

EMPLACEMENT, PETROLOGY
AND GEOCHEMISTRY OF
ULTRABASIC TO BASIC
INTRUSIVES AT AILLIK
BAY, LABRADOR

CENTRE FOR NEWFOUNDLAND STUDIES

**TOTAL OF 10 PAGES ONLY
MAY BE XEROXED**

(Without Author's Permission)

DAVID W. HAWKINS



National Library of Canada

Cataloguing Branch
Canadian Theses Division

Ottawa, Canada
K1A 0N4

Bibliothèque nationale du Canada

Direction du catalogage
Division des thèses canadiennes

NOTICE

The quality of this microfiche is heavily dependent upon the quality of the original thesis submitted for microfilming. Every effort has been made to ensure the highest quality of reproduction possible.

If pages are missing, contact the university which granted the degree.

Some pages may have indistinct print especially if the original pages were typed with a poor typewriter ribbon or if the university sent us a poor photocopy.

Previously copyrighted materials (journal articles, published tests, etc.) are not filmed.

Reproduction in full or in part of this film is governed by the Canadian Copyright Act, R.S.C. 1970, c. C-30. Please read the authorization forms which accompany this thesis.

**THIS DISSERTATION
HAS BEEN MICROFILMED
EXACTLY AS RECEIVED**

AVIS

La qualité de cette microfiche dépend grandement de la qualité de la thèse soumise au microfilmage. Nous avons tout fait pour assurer une qualité supérieure de reproduction.

S'il manque des pages, veuillez communiquer avec l'université qui a conféré le grade.

La qualité d'impression de certaines pages peut laisser à désirer, surtout si les pages originales ont été dactylographiées à l'aide d'un ruban usé ou si l'université nous a fait parvenir une photocopie de mauvaise qualité.

Les documents qui font déjà l'objet d'un droit d'auteur (articles de revue, examens publiés, etc.) ne sont pas microfilmés.

La reproduction, même partielle, de ce microfilm est soumise à la Loi canadienne sur le droit d'auteur, SRC 1970, c. C-30. Veuillez prendre connaissance des formules d'autorisation qui accompagnent cette thèse.

**LA THÈSE A ÉTÉ
MICROFILMÉE TELLE QUE
NOUS L'AVONS REÇUE**

EMPLACEMENT, PETROLOGY AND GEOCHEMISTRY OF
ULTRABASIC TO BASIC INTRUSIVES AT AILLIK BAY, LABRADOR

by

David W. Hawkins, B.Sc.

A Thesis submitted in partial fulfillment
of the requirements for the degree of
Masters of Science

Department of Geology
Memorial University of Newfoundland

October 1976

St. John's

Newfoundland

ABSTRACT

Intrusive into the Archean Hopedale Complex and Proterozoic Aillik Group in the vicinity of Aillik Bay, Labrador, are a suite of Mesozoic basic to ultrabasic dykes exhibiting the compositions minette, monchiquite, kimberlite, micaceous kimberlite, alnöite and carbonatite. The dykes were emplaced along several well-developed joint directions and exhibit a variety of emplacement and/or internal features which are interpreted to be the result of liquid immiscibility, flow differentiation, multiple intrusion, supercooling, carbonatitization and forceful injection. The monchiquites, kimberlites and carbonatites are usually banded and are gradational in composition along strike.

The kimberlites are clinopyroxene-bearing and contain two generations of olivine and mica with perovskite, ilmenite, magnetite and apatite, as well as high concentrations of magmatic carbonate as an interstitial matrix phase or more rarely as ocelli. They also contain abundant glimmeritic nodules which form part of the Mica-Amphibole-Rutile-Ilmenite-Diopside suite and are interpreted to be of cognate origin. The minettes and monchiquites are petrologically similar to other intrusions of these compositions and contain carbonate in the form of ocelli.

Field, petrological and chemical data indicate that the monchiquites, kimberlites and carbonatites are genetically related and crystallized from a common parent. The minettes appear to be unrelated to the ultrabasic magmatism and were intruded prior to the above suite.

The emplacement of the ultrabasic dykes is attributed to the initial separation of Greenland from North America during the formation of the Labrador Sea in the Mesozoic. The magma produced during this distension and rifting also gave rise to kimberlites and related rocks in Greenland.

TABLE OF CONTENTS

	Page
Abstract	i
List of Figures	vii
List of Tables	xiv

CHAPTER 1

INTRODUCTION

1.1 Preamble	1
1.2 Location and accessibility	2
1.3 Geographical setting	4
1.4 Regional geological setting	6
1.5 Previous studies	7
1.6 Acknowledgements	10

CHAPTER 2

GENERAL GEOLOGY OF THE AILLIK BAY AREA

2.1 Introduction	12
2.2 The Hopedale Complex	13
2.3 The Aillik Group	
2.3.1 Stratigraphy	14
2.3.2 Lithologies	
2.3.2.1 Metasediments	17
2.3.2.2 Mafic metavolcanics	17
2.3.2.3 Undifferentiated sediments (including acid volcanics)	23
2.4 Intrusive rocks	
2.4.1 Post-tectonic	23

CHAPTER 3

FIELD CHARACTER AND EMPLACEMENT HISTORY OF THE AILLIK BAY BASIC - ULTRABASIC DYKE SWARM

3.1	Introduction	26
3.2	Field Setting	27
3.3	Dyke Orientations	27
3.4	Intrusive relations between different compositional types	30
3.5	Detailed field characteristics	
3.5.1	Hornblende peridotites	
3.5.1.1	Lithology	31
3.5.1.2	Contact relationships and internal structure	31
3.5.2	Minettes	
3.5.2.1	Lithology	31
3.5.2.2	Contact relationships and emplacement features	33
3.5.2.3	Contact alteration	33
3.5.2.4	Internal structure	34
3.5.3	Monchiquites	
3.5.3.1	Lithology	34
3.5.3.2	Contact relationships and emplacement features	
	(a) Carbonate-poor monchiquite	34
	(b) Carbonate-rich monchiquite	35
	(c) Carbonate-bearing monchiquite pipe	39
	(d) Carbonate-bearing monchiquite diatreme	42
3.5.3.3	Contact alteration	46
3.5.3.4	Internal structure	
	(a) Carbonate-poor monchiquites	46
	(b) Carbonate-rich monchiquites	46
3.5.3.5	Carbonatitization	59
3.5.3.6	Nodules and xenoliths	59
3.5.4	Kimberlites	
3.5.4.1	Lithology	59
3.5.4.2	Contact relationships and emplacement features	63
3.5.4.3	Contact alteration	67
3.5.4.4	Internal structures	69
3.5.4.5	Serpentinization	72
3.5.4.6	Carbonatitization	74
3.5.4.7	Nodules and xenoliths	75

3.5.5	Carbonatites	
3.5.5.1	Lithology	75
3.5.5.2	Contact relationships and emplacement features	78
3.5.5.3	Contact alteration	78
3.5.5.4	Internal structures	79
3.5.5.5	Nodules and xenoliths	79

CHAPTER 4

PETROLOGY

4.1	Introduction	80
4.2	Petrology	
4.2.1	Hornblende Peridotites	82
4.2.2	Minettes	83
4.2.3	Monchiquites	86
4.2.3.1	Carbonate-rich dykes	86
4.2.3.2	Carbonate-poor dykes	93
4.2.4	Kimberlites	
4.2.4.1	Introduction	94
4.2.4.2	First generation mineral phases	
	(a) Nodules	96
	(b) Megacrysts in kimberlites	105
4.2.4.3	Second generation mineral phases	108
4.2.4.4	Crustal nodules	121
4.2.5	Carbonatites	
4.2.5.1	Introduction	125
4.2.5.2	Carbonatites	127
4.2.5.3	Metasomatic carbonatites	127
4.2.6	Alnoites	
4.2.6.1	Introduction and Petrology	128

CHAPTER 5

GEOCHEMISTRY

5.1	Introduction	133
5.2	Major and trace element geochemistry	
5.2.1	Hornblende-bearing peridotites	134
5.2.2	Minettes	134
5.2.3	Carbonate-rich monchiquites	139
5.2.4	Kimberlites	146
5.2.5	Carbonatites	150

5.3	Variation diagrams	
5.3.1	Introduction	153
5.3.2	Harker diagrams	153
5.3.3	FMA diagram	158
5.3.4	($\text{SiO}_2 + \text{SiO}_2 + \text{alkalis}$) vs volatiles vs ($\text{CaO} + \text{MgO} + \text{FeO} + \text{Fe}_2\text{O}_3 + \text{TiO}_2$) ternary diagram	160
5.3.5	K/Rb ratios	162
5.4	Mineral chemistry	
5.4.1	Olivine	164
5.4.2	Mica	165
5.4.3	Clinopyroxene	168
5.4.4	Opaque oxides	168

CHAPTER 6

DISCUSSIONS AND CONCLUSIONS

6.1	Tectonic setting of kimberlite magmatism and its relationship to the Aillik occurrences	170
6.2	Carbonate: Its origin in kimberlites and carbona- tites	175
6.3	A petrogenetic model for the Aillik Bay ultrabasic - basic dykes	180
6.4	Conclusions	182
	Bibliography	184
	Appendix I	212
	Appendix II	222
	Appendix III	226

LIST OF FIGURES

	Page
Figure 1.1: Index map showing the location of the Aillik Bay thesis area	3
Figure 1.2: General map of the Aillik Bay area	5
Figure 2.1: General geology of the Aillik Bay thesis area	15
Figure 2.2: Large plagioclase phenocrysts in a diabase porphyry near Buttress Point	25
Figure 3.1: Dyke orientations of the Aillik Bay basic-ultrabasic dyke swarm	28
Figure 3.2: Joint and dyke orientations of the Aillik Bay area	29
Figure 3.3: Large porphyritic hornblende crystals in a hornblende-bearing peridotite	32
Figure 3.4: Nonbanded carbonate-poor monchiquite intruding granophyre near Cape Makkovik	32
Figure 3.5: Brittle fracture development in a carbonate-rich monchiquite dyke near Cape Makkovik	36
Figure 3.6: A horned offset dyke from the east side of Aillik Bay	36
Figure 3.7: Geometric forms of the monchiquite termination structures	38
Figure 3.8: Pseudo-fold within an amoeboid termination structure	40
Figure 3.9: Lineation development on the fine grained non-ocelli-bearing bands within the marginal banded zone of a carbonate-rich monchiquite dyke	40
Figure 3.10: Orientation of lineation and pseudo-fold directions within the carbonate-rich monchiquite dykes	41
Figure 3.11: A rod-shaped intrusion cutting a kimberlites dyke on West Turnavik Island	43

Figure 3.12:	Location and shape of a carbonate-bearing monchiquite and its associated breccia to the west of Banana Lake	44
Figure 3.13:	Subangular to subrounded xenoliths in the monchiquite diatreme to the west of Banana Lake	45
Figure 3.14:	Type I banding in a carbonate-bearing monchiquite on the west side of Aillik Bay	48
Figure 3.15:	Schematic diagram showing variation in Type I banding	49
Figure 3.16:	A band of skeletal pyroxene growth in a carbonate-bearing monchiquite near Cape Makkovik	54
Figure 3.17:	Schematic diagram showing variation in Type II banding	55
Figure 3.18:	Lobate shaped arrangement in a core of a dyke with Type II banding	58
Figure 3.19:	Rounded fragments in a dyke with Type III banding	58
Figure 3.20:	Carbonatite selvage in the marginal area of a carbonate-rich monchiquite, East Turnavik Island	60
Figure 3.21:	Carbonate veinlets cutting a monchiquite dyke near the Tidal Flat area	60
Figure 3.22:	Relationship between mica and carbonate in the Aillik kimberlites	62
Figure 3.23:	Extremely net-veined kimberlite dyke on the east shore of Aillik Bay	64
Figure 3.24:	A kimberlite dyke on the east shore of Aillik Bay which exhibits a chill margin	64
Figure 3.25:	Brittle fracture development within a carbonate-rich kimberlite on the east shore of Aillik Bay	66

Figure 3.26:	Horned termination structures in a kimberlite dyke on the east shore of the Aillik Bay	68
Figure 3.27:	Dark fenite halo surrounding a sub-angular xenolith in a carbonate-rich micaceous kimberlite	68
Figure 3.28:	Photograph of a kimberlite dyke showing banding produced by the segregation of megacrystic and finer grained non-megacrystic bands where the latter pinch, swell and encompass thin xenolithic slivers	70
Figure 3.29:	Large lensoidal ocelli which are connected by thin carbonate veinlets within a carbonate-rich micaceous kimberlite	70
Figure 3.30:	Crescent shaped flow structure produced by the alignment of ocelli in a carbonate-rich kimberlite	73
Figure 3.31:	Serpentine veinlets cutting a carbonate-rich kimberlite near Aillik Village	73
Figure 3.32:	Carbonate-rich marginal zone of a carbonate-rich micaceous kimberlite on the east shore of Cape Makkovik	76
Figure 3.33:	Spherical glimmerite nodules within a carbonate-rich micaceous kimberlite	76
Figure 3.34:	Nodular core of a carbonate-rich kimberlite on the west shore of Cape Aillik	77
Figure 4.1:	Photomicrograph of large poikilitic hornblende crystals which enclose embayed olivine and augite crystals	84
Figure 4.2:	Photomicrograph showing augite, opaque oxides and poikilitic biotite crystals in a matrix composed of orthoclase and augite	84
Figure 4.3:	Photomicrograph of a re-crystallized olivine phenocryst which exhibits a granoblastic texture	88

Figure 4.4:	Photomicrograph of bladed to dendritic augite growths which form Type II banding	88
Figure 4.5:	Photomicrograph showing a poikilitic tabular plate of biotite which encloses acicular needles of augite	90
Figure 4.6:	Photomicrograph showing the matrix of a carbonate-rich monzonite composed of acicular to bladed opaque oxide growths with biotite and opaque oxides	90
Figure 4.7:	Photomicrograph showing the diffuse boundary of a carbonate-rich ocelli	92
Figure 4.8:	Photomicrograph showing olivine phenocrysts with concentric rings of augite, biotite and opaque oxides	92
Figure 4.9:	Photomicrograph of a micaceous kimberlite containing large subrounded megacrysts in a matrix of olivine, serpentine, opaque oxides, phlogopite and carbonate	98
Figure 4.10:	Photomicrograph of a glimmerite nodule (Group V mica) within kimberlite	98
Figure 4.11:	Photomicrograph showing large deformed phlogopite crystal in a glimmerite nodule core	100
Figure 4.12:	Photomicrograph showing granular olivine crystals in an olivine opaque oxide glimmerite	100
Figure 4.13:	Photomicrograph of a granoblastic dunite nodule	105
Figure 4.14:	Photomicrograph of a diopside glimmerite nodule which contains interstitial chains of diopside	105
Figure 4.15:	Photomicrograph of an amphibole-biotite-opaque oxide glimmerite with nonpleochroic amphibole	107
Figure 4.16:	Photomicrograph of a poikilitic opaque oxide crystal in an opaque-olivine glimmerite	107

Figure 4.17:	Photomicrograph of a micaceous kimberlite containing large subrounded megacrysts in a matrix of olivine, serpentine, opaque oxides and carbonate	108
Figure 4.18:	Photomicrograph of a first generation olivine crystal showing deformation bands	108
Figure 4.19:	Photomicrograph of a first generation mica which exhibits a slightly bent (001) cleavage	110
Figure 4.20:	Photomicrograph of a first generation perovskite megacryst	110
Figure 4.21:	Photomicrograph of a second generation olivine megacryst which is completely replaced by calcite	111
Figure 4.22:	Photomicrograph of an xenomorphic olivine crystal belonging to second generation	111
Figure 4.23:	Photomicrograph of a zoned mica megacryst which contains a core of Group Ia mica and a rim of second generation mica	114
Figure 4.24:	Photomicrograph of a second generation mica megacryst which contains abundant opaque oxides along the (001) cleavage	116
Figure 4.25:	Photomicrograph of a second generation titan-augite megacryst	116
Figure 4.26:	Photomicrograph of the matrix of a micaceous kimberlite which contains small acicular needles of augite	118
Figure 4.27:	Photomicrograph of a second generation titan-augite megacryst with a narrow phlogopite mantle	118
Figure 4.28:	Photomicrograph showing lath to microlithic shaped growths of calcite in a carbonate-rich kimberlite	120

Figure 4.29:	Photomicrograph of a carbonate-rich micaceous kimberlite showing the development of long acicular crystals of primary calcite . . .	120
Figure 4.30:	Photomicrograph of a flow cell in a carbonatite vein which intrudes a kimberlite . . .	122
Figure 4.31:	Photomicrograph of a second generation opaque oxide with an idiomorphic outline . . .	122
Figure 4.32:	Atoll development in a fractured opaque oxide crystal . . .	123
Figure 4.33:	Photomicrograph of an allotriomorphic-granular texture in a calcic-carbonatite . . .	127
Figure 4.34:	Photomicrograph of atoll development in an opaque oxide crystal . . .	127
Figure 4.35:	Photomicrograph of an ocelli-like structure within a metasomatic carbonatite . . .	129
Figure 4.36:	Photomicrograph of fenitized micas in a metasomatic carbonate . . .	129
Figure 4.37:	Photomicrograph of aegirine occurring as static growths within a dolomitic carbonatite	131
Figure 4.38:	Photomicrograph of melilite which occurs in a band of perpendicular growth . . .	131
Figure 5.1:	Histograms showing the variation in major and trace element abundances for the Aillik minettes . . .	137
Figure 5.2:	Histograms showing the variation in major and trace element abundances for the Aillik carbonate-rich monchiquites . . .	142
Figure 5.3:	Histograms showing the variation in major element abundances for the Callander Bay monchiquites . . .	143
Figure 5.4:	Histograms showing the variation in major and trace element abundances for the Aillik kimberlites . . .	147

Figure 5.5:	Histograms showing the variation in major element abundances for the Lesotho kimberlites	149
Figure 5.6:	Histograms showing the variation in major and trace element abundances for the Aillik carbonatites	152
Figure 5.7:	Harker variation diagrams for Aillik major element analyses	155
Figure 5.8:	Harker variation diagrams for Aillik trace element analyses	156
Figure 5.9:	FMA ternary diagram showing Aillik and Lesotho dyke analyses	159
Figure 5.10:	($\text{SiO}_2 + \text{Al}_2\text{O}_3 + \text{Alkalis}$) vs Volatiles vs ($\text{CaO} + \text{MgO} + \text{FeO} + \text{Fe}_2\text{O}_3 + \text{TiO}_2$) ternary diagram for Aillik (A) and Lesotho-Benfontein kimberlites (B)	161
Figure 5.11:	K/Rb diagram for the Aillik dyke analyses	163
Figure 5.12:	Variation diagrams exhibiting analyses of mica from megacrysts and nodules in kimberlite (A) (after Dawson and Smith, 1975a) and the Aillik kimberlites (B)	167
Figure 6.1:	Location of Labrador and Greenland kimberlites on a Bullard and Runcorn (1965) fit of the Continents	173
Figure 6.2:	Evolution of the Labrador Sea	174

LIST OF TABLES

	Page
TABLE 2.1: Stratigraphy of the Aillik Group near Cape Makkovik	18
TABLE 2.2: Stratigraphy of the Aillik Group	19
TABLE 2.3: Stratigraphy of the Aillik Group based on structural criteria	20
TABLE 2.4: Lithological content and relationship between six formations recognized within the Aillik Group	21
TABLE 2.5: Stratigraphy of the Aillik Group at Aillik Bay	22
TABLE 4.1: Mineralogical variation in the Aillik Bay glimmerite nodule suite	97
TABLE 4.2: Pleochroic schemes for Group Ia micas	102
TABLE 4.3: Pleochroic schemes for Group II micas.	103
TABLE 4.4: Pleochroic schemes for second generation micas	113
TABLE 5.1: Representative geochemical and petrographic data for the hornblende-bearing peridotites	135
TABLE 5.2: Representative geochemical and petrographic data for the minettes	136
TABLE 5.3: Average composition for the Aillik dykes compared to other dyke suites	138
TABLE 5.4: Representative geochemical and petrographic data for the carbonate-rich monchiquites.	140
TABLE 5.5: Representative geochemical and petrographic data for the Aillik kimberlites	145
TABLE 5.6: Representative geochemical and petrographic data for the Aillik carbonatites	151

CHAPTER 1

INTRODUCTION

1.1 Preamble

The term kimberlite was first introduced by Lewis (1887) to describe diamond-bearing porphyritic peridotites from Kimberley, South Africa. Early interest in kimberlitic rocks was principally economic because they were an important source of diamonds. Excellent syntheses of this early research were presented by Wagner (1914) and Williams (1932). Recent research work has concentrated particularly on the mantle-derived ultramafic nodules which kimberlites contain, as they afford an opportunity to study the petrology and geochemistry of mantle, and to interpret the physical processes operating therein (Rickwood, 1969; Rickwood and Mathias, 1970; Sobolev, 1970; Meyer and Brookins, 1971; Boyd and Nixon, 1973; Boullier and Nicolas, 1973).

Kimberlites are commonly spatially and temporally related to other alkaline igneous rocks and carbonatites (Dawson, 1970a; Ukhonov, 1965; Zhabin and Cherepyskaya, 1965) and certain varieties of kimberlite are chemically similar to these rocks, which suggests that they may be genetically related (Dawson, 1966, 1967b; Janse, 1975; Gittins et al., 1975).

Recent experimental studies in the systems CaO-MgO-SiO₂-CO₂-H₂O (Wyllie, 1966b; Franz and Wyllie, 1967), CaO-MgO-SiO₂-CO₂ (Irving and Wyllie, 1973, 1975; Wyllie and Huang, 1975), MgO-SiO₂-CO₂ (Huang and Wyllie, 1974), CaO-MgO-Al₂O₃-SiO₂-CO₂ (Wyllie, 1975) and CaO-CO₂, MgO-CO₂ (Huang and Wyllie, 1976) have attempted to assess this relationship.

The ultrabasic to basic dykes in the Aillik Bay area, Labrador, which were investigated in this thesis, range in composition from kimberlite (both carbonate-rich and micaceous varieties), lamprophyre (i.e. alnöite, monchiquite and minette - many of which are carbonate-rich) to carbonatite. This unique suite is of considerable petrogenetic significance as the kimberlites appear to be temporally, genetically and spatially related to the lamprophyres and carbonatites. The present study encompasses a petrological and geochemical investigation of this suite with a view to assessing the petrogenesis of the association.

1.2 Location and Accessibility

The thesis area is situated in the Makkovik Sub-province (as defined by Taylor, 1971) of the Nain Province (Fig. 1.1). The Aillik region occupies an area bounded by

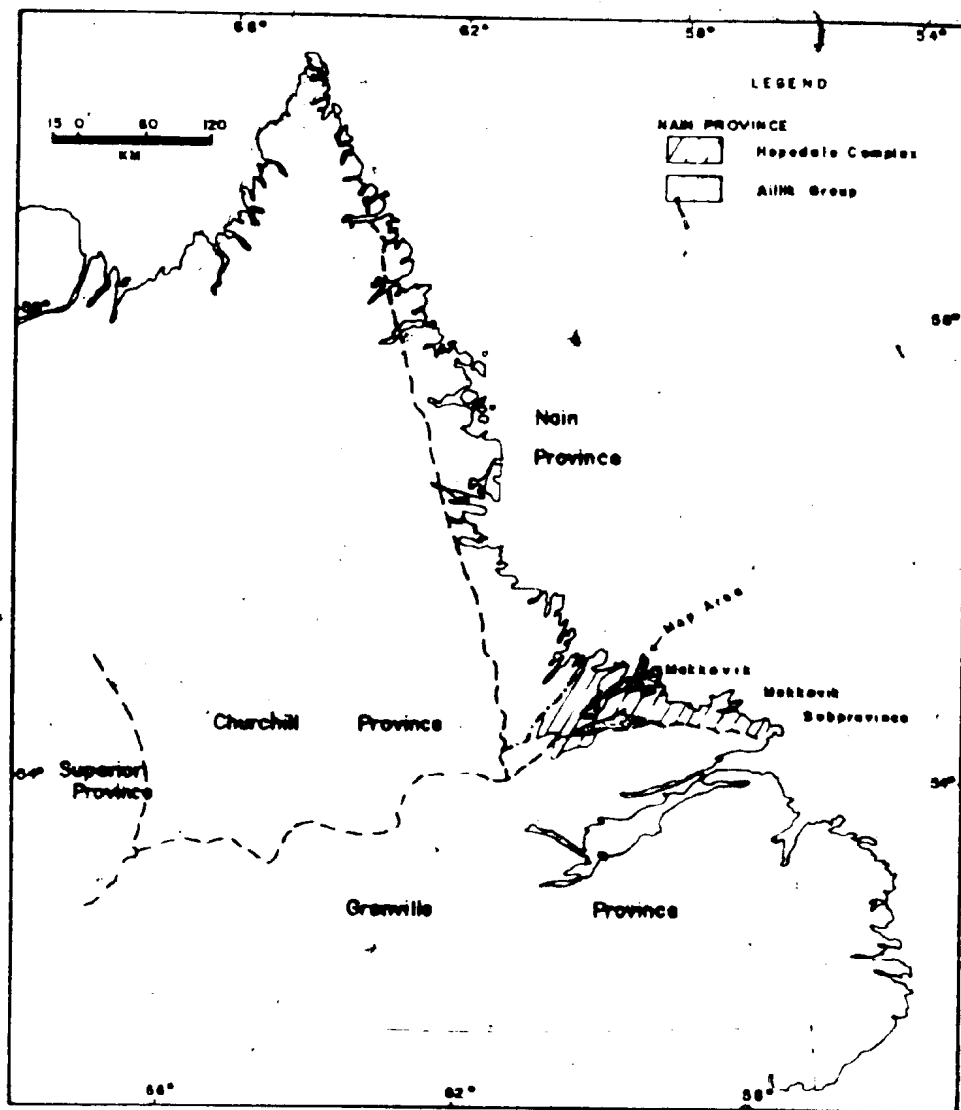


Figure 1.1 Index map showing the location of the Aillik Bay thesis area.

Makkovik Bay and Kaipokok Bay between latitude $55^{\circ} 10'$ N - $55^{\circ} 20'$ N and longitude $59^{\circ} 23'$ W - $59^{\circ} 08'$ W. Field work was carried out between June and September, 1973.

The settlement of Makkovik, approximately 12 km from the map area, was used as a logistical supply centre during the field season. The area was reached by float plane, chartered from Labrador Airways in Goose Bay. Access to the islands off the coast was by motorboat hired from local fishermen.

1.3 Geographical Setting

The topography of the map area (Fig. 1.2) is typical of regions glaciated during the Pleistocene. Hills have gentle slopes that seldom exceed 340 m in elevation. Joint and dyke controlled linear valleys up to 170 m wide and 30 m deep are a prominent feature of the landscape.

Rock exposure in the area is excellent along the coast, on the islands, and on exposed hill tops, however, outcrops in lowland areas are commonly poor.

A long fault-controlled, glacially scoured valley extends from south of Banana Lake towards Cape Makkovik. The valley is bottomed by a series of sphagnum and peat bogs

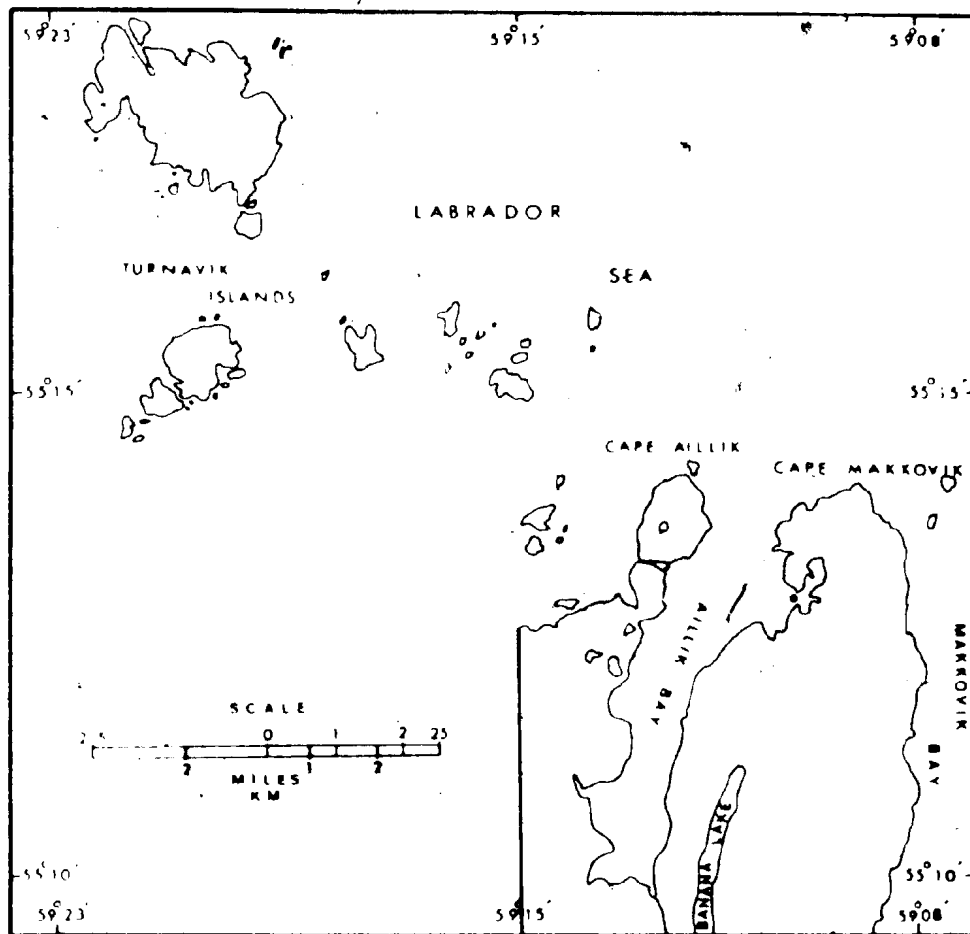


Figure 1.2 General map of the Aillik Bay area.

interspersed with small kettle holes and ponds.

Glacial ice flow with a mean direction towards 020 was indicated by numerous striations, grooves, chatter marks and stoss and lee forms. Glaciation is also evidenced by the occurrence of abundant erratic boulders and glacial-fluvial spillway morphology.

A prominent feature of the coastline areas is a series of raised marine beach berms and wave cut terraces. The most landward of the beach berms has a mean elevation of 17 m above the present sea level. This indicates an isostatic rebound since the Wisconsin Period of at least 17 m which has produced morphological features of an emergent and denuded coastline.

1.4 Regional Geological Setting

The Nain Province of the Canadian Shield (Fig. 1.1) is characterized by north-trending structures (Taylor, 1972). The northern part of the Province is dominated by a heterogeneous sequence of Archean gneisses which are intruded by Middle Proterozoic post-tectonic (Elsonian) anorthosite-adamellite plutons. The Archean gneisses are unconformably overlain by two Early Proterozoic supracrustal sequences (the Ramah and Mugford Groups). In the south, the Archean gneisses are also unconformably

overlain by Proterozoic supracrustal sequences; the Moran, Bruce River, Seal Lake and Aillik Groups (Smyth et al., 1975). A detailed account of the general geology within the Aillik Group is given in Chapter II and Appendix I.

1.5 Previous Studies

Prior to the later 1800's, Labrador was a land practically unknown to geologists. It had been visited only by trappers, fishermen or missionaries. The earliest workers involved with geological mapping were Steinhauer (1814), Lieber (1860) and Packard (1891). Daly (1902) provided the first descriptions of the sedimentary units and the numerous intrusive rocks at Aillik Bay.

Kranck (1939, 1953, 1961) provided the first detailed study of the Aillik area. He recognised the intense deformation of the Hopedale gneisses, the primary depositional structures in the Aillik Series and described the field relations and petrology of intrusive rocks in the area. He recognized the ultrabasic nature of certain lamprophyric dykes, which he termed "aillikites" and discussed their similarity with alnoites from Alno in Sweden. Unpublished theses by Cooper (1951), Moore (1951) and Riley (1951) present the results of detailed petrological studies carried out on specimens

collected by Kranck.

Regional reconnaissance mapping by the Geological Survey of Canada (Douglas, 1953; Christie et al., 1953) provided geological and economic syntheses of large areas of Labrador.

In 1954, British Newfoundland Exploration Company (Brinex) commenced geological mapping of their concession between Kaipokok Bay and Lake Melville. Piloski (1955) mapped the Aillik and Shoal Lake areas where occurrences of molybdenite, chalcopyrite, pyrite and uranium were recorded. Beavan (1958) discussed the uranium potential of Labrador with reference to the Central Mineral Belt.

King (1963) presented a detailed map of Cape Makkovik and discussed the petrology, stratigraphy, metamorphism and structure of the Aillik Group. He recognized the monchiquitic and alnoitic composition of the lamprophyre dykes in the Aillik area and provided well documented evidence for widespread metasomatism. A detailed synthesis of the stratigraphy, lithology and origin of the Aillik Group and associated intrusive rocks was presented by Gandhi et al. (1969). Clark (1971a, 1971b) redefined many of the units described by Gandhi et al. (1969) and divided the Aillik Group into an older and younger sequence on the basis of structure. In 1974 he (Clark, 1974) presented a detailed analysis of the stratigraphy and structure of the

Aillik Group. In this study he considered that many of the quartzite units within the succession were in fact acid pyroclastics, rhyolites or tuffaceous sediments.

The structure of the Aillik Group and Hopedale Gneiss was described by Sutton et al. (1971). They divided the orogenic history of the area into three major deformational episodes. The first produced major zones of intense deformation (large scale shear belts) during the early stages of the orogenic history. The second deformation resulted in the development of small tight folds and the third which was more widespread, produced large scale upright to recumbent folds.

In a recent study, King and McMillan (1975) on the basis of micropaleontological evidence have suggested that a diatremic (?) breccia in the Makkovik area is mid-Mesozoic in age. The breccia, which contains fragments of country rock including lamprophyre, overlies a lamprophyric dyke and is itself cut by lamprophyric and carbonatite dyklets. This implies at least a mid-Mesozoic age for the lamprophyric and carbonatite veinlets. If these veinlets are related to the lamprophyre below the breccia, then it is possible that the breccia and lamprophyric dykes are related to the same period of ultrabasic magmatism. King and McMillan (1975) suggest that the diatreme was emplaced into (now completely eroded) Jurassic sediments during the

initial opening of the Labrador Sea.

6 Acknowledgements

Financial support for this research was provided by the Federal Department of Regional Economic Expansion and by an N.R.C. Grant (No. A-8694) to Dr. K.D. Collerson.

The author is grateful to Dr. K.D. Collerson who suggested the project and provided supervision and guidance throughout the study. Dr. Collerson also allowed the author access to specimens of kimberlite from localities from Southern Africa and Lesotho. The thesis was read by Dr. Collerson who suggested numerous improvements. The author; however, accepts full responsibility for the ideas explained herein.

Assistance in mastering chemical analytical techniques was provided by Mrs. G. Andrews, Mr. D. Press and Mr. J. Vahtra of Memorial University. Mr. F. Thornhill produced many of the numerous thin sections used in this study. Draughting assistance was provided by the Newfoundland Department of Mines and Energy. The author was accompanied in the field by Mr. C. ~~Belong~~, whose enthusiasm and good humour were a constant source of inspiration.

Thanks are also due to Dr. A. King who provided many hours

of valuable discussion on aspects of the geology of the Cape Makkovik area and to Dr. D. Strong, Dr. C. Hughes and Dr. J. Malpas who provided stimulating discussion regarding the interpretation of the geochemistry of the Aillik dykes. Thanks must also be extended to L. Genge, D. Woodland and R. Hammond for typing this thesis.

CHAPTER 2

GENERAL GEOLOGY OF THE AILLIK BAY AREA

2.1 Introduction

The ultrabasic to basic dykes in the Aillik Bay area intrude a varied group of country rocks. The oldest rocks are Archean gneisses (Hopedale Complex; Sutton, 1972). The basement complex comprises migmatitically banded quartzofeldspathic gneisses, agmatites and amphibolites which are intruded by units of augen gneissic granite.

The gneisses are overlain by the Aillik Group, a sequence of early Proterozoic metavolcanic and metasedimentary rocks with an estimated thickness of 8500 m (Clark, 1974). The clastic sediments of the Aillik Group were deposited after considerable erosion of the basement gneisses (Gandhi *et al.*, 1969; Taylor, 1972). Acid to basic volcanic activity (including pyroclastic activity) contributed an important component to the stratigraphic succession (Taylor, 1972; Clark, 1971a, 1971b, 1974; Stevenson, 1970) and it is possible that certain "sedimentary units" could represent acidic volcanoclastic debris (Clark, 1974).

The Aillik Group was deformed and metamorphosed during the Hudsonian Orogeny circa 1.8 b.y. ago (Taylor, 1972). The grade

of metamorphism ranges from sub-greenschist to lower amphibolite facies (Gandhi et al., 1969; Clark, 1971a, 1974). Regression of the basement gneisses to greenschist facies assemblages probably occurred at this time.

Several units of pre-metamorphic (pre-Hudsonian) dykes and sills of augen schist and amphibolite occur in the area and were presumably emplaced prior to the deformation of the Aillik Group.

The basement gneisses and the Aillik Group are intruded by a complex suite of post-tectonic igneous plutonic to hypabyssal rocks ranging in composition from hornblende-gabbro, diorite, monzonite and granite. Diabase dykes commonly with large megacrysts of plagioclase and irregular xenoliths of anorthosite and leuco-gabbro are abundant in the area.

The last igneous activity was the emplacement of the ultra-basic to basic suite.

2.2 The Hopedale Complex

Rocks of the Hopedale Complex crop out in the northeastern part of the map area (Fig. 2.1), the most continuous exposures occurring on the Turnavik Islands and on Graplin Island. The oldest component of the gneiss complex consists of banded quartzo-

feldspathic gneiss and amphibolite. These gneisses are intruded by augen gneissic granite and show lateral variation into units of agmatitic migmatite. The sequence is characterized by a well developed quartzo-feldspathic layering that alternates with amphibolite bands on a scale of 10 to 15 cm. In some cases, particularly in the quartzo-feldspathic units, the large scale banding shows a finer layering on a scale of 1 to 10 mm. The large scale banding is commonly folded, contorted and boudinaged.

The unit of augen gneissic granite which intrudes the banded quartzo-feldspathic gneiss and amphibolites commonly contains xenoliths of these lithologies. It is characterized by megacrysts of alkali feldspar (mode 60 to 70 percent) in a matrix consisting of quartz, feldspar and biotite.

The migmatitic unit is an agmatitic breccia consisting of angular blocks of banded amphibolitic gneisses ranging in size from 10 to 50 m in diameter to fragments 1 to 5 cm in diameter in a neosome consisting of medium grained potassium feldspar-rich granite.

2.3 The Aillik Group

2.3.1 Stratigraphy

The first detailed stratigraphic subdivision of the Aillik

See Map 1
Back Pocket

Figure 2.1 General geology of the Aillik Bay thesis area.

Group was made by King (1963) in a study of the rocks at Cape Makkovik (Table 2.1). This work was extended by Gandhi et al. (1969) who presented a regional stratigraphic synthesis of the Aillik Group based on lithology, contact relationships, structure and geochronology (Table 2.2). They regarded the succession from the granoblastic feldspathic quartzite to the porphyritic arkosic quartzite to represent a conformable sequence.

Clark (1971a, 1971b) redefined many of the units proposed by Gandhi et al. (op. cit.); preferring to use non-genetic terms such as psammite to describe the quartzite units. He also divided the Aillik Group into a younger and older sequence (Table 2.3) using structural criteria.

The older sequence comprised units that contained fabrics and structures which were absent in the younger sequence. He regarded the older sequence as forming a structural succession although exact stratigraphic relations were unknown. The younger sequence, on the other hand, formed a conformable stratigraphic succession (based on sedimentological criteria such as cross-bedding and graded bedding). Clark (1974) redefined the stratigraphic succession in the Aillik Group and outlined six formations, each consisting of a number of individual members (Table 2.4). He also recognized the presence of an extensive suite of acid volcanics which had been suggested previously by Bridgwater (1970).

A combined structural and stratigraphic sequence of the Aillik Group in the Aillik Bay area is presented in Table (2.5.) Most units exposed in the map area (Fig. 2.1) are tentatively correlated with either the Big Island Formation or the Makkovik Formation (Clark, 1974).

2.3.2 Lithologies

2.3.2.1 Metasediments

Several metasediment horizons occur in the western part of the Aillik area (Fig. 2.1). The units contain well defined sedimentary structures such as bedding, flame structures and cross-bedding which indicate that the western sequences are upright. The sediments which consist mainly of arkoses or arkosic-quartzites contain variable amounts of feldspathic material. Marble horizons are commonly found as thin interbeds on the east side of Aillik Bay and have a distinctive salmon red color.

Two horizons of polymictic conglomerate are present within the sedimentary succession (Fig. 2.1), the largest outcrops occurring on the western side of Cape Aillik.

2.3.2.2 Mafic Metavolcanics

Two major horizons of basic metavolcanics are found in the thesis area (Fig. 2.1). They exhibit relict pillows in the

TABLE 2.1

Stratigraphy of the Aillik Group Near Cape Makkovik¹

Area west of Banana Lake shear zone

Chloritic amphibolite, biotite schist

Feldspathic quartzite-metamorphic granite

Chloritic amphibolite, biotite schist

Pure quartzite (meta-quartz sandstone)

Feldspathized banded quartzite

Micaceous grey quartzite

Quartzite gneiss-conglomerate gneiss

Tectonic conglomerate, crystalline limestone,
arkosic-quartzite

Tectonic shear zone

Quartzo-feldspathic mylonite gneiss (with
discoid plates and bands)

Mylonite quartzite, (with feldspar augen).

Area east of Banana Lake shear zone

Feldspathic quartzite (feldspathized in part);
minor bands of fine-grained grey quartzite and
biotite schist

¹ after King (1963).

TABLE 2.2
Stratigraphy of the Aillik Group²

Feldspathic prophyroblastic arkosic quartzite
Lineated gray feldspathic quartzite
Feldspathic quartzite (variable lithology)
Thin-bedded quartzite
Mafic lava (amphibolite) and associated tuffaceous beds
Conglomerate; paragneiss
Banded quartzite (varicolored)
Granoblastic feldspathic quartzite
----- Unconformity -----
Hopedale Gneiss

2 after Gandhi et al. (1969)

TABLE 2.3

Stratigraphy of the Aillik Group Based on Structural Criteria³

Younger Sequence

<u>Unit</u>	<u>Approx. Thickness</u>
Amphibolite (youngest)	6 - 33 m.
Porphyroclastic Psammite	33 m.
Conglomerate	17 - 200 m.
Cross-bedded Psammite (oldest)	17 - 700 m.

Older Sequence

Banded Psammite	~37 m.
Biotite - Hornblende - Feldspar Rock	17 m.
Variable Psammite	400 m.

³ after Clark (1971a)

TABLE 2.4

Lithological Content and Relationship Between Six Formations

Recognized within the Aillik Group⁴

<u>Big Island Formation</u>		<u>Pomiadluk Point</u>	<u>Makkovik Bay</u>
Rhyolite lavas, tuffs, mafic lavas, conglomerate and arkose		<u>Formation</u>	<u>Formation</u>
		Rhyolite lavas, tuffs and polymictic conglomerate	Arkose and mafic volcanics
		<u>Makkovik Formation</u>	
		Rhyolite lavas, tuffs and conglomerate	
		<u>Nesbith Harbour Formation</u>	
		Quartz-poor arkose, polymictic conglomerate and basaltic lavas	

Ranger Bight Complex

Amphibolite

⁴ after Clark (1974)

TABLE 2.5

Stratigraphy of the Aillik Group at Aillik Bay

<u>Cape Aillik</u>	<u>Cape Makkovik</u>
	Undifferentiated acid volcanics and quartzo-feldspathic sediments
	Quartzo-feldspathic Mylonite
	Sediments (possibly including acid volcanics) which show varying de- grees of secondary feldspathization
	Amphibolite, minor marble
	Sediments (possibly including acid volcanics) which show varying de- grees of secondary feldspathization
	Micaceous unit
	Undifferentiated sediments and acid volcanics
	Conglomerate, minor Banded Quartzo- marble feldspathic unit
	Arkosic-quartzite, cal-silicate breccia, marble
	?
Cross-bedded arkose and conglomerate	
?	
----- Unconformity -----	
Hopedale Complex	

southern exposures, but northwards they grade into tuffaceous horizons that contain pure quartzite lenses. This suggests that the northern sequences were deposited further from the source so they contain a sedimentary component. The volcanics contain 60 to 70 percent hornblende with feldspar and epidote.

2.3.2.3 Undifferentiated Sediments (Including acid volcanics)

Acid volcanic rocks are considered to form an important part of the Aillik Group at Aillik Bay. Most units were originally termed "quartzites" (King, 1963); however, this study has shown that rhyolites are also present in the succession although they were not separated during field mapping. The units commonly exhibit a well defined compositional layering; bands of quartzofeldspathic material alternating with more mafic bands on a 1 mm to 1 cm scale. Several units appear to locally have been subjected to regional potash metasomatism. The concentration of the feldspathizing solutions along brecciated zones (King, 1963), which are subparallel to the foliation has obliterated much of the original mineralogy; hence, the protolith could have been of igneous or sedimentary origin.

2.4 Intrusive Rocks

2.4.1 Post-tectonic

Dykes, sills and stocks ranging from granite to diorite are

common in the Aillik area. A large hornblendite to hornblende gabbro stock intrudes basement gneisses on the Turnavik Islands (Fig. 2.1) and contains abundant hornblende phenocrysts in a coarse grained feldspathic matrix. The stock contains numerous xenoliths of the basement gneisses as well as relicts of an earlier phase of hornblendite crystallization.

Diabase and diabase porphyry are most abundant in the northern part of the map area. The large porphyritic dykes (Fig. 2.2) contain phenocrysts that range from 2 to 12 cm in size. These feldspathic intrusions are regarded as being equivalent to the Gardar porphyritic dolerite dykes in Greenland described by Bridgwater and Harry (1968).



Figure 2.2 Large plagioclase phenocrysts in a diabase porphyry near Buttress Point.

CHAPTER 3
FIELD CHARACTER AND EMPLACEMENT HISTORY OF THE
AILLIK BAY BASIC-ULTRABASIC DYKE SWARM

3.1 Introduction

Several distinctive types of post-tectonic ultrabasic to basic intrusive rocks⁵ are recognized in the Aillik Bay area, viz; hornblende-bearing peridotites, minettes, monchiquites, carbonate-rich monchiquites, alnöites, kimberlites, (sensu stricto), micaceous kimberlites, carbonate-rich kimberlites, and carbonatites. Field, petrological and geochemical studies indicate that the lamprophyres (i.e. alnöites and monchiquites) together with the kimberlites and carbonatites are apparently genetically related whereas the hornblende-bearing peridotites and minettes are apparently not consanguineous, and are presumably related to an earlier magmatic event. The majority of the following discussion relates to the former suite.

The lamprophyres, kimberlites and carbonatites clearly post-date a major suite of diabase dykes which have a potassium-argon age of 956 ± 16 m.y. (Gandhi et al., 1969). Lëech et al. (1963) in a potassium-argon study of micas from three lamprophyres

5 A review of the terminology used is given in Appendix 2 and Chapter 4.

in the Aillik area concluded that the dykes have an average intrusive age of 570 m.y. In a more recent study, King and McMillan (1975) suggest that the lamprophyre suite may have a mid-Mesozoic age. This suggests that the earlier age determinations of Leech *et al.* (1963) were possibly influenced by excess argon in the micas and are therefore aberrant.

3.2 Field Setting

The ultrabasic to basic dykes (lamprophyres, kimberlites and carbonatites) in the Aillik Bay area comprise a well exposed north to northeast trending swarm (Fig. 3.1). They are petrologically similar to lamprophyric dykes found to the north and south along the Labrador coast (Kranck, 1953) and are also tentatively correlated with lamprophyric and kimberlitic dykes which intrude Archean gneisses and Proterozoic supracrustal rocks in West Greenland (Andrews and Emeleus, 1971; Escher and Watterson, 1972; Walton, 1966; Walton and Arnold, 1970).

The hornblende-bearing peridotites are poorly exposed and probably correlate with similar rocks in Southwest Greenland (Upton and Thomas, 1973).

3.3 Dyke Orientations

It is clear from Figures (3.2a and 3.2b) that there is a close correspondence between the attitudes of individual dykes

See Map 2

In Back Pocket

Figure 3.1 Dyke orientations of the Ailalik Bay basic-ultrabasic dyke swarm.

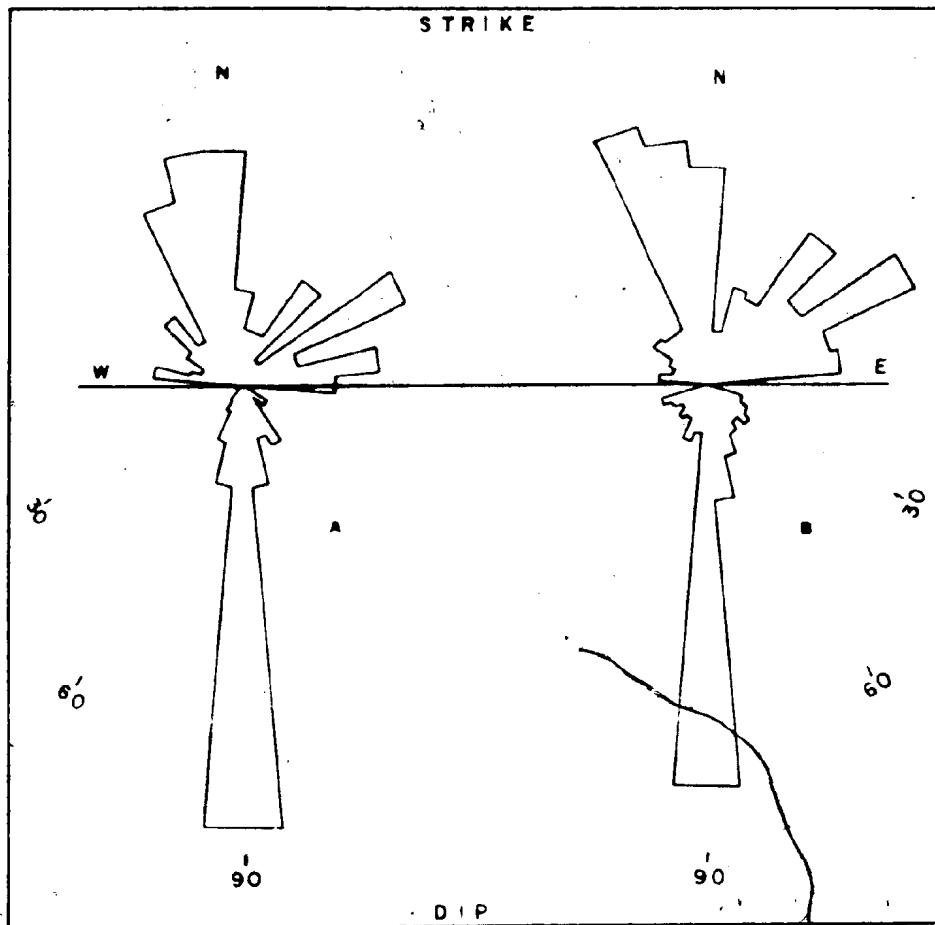


Figure 3.2 Joint (A) and dyke (B) orientations in the Aillik Bay area.

and the orientations of prominent joints in the area. Both dykes and joints dip nearly vertically and strike directions are commonly between 340 - 360, although significant nodes do occur between 035 - 045, 055 - 065 and 075 - 085. Throughout most of the area the dykes appear to have been emplaced along the most penetrative joints although in areas where joints are poorly developed, forceful features such as brittle fracturing, xenoliths and net-veining results.

3.4 Intrusive Relations Between Different Compositional Groups

From a study of intrusive relations between the different members of the lamprophyre-kimberlite-carbonatite suite, it is clear that the minettes were emplaced first as they are cut by kimberlite dykes. Most of the monchiquite dykes were also emplaced prior to the kimberlites; only a few examples were seen where they were intruded intermittently. At such localities, monchiquites postdate the kimberlites.

This intrusive sequence from minettes to carbonatites reflects a trend of increasing alkalinity and decreasing silica saturation and is discussed in detail in Chapter 5.

No hornblende-bearing peridotites have been observed to intrude dykes of the above suite; however, King (1963) on the basis of the ultrabasic character of the peridotites correlated them with the "lamprophyre suite". Results from this study

suggest that the peridotites are unrelated to the lamprophyric-kimberlitic suite. Instead they are tentatively correlated with the appinitic suite of hornblendites and hornblende-gabbros which intrude the Hopedale Complex on East Turnavik Island (Fig. 2.1).

3.5 Detailed Field Characteristics

3.5.1 Hornblende Peridotites

3.5.1.1 Lithology

Hornblende-bearing peridotites are the least widespread of all the intrusive rocks in the Aillik Bay area. They are medium to coarse grained, have a black to brown color and contain abundant poikilitic amphibole crystals ranging from .8 to 1 cm in diameter (Fig. 3.3).

3.5.1.2 Contact Relationships and Internal Structure

The hornblende-bearing peridotites occur as dykes that range in width from 1 to 2 m and in strike length from 5 to 10 m. They display sharp intrusive contacts which are invariably chilled against the country rocks. Most dykes have a massive habit and in contrast to some of the lamprophyres, kimberlites and carbonatites show no evidence of textural or mineralogical variation along strike.

3.5.2 Minettes

3.5.2.1 Lithology

Dykes classified as minettes are composed of phenocrysts of

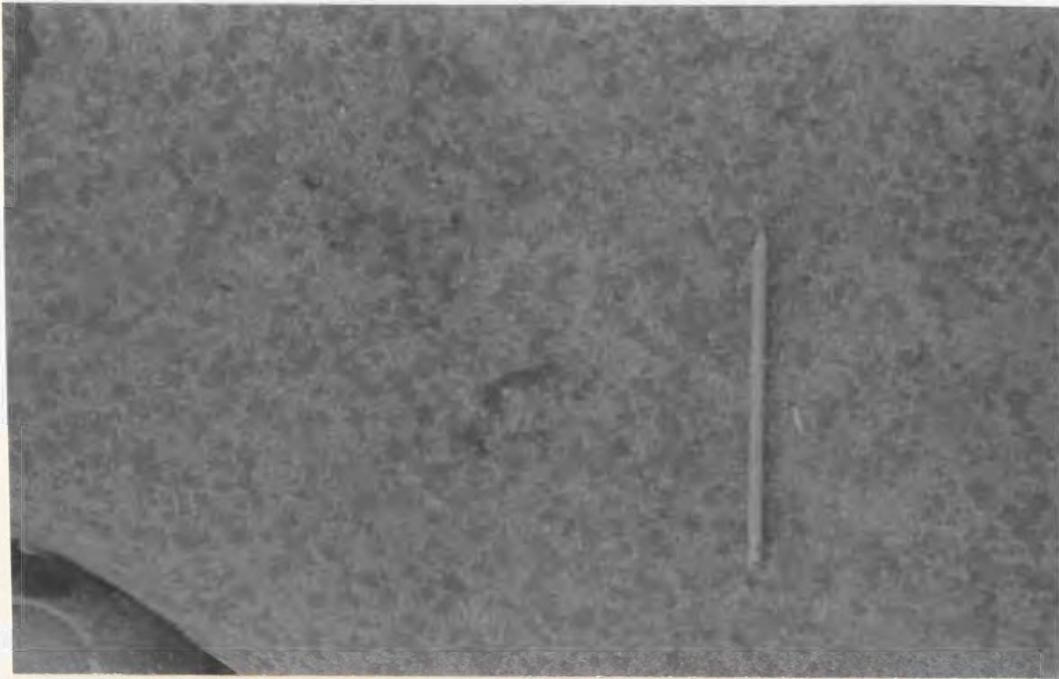


Figure 3.3 Large porphyritic hornblende crystals in a hornblende-bearing peridotite.



Figure 3.4 Nonbanded carbonate-poor monchiquite intruding granophyre near Cape Makkovik.

biotite, clinopyroxene and minor olivine in a groundmass of alkali feldspar. They are medium to fine grained and are black to brown in color. The minettes locally contain carbonate-bearing ocelli which are ellipsoidal to circular in shape and range in diameter from 1 to 3 mm.

3.5.2.2 Contact Relationships and Emplacement Features

The minette dykes have sharp regular contacts which are commonly chilled against the country rocks. The chill margins range in width from 1 to 2 cm and are characterized by a considerable decrease in grain size.

The minettes always follow prominent jointing directions and rarely show any variation in thickness or attitude along strike. Small angular xenolithic slivers of country rock are present in some dykes.

3.5.2.3 Contact Alteration

The contact rocks of the minettes rarely exhibit any alteration except for minor darkening in a few cases.

3.5.2.4 Internal Structure

The chill margins commonly grade outward into a marginal banded zone composed of alternating layers of ocelli-rich and ocelli-poor material on a scale of 1 to 3 cm wide. The ocelli-poor bands are finer grained than the ocelli-rich ones and commonly resemble

the chill marginal phase. Contacts between individual bands are sharp or gradational. In many dykes, the banded morphology is discontinuous along strike and in some dykes it is completely absent. The banding is similar to that observed in the carbonate-rich monchiquites and is interpreted to have a similar origin.

3.5.3 Monchiquites

3.5.3.1 Lithology

The monchiquites form two distinct groups viz; a carbonate-poor group and a carbonate-rich group. The carbonate-poor monchiquites are porphyritic and contain phenocrysts of clinopyroxene, biotite, olivine and opaque oxides up to 1 cm in diameter in a groundmass composed of very fine grained clinopyroxene, mica and opaque oxides. The carbonate-rich group are either porphyritic or nonporphyritic and contain abundant carbonate-bearing ocelli 1 to 8 mm in diameter. The ocelli commonly decrease in size and/or concentration toward dyke margins (a feature also noted in the monchiquite dykes at Callander Bay, Ferguson and Currie, 1972). Maximum concentrations of ocelli observed in individual dykes range from 3 to 20 percent.

3.5.3.2 Contact Relationships and Emplacement Features


(A) Carbonate-poor Monchiquites

The carbonate-poor monchiquites have sharp regular contacts and well developed chill margins. Most dykes are nonbanded; (Fig. 3.4); however, one dyke was seen to have a pronounced flow

lineation defined by the alignment of clinopyroxene phenocrysts.

(B) Carbonate-rich Monchiquites

The carbonate-rich monchiquite dykes have sharp, straight or irregular contacts and well developed chilled margins which range in width from 1 mm to 2 cm. In some dykes the chill margin exhibits a distinct mineral lineation which parallels the dykes margin. Individual dykes range in width from 4 cm to 1 m and in strike length from 15 to 270 m.



These dykes commonly display evidence of brittle fracturing (cf. Watterson, 1968) which implies that the monchiquite dykes were forcefully emplaced resulting in the rotation of blocks (Fig. 3.5) or slivers of country rock fragments into the dykes.

Most of the monchiquite dykes are vertically dipping (Fig. 3.2b) and have been emplaced in areas where jointing is well developed as continuous tabular bodies. In poorly jointed areas the monchiquites commonly terminate abruptly, bifurcate or become net-veined along strike. Dykes which terminate commonly reappear along strike in another coplanar joint plane giving the dykes a stepped appearance. Each segment of the stepped dyke has two termination heads (Fig. 3.6) which are similar to those described by Kaitaro (1953), Watterson (1968), Currie and Ferguson (1970, Fig. 3.7) and Pollard (1973). The termination heads have distinctive apophyses extending into the country rock from the outer edge of each part of the dyke across the line of offset giving



Figure 3.5 Brittle fracture development in a carbonate-rich monchiquite dyke near Cape Makkovik. Note the horned appearance of the apophyses and the concentration of country rock xenoliths within the core of the dyke.



Figure 3.6 A horned offset dyke from the east side of Aillik Bay. The dyke exhibits a distinct migration across its strike direction which is accomplished by several stepped sections. Each stepped dyke head contains a horned apophysis which extends across the line of offset.

them a horned appearance (Fig. 3.6).

The stepped dykes are considered by the author to have resulted from forceful emplacement of the monchiquite into discontinuous joint systems and are not considered to have formed by contemporaneous faulting with dyke injection (cf. Watterson, 1968). The propagation of apophyses at the head of each paired termination structure (Fig. 3.6) indicates that the stepped intrusions were emplaced simultaneously and that lateral migration towards one another occurred along the offset but parallel joints (Pollard, 1973).

Dyke intrusion was probably preceded by a volatile and/or fluid phase (Currie and Ferguson, 1970) which resulted in joint extension by a process of hydraulic fracturing (Phillips, 1972). The extension of discontinuous joints may account for the persistence of certain dykes in areas where joints are poorly developed. The occurrence of a fluid phase before intrusion is supported in the Aillik dykes by the presence of carbonate selvages in dykes which show no evidence of post or synemplacement carbonatization.

Some of the stepped dykes with small off-sets are interconnected by the apophyses, others are displaced by 10 cm to 1 m and no interconnection is apparent. Most stepped dykes with major offsets also exhibit a characteristic banding (Type II banding, see below, page 53).

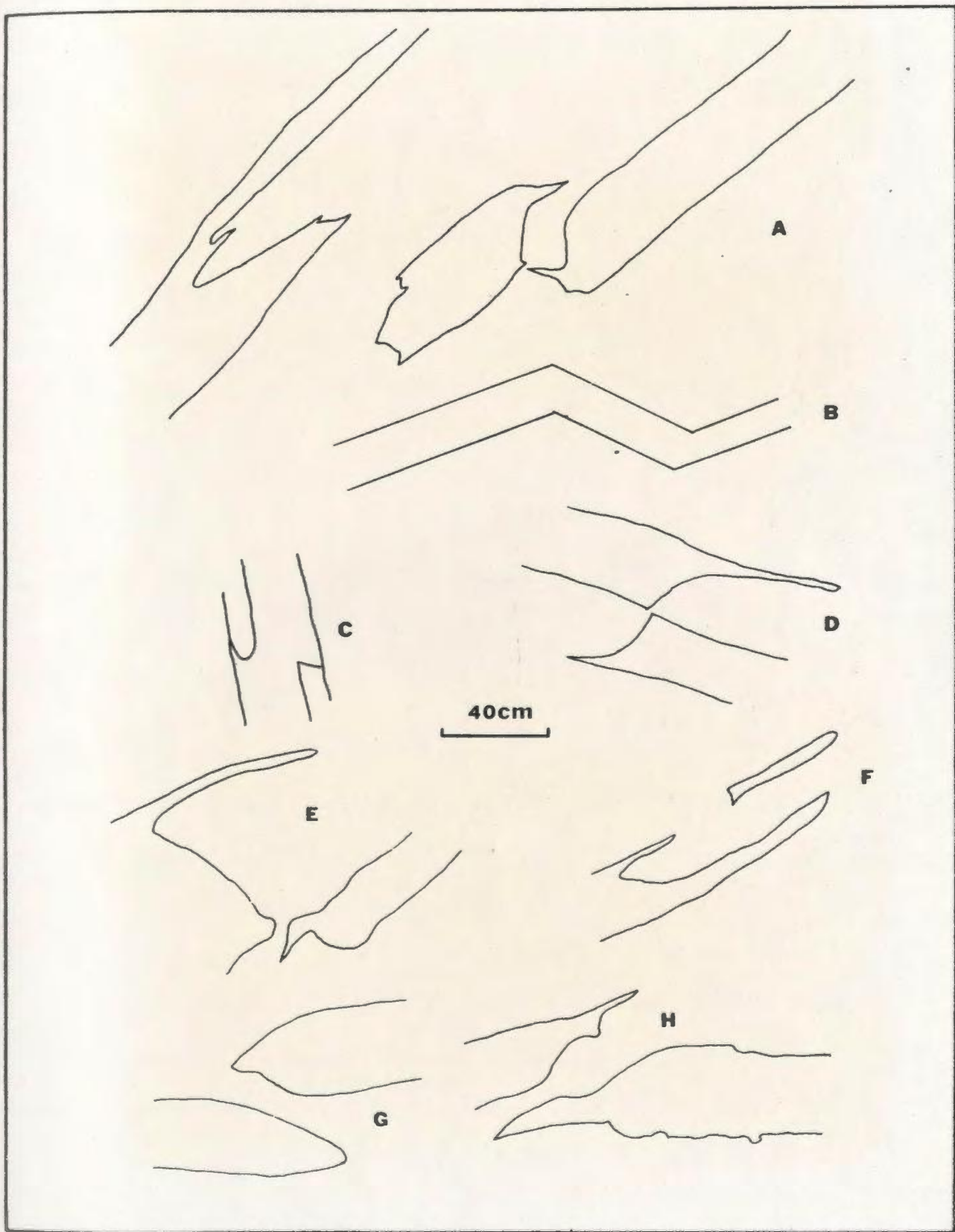


Figure 3.7 Geometric forms of the monchiquite termination structures (modified after Ferguson and Currie 1972).

Lobate or amoeboid termination structures are common in some of the monchiquite dykes (i.e. those which display Type II banding). In these structures, the banding appears to be folded around the termination. These "pseudo-folds" (Fig. 3.8) plunge at 40 to 80 degrees (Fig. 3.10). In some dykes, the "pseudo-folded" layering is not restricted to the termination area but can also be found in areas where a constriction of the dykes wall occurs. Some of the "pseudo-folds" exhibit weakly developed cleavage fans defined by fractures which radiate from the ocelli-rich core.

All termination structures regardless of shape display a core zone in which xenoliths and/or phenocrysts are concentrated. In many cases, the elongate xenoliths or phenocrysts are oriented with their long axis parallel to the dykes margin, producing a well defined flow lineation.

Many of the monchiquite dykes are characterized by the development of a strong lineation in a finer grained, nonocelli-bearing bands which comprise the marginal banded zone (Fig. 3.9). The lineations plunge between 0 to 90 degrees to either the north or south and show no apparent correlation between location or attitude (Fig. 3.10). These lineations are considered to be related to the emplacement of these dykes, although their exact nature is not fully understood.

(C) Carbonate-bearing Mochiquite Pipe



Figure 3.8 Pseudo-fold within an amoeboid termination structure.



Figure 3.9 Lineation development on the fine-grained nonocelli-bearing bands within the marginal banded zone of a carbonate-rich monchiquite dyke.

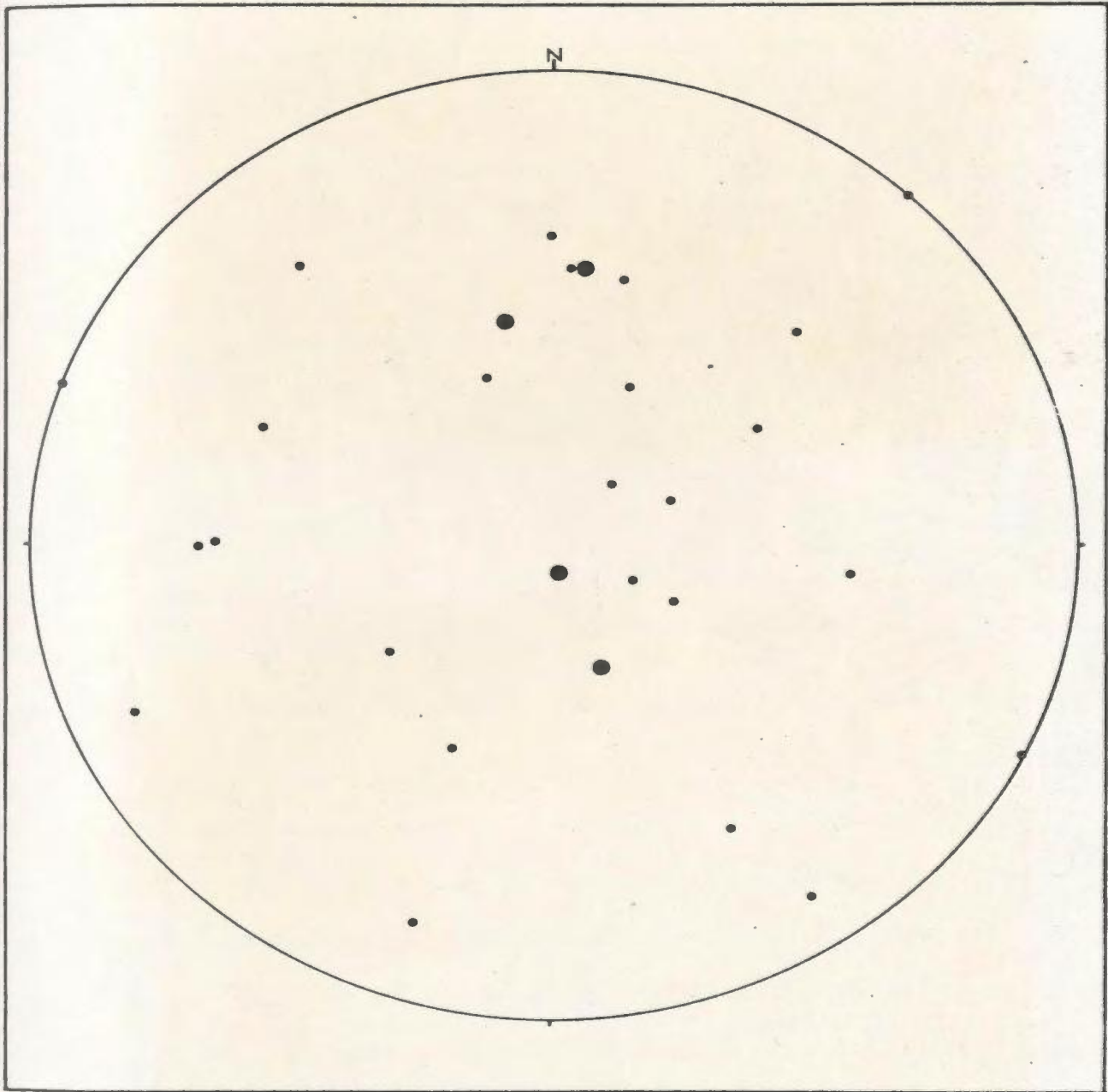


Figure 3.10 Orientation of lineation and pseudo-fold directions within the carbonate-bearing monchiquite dykes.

● "Pseudo-folds"

● "Lineations"

On West Turnavik Island a rod-shaped monchiquite intrusion (1 to 2 m in diameter) plunging at 45° to the northeast intrudes Archean gneisses of the Hopedale Complex and also cuts an earlier kimberlite dyke. It has a sharp intrusive contact and is partially chilled resulting in a perpendicular growth of dendritic clinopyroxene. The core of the intrusion contains abundant phenocrysts of clinopyroxene and country rock xenoliths. (Fig. 3.11)

(D) Carbonate-bearing Monchiquite Diatreme

A carbonate-bearing monchiquite and its associated breccia intrudes amphibolite west of Banana Lake (Fig. 2.1). The breccia occurs as an enlargement of an extensive carbonate-bearing monchiquite dyke as shown in Figure (3.12), and it contains numerous fragments of the surrounding country rocks (Fig. 3.13) i.e. amphibolites, metasedimentary units, intrusive rocks and acid metavolcanics. Clasts range in diameter from 1 mm to several centimeters and have angular to rounded outlines. The breccia has gradational contacts with the carbonate-rich monchiquite dyke and the clasts are cemented by a monchiquitic matrix. The occurrence appears to be similar to the Ford's Bight Breccia described by King and McMillan (1975).

The Aillik monchiquite diatremic breccia is interpreted to be either the base of a monchiquite diatreme (representing the contact between diatreme and hypabyssal facies; Dawson, 1971) or a blow on a dyke (Nixon, 1973)

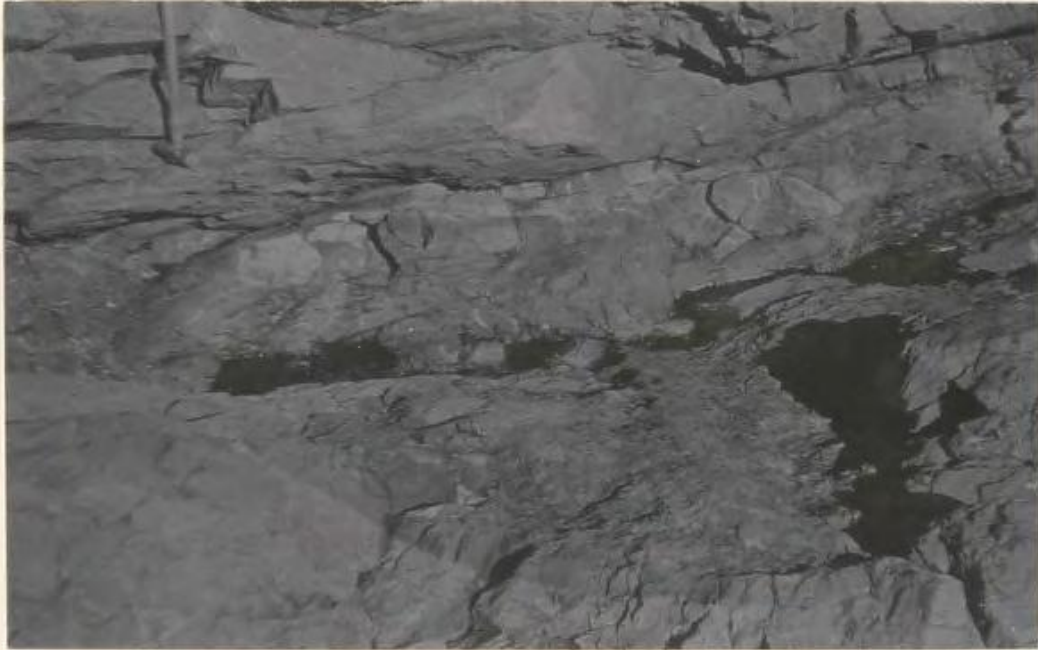


Figure 3.11 A rod-shaped intrusion cutting a kimberlite dyke on West Turnavik Island. The intrusion contains Type II banding and the dendritic pyroxene growth forms the chill margin.

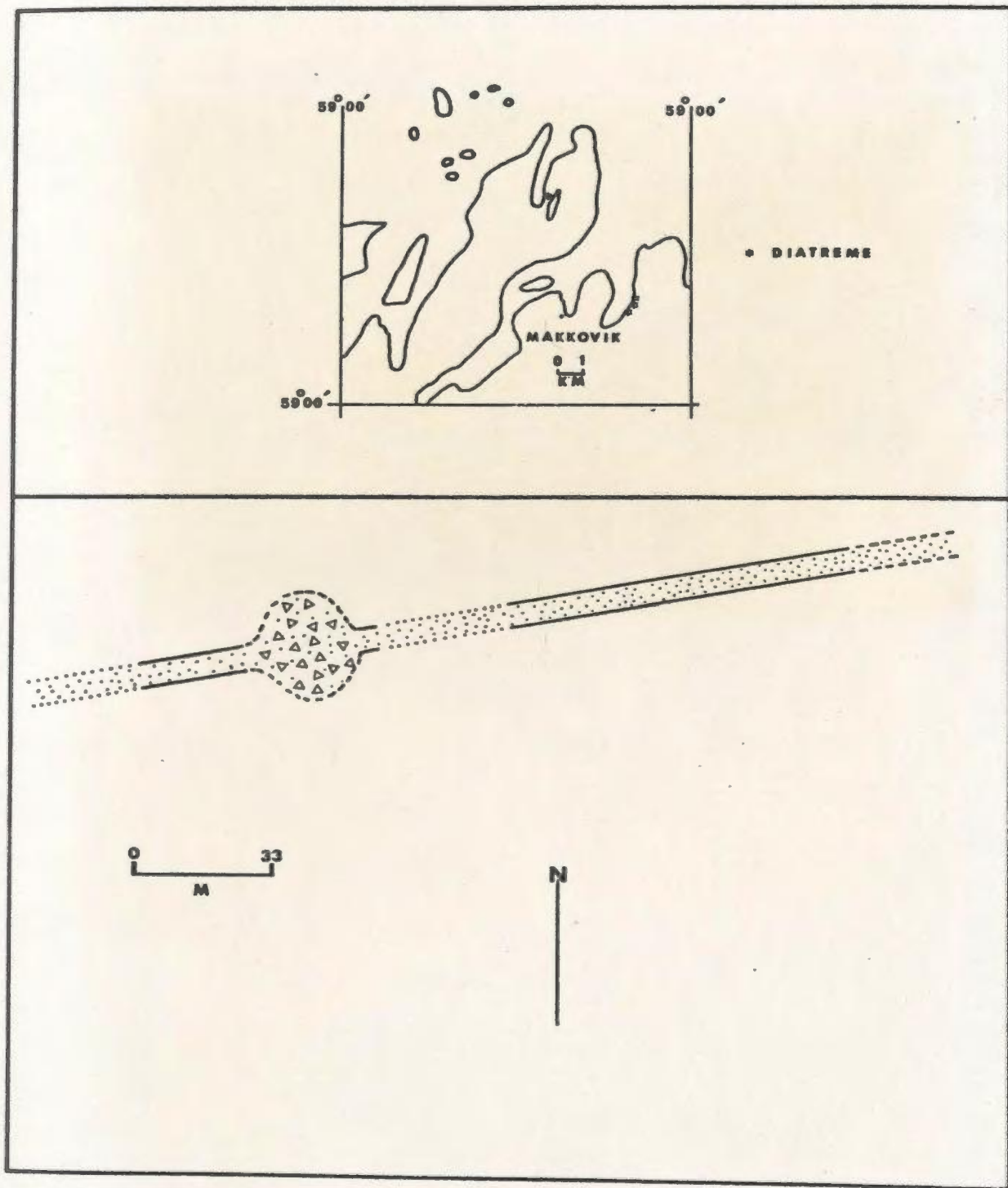


Figure 3.12 Location and shape of a carbonate-bearing monchiquite and its associated breccia to the west of Banana Lake.



Figure 3.13 Subangular to subrounded xenoliths in the monchiquite diatrema west of Banana Lake.

3.5.3.3 Contact Alteration

No marginal alteration was observed at the contacts of the carbonate-poor monchiquites. In contrast the carbonate-rich dykes commonly exhibit thin alteration (hematization or fenitization) halos (3 mm to 1 cm) in their contact rocks.

3.5.3.4 Internal Structures

(A) Carbonate-poor Monchiquites

Carbonate-poor monchiquites show no internal textural arrangements except for a mineral lineation in rare cases.

(B) Carbonate-rich Monchiquites

The carbonate-rich monchiquites are characterized by varying concentrations of carbonate-bearing ocelli. The ocelli are considered by the author to have formed as a result of liquid immiscibility (Ferguson and Currie, 1971; Phillips, 1973; Philpotts, 1972; Philpotts and Hodgson, 1968; Koster Van Groos and Wyllie, 1968b). It is considered unlikely that the Aillik ocelli are amygdules, late stage segregations or nucleation centres for leucocratic minerals (cf. Ferguson and Currie, 1971). Instead, the ocelli are considered to be of primary igneous origin, formed before the emplacement of the dykes. A more detailed account for their origin and texture is given in Chapters 4 and 6.

The carbonate-rich monchiquites exhibit three different varieties

of banding:

(1) Type I Banding

Dykes with Type I banding exhibit a bilaterally symmetrical marginal banded zone (between the chill margin and the core of the dyke) which ranges in width from 5 to 25 cm, depending on the thickness of the dyke.

The marginal banded zones consist of alternating layers of ocelli-rich and ocelli-poor bands between 5 mm to 5 cm and 2 mm to 1 cm in width respectively. The ocelli-poor bands are generally of uniform thickness; however, the ocelli-rich bands commonly increase in thickness towards the centre of individual dykes (Fig. 3.14).

Five distinct variances are present in dykes with Type I banding (Fig. 3.15) viz;

1a. Dykes that are poorly banded and contain ocelli-bearing bands in which the ocelli may or may not increase in size and/or concentration towards the dyke's core (Fig. 3.15a).

1b. Dykes that display a poorly developed marginal banded zone, each band displaying sharp contacts with material on either side. Each ocelli-bearing band shows increasing ocelli size towards the dykes core (Fig. 3.15b).

1c. Dykes that exhibit a well developed marginal banded zone. The ocelli-bearing bands may or may not show increasing



Figure 3.14 Type I banding in a carbonate-bearing monchiquite on the west side of Aillik Bay. Note the perfection of the banded arrangement and the increased size of the ocelli-bearing bands towards the core side of the dyke.

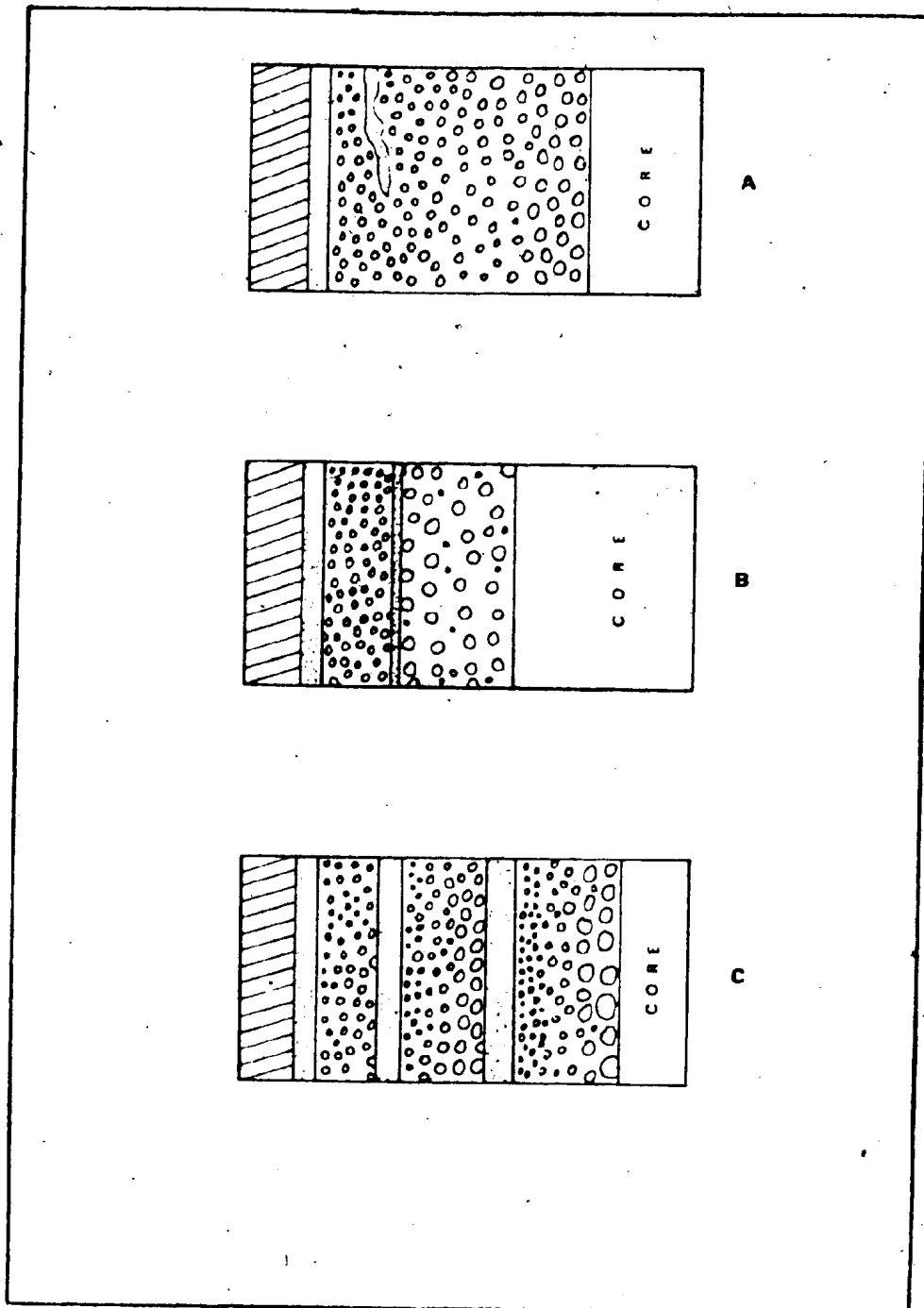


Figure 3.15 Schematic diagram showing variation in Type I banding.

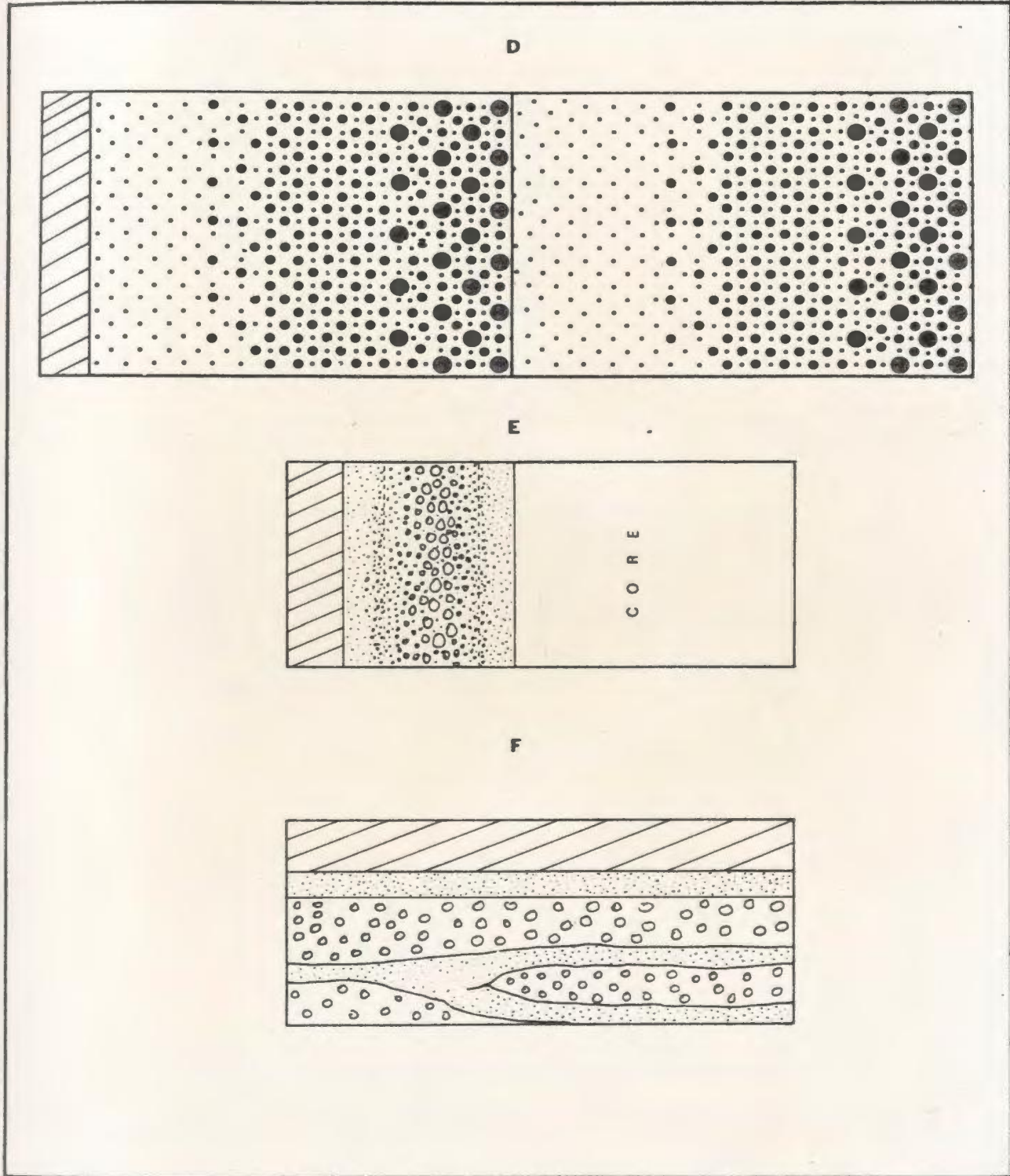


Figure 3.15 (continued)

size towards the dykes core (Fig. 3.15c).

1d. Dykes that have a well developed marginal banded zone, each fine grained band has gradational contacts with ocelli-bearing bands on the core side but has sharp intrusive contacts with the ocelli-bearing bands on the chill margin side. The ocelli size and/or concentration increases from each fine grained band into the ocelli-bearing bands on the core side of the dyke (Fig. 3.15d).

1e. Dykes with poorly developed marginal banded zones in which the fine grained bands have gradational contacts with ocelli-bearing bands on either side (Fig. 3.15e).

These marginal banded zones require the multiple or pulsating intrusion of magma (Bhattacharji, 1966, 1967; Simkin, 1967) containing dispersed carbonate-rich ocelli to explain their origin. The absence of ocelli in the finer grained bands may be a result of flowage differentiation (Bhattacharji, 1966); however, the effect of such a process upon an ocelli-bearing magma isn't known. These bands may also be interpreted as individual chill margins formed during multiple intrusion; however, they lack textures indicative of quenching and in contrast have a strong lineation defined by acicular minerals (see Chapter 4) possibly indicating rapid flow.

The distribution and size configurations observed in the

ocelli-bearing bands (Fig. 3.15) are interpreted by the author to have formed either under periods of flow differentiation and/or increasing ocelli size with each major magma pulse. The banding observed in Figure (3.15a) is considered to have formed by a process of flow differentiation upon emplacement of each successive ocelli-bearing band. The sharp contacts observed between the fine grained and ocelli-bearing bands are not easily explained by a simple flow differentiation model hence, slight chilling and/or increasing magma viscosity in this area is required to produce the extreme textural distinction. The banding present in Figure (3.15b) requires increasing ocelli size within each ocelli-rich layer towards the dykes core. There is no well documented evidence that ocelli decrease in size with cooling; however, Ferguson and Currie (1971) suggest that ocelli can increase in size provided there are gradually increasing periods at which temperatures are low enough for accumulation and coalescence of the ocelli. Thus, the increasing ocelli size in the ocelli-bearing bands may indicate that each pulse of ocelli-bearing material occurred at greater time intervals (therefore allowing the ocelli to increase in size towards the dyke's core). As in the above case, the fine grained bands are considered to be the result of flow differentiation. The banded arrangement shown in Figure (3.15c,d) is considered to represent the combined efforts of flow differentiation and increasing ocelli size with time.

(2) Type II Banding

Dykes with this type of banding are similar in many respects to dykes with Type I banding, displaying a well developed marginal banded zone. Type II banding is recognized by the presence of a band of skeletal pyroxene growth 1 - 3 cm wide in which the pyroxene elongation is perpendicular to the contact of the dyke (Fig. 3.16).

The skeletal pyroxene bands are commonly present on both sides of individual dykes at approximately equivalent distances from the edge of the dyke. Three varieties of perpendicular pyroxene growth are recognized:

- (i) As a band within the marginal banded zone (Fig. 3.17a)
- (ii) As a band within the chill margin (Fig. 3.17b)
- (iii) At the chill margin of the dyke (Fig. 3.17c)

The contact between the perpendicular growth zone and the adjacent monchiquite dyke is either sharp or gradational.

Similar shaped crystals have been observed in layered basic intrusions (Donaldson, 1974), kimberlite sills (Dawson and Hawthorne, 1973), picritic sills (Wyllie and Drever, 1963) and in feldspathic dolerite dykes (Platten and Watterson, 1969). They are interpreted to have developed by supersaturation during periods of supercooling (Preston, 1963; Lofgren and Donaldson, 1975). The development of the pyroxene growths at the chill margin in certain



Figure 3.16 A band of skeletal pyroxene growth in a carbonate-bearing monchiquite near Cape Makkovik. The growth forms a band within the chill margin. (Photograph courtesy of K.D. Collerson).

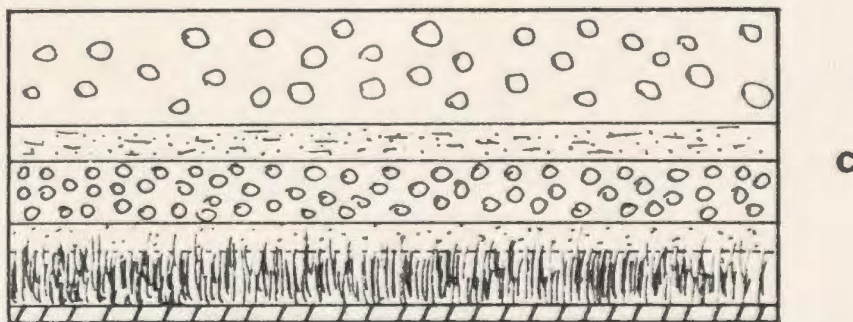
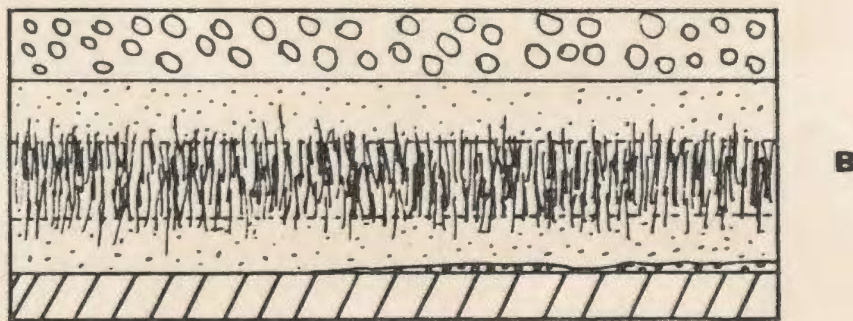
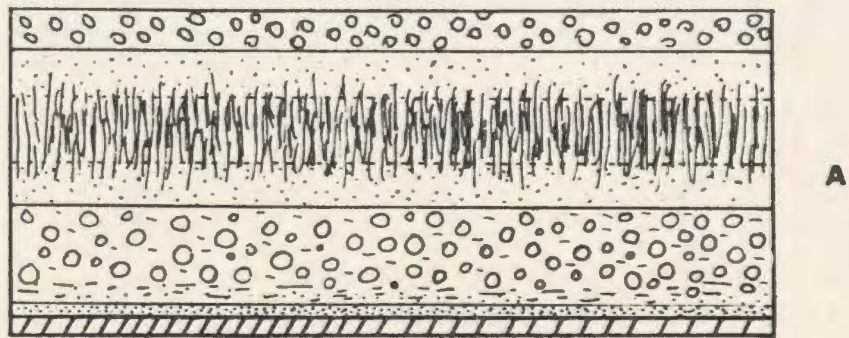


Figure 3.17 Schematic diagram showing variation in Type II banding.

°°° ocelli, ··· finegrained, ||| skeletal pyroxene
crystals.

Aillik dykes implies that rapid heat loss during intrusion (Drever and Johnston, 1957) was responsible for the supercooling (Fig. 3.17c).

The occurrence of skeletal crystals in bands within the marginal banded zone (3.17a) implies that supercooling may not always be ascribed to thermal cooling upon dyke injection. The case outlined above has been attributed to a sudden loss in vapor, either by deformational opening of joints or by pressure changes due to magma motion (Lofgren and Donaldson, 1975). "Blow" and/or diatreme formation may have been an important releasing mechanism in some of the Aillik dykes. The location of these pyroxene growths within the marginal banded zone implies that a supercooling event coincided with the formation of the marginal band (see above).

The formation of skeletal crystals (a structural analysis of acicular crystal growth is given by Fleet, 1975a, 1975b), are considered by Lofgren and Donaldson, (1975) to originate in a hydrostatic environment; however, Platten and Watterson (1969) conclude that such textures originate from rapid crystal growth in magmas undergoing flow.

Flow during preferred skeletal pyroxene growth is considered by the author to be an important feature as several bands containing such growths were observed to grade along strike into

fine grained (nonocelli-bearing) bands which display a strong mineral lineation.

Dykes with Type I and II banding commonly exhibit ocelli and phenocryst-rich cores that range in width from 1 to 30 cm. The carbonate-rich ocelli range from 3 - 5 mm in diameter and are present in concentrations ranging from 20 to 40 percent. Phenocrysts (olivine, biotite, clinopyroxene and opaque oxides) range in diameter from 3 mm to 2 cm.

In most cases the textural and compositional banding in the carbonate-bearing monchiquite dykes can be traced laterally for several meters without disruption; however, some dykes display bands which pinch, swell, divide or terminate along strike (Fig. 3.15a and e).

3. Type III Banding

These dykes are characterized by a brecciated core composed of lobate (Fig. 3.18) to subrounded (Fig. 3.19) fragments of monchiquite in a fine grained matrix. The core is bounded by either a marginal banded zone (as in Type I dykes) or it grades directly into a chilled margin.

The origin of these rounded and lobated structures cannot be explained solely on the basis of field evidence; a more detailed description of their origin is given in Chapter 4.



Figure 3.18 Lobate shaped arrangement in a core of a dyke with Type II banding.



Figure 3.19 Rounded fragments in a dyke with Type III banding.
(Photograph courtesy of K.D. Collerson).

3.5.3.5 Carbonatitization

Marginal selvages of carbonatite 3 to 12 cm wide and 30 to 40 cm in length are common in the dykes characterized by Type I banding and more rarely in those characterized by Type II and III banding. The selvages occur as semi-continuous bands, isolated pods (Fig. 3.20) or as anastomosing veinlets.

The dykes are also intruded by narrow transgressive veinlets of carbonate 1 - 2 mm in width and 5 to 30 cm in length. In some cases, these veinlets are apparently related either to carbonate-bearing ocelli or the carbonatite selvages; however, in other examples they are apparently unrelated to any observable local source of carbonate (Fig. 3.21).

3.5.3.6 Nodules and Xenoliths

Glimmeritic nodules are rarely observed in the carbonate-rich monchiquites. On the other hand, xenoliths and xenolithic slivers of the country rocks are not uncommon and range from 10 to 70 cm long and 1 mm to 5 cm wide. None of the carbonate-poor dykes contain xenoliths.

3.5.4 Kimberlites

3.5.4.1 Lithology

Kimberlite dykes and sills are the youngest intrusives in the Aillik Bay area. They are porphyritic containing



Figure 3.20 Carbonatite selvage in the marginal area of a carbonate-rich monchiquite, East Turnavik Island.



Figure 3.21 Carbonate veinlets cutting a monchiquite dyke near the Tidal Flat area.

megacrysts⁶ of olivine, phlogopite, ilmenite and magnetite in a fine grained matrix consisting of carbonate, phlogopite and opaque oxides. Carbonate is also present in ocelli (cf. Clarke and Mitchell, 1975). On weathered surfaces they range in color from yellowish brown to black depending on the amount of carbonate present.

The Kimberlites have been divided on the basis of mineralogy and modal composition into a number of different petrological types viz;

- (1) Kimberlites (sensu stricto) (Dawson, 1971)
- (2) Micaceous kimberlites (Dawson, 1971)
- (3) Carbonate-rich kimberlites
- (4) Carbonate-rich micaceous kimberlites

Each type appears to be genetically related in both space and time and they are commonly found within the same dyke-grading into one another along strike. Figure (3.22) shows the relationship between carbonate and mica within the Aillik dykes. The gradation of kimberlite into micaceous kimberlite is a common feature (Dawson, 1960, 1967a, 1971) and is usually attributed to the differential concentration of olivine or mica within individual dykes or sills.

The distinction between the carbonatites and extremely

6 For terminology see Appendix 2.

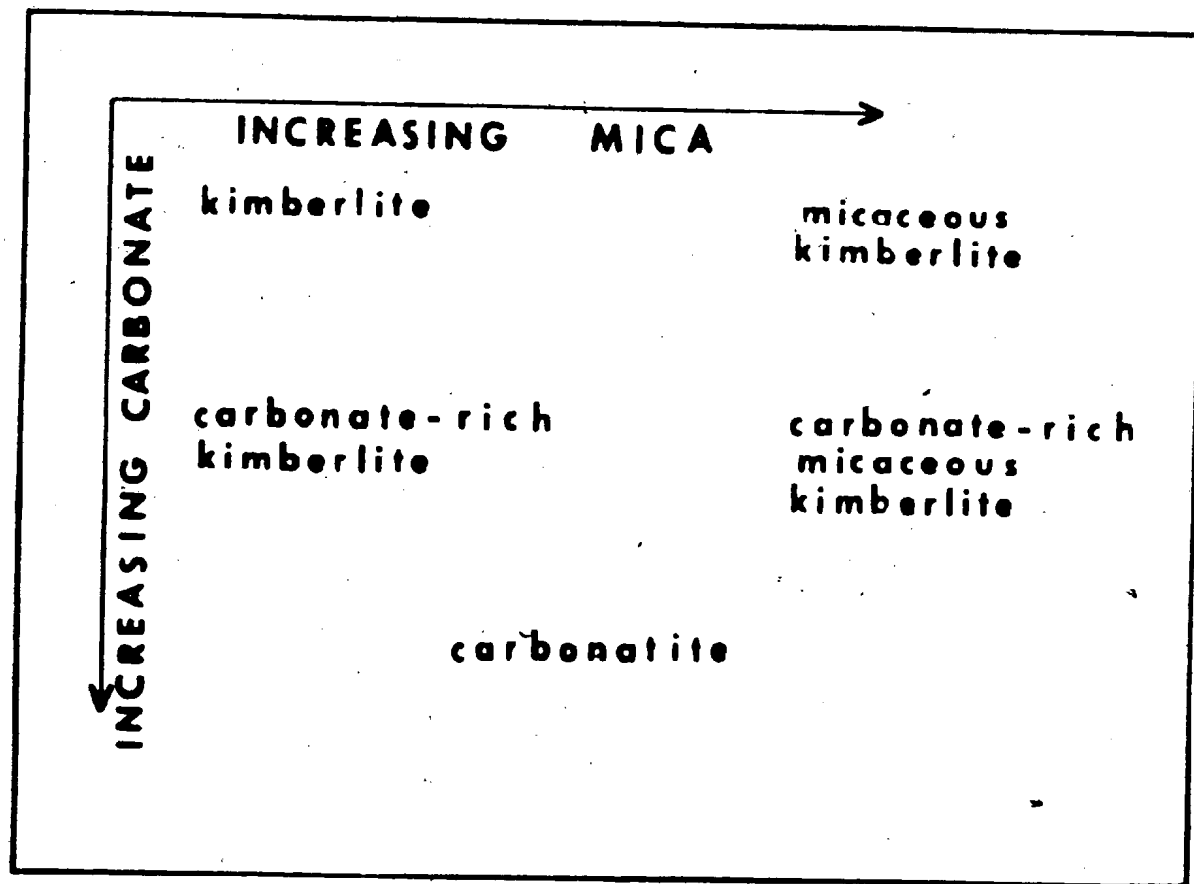


Figure 3.22 Relationship between mica and carbonate in the Aillik kimberlites.

carbonate-rich kimberlites is not always possible. Dykes that remain carbonate-rich for most of their length are classified as carbonatites and those that alternate between carbonatite and kimberlite are classified as carbonate-rich kimberlite. The carbonate-rich kimberlites have a recognizable kimberlitic mineralogy however, they have been subjected to the effects of syngenetic carbonatization.

3.5.4.2 Contact Relationships and Emplacement Features

The Aillik kimberlites show many features typical of hypabyssal kimberlite intrusions (Dawson, 1962, 1967a, 1971; Dawson and Hawthorne, 1970, 1973) and occur either as small discontinuous veinlets 10 - 20 cm in length or as dykes and sills greater than 40 m in length. Dyke widths are commonly proportional to their length, ranging from less than 1 mm to greater than 1 m. In general, the kimberlite dykes appear to be narrower than dykes of other compositions occurring in the area. Many of the kimberlite dykes are net-veined (Fig. 3.23). In contrast, the micaceous kimberlites tend to be more regular in form.

The kimberlites (sensu lato) (i.e., micaceous and carbonate-rich varieties) have sharp intrusive contacts with the country rocks. Some dykes are characterized by the development of a semicontinuous marginal chilled zone ranging in width from 1 mm to 1 cm (Fig. 3.24). Similar contact effects are described in South African (Dawson and Hawthorne, 1970, 1973) and Russian



Figure 3.23 Extremely net-veined kimberlite dyke on the east shore of Aillik Bay.



Figure 3.24 A kimberlite dyke on the east shore of Aillik Bay which exhibits a chill margin. (Photograph courtesy of K.D. Collerson).

(Kharkiv, 1967 quoted by Dawson and Hawthorne, 1973) kimberlites.

Many of the carbonate-rich dykes exhibit discontinuous to continuous flow banded selvages of carbonatite (5 mm to 13 cm wide) in the marginal zone. They show no evidence of chill margins, and are commonly transgressed by small veinlets of carbonatite which emanate from the marginal carbonatite selvages.

The contact zones have been divided on the basis of composition and texture into four distinct varieties viz;

- (1) Carbonate-free dykes which have a well developed chilled margin.
- (2) Carbonate-free dykes with no chilled margin.
- (3) Carbonate-rich dykes which display a marginal flow banded carbonatite selvege but have no obvious chilled margin.
- (4) Carbonate-rich dykes which have a chilled and flow banded margin.

In the field, all gradations between these four main types have been observed.

Intensity of jointing commonly increases near dyke margins (Andrews and Emeleus, 1975) and brittle fracture development is more widespread than in the monchiquites. Both features are believed to be related to forceful emplacement of gas emanations which precede the kimberlite magma (Andrews and Emeleus, 1975). The areas of jointing



Figure 3.25 Brittle fracture development within a carbonate-rich kimberlite on east shore of Aillik Bay.

and brittle fracture development (Fig. 3.25) commonly contribute loose fragments that become incorporated into the dykes as xenoliths or xenolithic shivers.

The discontinuous nature of joints in certain lithologies commonly results in the formation of termination structures. These structures usually occur in pairs (Fig. 3.26), allowing the emplacement of a dyke along a neighbouring joint plane to give it a stepped en échelon configuration. These structures differ greatly from those described for the monchiquites (see above, page 35), as they are more irregular and contain apophyses on both sides of the termination head.

Single dyke intrusions commonly bifurcate to form two or more separate dykes. In some cases, this results in self-intrusion when one of the subsidiary veins re-intrudes the main dyke.

3.5.4.3 Contact Alteration

The development of narrow fenite zones 0.5 to 1 m wide adjacent to the carbonate-rich dykes is a common feature, especially where the rocks are quartzo-feldspathic composition. The fenitized zones are dark in color and are composed of riebeckite, aegirine and alkali feldspar. Xenoliths also show fenite halos (Fig. 3.27) and many are completely fenitized. Hematized zones are also common, but are restricted to carbonate-poor dykes.



Figure 3.26 Horned termination structures in a kimberlite dyke on the east shore of Aillik Bay. (Photograph courtesy of K.D. Collerson).



Figure 3.27 Dark fenite halo surrounding a subangular xenolith in a carbonate-rich micaceous kimberlite.

3.5.4.4 Internal Structures

The Aillik kimberlites (sensu lato) show considerable variation in megacryst concentration; many dykes have megacryst-rich cores and finer grained margins. A similar texture was observed in the DeBeers mine, Kimberley (Wagner, 1914; Dawson and Hawthorne, 1970) however, it was interpreted to be a result of marginal quenching (Wagner, 1914). Bhattcharji (1966) has shown that a flowing magma containing solid and liquid phases segregates to form a concentration of solid phases toward the centre of the flowing magma (by flow differentiation) and marginal concentration of fluids and smaller solid phases (and not by marginal chilling of a hot kimberlite magma). This flow differentiation model is considered by the author to have operated in the Aillik dykes producing the above textural arrangements. This mechanism possibly accounts for the marginal concentration of carbonate in some of the carbonate-rich kimberlites.

The most common banding present in the Aillik dykes is produced by the segregation of megacrystic bands and finer grained nonmegacrystic bands (Fig. 3.28). The fine grained bands have sharp contacts with the megacrystic bands and consist mainly of a matrix material which in some cases is carbonate-rich. The megacrystic bands are generally wider and more continuous than the finer grained bands which seldom exceed 1 - 2 cm in width. The finer grained bands are usually developed parallel to the dykes



Figure 3.28 Photograph of a kimberlite dyke showing banding produced by the segregation of megacrystic and finer grained non-megacrystic bands where the latter pinch, swell and encompass thin xenolithic slivers. (Photograph courtesy of K.D. Collerson).

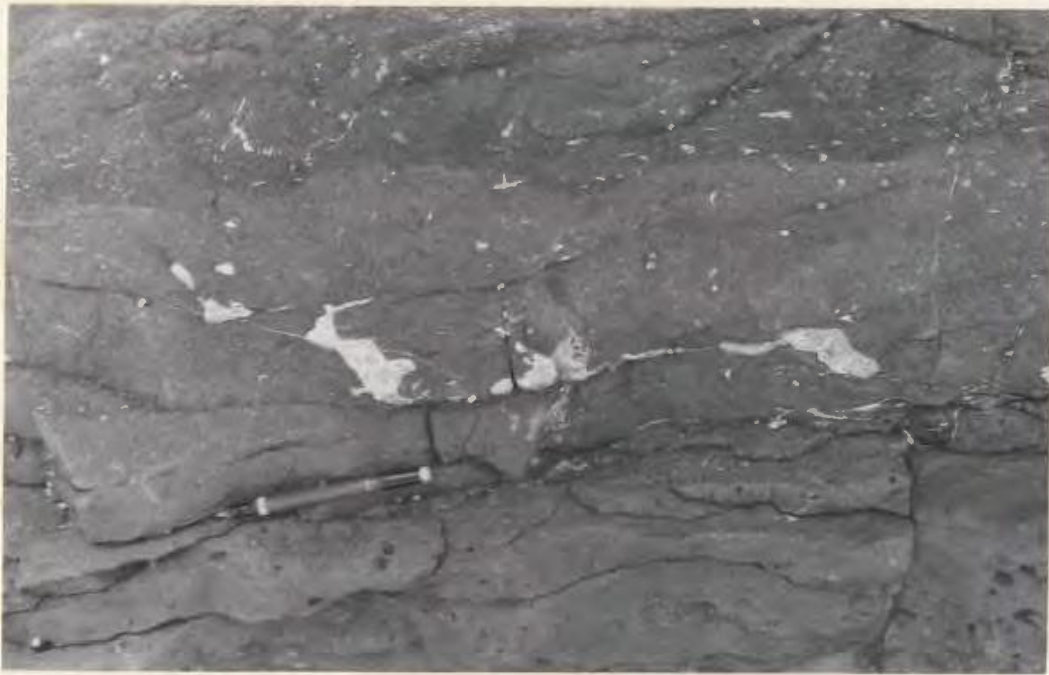


Figure 3.29 Large lensoidal ocelli which are connected by thin carbonate veinlets within a carbonate-rich micaceous kimberlite.

margin; however, they are commonly not paired as in the monchiquite dykes (see page 35). In some instances, the finer grained bands display delicate layering which may be developed oblique to the margin of the dyke; however, such instances are confined to layers having a high carbonate content. Similar textural arrangements have been observed in the Franspoort, Zonderwater, Kleinzonderhout, Wesselton, Byrnes, Benfontein and Roberts Victor intrusions in South Africa (Wagner, 1914; Dawson and Hawthorne, 1970, 1973). According to Dawson and Hawthorne (1970) the finer grained bands are not chill margin as the groundmass in the porphyritic layers is no finer than in the fine grained bands. The model proposed by Bhattacharji (1965) i.e. repeated injections (or pulsating magmatic flow) within a solid-liquid material to produce successive porphyritic and nonporphyritic layers may account for the textural variation present in both the African and Aillik kimberlites.

Carbonate-rich ocelli are present in many dykes. In some dykes these ocelli are concentrated in nonmegacrystic layers, a feature which accentuates the layering. Contacts between the ocelli-bearing layers and the ocelli-poor megacrystic layers are either sharp or gradational. In the carbonate-poor kimberlite dykes, the ocelli occur as randomly oriented ellipsoidal to rounded masses (Fig. 3.29) which are interconnected by thin carbonate veins. The ocelli do not occur in specific bands and their size appears to be independent of their location

within the dyke.

The carbonate-bearing ocelli are considered to have formed during a period of liquid immiscibility (cf. Ferguson and Currie, 1971) and most carbonate is regarded to be of primary origin. A more detailed explanation of the textures and origin of the carbonate are given in Chapters 4 and 6.

Flow structures formed by the alignment of megacrysts, ocelli, xenoliths or more rarely nodules are common in many of the Aillik kimberlite dykes (cf. Walton, 1965). The flow structures have crescent or arcuate shapes (Fig. 3.30) which are usually concave towards the intrusion direction. In some dykes these structures are found trending in opposite directions along a dyke's length or they may be joined to form concentric rings. These features indicate close proximity to a flow cell (Clark, 1974) and maybe taken as evidence that the dykes were intruded along specific locations within the fractures and were not emplaced along the whole length of a fracture system during one magmatic episode.

3.5.4.5 Serpentinization

Serpentinization is not always observable in hand specimens and in many cases fresh olivine could be seen protruding from weathered surfaces. One carbonate-rich dyke near Aillik Village did; however, contain discontinuous chrysotile veinlets 1 mm to



Figure 3.30 Crescent shaped flow structure produced by the alignment of ocelli in a carbonate-rich kimberlite. The dyke was emplaced from left to right. Note the thin carbonatite selvages along the marginal area of the dyke.



Figure 3.31 Serpentine veinlets cutting a carbonate-rich kimberlite near Aillik Village. Note the sharp contact between the nodular core and the marginal banded zone.

5 cm wide. These serpentine veinlets are regarded as a post consolidation effect as they cut both the margin and nodular core of the dyke (Fig. 3.31).

3.5.4.6 Carbonatization

The carbonate content as well as its behaviour during intrusion has greatly governed the textural and/or structural features observed in the Aillik kimberlites. The most carbonate-rich kimberlites either display a relict megacrystic texture or in other cases the carbonate-rich areas resemble carbonatites. Most of the carbonate appears to be syn-intrusive with the kimberlite magma. The higher mobility of the carbonate-rich fraction relative to the megacrystic kimberlite fraction has resulted in its segregation or partial segregation producing complex banding, veining and anastomosing relationships. The carbonate appears to have migrated laterally along the margins of the dykes. This migration probably continued after the consolidation of the kimberlite as many carbonate-rich veins brecciate and engulf fragments of kimberlite.

The transition from kimberlite to carbonate-rich kimberlite is commonly observed in the field and results from the local concentration of carbonate. The gradation usually occurs within a strike length from 10 cm to 1 m and may occur any number of times along the length of a dyke. The transition is often related to obstructions within dykes and frequently occurs in areas where the dykes narrow rapidly (i.e. termination structures).

3.5.4.7 Nodules and Xenoliths

Glimmerite and phlogopite-bearing pyroxenite cognate nodules are widespread in the Aillik Bay kimberlites. They are spherical to ellipsoidal in shape, range in diameter from 1 mm - 4 cm and have polished outer surfaces (Fig. 3.33 and 3.31). The core zones of some dykes are extremely rich in nodules (up to 80 percent of their volume, Fig. 3.34). In addition to the cognate nodules, most kimberlites contain variable concentrations of xenolithic slivers and/or fragments which were rafted from the exposed country rock walls. These fragments are angular to subangular in shape and range in length from 5 mm to 10 cm and in width from 1 mm to 1 cm. The concentration of these country rock xenoliths is quite variable, however it seldom exceeds 5 to 10 percent.

3.5.5 Carbonatites

3.5.5.1 Lithology

The carbonatites are composed of between 60 to 70 percent primary carbonate with minor amounts of phlogopite, opaque oxides, and occasional olivine pseudomorphs. They have been divided into two distinct varieties on the basis of their carbonate composition (Von Eckermann, 1948) viz;



Figure 3.32 Carbonate-rich marginal zone of a carbonate-rich micaceous kimberlite on the east shore of Cape Makkovik. Note the flow banding in the carbonate-rich area and the abundance of ocelli.



Figure 3.33 Spherical glimmerite nodules within a carbonate-rich micaceous kimberlite near Aillik Village.



Figure 3.34 Nodular core of a carbonate-rich kimberlite on the west shore of Cape Aillik.

- (1) Sbvites, consisting principally of calcite.
- (2) Beforsites, consisting principally of dolomitic carbonate.

The sbvites are commonly light grey to pinkish grey in color while the beforsites are generally cream in color.

3.5.5.2 Contact Relationships and Emplacement Features

The carbonatites have sharp intrusive contacts which are sinuous and irregular along strike. The beforsites commonly display chill margins; however, the sbvites are usually devoid of such features.

The carbonatites are typically net-veined and highly fractured contact zones are commonly developed. The dykes sometimes display termination structures and like the kimberlites show intensification of the regional joint directions next to the dyke's margin. Several carbonatite dykes grade into kimberlite in the termination structures.

3.5.5.3 Contact Alteration

The development of fenite in narrow zones adjacent to the dykes margins is a common feature. The fenitized zones range from 1 mm to 5 cm but increases to 15 - 20 cm in dykes which are strongly net-veined.

3.5.5.4 Internal Structures

The carbonatites are generally flow banded and some dykes near Cape Makkovik grade between sövite, beforosite or kimberlite along strike. A few of the sövites are megacrystic and the segregation of megacrysts in certain bands parallel to the dykes margin commonly enhances their flow-banded character.

3.5.5.5 Nodules and Xenoliths.

The carbonatites rarely contain nodules and only one glimmerite has been recovered. Most dykes contain abundant xenoliths whose dimensions are similar to those recorded for the kimberlites.

CHAPTER 4

PETROLOGY

4.1 Introduction

A genetic relationship between kimberlites, carbonatites and some varieties of lamprophyre has been postulated from field, petrological and geochemical evidence by a number of petrologists (Dawson, 1960, 1966, 1967b; Nikishov et al., 1972; Gold, 1963; Geiser, 1928 and Von Eckermann, 1967). Although this relationship has been vigorously criticized by Mitchell (1970), recent studies have indicated that such associations do exist, and all have possibly evolved from a common parent (Cornelissen and Verwoerd, 1975; Gittins et al., 1975; Robinson, 1975; Ferguson et al., 1975).

Genetic relationships between kimberlites and carbonatites have been described by Von Eckermann (1948, 1966, 1967), Dawson (1960, 1966, 1967), Egorov (1970), Saether (1957), King and Sutherland (1960a, 1960b), Garson (1962, 1965), Heinrich (1966), Tuttle and Gittins (1966), Marshintsev and Balakshin (1969), Kovalsky and Egorov (1966), Nikishov (1970), McGetchin et al. (1973), Watson, (1967a, 1967b) and Griffin (1973). The occurrence of kimberlites containing high concentrations of primary carbonate as a matrix phase also suggests that a possible link exists between kimberlites and carbonatites (Dawson and Hawthorne, 1973; Mitchell and Fritz, 1973; Ferguson et al., 1975; Janse, 1975). This suggestion is supported by recent experimental studies (Irving and Wyllie, 1975; Wyllie and Huang, 1975; Wyllie, 1966; Eggler, 1973, 1974, 1975),

which have emphasized the significance of CO_2 as a constituent of the mantle, and as an important volatile involved in the emplacement of kimberlite magmas.

Occurrences of kimberlite and/or carbonatite which are spatially, temporally and (possibly) genetically related to the emplacement of lamprophyre dykes (minettes, monchiquites) have been described by Allen and Balk (1954), McGetchin and Silver (1970), Kay and Gast (1970) and McGetchin et al. (1973). Carbonate-rich monchiquites genetically related to carbonatites are also described by Currie (1971) and Ferguson and Currie (1972) from the St. Lawrence rift system at Callander Bay and Brent Crater, Ontario.

Alnöitic lamprophyres which contain xenocrysts of picro-ilmenite, chrome-diopside and pyrope closely resemble some varieties of kimberlite (Allen and Deans, 1965). Alnöites are often spatially related to kimberlites (Watson, 1967b, Von Eckermann, 1948; Koenig, 1956, Brachvogel and Kovalsky, 1970) or they display a gradational mineralogical relationship with them (Bowen, 1922; Harvie, 1909; Martens, 1924). More recently melilite-bearing kimberlites have been described in Greenland (Escher and Watterson, 1972), hence the term alnöite may be superfluous to the geological literature.

The basic and ultrabasic dykes which outcrop in the Aillik Bay area are closely related in time and space. They are therefore an ideal association in which to examine the genetic relationship between kimberlites, carbonatites and lamprophyres. The following Chapter presents

the results of a detailed petrographic study aimed at providing mineralogical and textural data relevant to a comparative investigation of the different compositional groups.

All compositional variants were thin sectioned and examined petrographically. Modal analyses determined by point counting are presented in Chapter 5.

4.2 Petrology

4.2.1 Hornblende Peridotites

The hornblende-bearing peridotites are mineralogically distinct from the other dyke suites and are not considered by the author to belong to the consanguineous basic to ultrabasic suite. They are porphyritic rocks composed of large xenomorphic poikilitic crystals of hornblende (50 - 70%) (10 x 7.5 to 0.25 x 0.20 mm in size) enclosing smaller rounded crystals of olivine (20 - 30%) augite (1 - 5%) and hypersthene (0 - 2%). The hornblende is strongly pleochroic in two contrasting schemes: α - light green to light brownish green, β - olive green, γ - green; and α - colorless, β - pale greenish brown and γ - light brown, and it appears to replace irregular grains of clinopyroxene (Fig. 4.1) which display embayed crystal boundaries. This replacement is considered by the author to have occurred at a late stage in the crystallization history of the dykes when an increase in P_{H_2O} favoured the crystallization of hornblende. Although the hornblende is usually fresh, some late-stage chloritic alteration (0.5 - 2%) has been observed.

Olivine occurs as xenomorphic to idiomorphic crystals with embayed crystal boundaries (Fig. 4.1) which are interpreted to have formed by reaction during the early stages of crystallization of the melt (Cawthorn, 1975 personal communication). Many crystals also show marginal alteration to antigorite and/or chlorite.

Other minor phases include slightly pleochroic xenomorphic crystals of hypersthene (α - pink, β - yellowish brown, γ - pale green) and xenomorphic to hypidiomorphic crystals of apatite (0 - 3%) and opaque oxides (magnetite) (0.5 - 5%) which occur as randomly distributed crystals or as lenticular stringers along amphibole cleavages.

4.2.2 Minettes

The minettes have a medium-grained panidiomorphic-granular texture which is defined by idiomorphic crystals of olivine (5 - 10%), augite (30 - 40%), biotite (15 - 25%), and opaque oxides in a matrix of fine grained orthoclase (30 - 50%), biotite, opaque oxides and augite. Minor concentrations of carbonate-bearing ocelli are also present.

Xenomorphic to idiomorphic grains of olivine occur either as microphenocrysts, more rarely as a matrix phase or as glomerophyritic clusters. Many crystals exhibit antigorite pseudomorphs and several are mantled by coronas of biotite.

Prismatic crystals of brown to greenish brown augite occur either as a relatively fine grained matrix phase (Fig. 4.2) or more rarely as



Figure 4.1 Photomicrograph of large poikilitic hornblende crystals which enclose embayed olivine and augite crystals. Note the opaque oxides along cleavage traces in the amphibole. Plane light. Scale bar is 0.5 mm long.

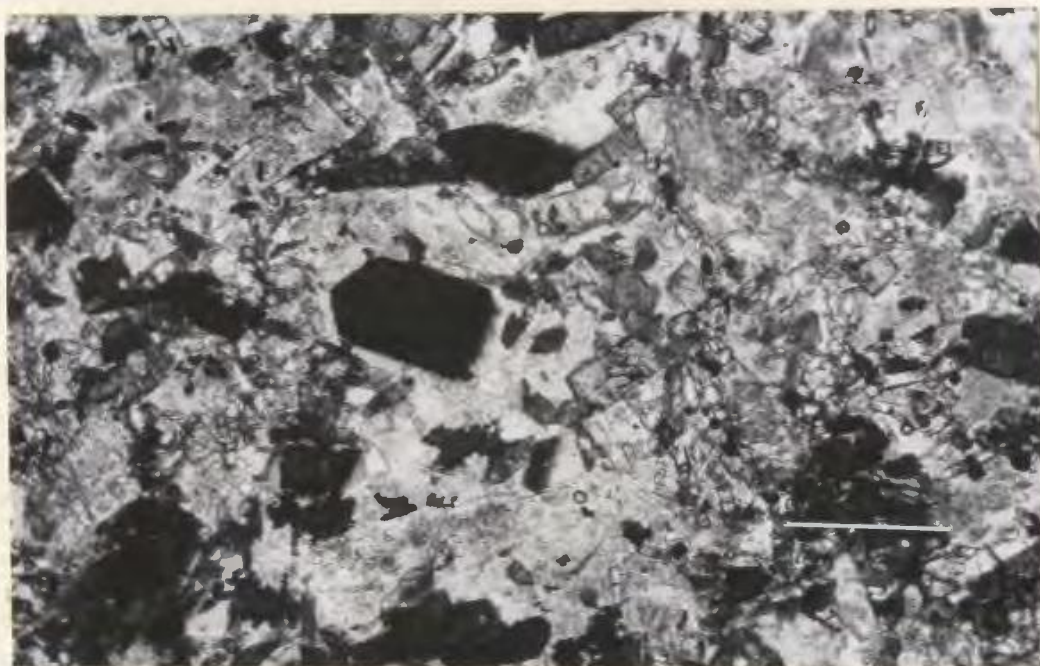


Figure 4.2 Photomicrograph showing augite, opaque oxides and poikilitic biotite crystals in a matrix composed of orthoclase and augite. Note the dark rim around mica in the upper centre of the photograph. Plane light. Scale bar is 0.5 mm long.

idiomorphic phenocrysts. The matrix crystals are commonly surrounded by a narrow mantle of aegirine which is interpreted to be an alteration product rather than compositional zoning of primary origin (cf. Wilkinson, 1957).

Biotite is present either as small lath to microlite-shaped crystals in the matrix or as large idiomorphic to hypidiomorphic tabular crystals which are often poikilitic to augite and/or opaque oxides. It has a normal pleochroism with α - yellow to yellowish brown, $\beta = \gamma$ - a dark rusty brown. The matrix crystals generally exhibit a thin incomplete rim of a mica with a dark, almost opaque, absorbance (Fig. 4.2); a feature commonly observed in minettes (Williams et al., 1955; Némec, 1973). Some phenocrysts display evidence of mechanical deformation, i.e. kinking of the (001) cleavage traces.

Idiomorphic to xenomorphic grains of opaque oxide (magnetite, ilmenite) occur as a matrix phase.

Interstitial medium to fine grained xenomorphic crystals of cloudy orthoclase containing finely disseminated granular opaque oxides, kaolin and small flakes of sericite are an important matrix phase.

Carbonate is present either as a component of irregular ocelli or more rarely as a matrix phase or in thin cross-cutting veinlets. The ocelli exhibit sharp contacts, are circular to lensoidal in shape and contain fine grained anhedral crystals of calcite (0.8×0.6 to 0.1×0.05 mm in size). More rarely granular crystals of zircon are

concentrated along the ocelli walls. Matrix carbonate (calcite) forms interstitial grains to the larger hypidiomorphic to xenomorphic orthoclase crystals. The cross-cutting calcite veinlets (0 - 10 mm wide) emanate either from the dykes margin or carbonate-bearing ocelli.

4.2.3 Monchiquites

The monchiquites, as described above (Chapter 3, page 34) have been divided into two varieties viz; a carbonate-rich group and a carbonate-poor group. Each will be described separately in the following section; however, a considerable overlap in mineral compositions exists. Similar intrusives have been described by Ferguson and Currie (1972), Woodland (1962), Strong and Harris (1974) and Walker and Ross (1954).

4.2.3.1 Carbonate-rich Dykes

The carbonate-rich monchiquites are porphyritic and contain randomly arranged idiomorphic to hypidiomorphic phenocrysts of olivine (5 - 50%), biotite (10 - 30%), augite (30 - 70%) and opaque oxides (10 - 30%) in a fine grained matrix composed of the above mineral species together with calcite (0 - 5%) analcime (0 - 2%) and apatite (0 - 5%). In addition, they contain abundant carbonate-bearing ocelli (10 - 40%) which are considered to represent an immiscible liquid fraction (Ferguson and Currie, 1971; Strong and Harris, 1974; Phillips, 1973) (see also Chapter 3, page 46).

Olivine occurs as xenomorphic to idiomorphic crystals, ranging in

size from 5.0 x 2.0 mm to 0.10 mm in diameter and forms either a seriate or hiatal texture (Moorhouse, 1959). Crystals rarely show evidence of mechanical deformation, although several dykes contain olivine with undulose extinction, subrounded grain boundaries (Walker and Ross, 1954) or recrystallized crystals with granoblastic textures (Fig. 4.3). The above mechanical deformation is considered to be the result of deformation of crystals during transportation and emplacement of the dykes. In general the finer grained crystals of olivine show a greater tendency toward alteration; however, a relationship is also considered to exist between this alteration and the presence of ocelli which suggests that it may be related to volatile release from the ocelli during their crystallization.

Brown to green-brown augite and more rarely purple titan-augite is the most common ferromagnesian mineral in the Aillik monchiquites (cf. Ferguson and Currie, 1972) occurring either as phenocrysts or as a matrix phase. Zoned prismatic augite phenocrysts commonly form a seriate texture with large crystals occurring either in independent or radiating glomeroporphyritic clusters and grade into acicular to columnar zoned matrix crystals which commonly exhibit a trachytic texture. Some augite crystals display undulose extinction and crystals proximal to ocelli or cross-cutting carbonate veinlets show alteration to aegirine. Zoned augite crystals with aegirine mantles are also described by Ferguson and Currie (1972) and are considered to represent primary crystallization features related to fractionation of the original magma. Monchiquite dykes with Type II banding (Chapter 3, page 53) exhibit

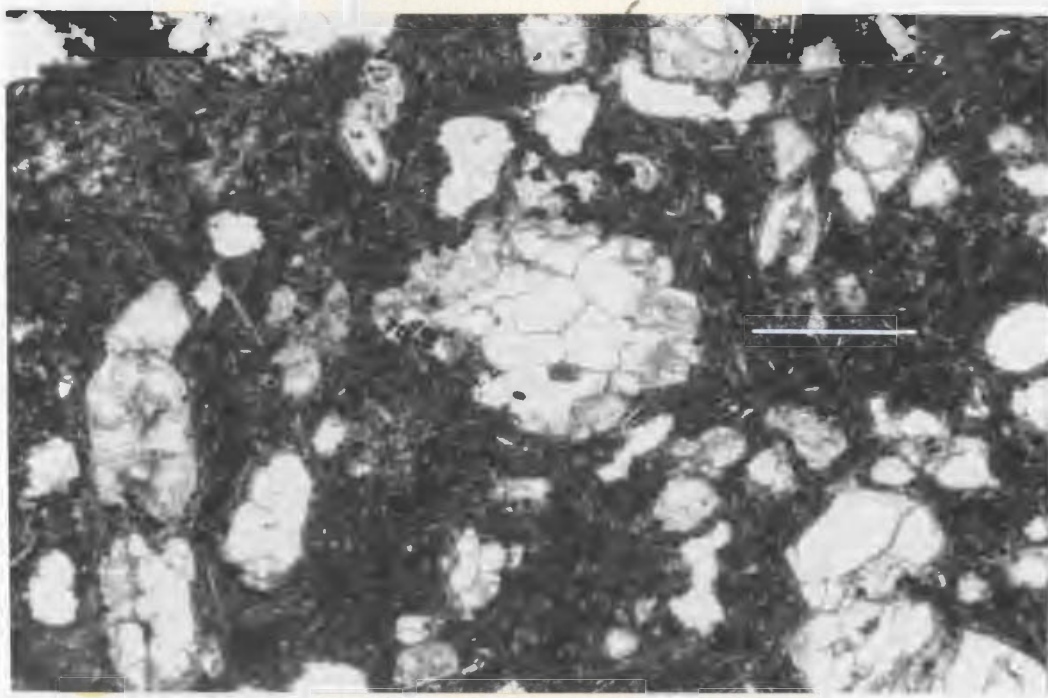


Figure 4.3 Photomicrograph of a recrystallized olivine phenocryst which exhibits a granoblastic texture. Plane light. Scale bar is 0.5 mm long.

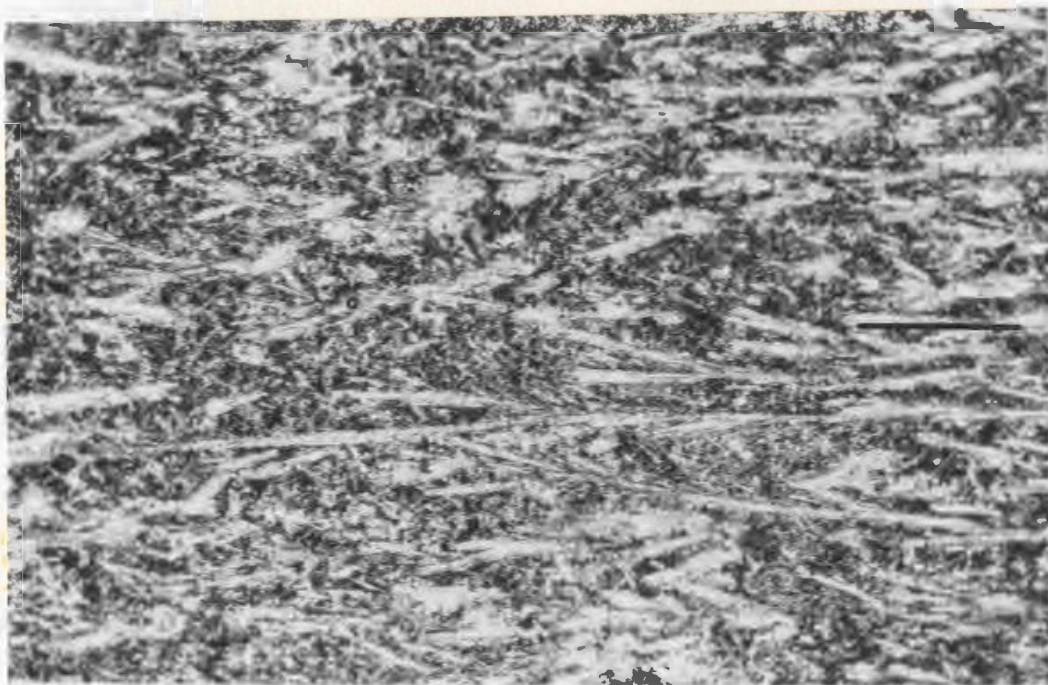


Figure 4.4 Photomicrograph of bladed to dendritic augite growths which forms Type II banding. Note the curvature of several of the crystals. Plane light. Scale bar is 0.5 mm long.

bladed augite growths which are interpreted by the author to result from supercooling. The augite is optically identical to those described above and crystal morphology ranges from acicular, to bladed, to dendritic. The crystals which occur in subparallel or anastomosing growths, exhibit length to breadth ratios of 40:1 to 10:1, although they seldom exceed 6 mm in length (Fig. 4.4).

Biotite forms lath, microlite or xenomorphic tabular poikilitic plates (cf. Ferguson and Currie, 1972) which display normal pleochroism with α - reddish brown to yellowish brown, $B = \gamma$ - dark brown and commonly enclose matrix augite (Fig. 4.5). The biotite commonly exhibits an outer rim with a strong, almost opaque absorbance (Fig. 4.5) (cf. Ferguson and Currie, 1972), which is interpreted to be an iron-rich mica (Rimsaite, 1969, 1971) and possibly the last phase to crystallize from the monchiquite magma.

Phenocrystal and matrix opaque oxides range in size from 3.25 x 3.20 to 0.05 mm in diameter and exhibit xenomorphic to idiomorphic outlines. Many of the oxides exhibit atoll development similar to that described by Stewart (1970) and Dawson and Hawthorne (1973). Dawson and Hawthorne (op. cit.) consider these textures to have resulted from two periods of opaque oxide crystallization. Bladed to acicular oxide growths are also present and are interpreted to have crystallized in response to rapid cooling (or supercooling); however, the occurrence of many of these crystals between acicular augite crystals may imply that their morphology was controlled by the acicular



Figure 4.5 Photomicrograph showing a poikilitic tabular plate of biotite which encloses acicular needles of augite. Note the rim of dark mica around a lath of biotite just below the tabular crystal. Plane light. Scale bar is 0.25 mm long.



Figure 4.6 Photomicrograph showing the matrix of a carbonate-rich monchiquite composed of acicular to bladed opaque oxide growths with biotite and opaque oxides. Plane light. Scale bar is 0.5 mm long.

interstitial spaces between the augite crystals (Fig. 4.6). Grains of magnetite are commonly altered and display a narrow incomplete rim of biotite; ilmenite in contrast is commonly altered to leucoxene.

Circular to lobate carbonate-bearing ocelli, 10.0 x 4.5 mm to 0.15 mm in diameter, are widespread in the monchiquites and contain varying proportions of calcite, siderite, analcime and chalcedony. The ocelli are characterized by either sharp or diffuse contacts, and elongate matrix minerals often project into them (Fig. 4.7). Xenomorphic to idiomorphic calcite crystals are clear, in contrast to siderite which is yellow in color and occurs in bladed or radiating growths which display spherulitic extinction.

Isotropic to weakly birefringent analcime (cf. Walker and Ross, 1954) occurs as xenomorphic grains which are usually associated with either siderite or bladed to radiating spherulitic chalcedony. Many of the ocelli are zoned (cf. Ferguson and Currie, 1972) with either a carbonate or chlorite rim and a silicate core.

In dykes exhibiting Type I banding (Chapter 3, page 47) i.e. a marginal banded zone formed by the alteration of ocelli-rich and ocelli-poor bands, the ocelli-poor bands are nonporphyritic and exhibit either a trachytic arrangement of acicular augite crystals or an increased content of opaque oxides. In contrast, the ocelli-rich bands are porphyritic containing olivine and opaque oxides although their matrix may be compositionally equivalent to the ocelli-poor bands. This confirms earlier conclusions that the nonocelli-



Figure 4.7 Photomicrograph showing the diffuse boundry of a carbonate-rich ocelli. This diffuse boundary is caused by the projection of augite and biotite across the ocelli wall. Plane light. Scale bar is 0.5 mm long.

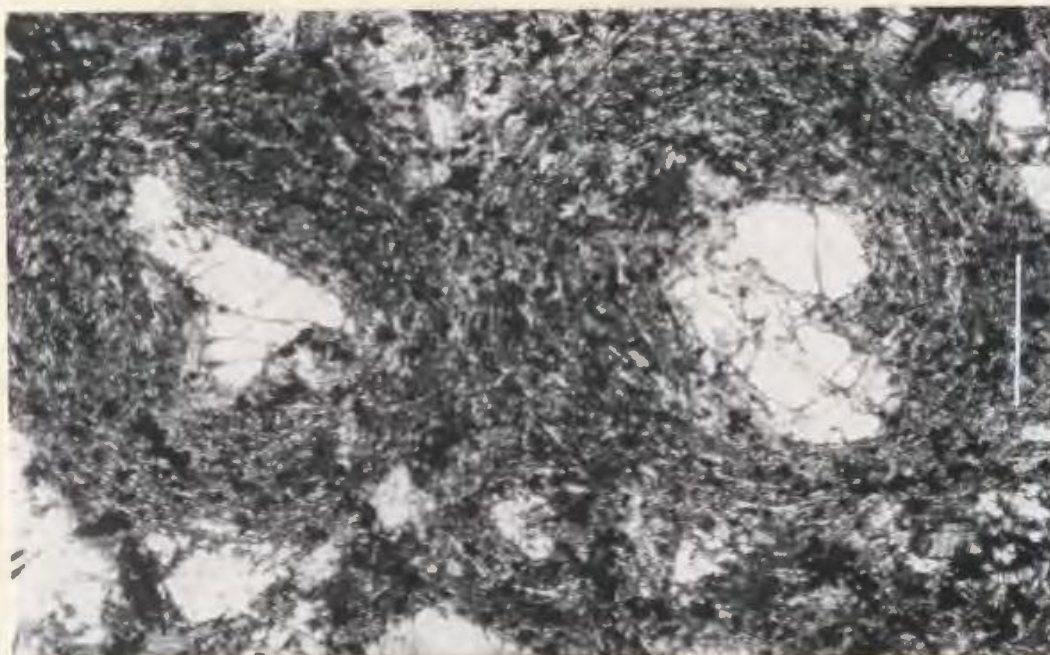


Figure 4.8 Photomicrograph showing olivine phenocrysts with concentric rings of augite, biotite and opaque oxides. Plane light. Scale bar is 0.5 mm long.

bearing bands are not chill margins and were produced by flow differentiation (Chapter 3, page 51).

In thin section, dykes with Type III banding (i.e. a core zone composed of lobate to circular fragments, (Chapter 3, page 57) show a slight variation in matrix augite and carbonate concentration where the variation occurs in subcircular patches 0.5 to 2 mm in diameter. No evidence for autobrecciation has been seen in thin section studies, thus this texture is considered to have resulted from differential weathering of the above patches.

Several dykes studied contain phenocrysts (usually olivine) which are surrounded by concentric rings, 0.5 to 0.25 mm in diameter, composed of circular aggregates of augite, with interstitial opaque oxides and poikilitic biotite (Fig. 4.8). The outermost augite layers display a trachytic texture which form shells around the other phenocrysts. These textures are interpreted to be the result of the nucleation of groundmass phases around olivine phenocrysts as the magma was undergoing rapid flow and possibly fast crystallization. As such, they closely resemble textures observed in autoliths from kimberlite (Ferguson et al., 1973).

4.2.3.2 Carbonate-poor dykes

The carbonate-poor monchiquites are also porphyritic and except for the absence of carbonate-bearing ocelli, contain similar mineral phases to those described in the carbonate-rich dykes. They contain

phenocrysts of augite, biotite, opaque oxides (magnetite, perovskite and possibly ilmenite) in a matrix of the above phases and apatite. Perovskite, a major mineral phase in the carbonate-poor dykes is rare to absent in carbonate-rich dykes and occurs as square to cubo-octahedral crystals which form a seriate texture.

4.2.4 Kimberlites

4.2.4.1 Introduction

The kimberlites are divided into four distinct types (see Chapter 3, page 61), however, they will be discussed collectively in this Chapter as they differ only in modal proportion. Most dykes are porphyritic (Fig. 4.9) and contain megacrysts⁷ of olivine (5 - 10 %), phlogopite and/or biotite (2 - 80 %), opaque oxides (picro-ilmenite, ilmenite, magnetite, chrome-spinel and perovskite) (5 - 30 %), apatite (0 - 17 %) and more rarely augite (0 - 20%) and carbonate-bearing ocelli (0 - 20 %). Most dykes exhibit an inequigranular texture and are medium to fine grained. They also contain abundant nodules (Chapter 3, page 75) which are characterized by high concentrations of phlogopite and/or biotite. A compositional comparison of sixty-eight nodules from the Aillik kimberlites examined in this study is given in Table 4.1. The classification of these nodules is based on that of Frantsesson (1970) and they are regarded as part of the M.A.P.I.D. (mica, amphibole, rutile, ilmenite, diopside) suite

⁷ See Appendix 2

of Smith et al. (1975) and Dawson and Smith (1975b). In thin section, the glimmerite nodules range in size from 5.0 x 6.0, to 0.5 mm in diameter and have elongate, pear-shaped or circular forms (Fig. 4.10). They are medium to fine grained and exhibit xenomorphic crystals which range in size from 3.0 x 1.5 mm to 0.05 mm in diameter. Besides containing high concentrations of mica they also contain olivine (not found in the M.A.R.I.D. Suite), apatite, opaque oxides (ilmenite and possibly magnetite), diopside (possibly chromium-bearing) and amphibole (possibly richteritic). A detailed microprobe study of these nodules is currently being carried out by K.D. Collerson. Results will be presented in a joint paper with the author. It is clear that peridotites are a relatively minor component of the suite which is in contrast with other nodule populations in kimberlite (cf. Nixon, 1973). The occurrence of glimmerite nodules in kimberlite is relatively rare and has been previously recorded from South Africa (Wagner, 1914; Williams, 1932; Erlank, 1973; Aoki, 1974; Dawson and Smith, 1975a, 1975b; Smith et al., 1975) and Russia (Frantseson, 1970; Sobolev et al., 1973). Electron probe studies (Dawson and Smith, 1975a, Aoki, 1974) have demonstrated that most nodule micas are of similar compositions to megacrysts (i.e. micas in kimberlite) and are unlike primary or secondary micas in peridotite nodules (cf. Carswell, 1975). The chemistry of these micas (Chapter 5, page 156) suggests that they crystallized from the kimberlite magma either in the upper mantle or lower crust (Aoki, 1974; Dawson and Smith, 1975a). Amphibole-bearing nodules (Erlank and Finger, 1970; Erlank, 1973; Aoki, 1974; Dawson and Smith, 1975b; Smith et al., 1975) which

are known to contain potassic richterite (Erlank and Finger, 1970; Aoki, 1974) are not considered to be stable below 110 km (cf. Kushiro, 1970 and Nishikawa et al., 1971). Recent experimental studies on the stability of richterite (Kushiro and Erlank, 1970); however, have demonstrated that this amphibole is stable to depths between 70 - 90 km in the absence of garnet or spinel. It therefore has a relatively limited field of stability and is possibly restricted to nodules in kimberlite. Similar depths of formation probably apply to the whole M.A.R.I.D. suite. The Aillik glimmerites are interpreted to represent cognate xenoliths which crystallized from a kimberlite magma; all mineral phases present in these nodules are therefore regarded as first generation crystals⁸. Megacrysts from the kimberlite which show evidence of mechanical deformation, abrasion and/or corrosion are also ascribed to first generation crystallization as they have clearly been transported from depth. They are regarded as having crystallized during an early stage of the consolidation of the magma, possibly during the formation of the glimmerite nodules or alternatively they may result from fragmentation of nodules during their transport to the surface.

4.2.4.2 First Generation Mineral Phases

(A) Nodules

Phlogopite and/or biotite occur as xenomorphic to idiomorphic laths

⁸ The author considers first generation crystals to be those mineral phases which were the first crystallization products from the kimberlite magma. All megacrysts which exhibit idiomorphic outlines and matrix crystals have been ascribed to second generation crystals as they appear to have crystallized close to their present location and show no evidence of mechanical deformation.

TABLE 4.1

Mineralogical Variation in the Aillik Bay Glimmerite Nodule Suite

<u>Nodule Type</u>	<u>No. of Observations</u>
Olivine - glimmerite	3
Olivine - ilmenite glimmerite	7
Olivine - apatite glimmerite	1
Olivine - apatite - ilmenite glimmerite	2
Olivine - clinophyroxene - ilmenite - amphibole glimmerite	1
Glimmerite	21
Diopside glimmerite	5
Apatite glimmerite	8
Ilmenite glimmerite	5
Ilmenite - apatite glimmerite	3
Diopside - ilmenite glimmerite	3
Diopside - apatite glimmerite	2
Diopside - apatite - ilmenite glimmerite	2
Opaque oxide dunite	1
Mica dunite	1
Opaque oxide - mica dunite	1
Mica - opaque oxide - amphibole nodule	2

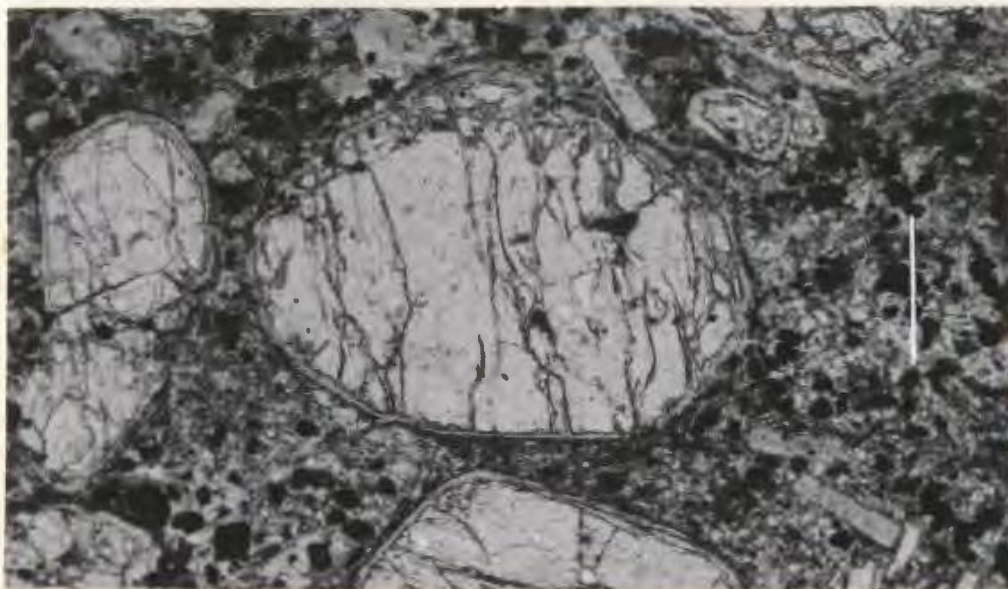


Figure 4.9 Photomicrograph of a micaceous kimberlite containing large subrounded megacrysts in a matrix of olivine, serpentine, opaque oxides, phlogopite and carbonate. Note the anti-gorite mantles around the olivine crystals. Plane light. Scale bar is 0.5 mm long.



Figure 4.10 Photomicrograph of a glimmerite nodule (Group V mica) within kimberlite. The nodule is subrounded and contains interstitial granular diopside. Plane light. Scale bar is 0.5 mm long.

which range in size from 0.5 x 0.35 to 0.10 x 0.05 mm and commonly exhibit a granoblastic to decussate texture. Larger deformed laths of mica (up to 3.0 x 1.5 mm in size) with strongly kinked (001) cleavage traces are present in some nodules. These larger laths are commonly surrounded by an extensive development of fine grained decussate mica with intricately sutured grain boundaries (Fig. 4.11) and are regarded as a recrystallization product of an earlier more extremely deformed mica. The deformation observed in the Aillik Bay glimmerites is considered by the author to have occurred during nodule incorporation into the kimberlite host and subsequent deformation during transportation to the surface. Although the recrystallization textures are superficially similar to those found in granular and some sheared mantle-derived peridotite nodules from kimberlites (Nixon and Boyd, 1973; Boullier and Nicolas, 1973, 1975; Cox *et al.*, 1973), the Aillik textures are nevertheless considered to be the result of thermal metamorphism by the hot kimberlite host after incorporation of the nodule, rather than mantle deformation processes.

Five varieties of mica (phlogopite and/or biotite) have been recognized as the basis of color and pleochroism⁹ in the Aillik glimmerites.

9 Pleochroism as used in this thesis refers to normal, reverse or non-pleochroic micas. Normal pleochroism in micas results from the electronic interaction between d - orbitals centered on transition metal ions and/or from a cation of low oxidation number to one of high number (Faye, 1968; Faye and Hogarth, 1969). In biotite and some phlogopites this results from the $Fe^{2+} \rightarrow Fe^{3+}$ interaction (Faye and Hogarth, 1968) in the octahedral layers which lie parallel to (001). Reverse pleochroism, however, cannot be attributed to Fe^{3+} in the octahedral layers and is found to be related to Fe^{3+} occupancy in tetrahedral sites as well as substitution of Al^{3+} for Fe^{3+} in the layers.

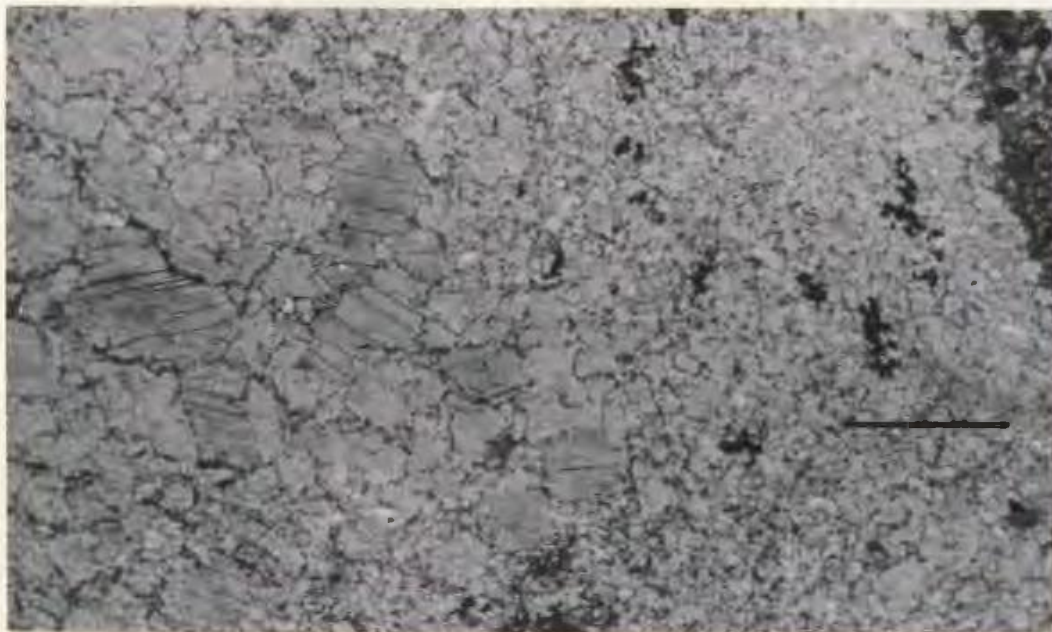


Figure 4.11 Photomicrograph showing large deformed phlogopite crystals in a glimmerite nodule core. The large crystals grade towards the nodules margin into recrystallized micas with decussate texture. Plane light. Scale bar is 0.5 mm long.



Figure 4.12 Photomicrograph showing granular olivine crystals in an olivine opaque oxide glimmerite. Note the decussate texture displayed by the mica crystals. Plane light. Scale bar is 0.5 mm long.

Group I micas exhibit reverse pleochroism ($\alpha > \beta = \gamma$) and can be divided into two subgroups on the basis of color. The first variety varies in pleochroic scheme as shown in Table 4.2. These micas are possibly titan-rich phlogopites and the variance in their color of the α ray is related to varying proportions of iron (Fe^{3+} , Fe^{2+}) to titanium in the mica structure (Deer et al., 1971; Rimsaite, 1968). The second variety (Group Ib) also show reverse pleochroism and exhibit α - greenish brown to dark reddish orange, $\beta = \gamma$ - green to light greenish brown schemes. Group II micas display normal pleochroism and their color variations are shown in Table 4.3. Group III micas display both normal and reverse pleochroism; $\alpha = \beta$ - a dark reddish brown to reddish green, γ - a dark greenish brown to green. The absorption of α and γ is moderate to high and in some cases $\alpha = \beta = \gamma$. Group IV micas are nonpleochroic but may grade into reverse or normal pleochroism with slight change in absorption. The pleochroic scheme ranges from α - a light reddish brown to clear, β - a light brownish green to clear, γ - a light green, light brownish to clear color. Group V micas are confined to two nodules (specimen numbers¹⁰ 51 - 1, 13 - 4) and are characterized by a distinct pleochroic mica with $\alpha = \beta$ - a pale yellow and γ - a brown to greenish brown. Specimen (13 - 4) contains a mica with a Group Ia core and a rim comparable to that observed in specimen (51 - 1). In summary, three important trends are seen in the mica suite.

(i) The distinct trend in color from clear to either brown green or orange is interpreted to indicate varying concentrations of

¹⁰ Specimens housed in the Department of Geology, M.U.N. under the Labrador collection.

TABLE 4:2

Pleochroic Schemes for Group Ia Micaceous Minerals

- | | | |
|-------------------------------|---|---|
| (Absorption moderate to high) | - | Light reddish to orange brown, dark reddish to orange brown |
| (Absorption Low) | - | Light yellow to light green, light reddish green to light reddish brown |

TABLE 4.3

Pleochroic Schemes for Group II Mica

- | | |
|---------------------------------------|--|
| 1 = (Absorption Low) | - clear to yellow, light greenish
yellow to brownish yellow, light
greenish brown to brown |
| 2 = 3 = (Absorption moderate to high) | - light green to green, light greenish
brown to greenish brown, brown to
dark brown |

FeO, Fe₂O₃, TiO₂, and Al₂O₃ in the mica structure (Deer et al., 1971; Rimsaite, 1969).

(ii) The distinct gradation from nonpleochroic micas to those with either normal or reverse pleochroism in the suite is attributed to compositional changes within the various groups (Faye and Hogarth, 1969; Hogarth, 1964; Faye, 1968).

(iii) Zoning relationships indicate that micas with reverse pleochroism crystallized before those which display normal pleochroism.

In thin section, xenomorphic olivine ranging in size from 1.0 x 0.9 mm to 0.10 x 0.10 mm occurs as optically continuous granular crystals (Fig. 4.12) which may form partially connected interstitial chains. Fresh olivine crystals often exhibit increasing serpentinization towards the nodule margins and several carbonatitized nodules only contain antigorite. Several dunitic nodules studied exhibit a granoblastic texture (Fig. 4.13) which is considered to have formed by recrystallization from larger strained crystals.

Xenomorphic green diopside (possibly chrome-bearing) ranges from 1.0 x 0.75 to 0.10 x 0.05 mm in size and occurs either as small granular crystals (Fig. 4.10) or lenticular chains which are in optical continuity (Fig. 4.14). Most crystals are interstitial to the micas, however, poikilitic crystals were also observed.

Nonpleochroic to pleochroic amphibole (richterite?) with $\alpha - a$

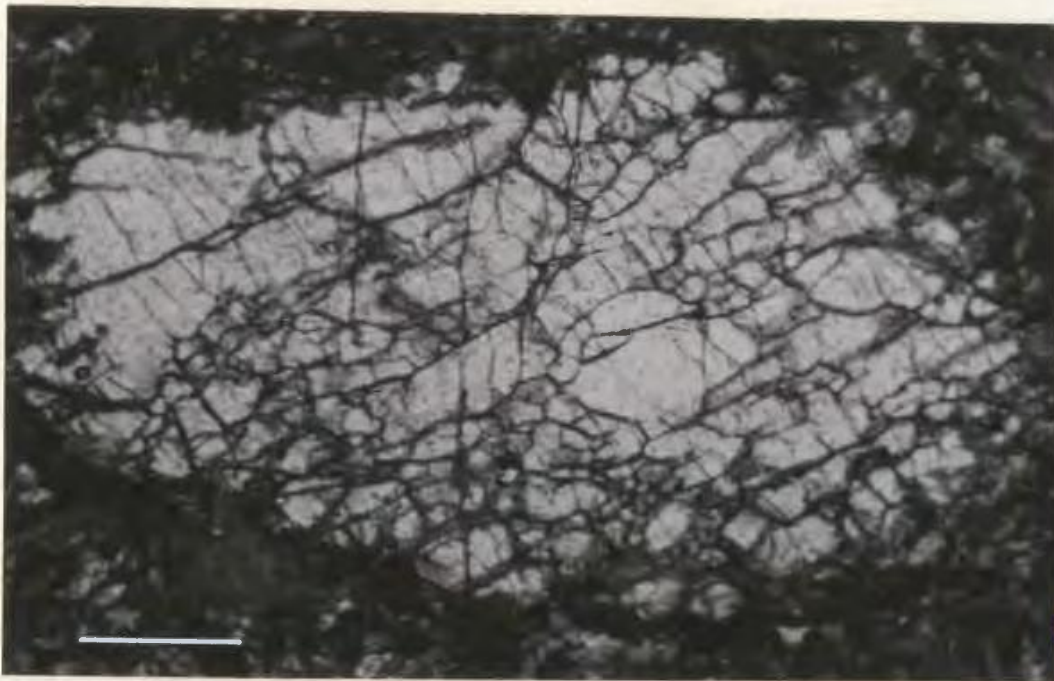


Figure 4.13 Photomicrograph of a granoblastic dunite nodule. Plane light. Scale bar is 0.5 mm long.

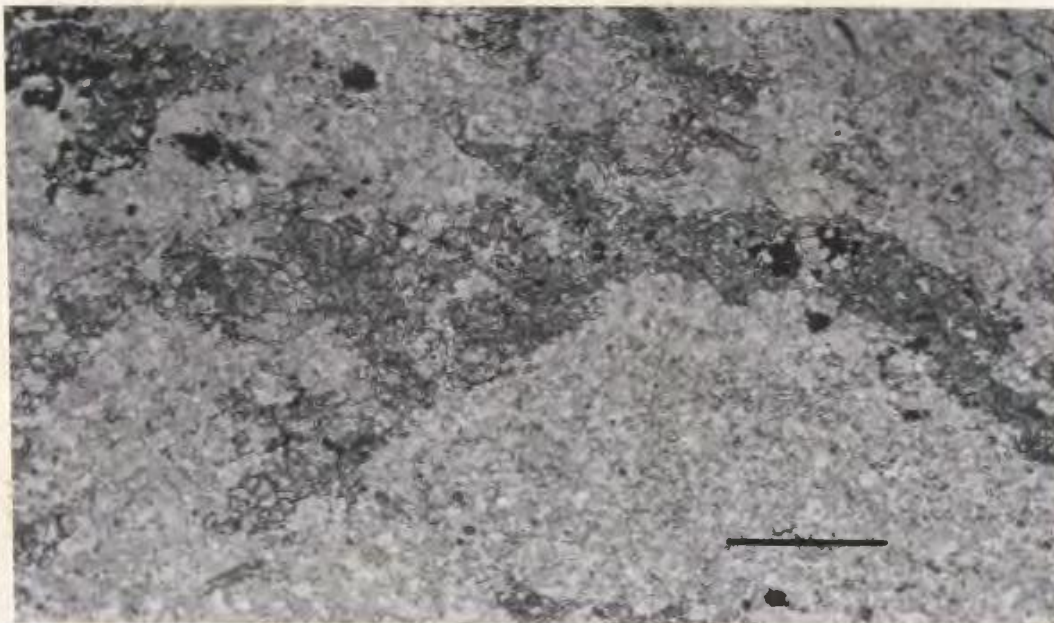


Figure 4.14 Photomicrograph of a diopside glimmerite nodule which contains interstitial chains of diopside. Plane light. Scale bar is 0.5 mm long.

colorless to light brown, β - colorless to light brown and γ - a colorless to brown occurs as xenomorphic to hypidiomorphic crystals (Fig. 4.15). Most nonpleochroic crystals are strained and exhibit undulose extinction while the pleochroic crystals occur as poikilitic grains with inclusions of olivine, mica and partially re-absorbed clinopyroxene.

Xenomorphic apatite forms interstitial crystals which range in size from 0.75×0.20 to 0.10×0.05 mm. Opaque oxides (ilmenite, and possibly magnetite) usually form xenomorphic crystals with either an interstitial or more rarely a poikilitic texture (Fig. 4.16). Although most magnetite crystals are fresh, ilmenite commonly exhibits marginal coronas of leucoxene or perovskite.

(B) Megacrysts in Kimberlite

Olivine megacrysts which are regarded as first generation occur as xenomorphic rounded to subrounded crystals ranging in size from 4.0 to 5.5 mm in diameter (Fig. 4.17). They are usually extensively fractured and commonly exhibit undulose extinction and/or deformation bands (Fig. 4.18). Although most crystals are fresh, thin coronas of antigorite are commonly developed.

Group Ia, II, III and IV micas of the nodule suite are found either as lath to tabular shaped megacrysts or more rarely as microlitic matrix crystals, and range in size from 4.0×1.25 to 0.10×0.05 mm. They exhibit comparable pleochroic schemes to those described in the nodules; however, Group III mica crystals in the kimberlite grade into Group II;



Figure 4.15 Photomicrograph of an amphibole - biotite - opaque oxide glimmerite with nonpleochroic amphibole (richterite?). Plane light. Scale bar is 0.25 mm long.



Figure 4.16 Photomicrograph of a poikilitic opaque oxide crystal in an opaque - olivine glimmerite. Plane light. Scale bar is 0.5 mm long.

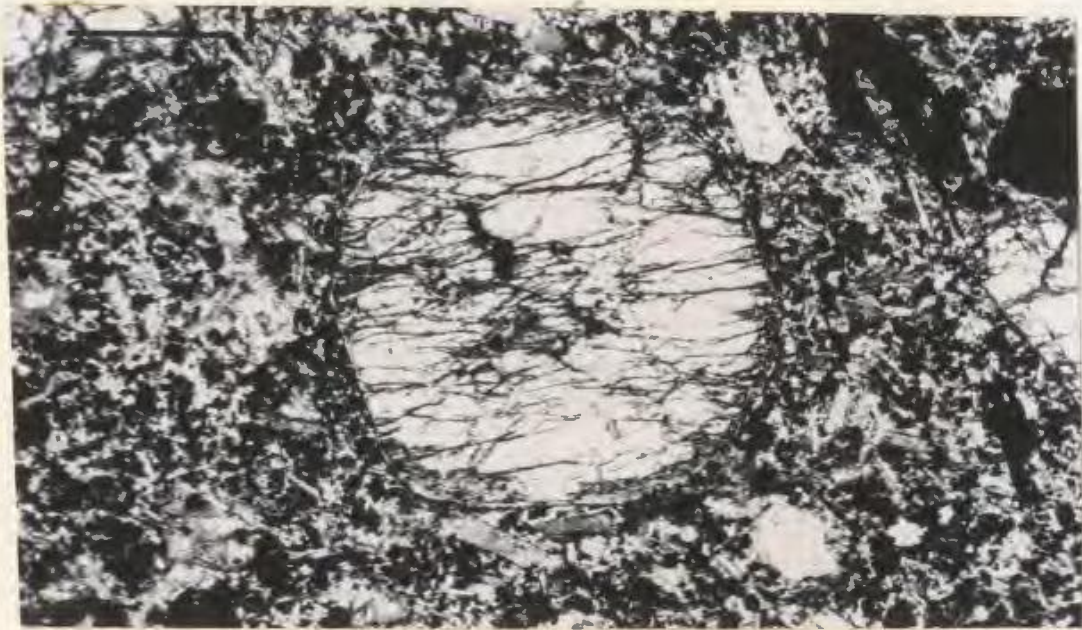


Figure 4.17 Photomicrograph of a micaceous kimberlite containing large subrounded megacrysts in a matrix of olivine, serpentine, opaque oxides, phlogopite and carbonate. Note the intense fracturing in the megacryst. Plane light. Scale bar is 0.5 mm long.

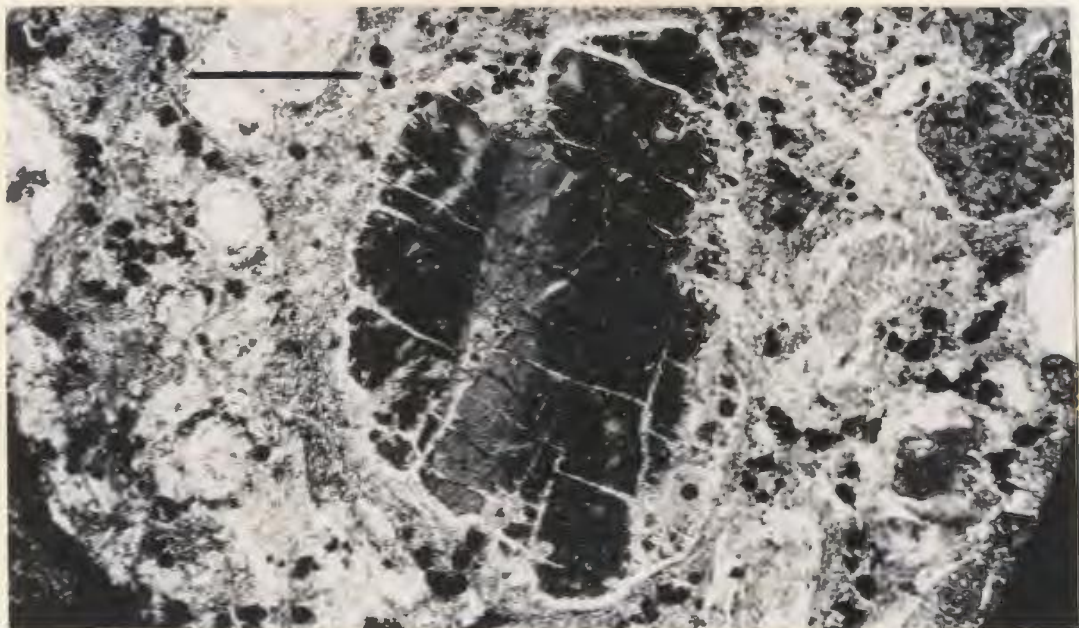


Figure 4.18 Photomicrograph of a first generation olivine crystal showing deformation bands. Crossed polars. Scale bar is 0.5 mm long.

a feature not observed in the nodules. Most crystals show mechanical deformation features (i.e. kinked and/or folded (001) cleavage (Fig. 4.19) or rounded tabular plates) which are attributed to deformation during transport (cf. Reid et al., 1975).

Xenomorphic apatite crystals are also present and range in size from 1.3 x 0.5 to 0.35 x 0.20 mm.

In thin section opaque oxides (ilmenite, magnesium-rich ilmenite, perovskite and possibly magnetite) occur as xenomorphic crystals which range in size from 6.0 x 2.0 to 0.05 x 0.05 mm and commonly exhibit rounded (Fig. 4.20), subrounded or fractured grain boundaries. They commonly contain inclusions of apatite, augite, phlogopite, olivine and carbonate.

4.2.4.3 Second Generation Mineral Phases

Second generation olivines are present either as large xenomorphic to idiomorphic megacrysts (4.0 x 3.0 mm) or small hypidiomorphic matrix crystals (0.25 x 0.10 mm) which commonly exhibit a seriate or more rarely a hiatal texture. The larger megacrysts may show evidence of mechanical deformation and a complete gradation possibly exists between first and second generation crystals. Most megacrystic olivine grains display antigorite mantles, and many are completely pseudomorphosed by calcite (Fig. 4.21), antigorite and/or talc. Matrix crystals are always partially (Fig. 4.22) or completely replaced by antigorite.

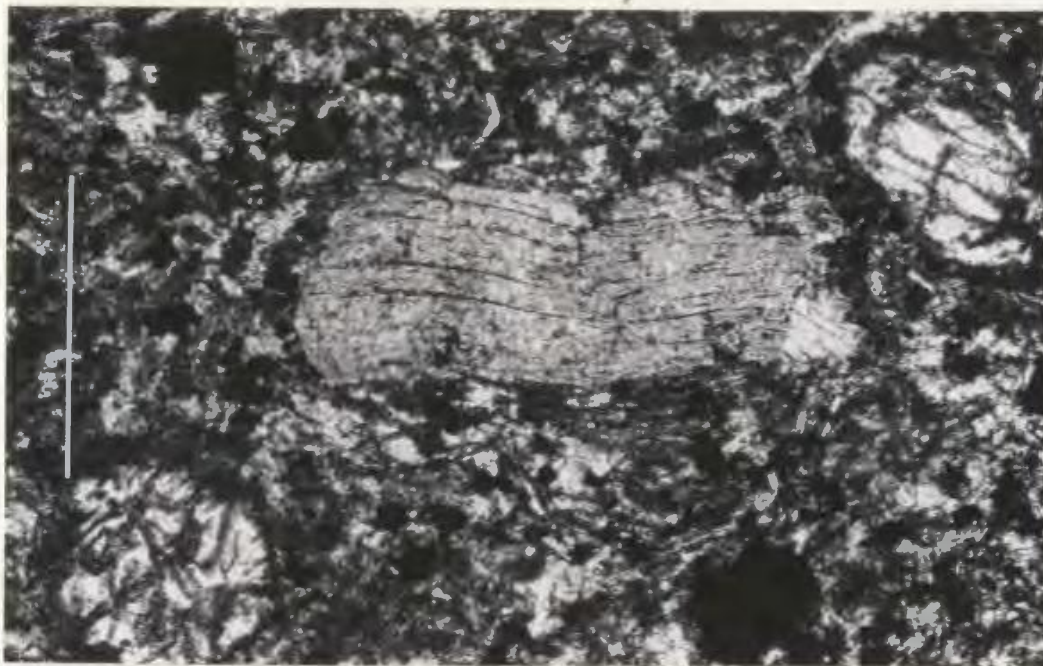


Figure 4.19 Photomicrograph of a first generation mica which exhibits a slightly bent (001) cleavage. Plane light. Scale bar is 0.25 mm long.



Figure 4.20 Photomicrograph of a first generation perovskite megacryst. Note the rounded grain boundary and the inclusions of carbonate. Plane light. Scale bar is 1 mm long.

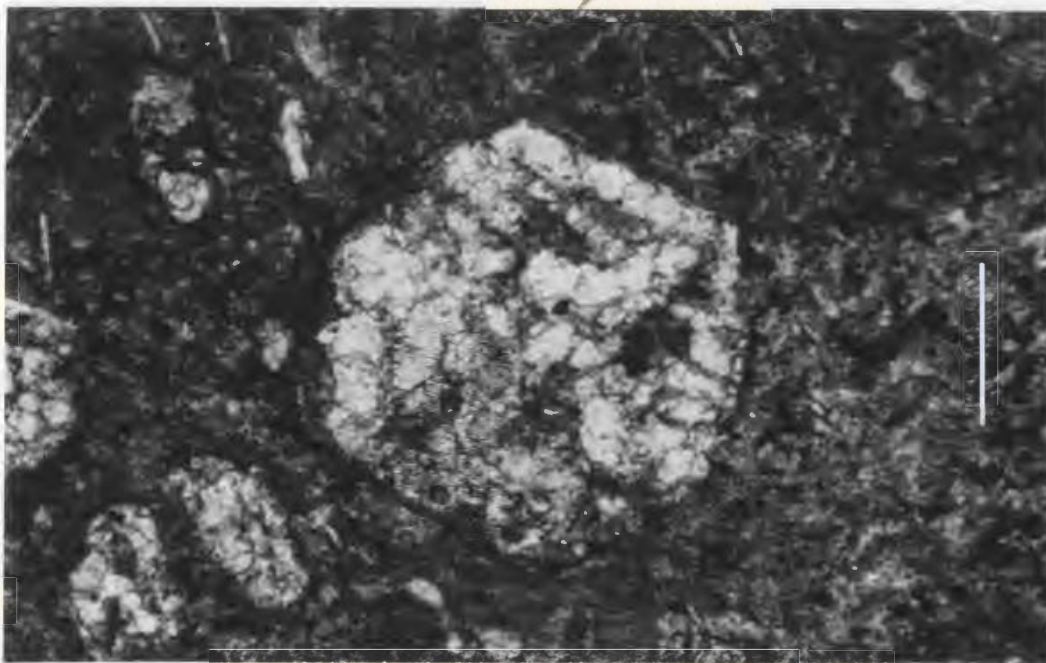


Figure 4.21 Photomicrograph of a second generation olivine megacryst which is completely replaced by calcite. Plane light. Scale bar is 0.5 mm long.

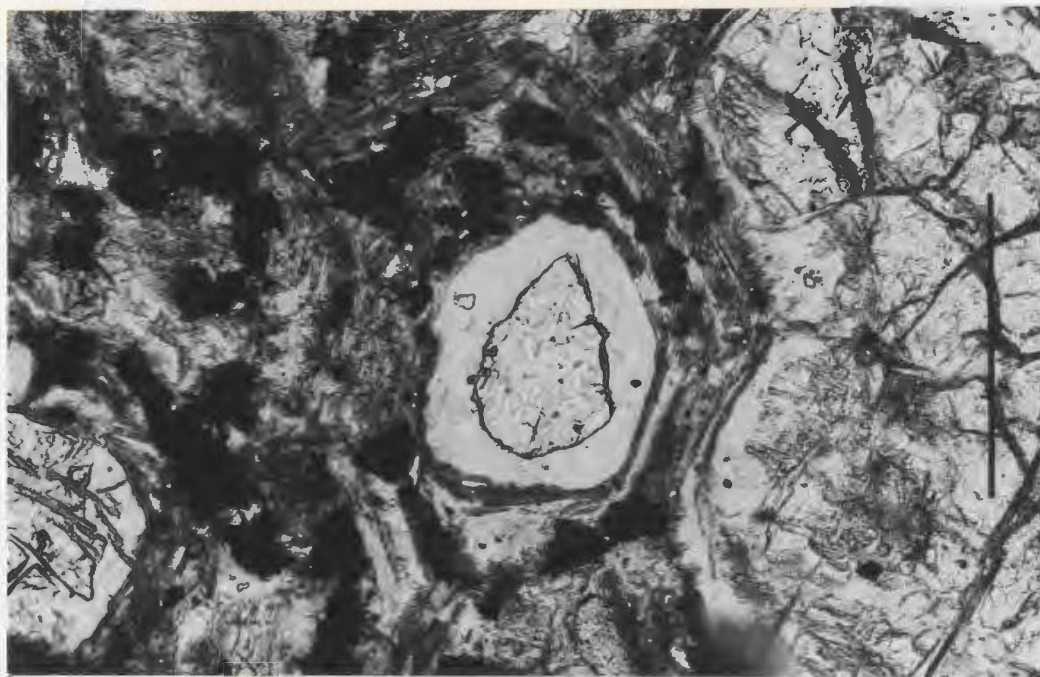


Figure 4.22 Photomicrograph of a xenomorphic olivine crystal belonging to second generation. Note the mantle of antigorite. Plane light. Scale bar is 0.25 mm long.

Olivine, regardless of generation, may exhibit mantles of lath-like aggregates of phlogopite which display reverse pleochroism; α - dark orange brown to reddish brown, $\beta = \gamma$ - light brown to reddish yellow. Similar phlogopite occurrences have been described previously in kimberlites from South Africa (Dawson, 1962) and also in lamprophyres (Mukherjee, 1961). They are interpreted to represent either reaction between the kimberlite magma and the first precipitated olivine (Luth, 1967) or possibly between alkali-aluminum-bearing fluids and serpentine (Dawson, 1962).

Micas belonging to second generation exhibit normal pleochroic schemes (Table 4.4) and occur either as megacrysts or more commonly as matrix crystals. The idiomorphic to hypidiomorphic megacrysts are commonly poikilitic and enclosed grains of olivine, opaque oxides, augite and apatite. Prismatic matrix crystals commonly exhibit a trachytic texture and form anastomosing layers around the larger crystals.

Megacrysts and/or matrix crystals displaying kinked and/or folded (001) cleavages are regarded as having been abraded during transportation. Second generation mica is also found as rims around first generation micas of Group Ia, II, III and IV producing zoned crystals (Fig. 4.23) exist independently of the first generation megacrysts and are present either as megacrysts or matrix phases.

Both first and second generation micas contain inclusions of opaque oxides either along the (001) cleavage or as mantles (cf. Dawson, 1962).

TABLE 4.4

Pheochroic Schemes for Second Generation Micas

$\alpha = \beta$ (absorption low to moderate) - light brown to yellowish brown, light brownish yellow to light reddish brown, yellow to dark brownish yellow, pale brown to light greenish brown, green to light green.

γ = (absorption moderate to high) - reddish brown to dark reddish brown, brown to dark brownish yellow, yellow to pale brown, light greenish brown to green, light green.

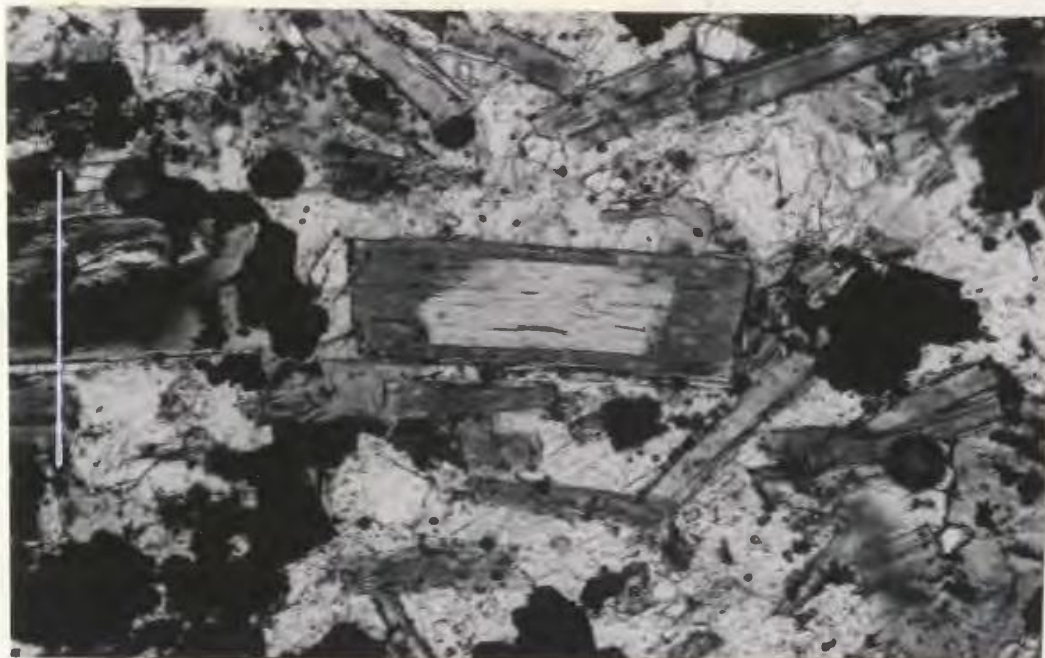


Figure 4.23a Photomicrograph of a zoned mica megacryst which contains a core of Group Ia mica and a rim of second generation mica. Plane light. (Parallel to analyzer). Scale bar is 0.25 mm long.



Figure 4.23b Plane light. (Perpendicular to analyzer). Scale bar is 0.25 mm long.

Similar oxide mantles on kimberlite megacrysts have been described by Mitchell (1970), Mitchell and Fritz (1973) and Dawson (1962, 1967a) and are regarded as either reaction products (Mitchell, 1970) or exsolution phenomena (Dawson, 1962). In carbonate-rich dykes, micas are commonly fenitized and are replaced either by opaque oxides (Fig. 4.24) or by aggregates of carbonate, chlorite and opaque oxides. Other crystals exhibit bleached outer rims that ranges in width from 0.5 to 0.15 mm, and have normal pleochroic schemes with α - a light yellow and γ - a light green. These bleached zones have been identified as vermiculite; a phase commonly found associate with kimberlitic phlogopites (Mitchell, 1970; Smirnov, 1959; Dawson, 1967a). Many matrix micas display thin incomplete rims of phlogopite with reverse pleochroism (α - orange to reddish brown, $\beta = \gamma$ - green to yellow) which are similar to micas previously described as mantles around olivine megacrysts (see above, page 112). Zoned micas have also been described by Emeleus and Andrews (1975) and are interpreted by the author to be either the reaction product between mica and the carbonate-rich matrix or the last mica to crystallize from the kimberlite magma.

Augite, salite, diopside or more rarely titan-augite occurs either as zoned xenomorphic to idiomorphic megacrysts or as matrix crystals which range in size from 1.5 x 0.5 to 0.10 x 0.05 mm and exhibit a hiatal texture. The xenomorphic megacrysts are often fractured or subrounded and comonly exhibit undulose extinction. Many megacrysts display mantles of opaque oxide (Fig. 4.25) which are considered by the author to



Figure 4.24 Photomicrograph of a second generation mica megacryst which contains abundant opaque oxides along the (001) cleavage. Plane light. Scale bar is 0.5 mm long.

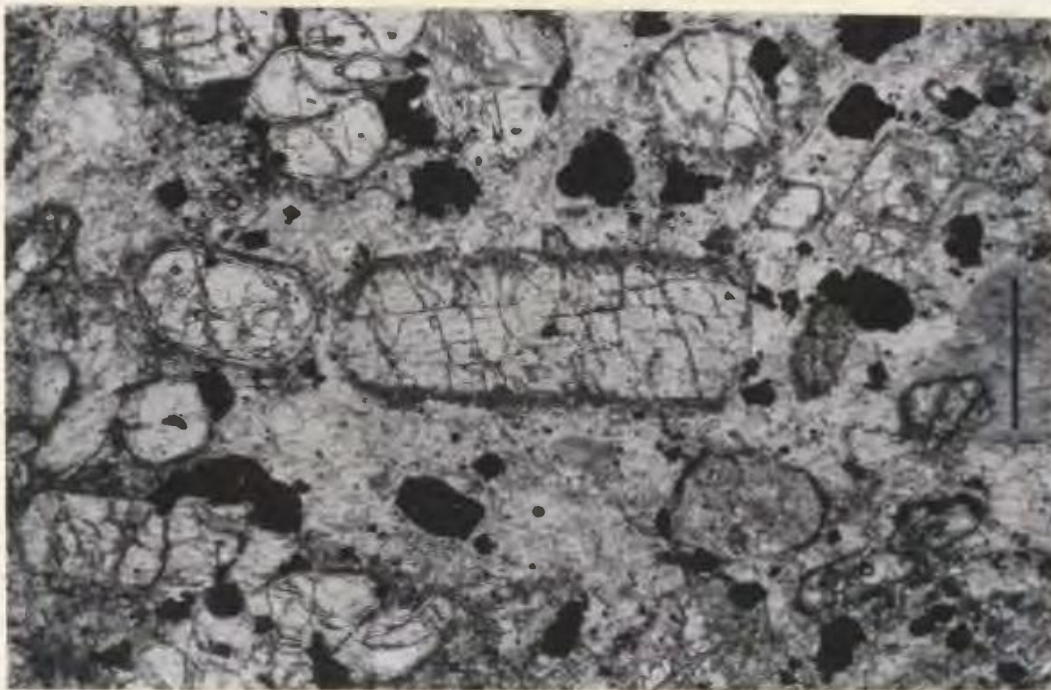


Figure 4.25 Photomicrograph of a second generation titan-augite megacryst. Note the diffuse boundary which is rich in opaque oxides. Plane light. Scale bar is 0.5 mm long.

have been produced by reaction of the clinopyroxene with the carbonate-rich matrix. A complete gradation exists between idiomorphic to xenomorphic crystals, however, all are classified as second generation, as augite is rare to absent in the nodule suite. Matrix augite has a green, greenish brown to pale yellow color and forms small acicular to columnar needles (0.20×0.15 to 0.10×0.05 mm in size) (Fig. 4.26). Most crystals are zoned and form either radiating clusters or discrete crystals. The extreme zoning observed in the megacrysts and matrix crystals indicates differentiation prior to emplacement and/or crystallization over a wide temperature interval. Several carbonatized kimberlites contain augite crystals that exhibit phlogopite mantles (Fig. 4.27) which are similar to those observed around olivine and matrix mica crystals (see above).

Circular to lobate carbonate-rich ocelli are found to occur individually (Fig. 4.29) or in carbonate-rich bands or veins. They are either monominerallic (carbonate-bearing) or contain varying concentrations of calcite, siderite, mica, opaque oxides, augite or quartz (cf. Dawson and Hawthorne, 1973). The calcite occurs as acicular to granular crystals, in contrast to the siderite which forms granular to bladed radiating growths. Several carbonate-rich dykes contain vugs consisting of quartz which occurs either as radial spherulitic growths or as xenomorphic crystals with undulose extinction. Calcite, siderite, and chlorite are also found. The ocelli are regarded as liquid immiscible fractions which developed prior to, and also contemporaneous with, dyke emplacement. Features in kimberlites attributable to liquid

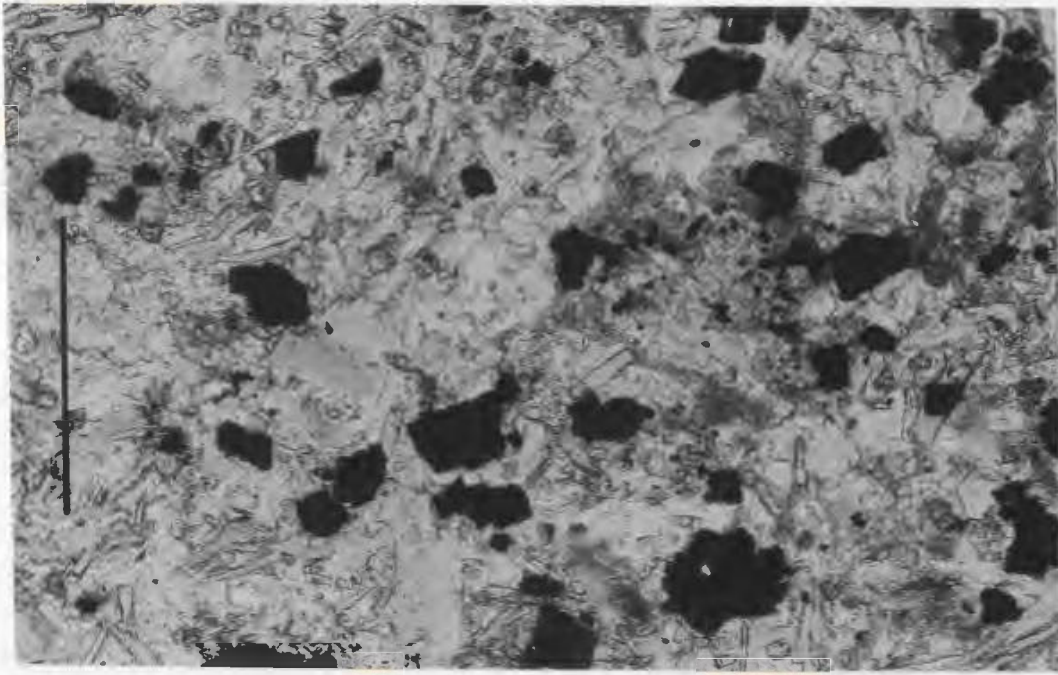


Figure 4.26 Photomicrograph of the matrix of a micaceous kimberlite which contains small acicular needles of augite. Note the idiomorphic to xenomorphic nature of the opaque oxides, biotite and calcite. Plane light. Scale bar is 0.25 mm long.

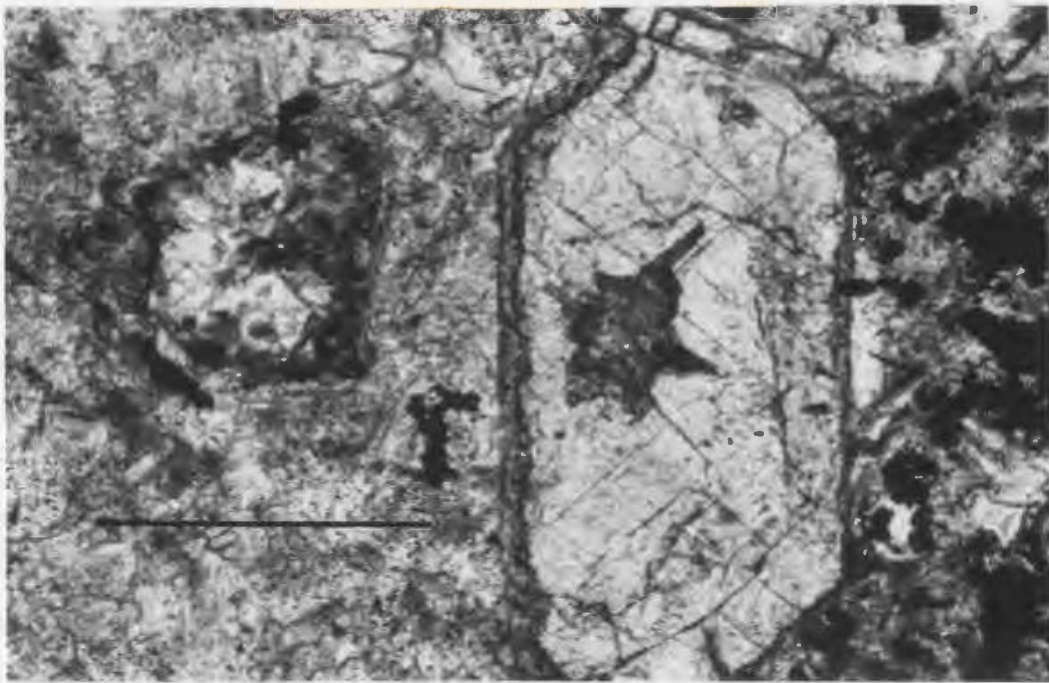


Figure 4.27 Photomicrograph of a second generation titan-augite megacryst with a narrow phlogopite mantle. Plane light. Scale bar is 0.25 mm long.

immiscibility which result in the formation of a carbonatitic residue have been described previously by Dawson and Hawthorne (1973); Clement (1975); and Clarke and Mitchell (1975).

Xenomorphic calcite and/or dolomite is commonly present as an interstitial matrix phase and ranges in size from 0.50 x 0.25 to 0.05 x 0.05 mm. Calcite also occurs either as xenomorphic poikilitic patches, or as randomly oriented and/or trachytic microlites. Lath-shaped crystals are also present (Fig. 4.28) and exhibit length to breadth ratios of 15:1 to 5:1. These are considered by the author to be primary in origin (cf. Watson, 1955; Dawson and Hawthorne, 1970, 1973; Zhabin and Cherepyskaya, 1965; Johnson, 1961; Gittins, 1963, 1973; Wyllie and Boettcher, 1969) and do not replace an earlier phase (cf. Dawson and Hawthorne, 1973).

Dendritic to acicular skeletal calcite crystals exhibiting length to breadth ratios of 1:45 to 1:25 occur in several dykes (Fig. 4.29) (cf. Dawson and Hawthorne, 1973) and are interpreted to be quench features (cf. Lofgren and Donaldson, 1975; Wyllie and Boettcher, 1969; Dawson and Hawthorne, 1973). Carbonate-rich dykes are commonly cut either by bands (formed by flow differentiation; see Chapter 3, page 62) or veins of carbonate, which clearly postdate kimberlite intrusion. One vein studied exhibited flow cells outlined by small acicular needles of apatite and xenolithic slivers of country rock (Fig. 4.30).

Idiomorphic to hypidiomorphic opaque oxide (magnesium-rich ilmenite, ilmenite, magnetite and perovskite) megacrysts and matrix

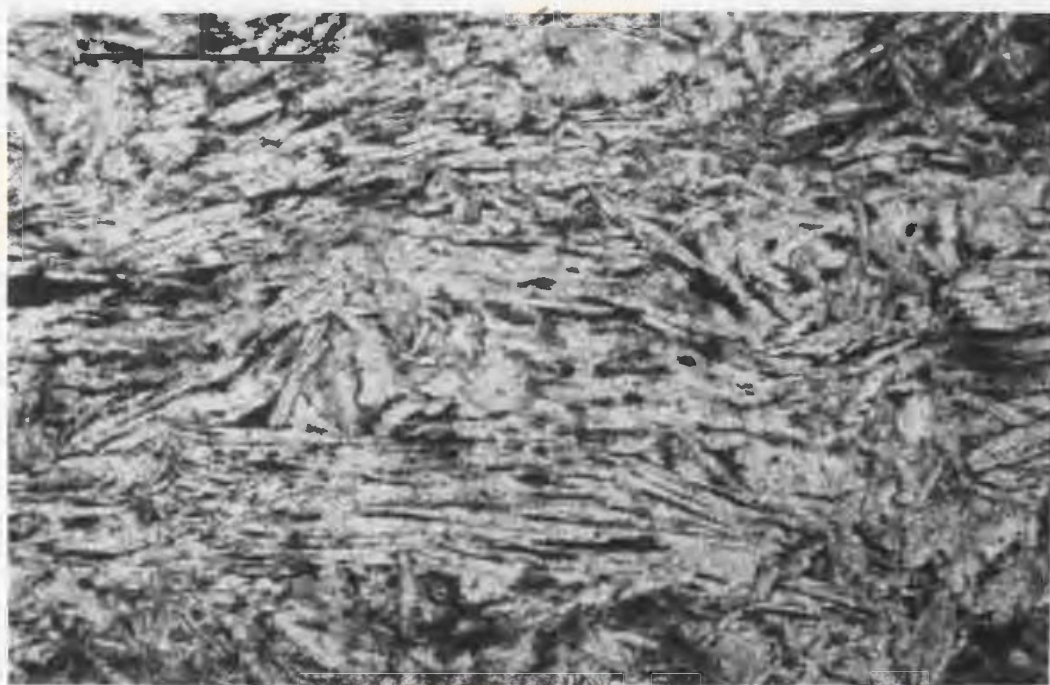


Figure 4.28 Photomicrograph showing lath to microlithic shaped growths of calcite in a carbonate-rich kimberlite. Note the acicular interstitial opaque oxides. Plane light. Scale bar is 0.5 mm long.

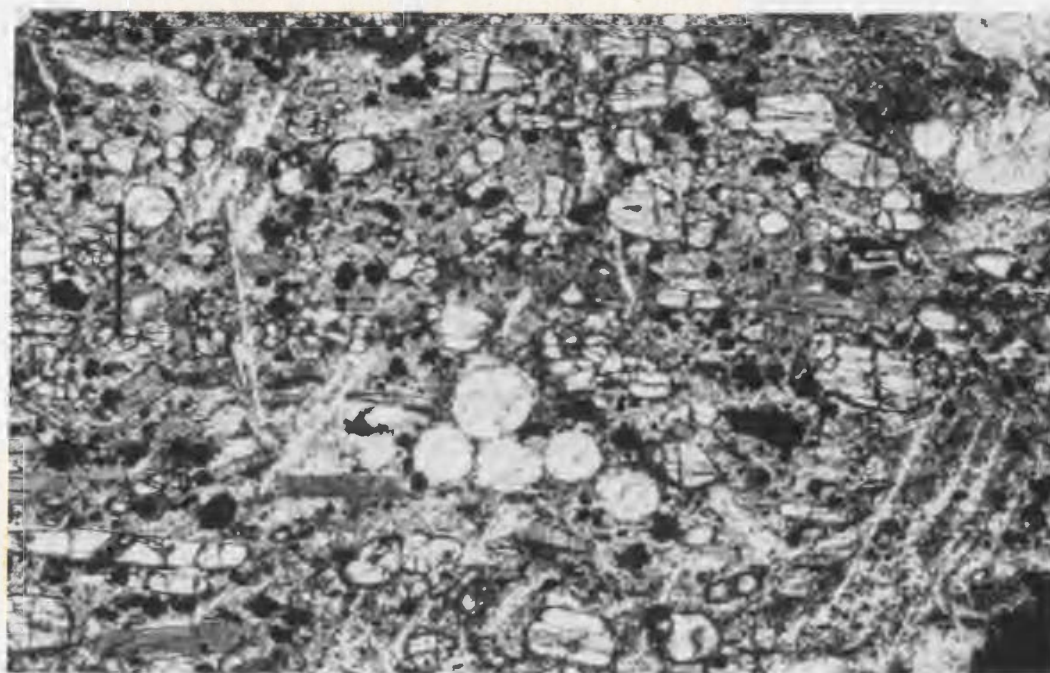


Figure 4.29 Photomicrograph of a carbonate-rich micaceous kimberlite showing the development of long acicular crystals of primary calcite. Plane light. Scale bar is 1 mm long.

crystals (Fig. 4.31) range in size from 2.0×1.5 to 0.05×0.05 mm and commonly exhibit a hiatal texture. Bladed to acicular growths are also common (Fig. 4.28) but are restricted to crystals which form an interstitial phase to carbonate laths. Atoll development (Fig. 4.32) is widespread in this generation and consists of opaque oxide crystals with an internal ring or core of carbonate. Similar arrangements to those in the Aillik dykes have been described in South African kimberlites (Dawson and Hawthorne, 1973) and are interpreted to have formed as a result of two stages of opaque oxide growth. Ilmenite (either megacrysts or matrix crystals) commonly exhibit perovskite-rich mantles (cf. Haggerty et al., 1975; Mitchell, 1970; Dawson, 1971; Haggerty, 1973) and are taken as evidence that a reaction occurred between ilmenite and carbonate. Leucoxene is also a common alteration product and forms greyish coatings around the crystal margins. Magnesium-rich ilmenite is an important kimberlite indicator mineral (Dawson, 1967a; Mitchell, 1970) and its abundance in the Aillik dykes provides a positive link with other kimberlite occurrences (Haggerty et al., 1975).

4.2.4.4 "Crustal" Nodules

A small suite of nodules derived from the basement gneisses and associated intrusive rocks has also been recognized in the Aillik kimberlites. The gneiss fragments are quartzo-feldspathic and in addition to quartz and plagioclase, they contain biotite, amphibole and more rarely potassium feldspar or diopside. All nodules studied in thin section exhibit a well developed mineralogical banding produced by

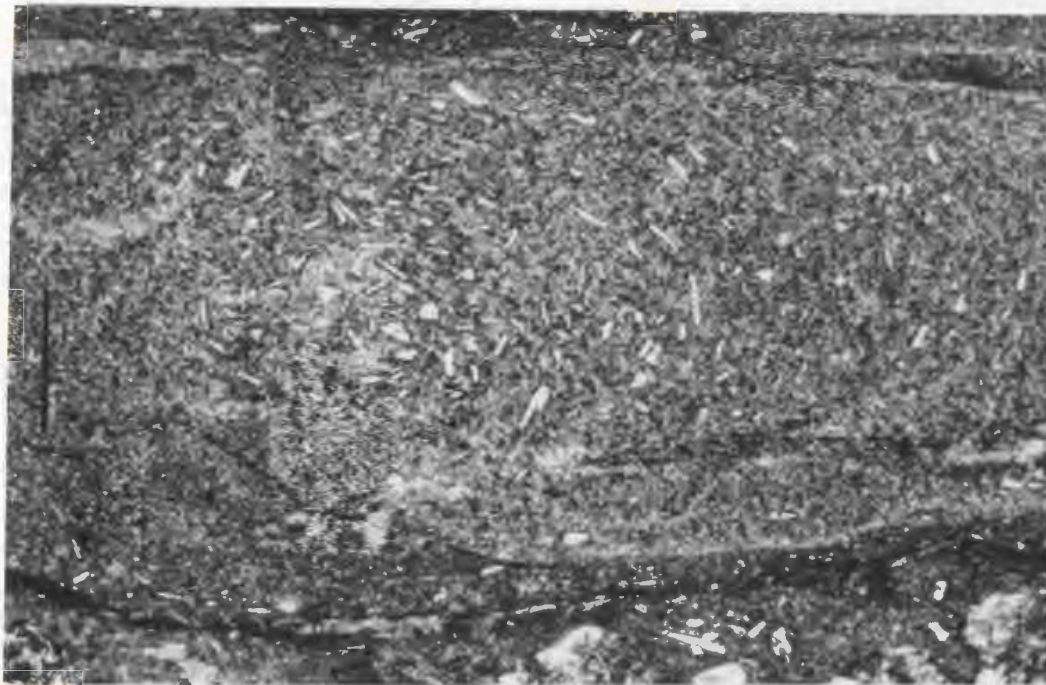


Figure 4.30 Photomicrograph of a flow cell in a carbonatite vein which intrudes a kimberlite. Note the concentric arrangement of acicular apatite and country rock fragments. Plane light. Scale bar is 1 mm long.

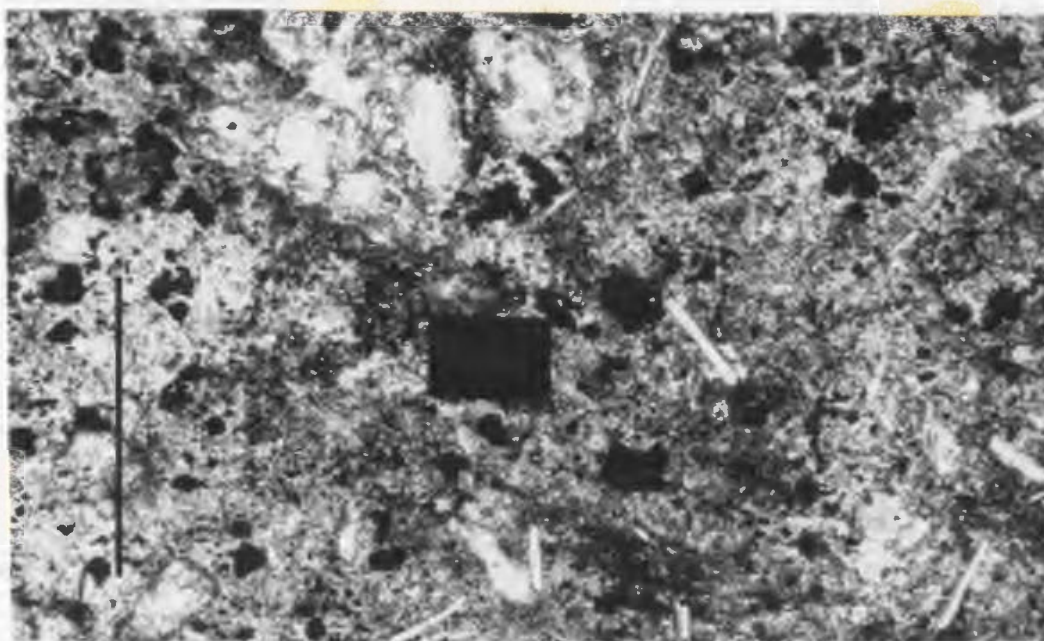


Figure 4.31 Photomicrograph of a second generation opaque oxide with an idiomorphic outline. Plane light. Scale bar is 0.25 mm long.

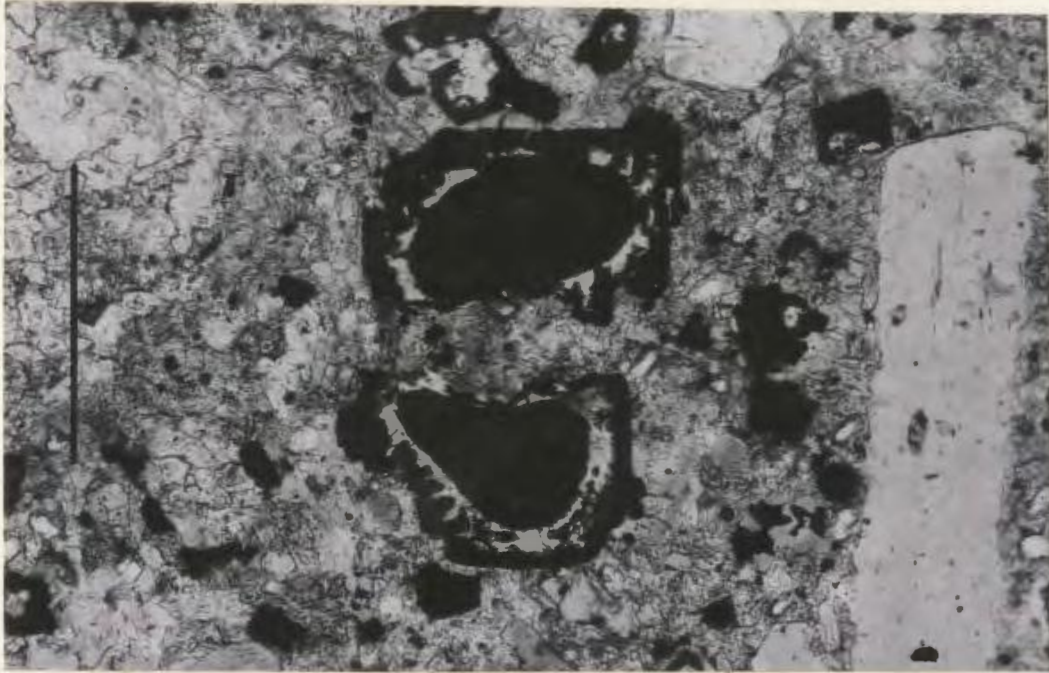


Figure 4.32 Atoll development in a fractured opaque oxide crystal.
Plane light. Scale bar is 0.25 mm long.

alternating feldspathic and ferromagnesian layers. The grade of metamorphism represented by the gneiss fragments is believed to be amphibolite facies. The intrusive rocks are medium to coarse grained and contain major concentrations of plagioclase and/or microcline together with hornblende, biotite, and smaller amounts of quartz, opaque oxides, apatite and secondary aegirine.

Unaltered nodules are uncommon; most show moderate to extreme effects of either fenitization and/or carbonatization. The fresh nodules are similar to the basement gneiss exposed elsewhere in the map area (the Hopedale Complex) and are not considered to represent deep crustal levels (cf. Nixon, 1973) in which granulites and eclogites are an important component.

Although initial alteration proceeds along grain boundaries, microbrecciation is also common in many nodules and the fractures are usually filled with small needles of aegirine and grains of carbonate. Plagioclase and/or microcline usually show the earliest effects of alteration, becoming cloudy and displaying the crystallization of aegirine, sericite, and carbonate. Magnetite mantles are commonly developed on the micas and original amphibole appears dark. Aegirine which first occurs in fracture fillings, eventually forms static growths or develops as mantles around biotite and amphibole. Several nodules show the extensive growth of phlogopite aggregates as interstitial layers between feldspars. With increasing intensity of alteration, the small aegirine needles increase in grain size to form larger prismatic crystals, and carbonate becomes more common.

Plagioclase and/or microcline are eventually completely pseudomorphosed by carbonate and/or sericite and several nodules develop a carbonatitic aspect. The original gneissic banding is almost totally obliterated in the most highly altered nodules.

The fenitization observed in the highly altered nodules is interpreted by the author to have been produced by the carbonatitic fraction present in the matrix of the Aillik kimberlites and is similar to fenitization effects described elsewhere in association with carbonate-rich kimberlites (Ferguson et al., 1973; Ferguson, et al., 1975).

4.2.5 Carbonatites

4.2.5.1 Introduction

The distinction between carbonate-rich kimberlites and carbonatites is not always obvious in the field nor under the microscope. It has been made by some Russian petrologists (cf. Frantsesson, 1970) on the occurrence of pyrochlore, baddeleyite and rare earth-bearing carbonates; however, this mineralogical distinction has been shown to be invalid, as some diamond-bearing carbonate-rich kimberlites also contain the above phases (Frantsesson, 1970). Frantsesson (1970) considers that the distinction should be based upon the presence of absence of relict textures. Those intrusions which can be seen to have contained kimberlitic phases regardless of the state of preservation should be classified as carbonate-rich kimberlites or metasomatic carbonatites. The author has followed the guidelines

established by Frantsesson (1970) and has outlined several varieties of metasomatic carbonatites and carbonatites (sensu stricto).

4.2.5.2 Carbonatites

The carbonatites are fine grained rocks which contain 50 to 90 percent calcite and/or dolomite with minor amounts of barite (0 - 25%), opaque oxides (0 - 15%) and apatite (1 - 10%). In thin section they have a conspicuous allotrimorphic-granular texture (Fig. 4.33) and many exhibit aligned lensoidal or platy carbonate crystals which produce a distinct mineral lineation. Massive xenomorphic to idiomorphic opaque oxides (magnetite, and possibly ilmenite) are common matrix phases and exhibit an interstitial texture. Atoll development is not uncommon (Fig. 4.34) and resembles similar textures observed in the kimberlites (see above, page 121).

Xenomorphic pleochroic barite (α - clear, B - pale yellow, γ - yellowish brown) was observed in a dyke at location 418 (see map 3, back pocket), occurring either as vein-like structures developed subparallel to the dykes margin or as poikilitic interstitial growths. Other phases in the carbonatites include apatite, which forms either megacrysts or matrix phases, xenomorphic quartz and interstitial xenomorphic chlorite patches. The chlorite is slightly pleochroic with α - a pale brown and $B = \gamma$ - green.

4.2.5.3 Metasomatic Carbonatites

The metasomatic carbonatites contain abundant carbonate (40 - 80%).

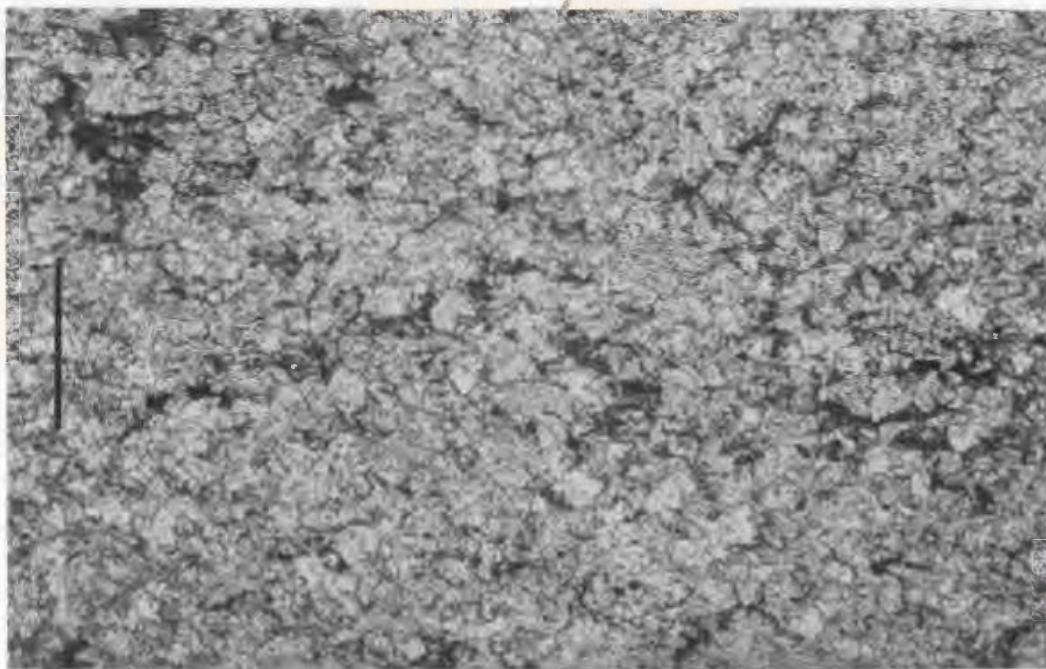


Figure 4.33 Photomicrograph of an allotriomorphic-granular texture in a calcic-carbonatite. Plane light. Scale bar is 0.5 mm long.

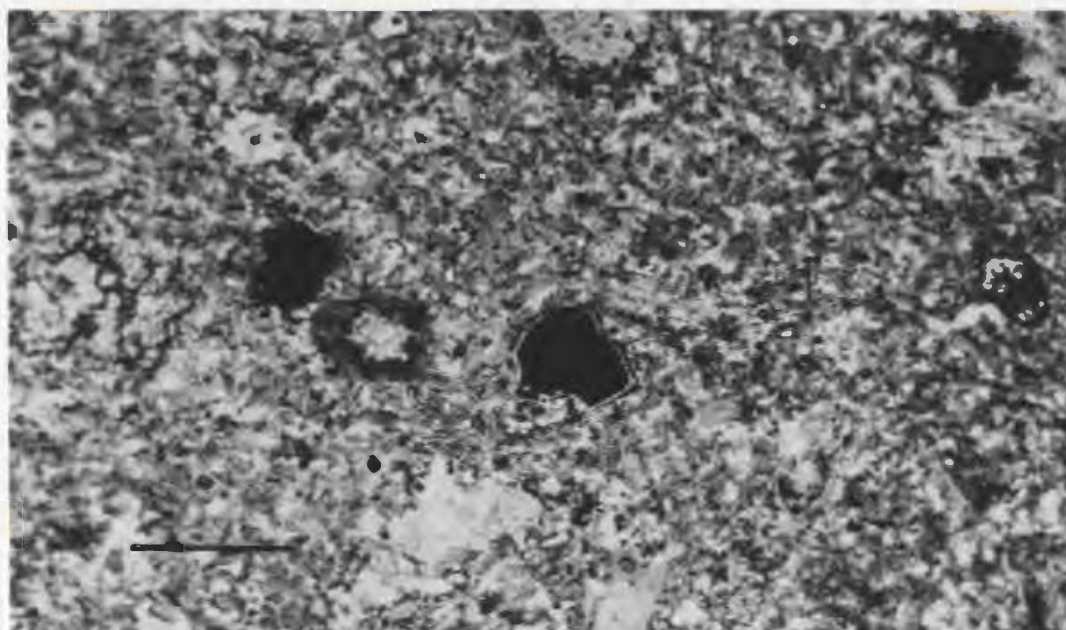


Figure 4.34 Photomicrograph of atoll development in an opaque oxide crystal. Plane light. Scale bar is 0.5 mm long.

with biotite and/or phlogopite (0 - 15%), opaque oxides (5 - 20%), relict olivine (0 - 10%) and apatite (0 - 10%). These carbonatites are characterized by replacement textures and carbonate occurs either as a matrix or more commonly as a secondary alteration phase. The carbonate occurs in a variety of habits, but most are closely comparable to those described in the kimberlites or carbonatites. Ocelli-like structures with fine grained carbonate-rich cores and opaque oxide mantles are present in one dyke (specimen 364). These are regarded as irregular shaped ocelli or alternatively as carbonatite xenoliths transported from depth (Fig. 4.35).

Phlogopite and/or biotite occurs as either lath to microlitic shaped megacrysts or matrix crystals with pleochroic schemes comparable to second generation crystals in the kimberlites; implying that several of these dykes may represent mica-bearing carbonatites. Most mica is chloritized and/or fenitized (Fig. 4.36) and contains abundant carbonate or opaque oxides along cleavage traces. Atoll textured opaque oxides and prismatic apatite crystals similar to those observed in the kimberlites are present in many of the metasomatic carbonatites. Acicular green to greenish brown crystals of secondary aegirine occur as static growths in the metasomatic carbonatite matrix (Fig. 4.37) and also in country rock xenoliths.

4.2.6 Alnöites

4.2.6.1 Introduction and Petrology

Melilite-bearing intrusions are rare in the Aillik area and have only been recognized at one location (specimen 513; Map 3, back pocket).

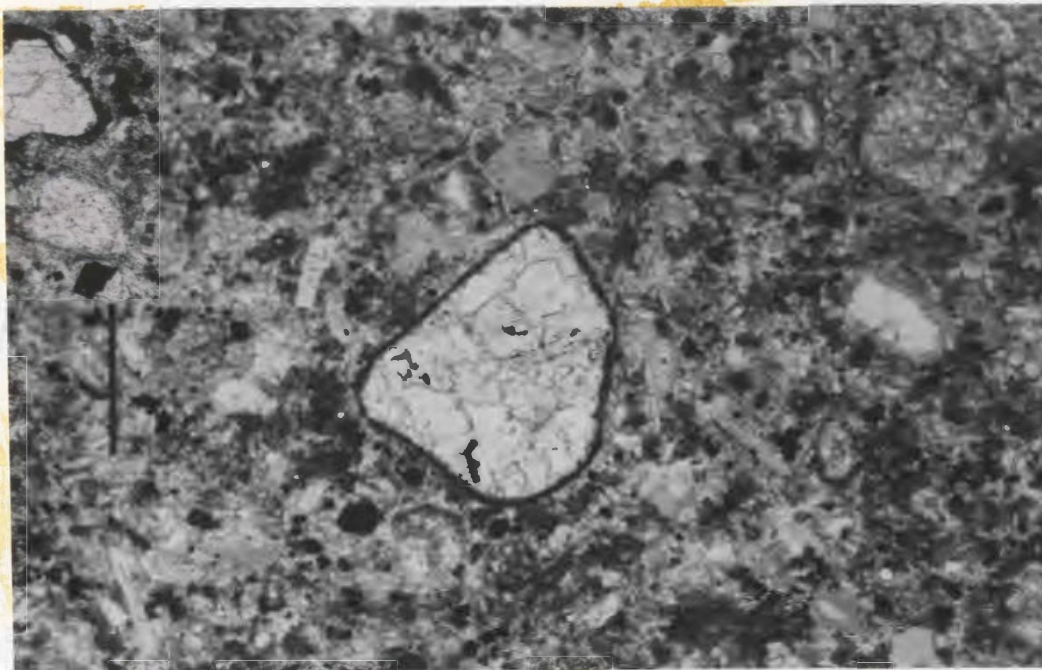


Figure 4.35 Photomicrograph of an ocelli-like structure within a metasomatic carbonatite. Note the oxide rim. Plane light. Scale bar is 0.5 mm long.

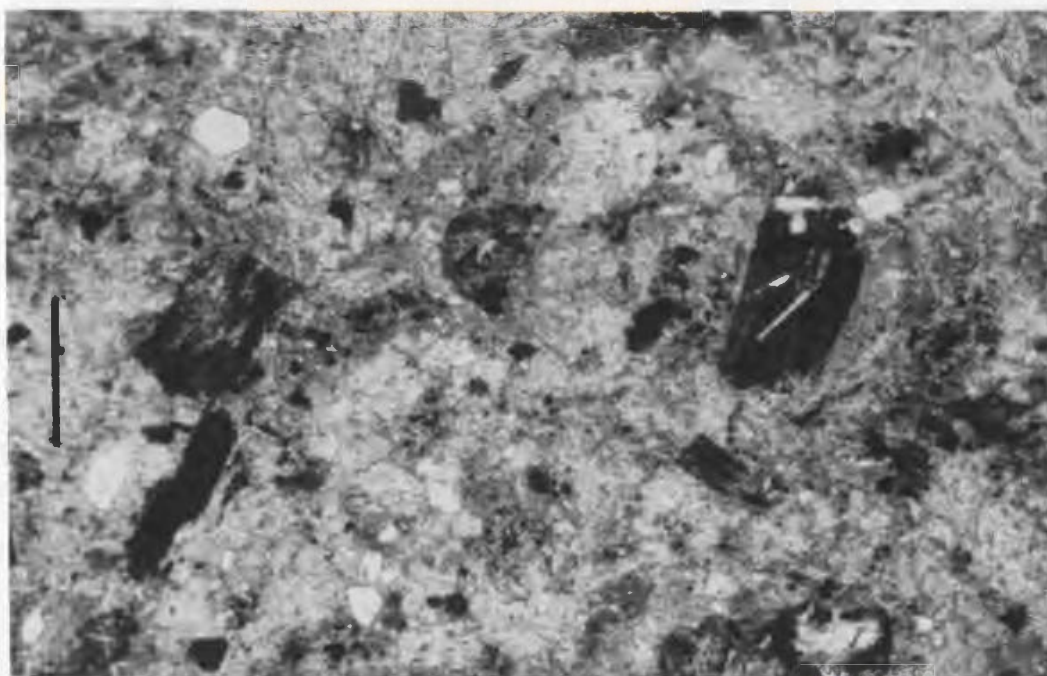


Figure 4.36 Photomicrograph of fenitized micas in a metasomatic carbonatite. Plane light. Scale bar is 0.5 mm long.

Its alnöitic nature was not obvious in the field and it was previously classified as kimberlite. The dyke is composed of olivine, phlogopite and/or biotite, opaque oxides, augite and apatite as well as melilite. Olivine is only present as second generation megacrysts and/or matrix crystals which are seriate in texture. Phlogopite and/or biotite occurs in two generations with the first occurring in glimmerite nodules and as megacrysts. These micas are comparable to those in the kimberlites and belong to Groups I, II or III (see page 101). Second generation crystals are present as megacrysts and matrix crystals but are also found in rims on zoned crystals like those on the kimberlites (see page 112). Clinopyroxene is present both as first and second generation phases and has similar textures and compositions to kimberlite clinopyroxenes. Melilite occurs as small clear to yellow crystals which range from 0.75×0.20 to 0.20×0.10 mm in size. They form a band of perpendicular growth (Fig. 4.38) and are found on both sides of the dyke and at equal distances from the margin. The melilite in this band occurs both as fresh crystals and as crystals pseudomorphosed by carbonate and an unidentified phase. Mineral phases belonging to the spinel group, phosphates and carbonates show similar texture, alteration and composition to those present in the kimberlites.

Although early definitions of kimberlite included melilite as a primary and essential phase (Shand, 1934; Williams, 1932) recent definitions have excluded it (Mitchell, 1970; Dawson, 1967, 1971, 1972a) and it has been regarded as an indicator mineral of alnöites (Mitchell, 1970). Recent studies on kimberlites from Greenland (Escher and Watterson,



Figure 4.37 Photomicrograph of aegirine occurring as static growths within a dolomitic carbonatite (beforsite). Plane light. Scale bar is 0.5 mm long.

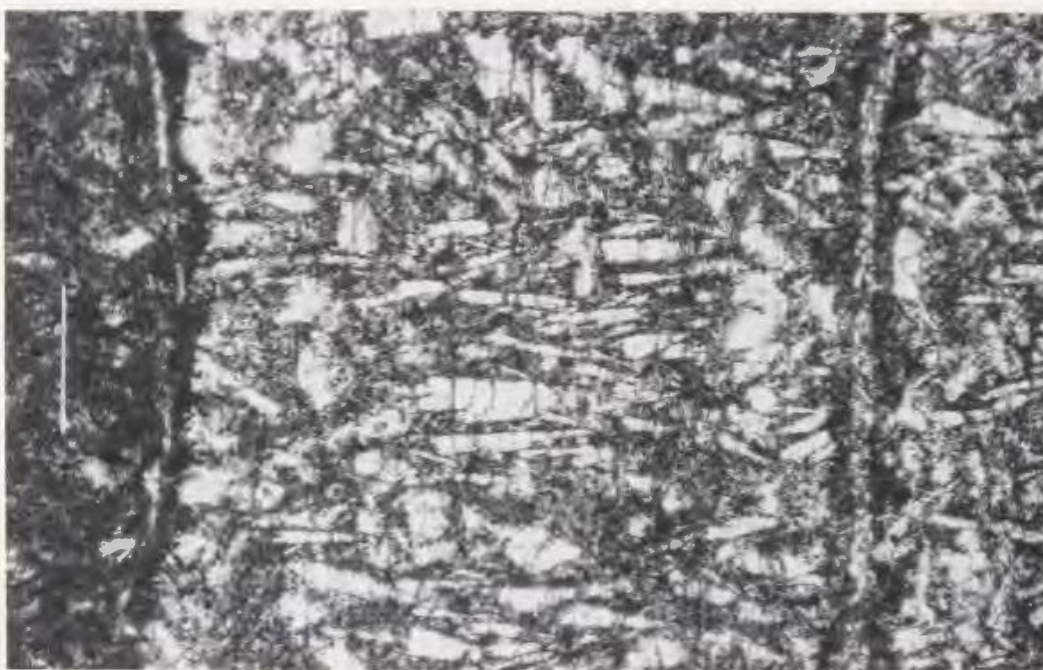


Figure 4.38 Photomicrograph of melilite which occurs as a band of perpendicular growth. Plane light. Scale bar is 0.5 mm long.

1972) however, have shown that kimberlites may contain melilite.

Therefore, further studies of alnöites are necessary to more accurately document their petrological affinity.

CHAPTER 5

Geochemistry

5.1 Introduction

A chemical relationship implying a possible genetic connection between kimberlites, carbonatites and some lamprophyres has been suggested by a number of authors (Dawson, 1960, 1966, 1967b; Ferguson *et al.*, 1975; McGetchin *et al.*, 1973). These findings support similar conclusions which are based on field and petrological evidence (see Chapter 4, page 80). Field and petrological data (Chapters 3 and 4) indicate that a genetic and/or co-magmatic relationship may exist between the various dyke groups mapped in the Aillik area. A geochemical study of these dykes has been undertaken in an attempt to confirm this interpretation. The study has enabled the chemical variation within the individual dyke suites to be assessed and a more complete classification of the dyke swarm has been made.

Seventy-four specimens were analysed; 38 kimberlites, 21 monchiquites, 5 minettes, 7 carbonatites, 2 hornblende-bearing peridotites and 1 glimmerite nodule. Major elements were determined by atomic absorption spectroscopy, x-ray fluorescence, titration, colourimetry, loss on ignition, by fusion and trace elements by x-ray fluorescence. Details of the sample preparation, analytical methods, precision and accuracy of the analyses are given in Appendix 3.

5.2 Major and Trace Element Geochemistry (Elemental Abundances)

5.2.1 Hornblende-bearing Peridotites

Representative chemical analyses and C.I.P.W. norms of the hornblende-bearing peridotites are given in Table 5.1. A comparison of these data with data presented in Tables 5.2, 5.3, 5.4, and 5.5 confirms the earlier conclusions (see Chapter 3 and 4) that the hornblende-bearing peridotites are unrelated to the basic-ultrabasic dyke swarm. The two peridotites studied show a large variation in MgO , CaO and FeO (Table 5.1) which is related to variation in olivine and hornblende concentrations. The large variation in Fe^{2+} and Fe^{3+} between these two dykes is related to the highly chloritized nature of dyke 449.

5.2.2 Minettes

The minettes display little variation in major element chemistry (Table 5.2); a feature which may be related to the relatively small number of these dykes analysed. Most dykes are of basic composition (SiO_2 40-45%) (Fig. 5.1) and exhibit only slight variation in K_2O (5-7%); TiO_2 (3-5%), Al_2O_3 (2-6%), MnO (0.1-0.2%), P_2O_5 (1.0-1.5%), H_2O (nd.-3.5%) and CO_2 (nd.-15.0%) which reflect variations in the modal abundances of opaque oxides, biotite, augite, olivine, and carbonate in the minettes.

The average chemical composition of the Aillik minettes (Table 5.3) differs significantly from average values presented by Métais and Chayes (1963), which are lower in SiO_2 , Al_2O_3 , H_2O and higher in TiO_2 , total Fe, MgO , CaO and H_2O compared to the Aillik dykes.

TABLE 5.1

Representative Geochemical and Petrographic Data for the Hornblende-bearing Peridotites

Sample No.	449	336
SiO ₂	42.22	41.48
TiO ₂	0.33	0.49
Al ₂ O ₃	5.92	7.95
Fe ₂ O ₃	1.07	5.34
FeO	10.61	4.56
MnO	0.19	0.18
MgO	28.53	23.21
CaO	4.62	10.55
Na ₂ O	0.55	1.69
K ₂ O	0.43	0.69
P ₂ O ₅	N.D.	0.10
CO ₂	0.71	0.86
H ₂ O	4.93	3.23
Total	100.11	100.33
<u>Trace (PPM)</u>		
Zr	47	61
Sr	160	381
Rb	21	20
Zn	84	60
Cu	40	56
Ba	210	284
Ni	381	455
Cr	1329	1900
Nb	10	12
<u>C.I.P.W.</u>		
<u>Norm</u>		
Or	4.19	2.66
Ab	2.64	4.88
An	12.39	13.01
Ne	6.52	
Ca	2.00	1.69
Dp	27.62	5.10
Hy		17.01
Ov	35.07	53.05
Mag	7.95	1.63
Il	0.96	0.66
Cr	0.42	0.30
Ap	0.24	
<u>Modes</u>		
Hornblende		66.5
Olivine		25.7
Biotite		4.3
Ore		1.4
Calcite		0.4
Chlorite		1.7

TABLE 5.2

Representative Geochemical and Petrographic Data for the Minettes

Sample No.	210-2	324-A	224-1	221-A	209-1
SiO ₂	45.01	43.65	44.47	41.43	44.89
TiO ₂	4.06	4.13	4.12	3.68	4.12
Al ₂ O ₃	9.29	8.88	9.25	8.49	9.55
Fe ₂ O ₃	4.13	4.88	4.28	3.67	3.53
FeO	7.50	6.85	7.20	7.03	8.01
MnO	0.12	0.17	0.14	0.12	0.13
MgO	10.43	9.82	11.08	10.25	11.09
CaO	7.35	8.71	7.28	6.66	7.54
Na ₂ O	2.15	1.28	1.60	2.66	1.34
K ₂ O	6.68	6.04	6.44	5.60	6.60
P ₂ O ₅	1.06	1.09	1.04	1.04	1.12
CO ₂	1.55	2.21	1.49	10.03	1.71
H ₂ O	0.76	3.22	2.44	0.12	0.83
Total	100.18	100.83	100.80	100.78	100.46
<u>Trace (PPM)</u>					
Zr	530	451	540	657	547
Sr	936	946	1412	1748	1075
Rb	113	113	101	94	116
Zn	121	114	114	111	123
Cu	29	34	31	32	34
Ba	1839	1832	1849	1914	2123
Ni	193	223	189	203	191
Cr	168	373	169	262	159
Nb	75	86	79	82	85
<u>C.I.P.W.</u>					
<u>Norm</u>					
Or	29.88	36.45	38.60	39.07	29.60
Ab		6.24	1.10	2.19	
An		0.66		0.55	5.93
Ne	5.76	2.61	5.85	4.97	
Lc	7.65				
Na-Carb					12.32
Ca	3.54	5.13	3.44	3.90	8.77
Dp	16.34	17.81	16.63	15.54	14.59
Ny					0.88
Ac	6.72		1.62		
Ov	17.21	13.19	16.86	18.18	9.69
Mag	2.64	7.23	5.48	5.13	4.76
IL	7.74	8.01	7.94	7.84	6.25
Cr	0.04	0.08	0.04	0.03	0.05
Ap	2.47	2.59	2.45	2.61	2.16
<u>Modes</u>					
Olivine		8.7	4.4		
Augite		37.3	33.8		
Biotite		25.5	30.1		
Orthoclase		22.0	28.0		
Ore		5.7	3.7		
Carbonate		0.8	0.0		

Figure 5.1 Histograms showing the variation in major and trace
element abundances in the Ailalik minettes.

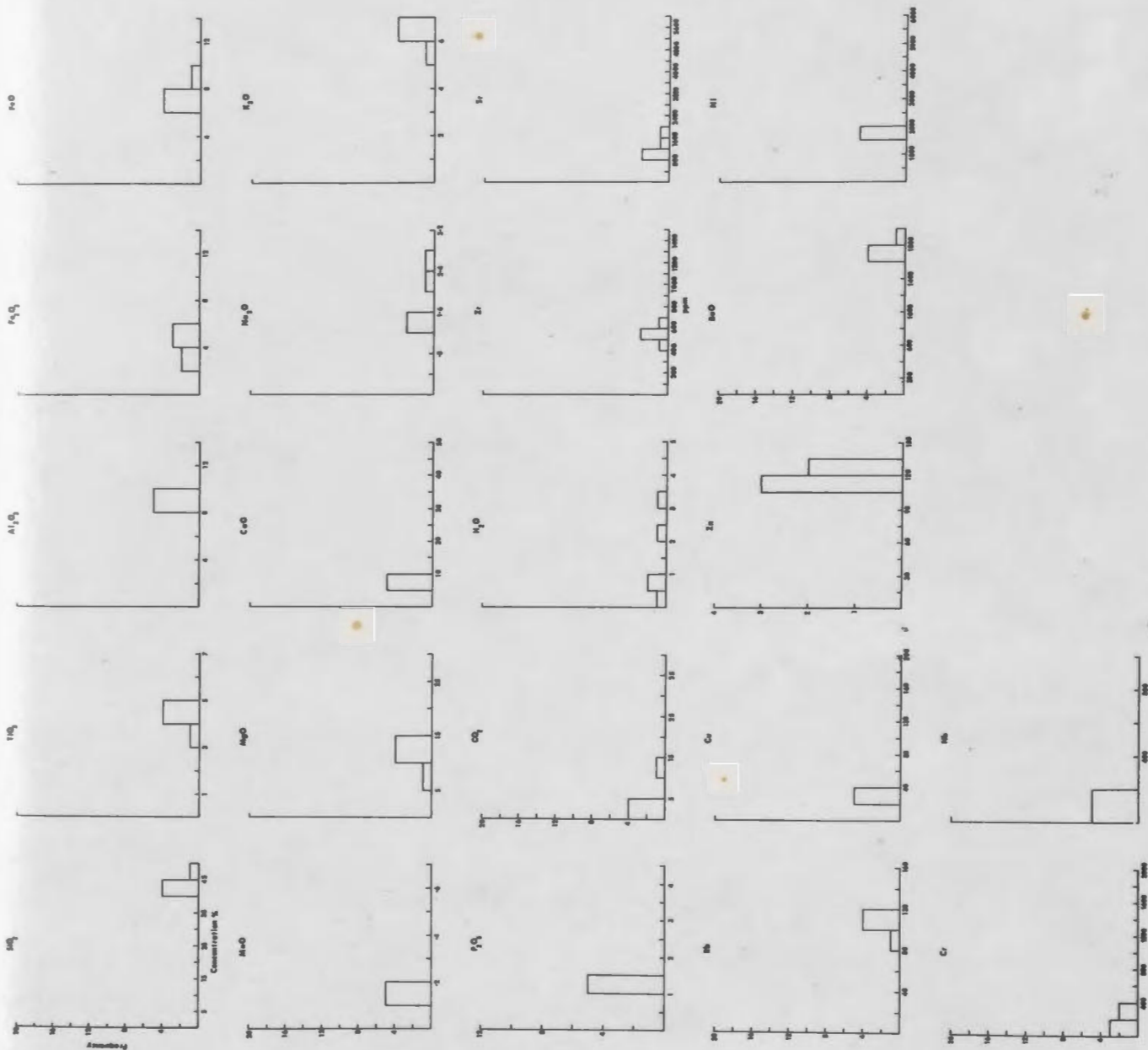


TABLE (5.3)
Average Composition of the Aillik Dykes Compared to Other Dyke Suites

	A	B	C	D	E	F	G	H	I	J	K	L	M
No. of Analyses	64	5	61		20			339	25	38	140	200	7
Element													
SiO ₂	51.17	43.91	40.68	37.56	32.26	31.10	35.20	27.81	33.21	22.16	10.29	9.14	13.52
TiO ₂	1.36	4.02	2.34	3.75	4.96	2.03	2.32	1.63	1.97	3.07	0.73	0.62	1.33
Al ₂ O ₃	13.87	9.09	13.20	10.40	6.14	4.90	2.32	3.40	4.45	3.47	32.9	2.77	3.03
Fe ₂ O ₃	3.27	4.10	4.87	4.86	5.10	N.D.	N.D.	5.40	6.74	5.07	3.46	4.13	2.02
FeO	4.16	7.32	6.47	7.24	9.09	10.50+	9.80+	2.82	3.43	6.84	3.60	4.17	5.27
MgO	6.92	10.53	9.17	9.56	12.47	23.90	27.90	25.53	22.78	16.53	5.79	6.39	12.95
CaO	6.58	7.51	11.02	12.42	14.93	10.60	7.60	12.21	9.36	20.59	36.10	32.52	27.30
Na ₂ O	2.12	1.81	3.06	1.64	1.27	0.31	0.32	0.33	0.19	0.36	0.42	0.97	0.69
K ₂ O	5.49	6.27	2.16	3.64	1.76	2.10	0.98	0.66	0.79	1.84	1.36	1.40	1.12
MnO	N.D.	0.14	N.D.	0.96	0.22	0.10	0.11	0.12	0.17	0.28	0.68	0.69	0.36
H ₂ O	2.42	1.47	3.52	3.32	2.29	5.90	7.40	N.D.	10.70	2.36	1.44	1.37	2.01
P ₂ O ₅	N.O.	1.07	N.D.	0.20	1.65	0.66	0.72	0.50	0.65	1.89	2.09	1.77	2.02
CO ₂	13.0	3.40	1.38	4.70	7.56	7.10	3.30	N.D.	4.98	15.60	28.52	27.96	27.59
Reference	1		1	2		3	3	4	5		6	7	

- 1 Metais and Chayes (1963)
- 2 Ferguson and Currie (1972)
- 3 Dawson (1961)
- 4 Davidson (1967)
- 5 Nixon (1973)
- 6 Heinrich (1966)
- 7 Gold (1966)

- A Minette
- B Aillik Minette
- C Monchiquite
- D Callander Bay Carbonate-Rich Monchiquite
- E Aillik Carbonate-Rich Monchiquite
- F Micaceous Kimberlite
- G Basaltic Kimberlite

- H Siberian Kimberlite
- I Lesotho Kimberlite
- J Aillik Kimberlite
- K Carbonatite
- L Carbonatite
- M Aillik Carbonatite

N.D. - Not Determined
+ - Total Iron as FeO

Trace element variations tend to be wider than those of the major oxides (Fig. 5.1). They contain significant amounts of Sr (800 - 2000 ppm), Zr (400 - 700 ppm), Ba (1600 - 2000 ppm), Ni (1500 - 2000 ppm) and Cr (nd. - 400 ppm). Nb is invariably less than 200 ppm and it appears to be highest in dykes containing carbonate-bearing ocelli.

5.2.3 Carbonate-Rich Monchiquites

Chemical analyses, C.I.P.W. norms and modes of the carbonate-rich monchiquites are presented in Table 5.4. Most dykes are ultrabasic (SiO_2 20-40%) and contain Fe_2O_3 , Al_2O_3 , TiO_2 , Na_2O , FeO , H_2O and CO_2 concentrations which are comparable to those observed in the minettes (compare Fig. 5.1 and 5.2); however, the range of each oxide may be slightly higher or lower. MgO (5-25%), CaO (5-20%) and P_2O_5 (nd.-4%) occur in higher concentrations than in the minettes; however, K_2O (nd.-3%) is lower. The large variation in TiO_2 , total Fe, MgO , Al_2O_3 , CO_2 , and P_2O_5 is regarded as reflecting modal variations in opaque oxides, olivine, biotite, analcime, carbonate and apatite.

Histograms showing major oxide concentrations in the carbonate-rich monchiquites from Callander Bay and Brent Crater, Ontario (Ferguson and Currie, 1972; Currie, 1971) are given in Figure 5.3, for comparison with the Aillik dykes. It is clear that SiO_2 , Fe_2O_3 , CaO , TiO_2 , MnO and H_2O concentrations are comparable to those in the Aillik dykes. K_2O (nd.-5%), Al_2O_3 (nd.-12%) and CO_2 (nd.-35%) are distinctively higher in

TABLE 5.4

Representative Geochemical and Petrographic Data for the Carbonate-Rich Monchiquites

Sample No.	29	227-1	269	307	475	220	200	20	138	228	355	311	3-1	268-A	76
SiO ₂	32.37	33.01	34.86	33.40	32.23	31.04	32.00	30.94	34.78	32.74	32.41	29.13	31.26	35.10	32.85
TiO ₂	5.79	4.74	5.77	5.51	4.18	5.46	5.27	4.09	3.56	4.92	6.21	4.68	3.74	6.31	3.75
Al ₂ O ₃	6.46	5.27	7.34	7.42	5.78	7.48	7.77	3.42	4.15	5.96	6.48	4.68	5.87	7.53	4.74
Fe ₂ O ₃	3.53	4.05	4.61	5.55	4.13	4.34	6.93	4.04	3.62	4.70	6.33	4.14	4.95	6.07	4.20
FeO	11.49	10.42	9.96	8.58	9.74	8.96	7.66	9.24	9.72	7.86	8.22	10.47	9.01	9.43	9.12
MnO	0.20	0.21	0.21	0.22	0.20	0.22	0.26	0.20	0.17	0.21	0.24	0.19	0.24	0.22	0.21
MgO	12.34	13.60	10.40	8.71	16.30	9.20	8.80	18.16	21.29	10.66	8.00	13.18	12.95	9.70	19.82
CaO	12.42	12.10	12.02	16.01	11.09	19.04	19.46	13.10	7.59	16.25	19.73	15.84	14.81	13.40	13.65
Na ₂ O	1.65	1.67	1.83	1.82	1.18	1.43	1.24	0.55	0.51	1.87	1.12	0.63	1.01	1.47	0.40
K ₂ O	1.48	0.88	1.65	2.21	1.47	1.70	2.25	1.09	1.85	1.11	1.29	1.13	2.27	2.68	1.75
P ₂ O ₅	1.31	0.99	1.02	1.74	1.12	2.01	2.33	1.33	0.23	2.19	2.35	1.46	2.15	1.26	1.42
CO ₂	10.07	11.49	7.30	7.16	11.33	6.63	3.15	11.50	10.57	8.95	4.18	7.86	8.54	5.63	5.13
H ₂ O	2.84	1.88	2.74	1.87	1.72	3.33	2.34	1.52	1.74	2.27	2.97	2.96	1.54	1.59	3.32
Total	101.95	100.31	99.66	100.20	100.47	100.84	99.46	99.58	99.78	99.69	99.53	99.35	98.34	100.39	100.36

Trace (PPM)

Zr	362	364	374	713	578	545	1393	363	176	918	423	238	640	450	396
Sr	794	793	850	2805	833	1179	2678	1139	347	3352	619	453	1940	1177	1119
Rb	44	44	48	48	54	53	68	44	67	30	39	75	69	63	61
Zn	111	88	92	104	93	96	90	95	81	94	81	95	118	115	91
Cu	69	75	89	90	68	117	123	56	57	97	140	54	62	96	71
Ba	594	564	661	951	699	1024	902	641	568	918	932	573	952	942	535
Ni	222	445	265	135	372	97	84	450	613	161	72	226	247	147	450
Cr	316	642	499	172	837	132	62	813	739	423	6	276	237	220	789
Nb	196	72	73	125	756	126	301	106	43	131	224	72	110	116	100

C.I.P.W.

Norm

Or			10.04	13.24		10.14				6.71	7.88	7.14	13.82	16.00	9.09
Ab			15.95	13.25						16.18	0.05	5.70	8.81	12.57	
An	12.09	10.52		5.63	10.29	9.18	9.51	6.65	5.25	4.70	9.15	7.06	4.93	6.10	6.14
Ne				1.28		6.71	6.01				5.28				1.88
Lc	6.25	3.64			6.13	0.11	11.03	4.66	7.68						1.21
Na-carb.	3.25	6.34			8.04			5.56	10.39						
Ca	17.56	17.35	17.10	16.51	15.60	15.43	7.58	18.89	11.73	20.82	9.83	19.12	20.01	12.94	11.99
Dp	24.58	29.96	0.29	14.73	18.65	25.27	28.99	15.29	20.60	5.26	38.50	11.17	1.32	13.71	16.73
Hy			20.88							17.28		8.67	10.54	1.20	
Qv	18.46	16.73	7.97	12.44	26.25	11.28	9.92	33.34	32.95	7.24	1.97	21.53	20.65	13.48	35.81
Mag	4.67	5.24	6.88	8.16	5.39	6.44	10.63	5.41	4.70	6.97	9.49	6.42	7.40	8.89	6.26
Il	10.03	8.04	11.19	10.61	7.15	10.62	10.59	7.17	6.06	9.56	12.20	9.50	7.32	12.11	7.23
Cr	0.06	0.12	0.11	0.04	0.16	0.03	0.01	0.16	0.14	0.09		0.06	0.05	0.05	0.17
Ap	2.55	2.05	2.44	4.10	2.34	4.78	5.73	2.85	0.48	5.20	5.65	3.63	5.15	2.96	3.39
Kp															

Modes

Olivine	21.7		10.1						33.5					8.3	
Augite	39.7		53.3						31.1					50.6	
Biotite	11.9		10.9						12.7					17.3	
Ore	15.5		17.9						12.0					16.7	
Carbonate-bearing ocelli	11.2		7.6						10.7					7.1	

	318-3	491-1	470	204-1	204-2
SiO ₂	22.22	30.77	33.29	35.57	35.22
TiO ₂	3.45	3.75	5.65	5.94	6.41
Al ₂ O ₃	3.82	3.95	9.25	8.34	7.72
Fe ₂ O ₃	7.57	6.49	6.46	4.51	5.68
FeO	8.69	6.15	7.88	9.76	9.44
MnO	0.30	0.23	0.26	0.20	0.22
MgO	10.93	20.25	7.08	7.98	10.14
CaO	19.95	14.44	18.26	15.47	14.03
Na ₂ O	0.86	0.39	1.83	2.32	1.53
K ₂ O	1.49	2.03	2.67	1.84	2.37
P ₂ O ₅	3.83	1.35	2.78	1.08	1.14
CO ₂	13.02	7.14	2.96	5.18	3.46
H ₂ O	1.45	3.67	2.88	1.51	1.57
Total	97.58	100.61	100.25	99.70	98.93

Trace (PPM)

Zr	1045	503	867	380	471
Sr	1524	2267	2428	1240	1079
Rb	38	54	76	43	66
Zn	134	81	109	96	97
Cu	49	65	147	90	107
Ba	925	2065	1160	728	688
Ni	135	442	63	112	172
Cr	17	577	13	500	321
Nb	316	151	243	73	94

C. I. P. W.

Norm

Or		12.33		11.05	14.36
Ab		1.53		9.08	2.38
An	5.93	3.12	6.61	7.05	7.38
Ne		1.01	8.65	5.89	5.90
Lc	3.93		12.76		
Na-carb.	2.79				
Ca	26.52	16.69	6.94	11.97	8.07
Dp		12.71	35.67	24.76	27.12
Hy					
Ov	32.74	32.37	1.99	9.43	11.07
Mag	10.81	9.67	9.66	6.64	8.44
Il	6.45	7.32	11.06	11.46	12.48
Cr		0.13		0.11	0.07
Ap	8.76	3.22	6.66	2.55	2.72
Kp	2.08				

Figure 5.2 Histograms showing the variation in major and trace element abundances in the Aillik monchiquites.

S

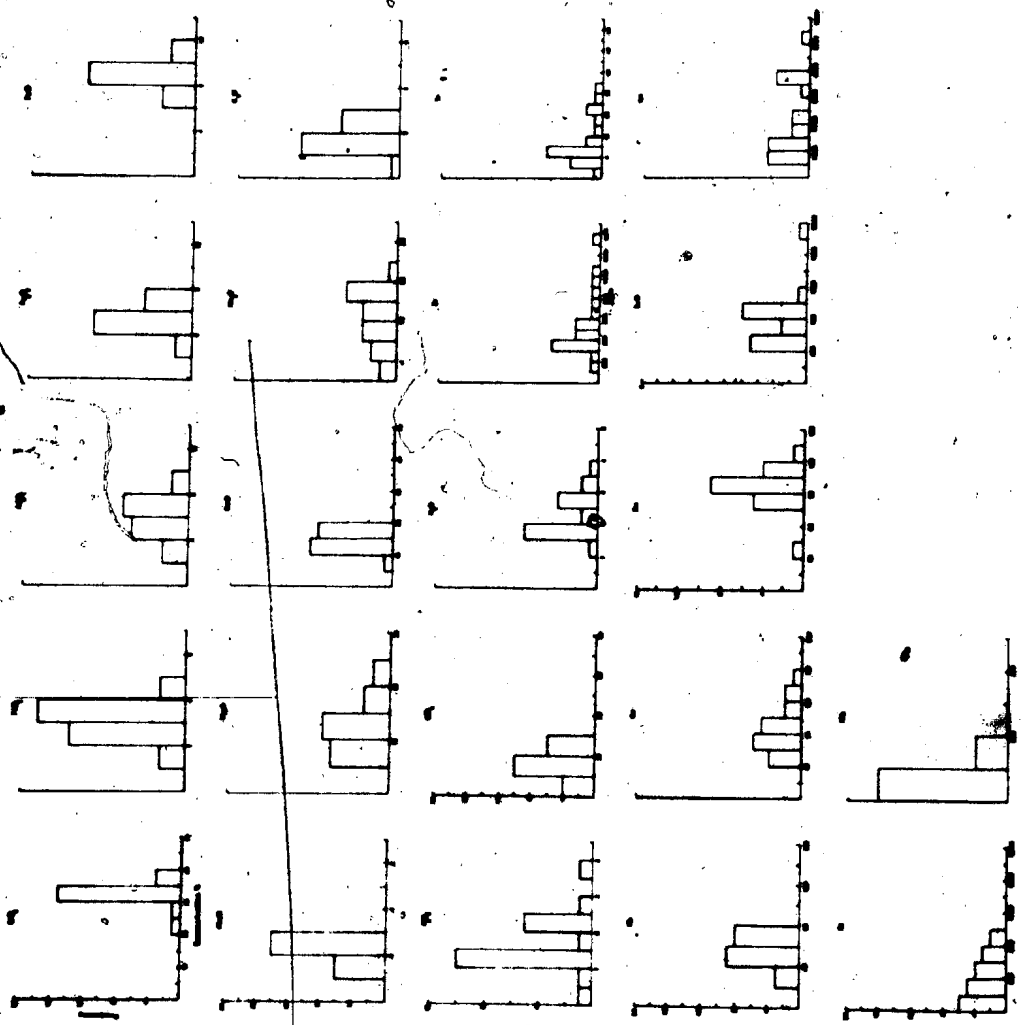
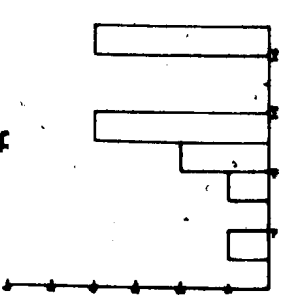
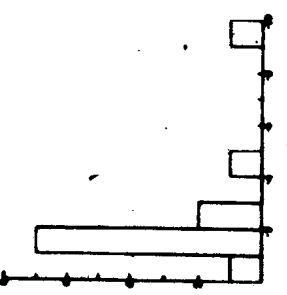
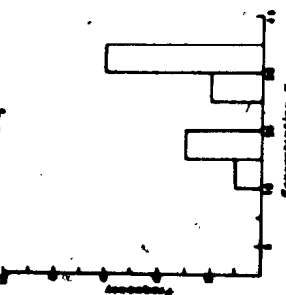
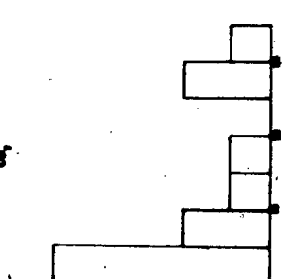
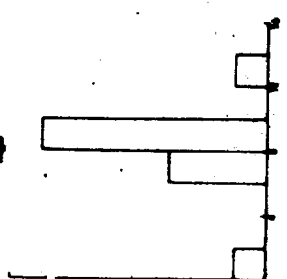
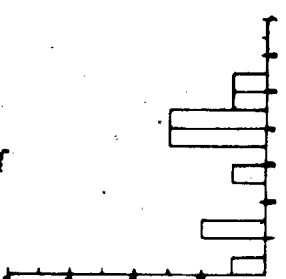
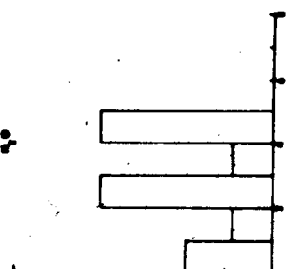
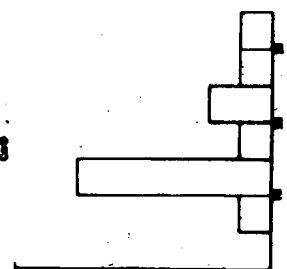
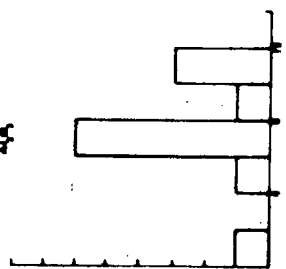
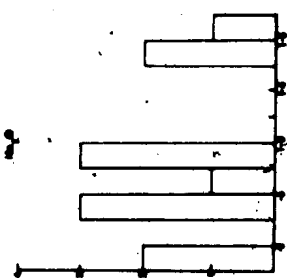
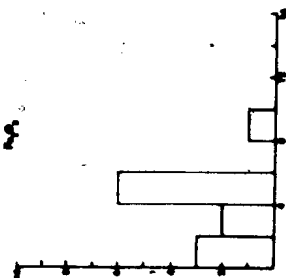
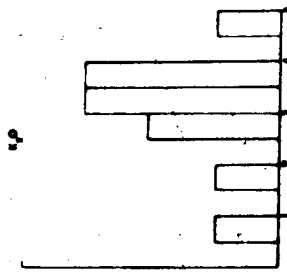
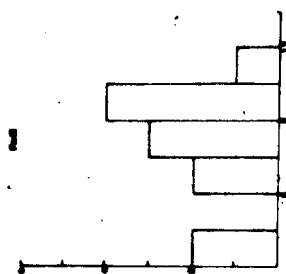


Figure 5.3 Histograms showing the variation in major element abundances for the Callander Bay monchiquites.



several of the Ontario dykes reflecting higher biotite and carbonate contents. Contents of MgO and P_2O_5 are higher in the Aillik dykes and reflect increased olivine and apatite.

Apart from lower SiO_2 and higher CaO and CO_2 (reflecting increased carbonate contents), the monchiquites at Aillik Bay are of similar composition to the average monchiquite analysis given by Métais and Chayes (1963), Table 5.3.

Trace element variation is more pronounced in the monchiquites relative to the minettes. Ba (400-2000 ppm) and Cu (40-160 ppm) are generally higher in the monchiquites. Rb and Nb occur in similar concentrations in the monchiquites as in the minettes, however, Zr (100-1400 ppm), Sr (nd.- 3600 ppm), Ni (500-5500 ppm) and Cr (100-1400 ppm), may be comparable or distinctively higher in some dykes.

5.2.4 Kimberlites

The kimberlites are distinctly ultrabasic in composition (SiO_2 , 10-30%) and exhibit a very wide compositional range (Fig. 5.4). Contents of Fe_2O_3 (2-14%), TiO_2 (3-7%), FeO (2-10%), H_2O (0.5-4.5%) and MnO (0.2-0.4%) are in similar or slightly higher concentration than in the carbonate-rich monchiquites and minettes; however, P_2O_5 , K_2O , MgO , Al_2O_3 , Na_2O , and H_2O are present in amounts comparable to values obtained for the carbonate-rich monchiquites. CaO (10-35%) and CO_2 (nd.-30%) are considerably higher in the kimberlites and reflect their high carbonate contents.

TABLE 5.5
REPRESENTATIVE GEOCHEMICAL AND PETROGRAPHIC DATA FOR THE AILLIK KIMBERLITES

Sample No.	205-4	212	211-1-B	211-4-B	205	51-1	25-1	416	496-1	496-2	454	453-2	453-3	453-4	13-1	6-1	258-3	270
SiO ₂	20.60	24.88	23.97	23.22	19.94	26.60	28.92	27.55	13.89	25.03	24.68	24.23	24.45	22.11	19.29	25.29	29.41	25.64
TiO ₂	3.70	3.36	3.14	3.00	3.24	2.70	4.37	4.06	1.79	2.83	2.83	2.98	2.75	2.65	3.34	3.85	3.07	3.92
Al ₂ O ₃	3.75	3.63	3.80	3.13	2.80	4.19	5.72	5.42	2.27	2.98	3.33	3.37	3.37	2.54	3.36	5.14	3.68	2.99
Fe ₂ O ₃	8.16	5.89	5.18	5.32	11.60	3.15	4.07	6.12	3.76	5.23	5.34	6.49	13.42	7.17	7.69	2.22	4.73	5.49
FeO	7.02	7.01	7.23	6.53	7.36	7.74	7.26	6.55	4.70	8.92	7.72	6.92	6.50	4.54	5.68	9.54	7.78	7.92
MnO	0.30	0.26	0.29	0.24	0.27	0.21	0.26	0.29	0.27	0.39	0.31	0.28	0.26	0.28	0.30	0.29	0.24	0.24
MgO	16.36	18.85	19.61	17.85	17.60	16.90	14.05	15.30	12.35	23.79	24.82	25.37	20.63	13.15	12.91	10.09	24.00	24.50
CaO	18.80	17.79	19.52	21.38	18.85	14.79	19.27	16.97	34.77	16.74	17.58	17.31	17.42	18.15	25.82	21.09	14.91	13.23
Na ₂ O	0.13	0.14	0.14	0.11	0.07	0.76	0.71	0.60	0.28	0.14	0.13	0.10	0.31	0.39	0.10	0.42	0.20	0.22
K ₂ O	2.23	2.21	2.23	2.11	1.95	1.86	3.41	2.88	0.82	1.18	1.72	1.41	1.67	1.59	1.76	1.90	1.88	1.52
P ₂ O ₅	2.32	1.84	2.21	4.05	3.18	1.68	1.64	1.85	1.39	2.69	1.94	2.09	2.06	2.03	1.95	2.03	1.29	1.50
Co ₂	13.27	9.47	11.14	9.97	11.35	15.70	9.27	10.74	22.89	7.96	8.17	7.71	15.64	15.45	16.06	16.13	7.97	9.68
H ₂ O	2.76	4.08	1.53	1.65	1.94	4.12	1.34	2.00	0.66	2.48	1.95	2.38	2.72	5.07	1.19	1.66	2.25	3.89
Total	99.40	99.41	99.99	99.56	100.15	100.40	100.29	100.33	99.85	100.36	100.52	100.64	111.20	99.12	99.75	99.65	100.69	100.44

Trace (PPM)

Zr	576	618	707	1040	513	408	642	571	1520	759	553	711	354	430	614	613	359	356
Sr	1220	2198	2795	3137	1512	1441	3761	1150	10907	3489	3432	3548	1602	2162	1466	1199	1523	1903
Rb	65	65	62	62	59	40	92	64	21	34	48	41	51	44	59	47	59	44
Zn	70	81	75	61	69	87	89	81	60	88	88	90	76	78	121	92	84	83
Cu	69	81	74	79	65	47	82	71	33	41	41	67	59	48	72	63	56	34
Ba	1681	1265	1097	982	1617	902	2262	2252	1141	1540	1350	1240	1307	1292	1289	857	1155	871
Ni	181	353	323	278	176	449	151	236	170	414	385	416	400	375	158	170	530	462
Cr	192	763	681	554	144	589	155	219	192	414	425	474	220	258	158	124	595	584
Nb	266	176	195	232	224	165	277	200	367	388	223	204	192	186	236	184	173	187

C.I.P.W.

Norm

Or					4.21			17.27									3.03	
Ab								3.83										
An	3.57	2.91	3.24	1.90	1.59	5.52	2.39	3.64	2.55	4.17	3.58				4.40	7.97	3.64	
Ne		0.68	0.66	0.53	0.33		3.32	0.72	1.37	0.67	0.62				0.46		0.93	
Lc		10.84	10.60	10.23	5.88	4.01	16.10			2.19					8.27	1.50	6.45	
Kp	18.37					2.89			5.14	2.53	9.56					4.95		
Na carb.	1.83					12.77										3.58		
Ca	27.84	22.80	25.98	23.72	26.22	21.10	21.49	24.78	53.73	18.80	19.41				37.04	31.37	18.36	
Dp		5.76	0.16	4.17	0.35		14.28	1.24							7.29		7.01	
Ov	39.82	36.52	29.89	35.46	31.08	40.97	24.03	27.30	27.87	51.61	53.18				20.66	36.15	44.56	
Mag	11.59	9.04	7.70	8.07	15.42	4.24	6.01	9.00	5.63	7.87	8.09				90.81	3.05	6.95	
Lt	6.88	6.75	6.12	5.96	6.25	4.76	8.46	7.82	3.51	5.58	5.62				6.43	6.93	5.91	
He					1.15										1.11			
Cr	.04	0.17	0.15	0.12	0.03	0.12	0.03	0.05	0.04	0.06	0.10				0.03	0.03	0.13	
Ap	5.28	4.53	5.51	9.85	7.51	3.63	3.88	4.36	3.33	6.49	4.71				4.60	4.47	3.04	

Modes

Olivine		22.9								39.3		38.5			21.6			
Phlogopite		23.5								21.2		17.3			18.3			
Ore		12.1								12.7		15.5			10.4			
Augite		3.7								6.1		7.0			0.1			
Apatite		1.5								0.5		1.7			7.5			
Matrix (mainly carb.)		36.4								20.2		20.0			42.5			

328	240A-B-1	240-A-1	240-B-1	493-1	14-2	302	303-A	303-C	296-B	296-A	19-1	19KC-B	230-1	10-1	207-1	487-1	317	266-1	506-1
-----	----------	---------	---------	-------	------	-----	-------	-------	-------	-------	------	--------	-------	------	-------	-------	-----	-------	-------

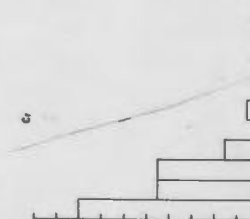
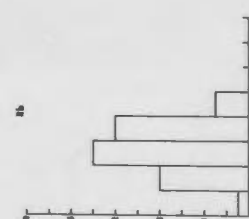
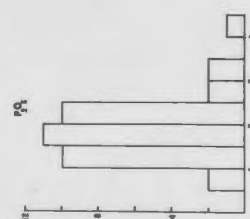
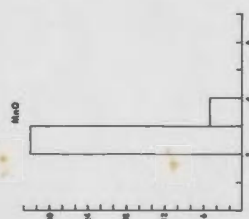
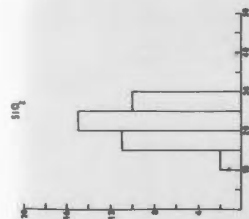
28.38	21.91	23.10	21.17	21.71	26.43	25.66	17.86	20.22	19.63	18.44	19.97	17.75	16.86	13.23	18.03	22.80	15.68		
3.18	2.75	3.25	3.04	4.34	3.26	3.61	3.45	3.38	3.32	2.83	2.25	1.84	2.56	1.58	2.80	3.69	2.22		
3.11	3.14	3.50	3.39	3.93	3.10	3.77	3.59	3.03	4.18	3.47	3.06	3.28	3.10	1.92	2.63	2.99	2.91		
3.26	3.19	3.79	2.71	5.27	4.08	2.50	4.63	3.66	3.72	3.88	3.55	3.19	4.25	2.52	7.13	5.92	6.08		
7.76	6.46	7.82	5.77	6.27	8.39	8.63	6.26	7.49	7.87	7.68	6.26	4.52	6.09	4.91	5.88	6.21	6.95		
0.21	0.27	0.27	0.30	0.24	0.22	0.26	0.26	0.26	0.28	0.36	0.35	0.36	0.27	0.26	0.28	0.27	0.26		
23.40	12.63	16.00	8.19	15.03	21.02	21.88	14.00	14.00	14.66	13.63	12.77	8.07	9.94	9.33	15.43	19.00	20.70		
12.40	21.33	15.65	26.52	22.00	12.91	12.35	24.30	20.78	19.27	19.15	22.49	30.06	30.33	32.23	24.43	20.52	26.63		
0.30	0.38	0.58	0.14	0.84	ND	0.31	0.32	0.49	0.40	0.61	0.76	0.72	1.04	0.63	0.11	0.10	0.06		
1.84	1.66	2.28	0.91	2.32	1.68	2.32	2.19	2.17	2.62	2.44	2.10	1.66	1.08	0.73	1.93	1.70	0.58		
0.88	1.13	1.11	1.02	1.64	1.51	1.07	1.96	2.15	2.03	1.93	1.47	0.84	2.58	2.43	3.35	1.42	2.38		
11.86	22.01	19.69	25.14	15.93	14.48	14.26	20.33	21.14	20.86	21.61	22.46	25.60	20.89	27.11	14.32	14.96	15.72		
3.77	1.60	2.89	2.10	1.08	3.56	4.01	1.83	2.22	1.94	2.68	2.46	2.85	0.90	2.55	3.61	1.01	0.77		
100.35	98.46	99.93	100.40	100.60	100.64	100.63	100.98	100.99	100.78	98.71	99.95	100.74	99.89	99.43	99.93	100.59	100.94		

325	394	571	375	638	295	486	752	690	774	652	325	316	690	301	730	491	855		
1271	960	1150	978	1759	1172	2075	1846	1501	3460	3049	2085	1611	2317	1528	3129	1594	3830		
58	51	64	31	71	63	87	80	94	76	53	53	41	27	20	64	58	28		
85	68	81	42	64	80	88	60	66	86	104	67	79	105	79	77	75	63		
44	49	71	64	81	50	30	72	60	43	42	31	31	48	38	64	61	42		
1163	2106	2252	1978	1216	1035	2374	925	990	2532	2574	2017	2395	1142	1757	1824	807	1613		
539	230	236	204	188	541	494	131	136	157	154	277	226	88	216	153	317	206		
797	218	219	171	317	1011	194	219	206	64	35	98	65	11	203	192	570	151		
163	295	200	359	259	138	202	222	239	384	448	368	317	225	196	255	275	233		

													6.43						
													3.23						
2.94													0.61		1.03				
													3.06		0.53				
3.03															8.55				
5.93															0.61				
6.79																			
19.57													47.87		34.19				
													1.67						
52.22													19.99		30.43				
4.55													6.21		10.85				
5.82													4.90		5.58				
0.17															0.04				
1.97													6.04		8.17				

	39.8	38.2	15.3
	5.8	13.0	25.1
	11.7	10.1	2.2
		3.9	0.2
	42.7	34.8	57.2

Figure 5.4 Histograms showing the variations in major and trace element abundances for the Aillik kimberlites.

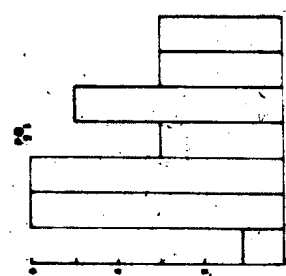
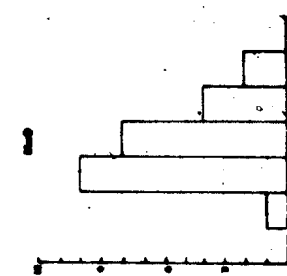
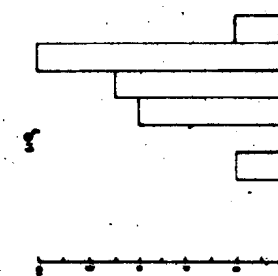
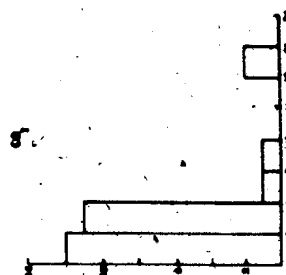
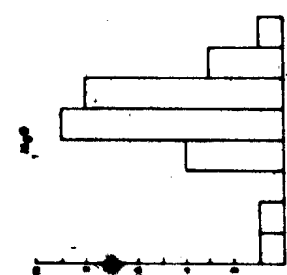
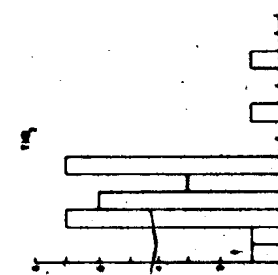
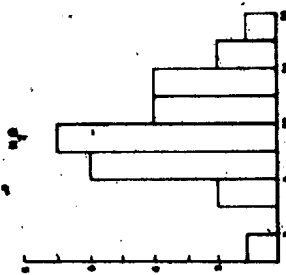
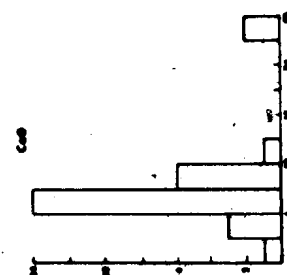
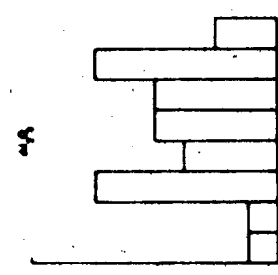
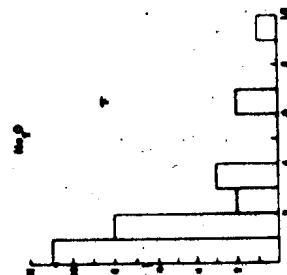
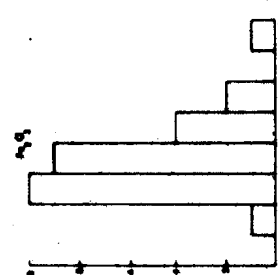
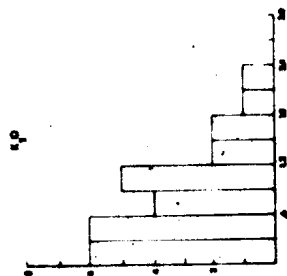
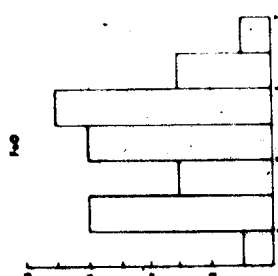


Histogram plots for the Lesotho kimberlites (calculated from analyses presented by Nixon, 1973) are shown in Figure 5.5 for comparison with the Aillik data. The values of Fe_2O_3 , K_2O , Al_2O_3 , MnO and Na_2O are comparable to the Aillik dykes however TiO_2 , P_2O_5 , CaO , FeO , and CO_2 are distinctively lower in the Lesotho dykes and SiO_2 is higher (compare Figs. 5.4 and 5.5). MgO exhibits a similar range for both kimberlite suites however a greater proportion of dykes from Lesotho have high MgO contents.

The Aillik dykes differ significantly from average kimberlite analyses presented in Table 5.3 as they have low SiO_2 and MgO and higher TiO_2 , Total Fe, CaO , and CO_2 . Concentrations of Al_2O_3 , Na_2O , K_2O and H_2O fall within the range of kimberlite compositions. The major difference in the major element chemistry between these two kimberlite occurrences appears to be the increased carbonate and opaque oxide contents of the Aillik dykes.

Trace element contents observed in the Aillik kimberlites are extremely variable. Zr (200-1400 ppm), Sr (nd.-4000 ppm), Ni (500-4500 ppm), Cr (nd.-1200 ppm) and Cu (20-100 ppm) are similar to the variations observed in the carbonate-rich monchiquites; however, they are distinctively higher than those in the minettes. Values for Rb (nd.-100 ppm) and Ba (600-2000 ppm) are comparable to those obtained from the carbonate-rich monchiquites and minettes. Nb (nd.-600 ppm) is significantly higher in the kimberlites reflecting the carbonatitic nature of the matrix (Heinrich, 1966).

Figure 5.5 Histograms showing the variation in the major element abundances for the Lesotho kimberlites.



5.2.5 Carbonatites

Geochemical and petrographic data for several carbonatites and metasomatic carbonatites are presented in Table 5.6. They are characterized by low amounts of SiO_2 (nd.-25%); the higher concentrations being from metasomatic carbonatites (Fig. 5.6). Values for P_2O_5 (nd.-4%), FeO (nd.-10%) and H_2O (1-3.5%) are comparable with concentrations observed within the kimberlites; however TiO_2 (nd.-3%), and Fe_2O_3 (nd.-8%) are slightly lower in the carbonatites. CaO , Al_2O_3 , Na_2O , MnO and CO_2 exhibit a similar range as in the kimberlites; however CO_2 (10-40%) and CaO (nd.-40%) are usually higher (reflecting their carbonatitic nature).

The Aillik carbonatites fall within the range for average carbonatite compositions (Gold, 1966) (Table 5.3); however, the Aillik dykes exhibit higher SiO_2 and lower CaO which reflects higher concentrations of silicate phases. The average analysis has also been affected by the addition of metasomatic carbonatite compositions.

Values for Ba, Zr, Rb, Ni, Cr and Cu are generally present in concentrations lower than those observed in the kimberlites and reflect decreased contents of opaque oxides, olivine and mica. Sr (nd.-5600 ppm) and Nb (nd.-1000 ppm) are higher than in the kimberlites and are similar to those observed in other carbonatites (Heinrich, 1966; Tuttle and Gittins, 1966).

TABLE 5.6
Representative Geochemical and Petrographic Data for the Aillik Carbonatites

Sample No.	413	365	325-4	349-1	364	315	332	231-1
SiO ₂	18.71	6.45	11.27	11.00	23.48	18.05	4.11	13.50
TiO ₂	2.58	0.74	0.69	0.11	1.64	2.63	0.01	13.0
Al ₂ O ₃	4.36	1.66	1.45	0.88	6.29	6.08	0.01	3.67
Fe ₂ O ₃	5.54	0.03	2.27	0.61	2.06	0.94	0.70	2.68
FeO	3.50	4.67	5.00	2.56	8.13	9.85	1.13	4.65
MnO	0.25	0.28	0.30	0.38	0.23	0.23	0.59	0.50
MgO	11.11	7.63	12.05	11.90	14.98	15.45	15.20	10.07
CaO	29.54	37.90	32.58	37.00	16.60	15.80	32.75	26.59
Na ₂ O	0.31	0.40	0.09	0.10	0.88	0.90	0.47	1.24
K ₂ O	1.40	0.68	0.33	ND	1.97	1.10	0.15	1.98
P ₂ O ₅	1.59	3.93	4.33	0.61	1.58	1.61	0.08	2.96
CO ₂	20.77	33.19	28.09	33.37	18.36	26.77	39.14	27.98
H ₂ O	1.03	1.04	1.41	2.04	3.46	1.35	2.83	1.87
Total	100.69	98.60	99.86	100.56	99.66	100.86	97.17	98.99

Trace (PPM)

Zr	598	500	543	470	376	596	282	518
Sr	3467	4572	787	5464	2594	2073	2632	4366
Rb	35	11	6	N.D.	25	71	N.D.	18
Zn	77	83	41	94	142	99	119	114
Cu	54	33	21	12	33	35	16	15
Ba	1310	1551	1806	829	300	826	493	819
Ni	126	53	77	44	150	336	36	51
Cr	23	2	10	2	678	578	3	3
Nb	338	961	252	260	424	187	72	963

C.I.P.W.

NORMS

Or	8.28		
Ab	2.62		
An	6.34	1.03	
Ne		0.53	
Lc		8.86	
Kp		0.39	
Co	.01		

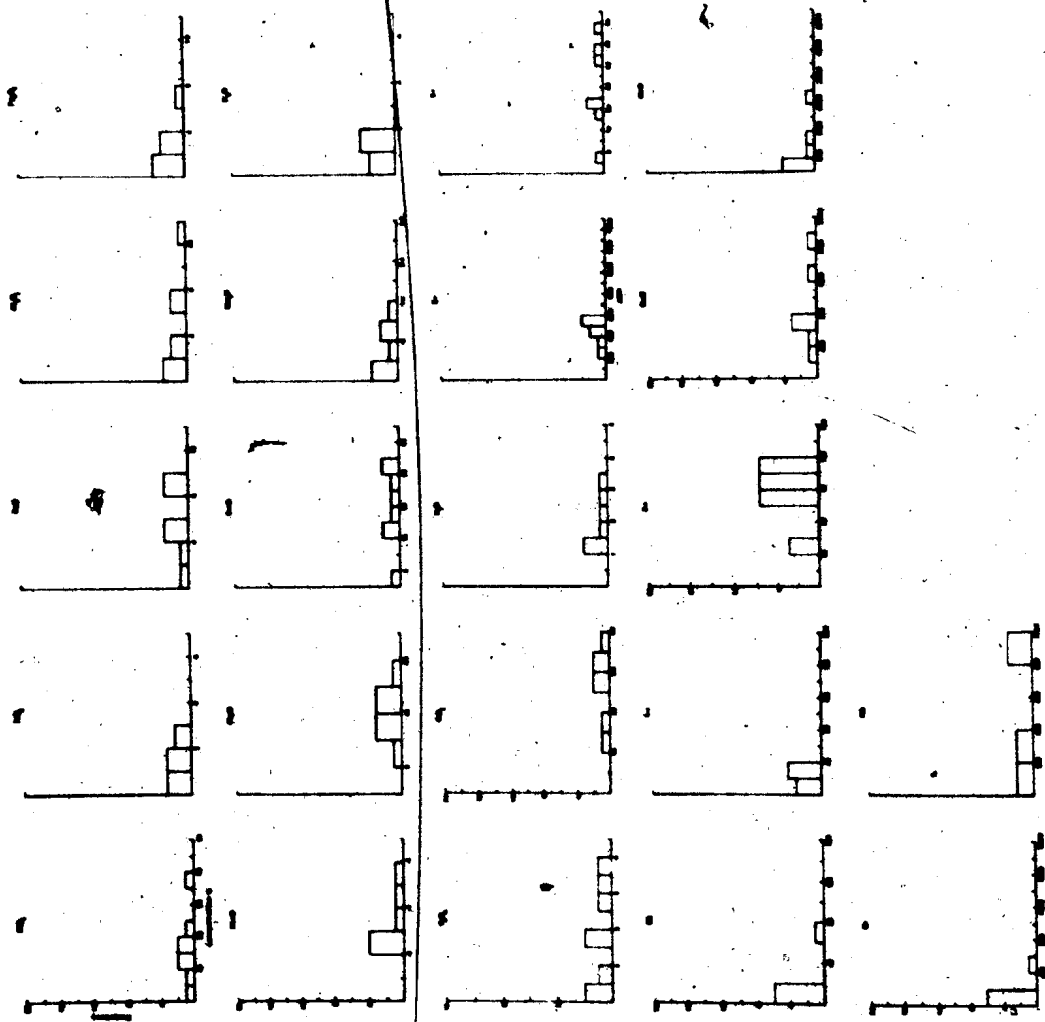
Na-Carb.

Ca	47.25	34.21
Hy	1.78	
Ov	18.14	30.32
Mag	4.61	10.86
Il	4.90	5.59
He	2.36	
Cr	0.01	0.04
Ap	3.70	8.18

Modes

Calcite	100.0	97.0
Ore		2.0
Chlorite		1.0

Figure 5.6 Histograms showing the variation in major and trace element abundances for the Aillik carbonatites.



5.3 Variation Diagrams

5.3.1 Introduction

Variation diagrams are presented in Figures 5.7 to 5.11 to depict chemical variations within the individual compositional groups of dykes and to demonstrate a possible co-magmatic relationship between the suite as a whole.

5.3.2 Harker Diagrams

Harker variation diagrams constructed from analyses given in Tables 5.2 and 5.4 to 5.6, are presented in Figures 5.7 and 5.8. A correlation matrix listing Pearson correlation coefficients for all dyke compositions is given in Table 5.7. This statistical investigation has enabled a detailed analysis of significant variations within the dyke swarm. Al_2O_3 (+0.86) and CO_2 vs CaO (+0.73) (Fig. 5.7) show a positive correlation for all dyke suites, although a significant increase in the Al_2O_3 occurs within the carbonate-rich monchiquites. The CO_2 vs CaO variation implies that these elements are mainly confined to calcium carbonate and occur in increasing concentrations from the minettes to the carbonatites. TiO_2 (+0.57) and FeO (+0.59) show a positive correlation for the kimberlites, carbonatites, and carbonate-rich monchiquites; however, the minette analyses lie below the trend outlined by the above dykes (Fig. 5.7). Negative correlations are exhibited by CaO , CO_2 , and MnO (-0.87, -0.84, and -0.70 respectively) and the fields outlined by the chemical analyses of the kimberlites, carbonatites and carbonate-rich

[illegible]

Figure 5.7 Harker variation diagrams for Aillik major element analyses.

- ▲ minettes, ■ monchiquites,
- kimberlites, ○ carbonatites

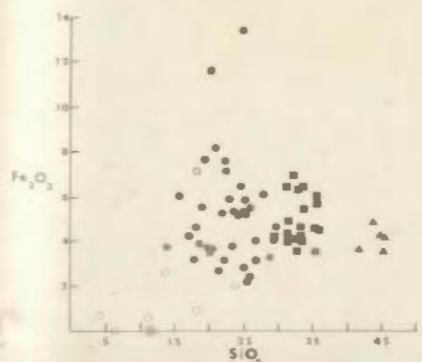
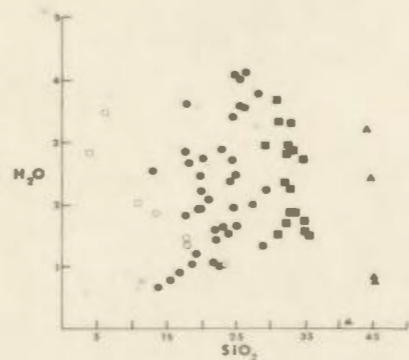
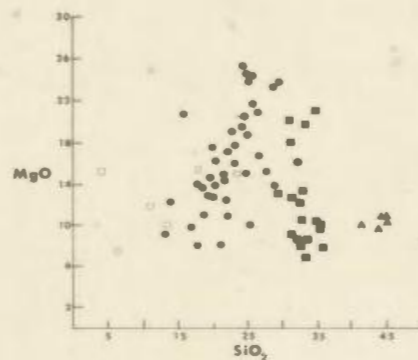
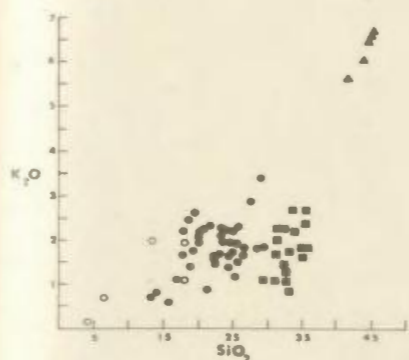
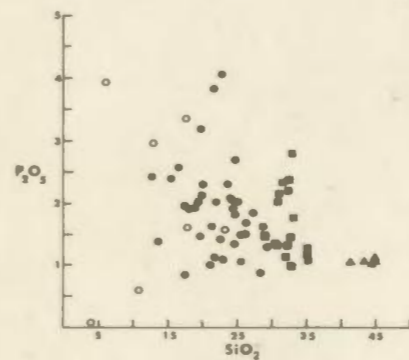
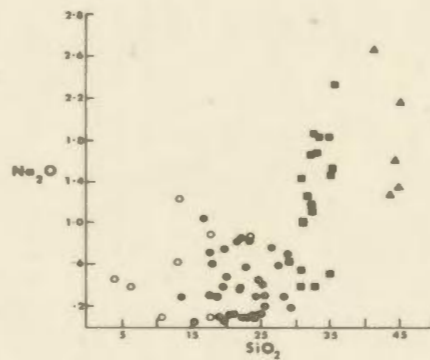
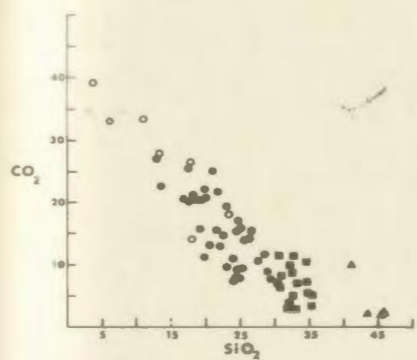
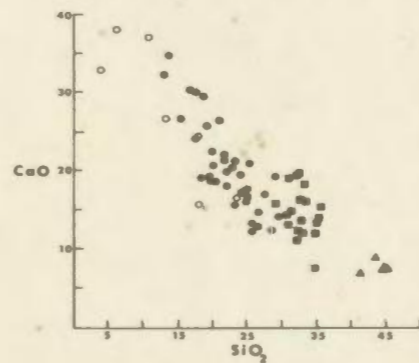
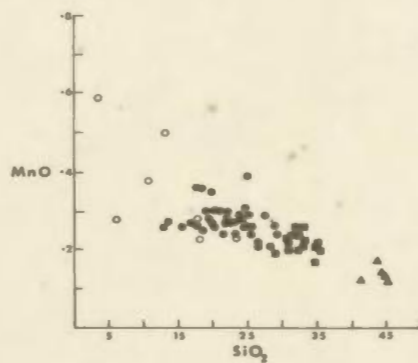
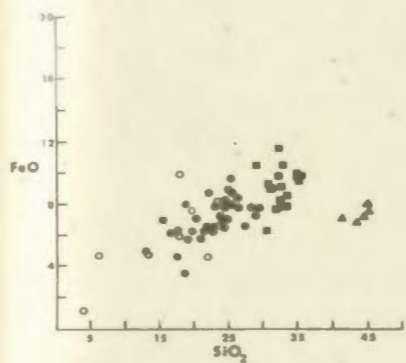
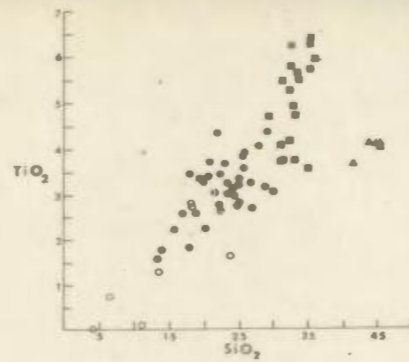
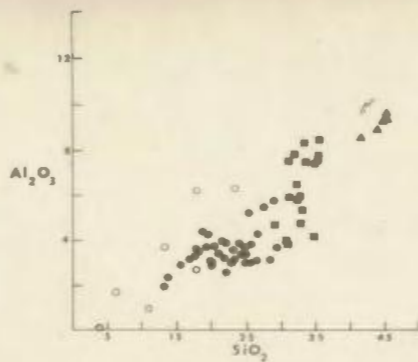
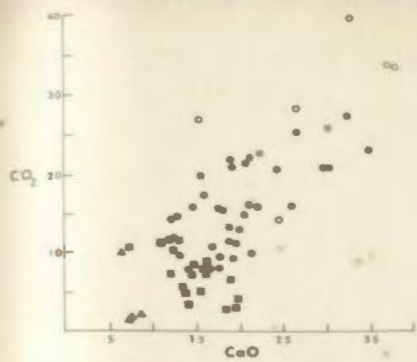
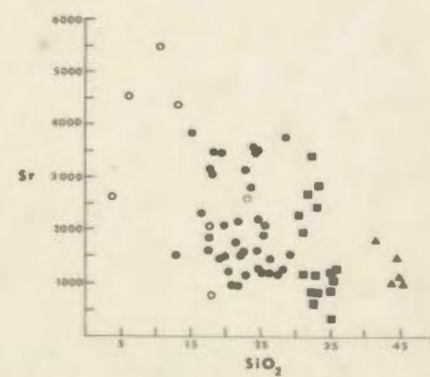
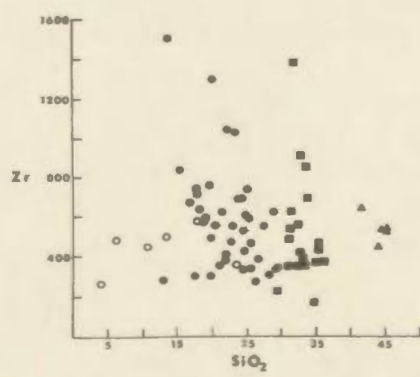
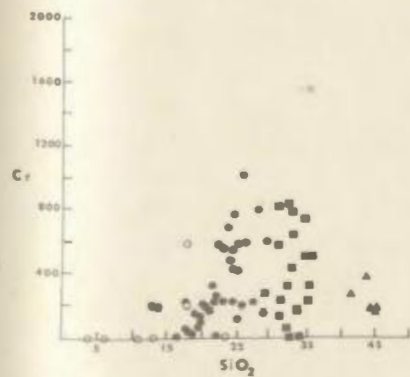
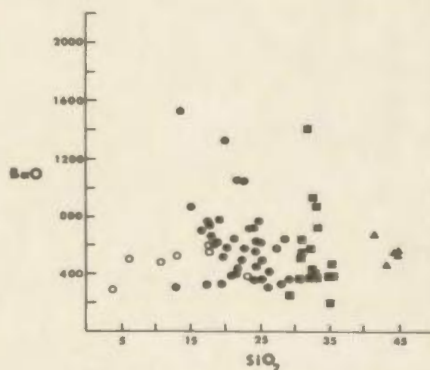
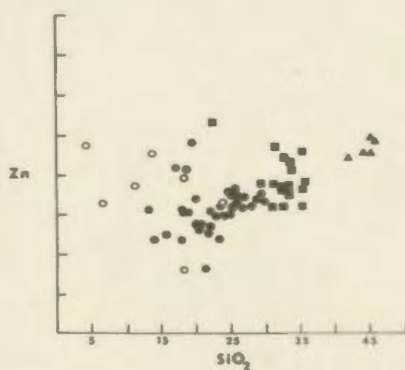
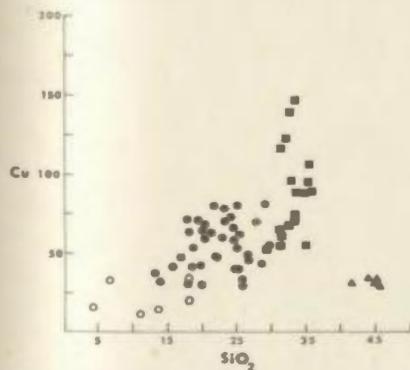
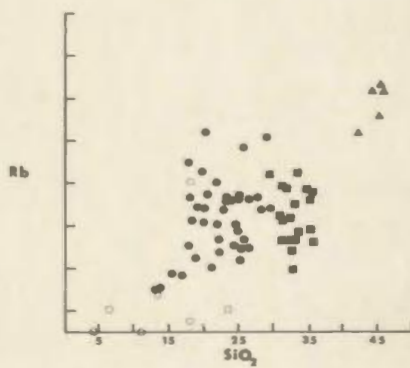
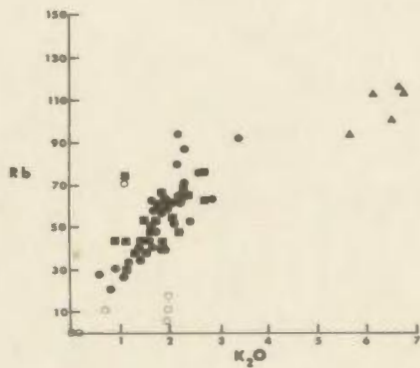
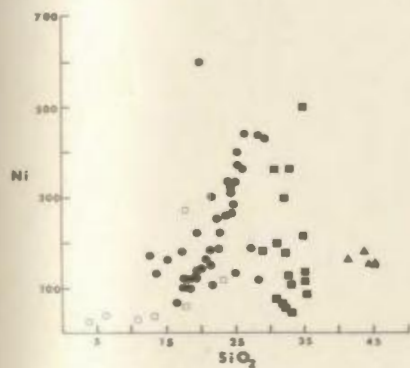
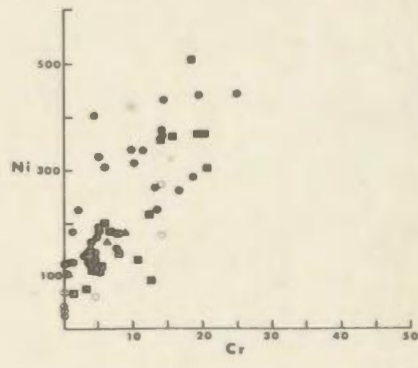
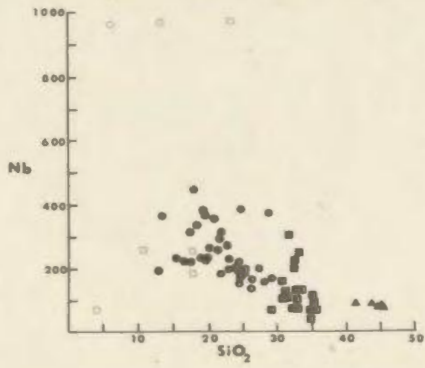
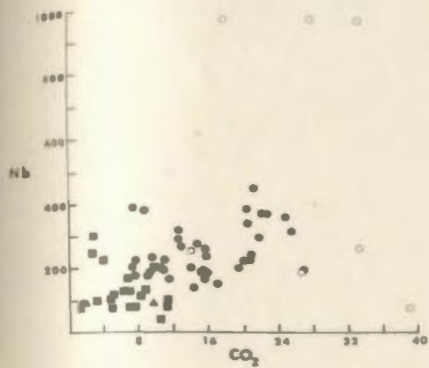


Figure 5.8 Harker variation diagrams for Aillik trace element analyses.



monchiquites are distinct in the MnO and CO₂ plots but overlap in the CO₂ (Fig. 5.7). Diagrams depicting concentrations of Fe₂O₃, H₂O, Na₂O, K₂O, MgO and P₂O₅ show no correlation for the dyke suite although K₂O and MgO exhibit a positive correlation for the minettes and the kimberlites respectively.

Nb vs CO₂ (+0.50) exhibits a positive correlation (Fig. 5.8) for the minettes, carbonate-rich monchiquites and kimberlites; however, the carbonatites show a irregular distribution and a marked division is apparent between the carbonatites and metasomatic carbonatites. The carbonatites exhibit high Nb contents while the metasomatic carbonatites have lower values and are comparable with the kimberlites. Ni vs Cr (+0.66) (cf. Frantsesson, 1970) also shows a positive correlation but considerable overlap occurs between the various dyke groups. Most carbonate-rich monchiquites are characterized by normal ultramafic ratios $Cr/Ni \geq 1$ (Dawson, 1967b, Fesq et al., 1975); however, several kimberlites exhibit low ratios. Rb vs K₂O (+0.79) shows positive correlation for the carbonate-rich monchiquites and kimberlites; however, the minettes plot below the other dykes.

The correlations observed for MnO, Al₂O₃, CaO and CaO vs CO₂ indicate that the carbonatites, kimberlites and carbonate-rich monchiquites form a consanguineous series. The offset of the minette analyses in respect to some elements in certain diagrams (CO₂, FeO and TiO₂) possibly implies that the minettes are not related to the bulk of the ultrabasic.

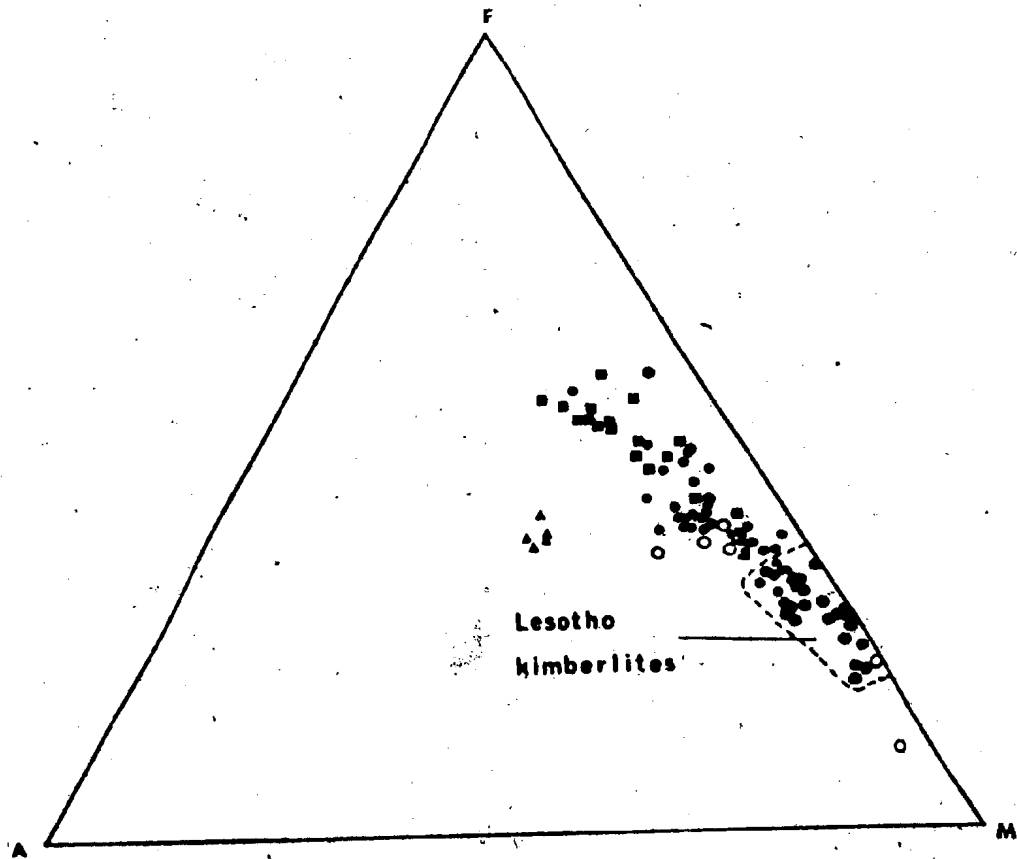
suite. The carbonatites and kimberlites usually exhibit a good correlation (plot on a straight line) although analyses may overlap. The above results are interpreted to suggest that the carbonatites have evolved from a kimberlitic magma either as a result of liquid immiscibility (cf. Dawson and Hawthorne, 1973; Mitchell and Fritz, 1973; Clement, 1975; Ferguson et al., 1975) and/or fractional crystallization of a magma of kimberlitic composition (cf. Janse, 1975; Gittins et al., 1975). In general the kimberlites and carbonate-rich monchiquites also show a good correlation with respect to major and trace element chemistry and exhibit a considerable degree of overlap with respect to their chemical composition suggesting that they too are co-magmatically related.

5.3.3 FMA Diagram

Analyses of the four major groups of dykes in the Aillik area are plotted in a ternary FMA diagram in Figure 5.9. The carbonatites, kimberlites and carbonate-rich monchiquites plot on an Fe enrichment trend which differs from that displayed by the minettes. The fields of kimberlite, carbonatite and carbonate-rich monchiquite also show a considerable degree of overlap which suggests that they may form part of a consanguineous series which differentiated from a common parent. The location of the minettes in the diagram implies that they may be unrelated to the other dyke groups. Also shown in Figure 5.9 are the analyses for Lesotho kimberlites. They are characterized by higher concentrations of MgO compared to the Aillik dykes; however, they do exhibit a trend towards iron enrichment and overlap with the Aillik dykes.

Figure 5.9 FMA ternary diagram showing Aillik and Lesotho dyke analyses.

- | | |
|-----------------------|----------------|
| ▲ minettes | ■ monchiquites |
| ● kimberlites | ○ carbonatites |
| ● Lesotho kimberlites | |



5.3.4 ($\text{SiO}_2 + \text{Al}_2\text{O}_3 + \text{Alkalis}$) vs Volatiles vs ($\text{CaO} + \text{MgO} + \text{FeO} + \text{Fe}_2\text{O}_3 + \text{TiO}_2$) Ternary Diagram

This ternary diagram was first used by Dawson (1960) to show that by increasing the CaO/MgO ratios and/or decreasing SiO_2 , kimberlites grade either into alnöites or carbonatites. It was intended to exhibit the genetic relationship between kimberlites, carbonatites and alnöites; however, Mitchell (1970) criticized its use on the basis of the following arguments:

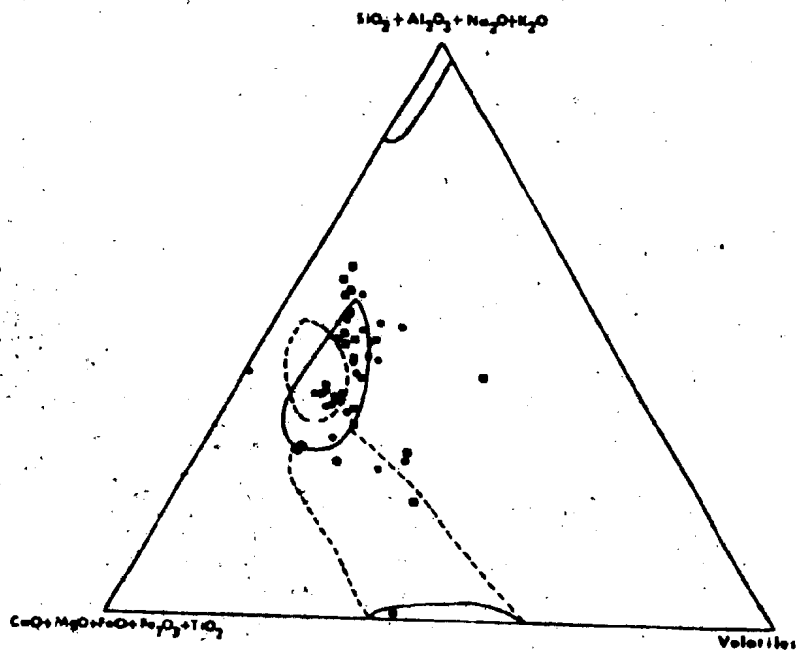
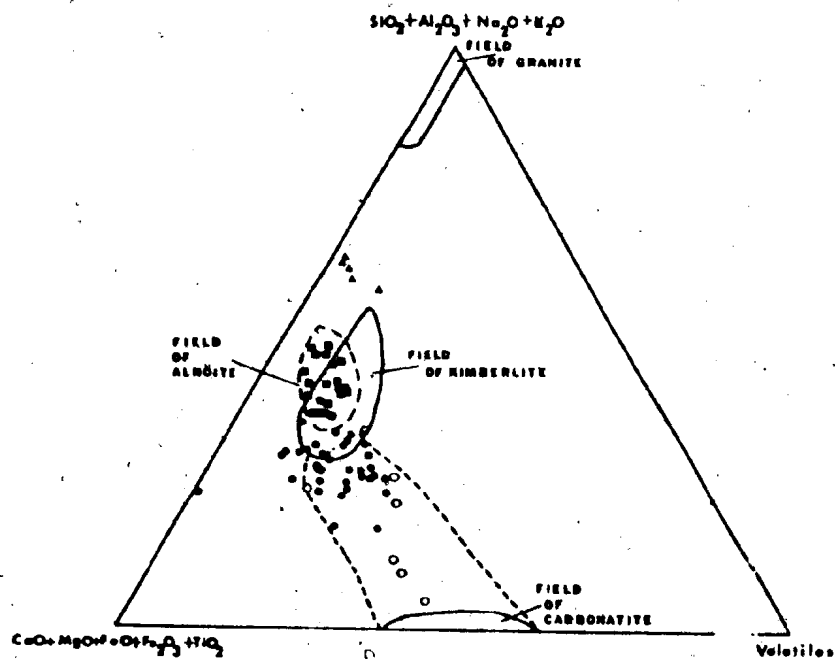
1. The rocks plotted by Dawson (1960) do not represent a continuous series produced by fractional crystallization of a common parental magma, and
2. Chemical gradations can be produced between any given series of rock types if enough selectively of oxides present and choice of analysis is used.

Recent studies (Gittins *et al.*, 1975; Janse, 1975) however, partially support Dawson's (1960) original contention. When plotted on a similar ternary diagram, the Aillik dykes define a broad gradational compositional band which truncates above the carbonatite field (Fig. 5.10a). The carbonate-rich monchiquites plot within the alnöite field; however, overlap does occur with the kimberlites. The kimberlites and carbonatites also overlap but a distinct gradation into the carbonatite field is discernable and the majority of the kimberlite analyses are restricted to the carbonate-rich kimberlite field. The minettes lie above the kimberlite and carbonate-rich monchiquite analyses and are apparently unrelated to the other dykes. Similar trends have been reported in

Figure 5.10a Dawson's ternary diagram containing Aillik dyke analyses.

Same symbols as in Figure 5.9.

Figure 5.10b Dawson's ternary diagram containing Lesotho kimberlite (●) and Callander Bay monchiquite (■) analyses.

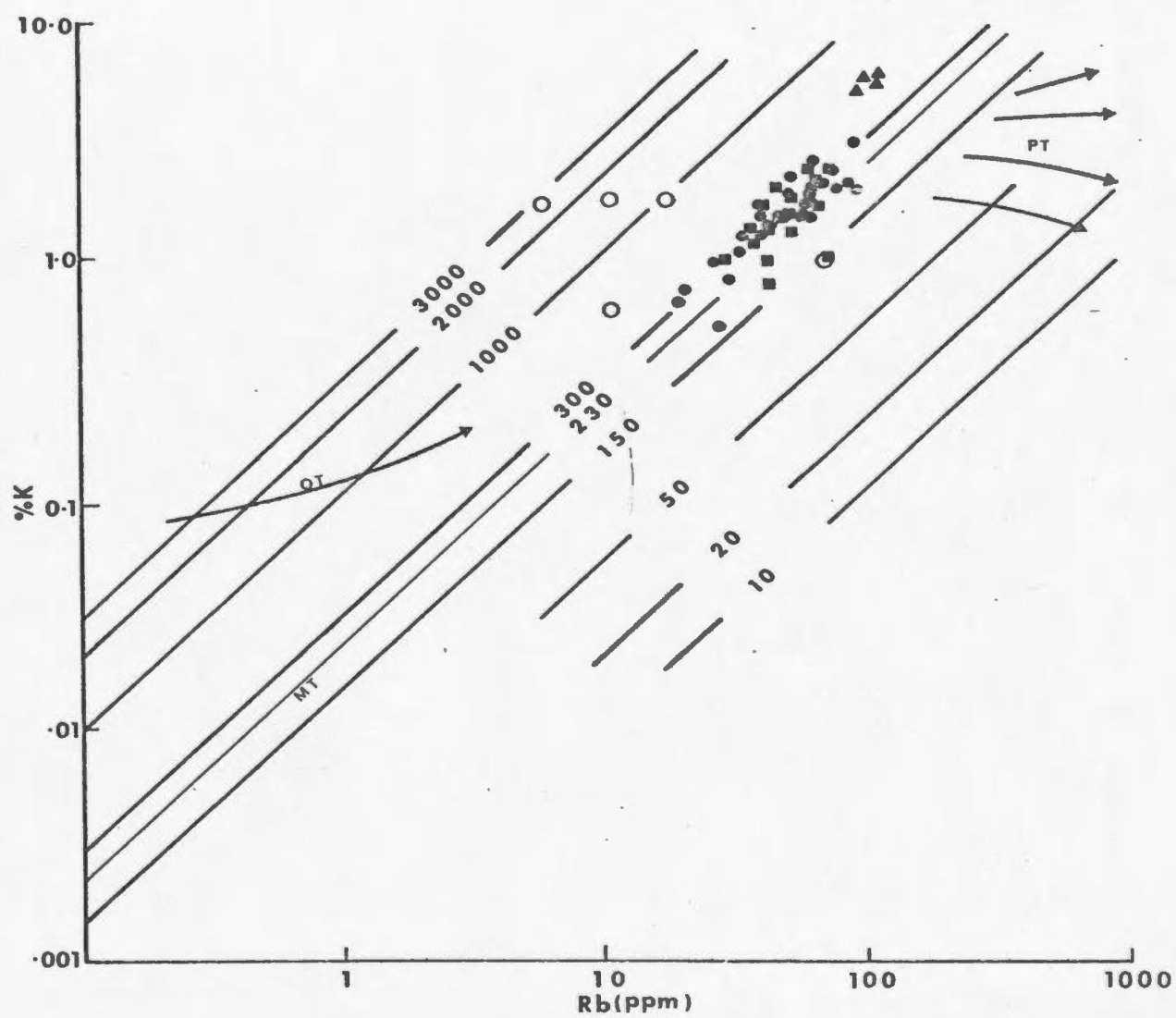


kimberlites and carbonatites by Gittins et al. (1975) and Janse (1975) and are interpreted for the Aillik dykes, by the author to represent a differentiation sequence from lamprophyre (monchiquite) to carbonatite. For comparison, analyses of Lesotho (Nixon, 1973) and Benfontein kimberlites (Dawson and Hawthorne, 1973) are plotted in Figure 5.10b. The Lesotho kimberlites plot within the kimberlite and alnöite fields; however, they plot above the field of the Aillik dykes (compare Figs. 5.10a and 5.10b). The Benfontein analyses are similar to the Aillik kimberlites and their position in the diagram probably reflects their higher carbonate contents. From Figures 5.10a and 5.10b it is clear that the alnöite and kimberlite fields outlined by Dawson (1960) apparently have little value for dyke classification. The diagrams do, however, demonstrate that the kimberlites, carbonatites and carbonate-rich monchiquites probably evolved from a common parent by some form of crystal-liquid fractionation. The monchiquites were probably the first product to crystallize from the parental magma, with differentiation of (the parental magma) gave rise to kimberlites and carbonatites.

5.3.5 K/Rb Ratios

A large number of the Aillik kimberlites and carbonate-rich monchiquites exhibit K/Rb ratios in the range 130-300 (Fig. 5.11) which correspond to Shaw's (1968) main trend. The remaining analyses exhibit slightly

Figure 5.11 K vs Rb diagram for the Aillik dyke analyses. Symbols same as in Figure 5.9.



abnormal ratios between 300 and 400. Rocks with K/Rb ratios above 400 include the carbonatites and the minettes with ratios in the range 400-3000 and 500, respectively.

Both Taylor (1965) and Shaw (1968) have suggested that consanguineous igneous rock series display decreasing K/Rb ratios with increasing degree of fractionation. The fact that the Aillik kimberlites and monchiquites show a positive correlation (Fig. 5.11) with decreasing K/Rb ratio implies that these two dyke groups are genetically related. The position of the minettes and carbonatites with higher K/Rb ratios compared to the kimberlites and monchiquites does not support a simple differentiation sequence and the significance of the observed trends is not known at present.

The K/Rb ratios exhibited by the Aillik kimberlites are unlike kimberlites from South Africa (Dawson, 1960; Fesq *et al.*, 1975) as the latter exhibit ratios in the range of 80 to 250. The Aillik dykes show no evidence for potassium enrichment relative to other kimberlite dykes and their K/Rb ratios is probably related to Rb depletion in the parental magma.

5.4 Mineral Chemistry

5.4.1 Olivine

Limited probe data (Collerson, 1973, personal communication) show that they have forsterite contents which range from Fo 83.2 to Fo 86.6. These forsterite contents compare with matrix olivine compositions

from other kimberlite occurrences (Dawson, 1971; Mitchell, 1970; Lee and Lawrence, 1968; Mitchell and Fritz, 1973); however, the olivines probed are of unknown generation and are probably phenocrysts, not xenocrysts (Dawson and Hawthorne, 1973).

5.4.2 Mica

Probe analysis for micas of unknown generation and several glimmerite nodule micas are compared with analyses of biotite, phlogopite and megacrysts from kimberlite in Table 5.8. The Aillik micas are titanium-rich phlogopites; however they exhibit lower SiO_2 and higher FeO relative to kimberlite megacrysts.

Geochemical studies by Carswell (1975) have indicated that primary and secondary peridotite micas can be differentiated on the basis of their TiO_2 , Cr_2O_3 , Al_2O_3 , MgO, Na_2O and SiO_2 contents. Electron probe studies on micas occurring as megacrysts and in glimmerite nodules (Dawson and Smith, 1975a) confirm the work of Carswell (1975) and show that Cr_2O_3 , TiO_2 and FeO contents serve to distinguish many primary mica phenocrysts in kimberlite from those which are true xenocrysts (fragmented from mica peridotite (Fig. 5.12a)). The data also indicate that most micas in kimberlite are genetically related to glimmerite nodules and that the latter apparently crystallized from a magma of kimberlitic composition either in the upper mantle or lower crust (cf. Dawson and Smith, 1975a): Figure 5.12b is similar to Figure 5.12a; however, it contains

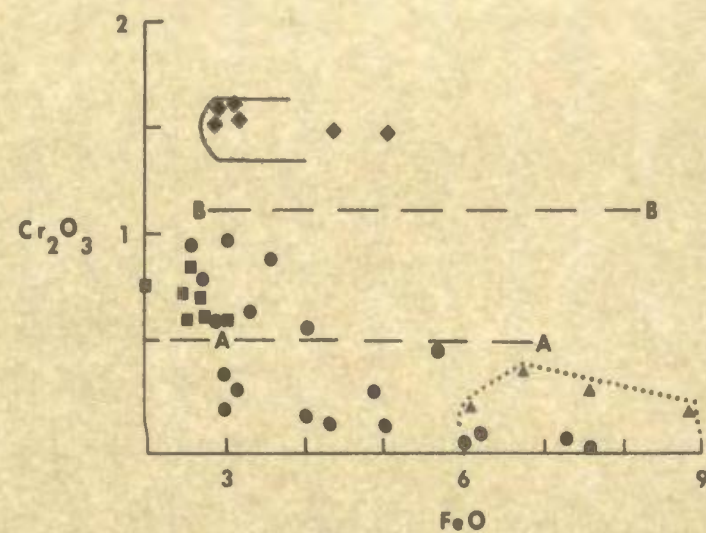
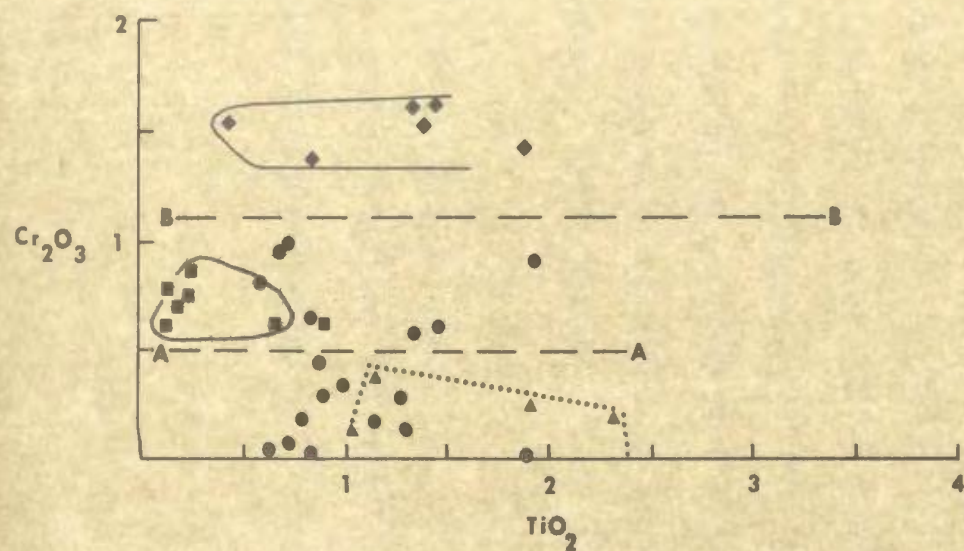
TABLE 5.8
PRIMER ANALYSIS OF THE ALLIUM NIGRUM 85-111-85 MEAL FROM OTHER LOCATIONS

Element	1	2	3	4	5	6	7	8	9	10	11	12	13	14	15	16	17	18	19	20	21	22	23	24	25	26	27	28	29	30	31	32	33	34	35	36	37	38	39	40	41	42	43	44	45	46	47	48	49	50	51	52	53	54	55	56	57	58	59	60	61	62	63	64	65	66	67	68	69	70	71	72	73	74	75	76	77	78	79	80	81	82	83	84	85	86	87	88	89	90	91	92	93	94	95	96	97	98	99	100	101	102	103	104	105	106	107	108	109	110	111	112	113	114	115	116	117	118	119	120	121	122	123	124	125	126	127	128	129	130	131	132	133	134	135	136	137	138	139	140	141	142	143	144	145	146	147	148	149	150	151	152	153	154	155	156	157	158	159	160	161	162	163	164	165	166	167	168	169	170	171	172	173	174	175	176	177	178	179	180	181	182	183	184	185	186	187	188	189	190	191	192	193	194	195	196	197	198	199	200	201	202	203	204	205	206	207	208	209	210	211	212	213	214	215	216	217	218	219	220	221	222	223	224	225	226	227	228	229	230	231	232	233	234	235	236	237	238	239	240	241	242	243	244	245	246	247	248	249	250	251	252	253	254	255	256	257	258	259	260	261	262	263	264	265	266	267	268	269	270	271	272	273	274	275	276	277	278	279	280	281	282	283	284	285	286	287	288	289	290	291	292	293	294	295	296	297	298	299	300	301	302	303	304	305	306	307	308	309	310	311	312	313	314	315	316	317	318	319	320	321	322	323	324	325	326	327	328	329	330	331	332	333	334	335	336	337	338	339	340	341	342	343	344	345	346	347	348	349	350	351	352	353	354	355	356	357	358	359	360	361	362	363	364	365	366	367	368	369	370	371	372	373	374	375	376	377	378	379	380	381	382	383	384	385	386	387	388	389	390	391	392	393	394	395	396	397	398	399	400	401	402	403	404	405	406	407	408	409	410	411	412	413	414	415	416	417	418	419	420	421	422	423	424	425	426	427	428	429	430	431	432	433	434	435	436	437	438	439	440	441	442	443	444	445	446	447	448	449	450	451	452	453	454	455	456	457	458	459	460	461	462	463	464	465	466	467	468	469	470	471	472	473	474	475	476	477	478	479	480	481	482	483	484	485	486	487	488	489	490	491	492	493	494	495	496	497	498	499	500	501	502	503	504	505	506	507	508	509	510	511	512	513	514	515	516	517	518	519	520	521	522	523	524	525	526	527	528	529	530	531	532	533	534	535	536	537	538	539	540	541	542	543	544	545	546	547	548	549	550	551	552	553	554	555	556	557	558	559	560	561	562	563	564	565	566	567	568	569	570	571	572	573	574	575	576	577	578	579	580	581	582	583	584	585	586	587	588	589	590	591	592	593	594	595	596	597	598	599	600	601	602	603	604	605	606	607	608	609	610	611	612	613	614	615	616	617	618	619	620	621	622	623	624	625	626	627	628	629	630	631	632	633	634	635	636	637	638	639	640	641	642	643	644	645	646	647	648	649	650	651	652	653	654	655	656	657	658	659	660	661	662	663	664	665	666	667	668	669	670	671	672	673	674	675	676	677	678	679	680	681	682	683	684	685	686	687	688	689	690	691	692	693	694	695	696	697	698	699	700	701	702	703	704	705	706	707	708	709	710	711	712	713	714	715	716	717	718	719	720	721	722	723	724	725	726	727	728	729	730	731	732	733	734	735	736	737	738	739	740	741	742	743	744	745	746	747	748	749	750	751	752	753	754	755	756	757	758	759	760	761	762	763	764	765	766	767	768	769	770	771	772	773	774	775	776	777	778	779	780	781	782	783	784	785	786	787	788	789	790	791	792	793	794	795	796	797	798	799	800	801	802	803	804	805	806	807	808	809	810	811	812	813	814	815	816	817	818	819	820	821	822	823	824	825	826	827	828	829	830	831	832	833	834	835	836	837	838	839	840	841	842	843	844	845	846	847	848	849	850	851	852	853	854	855	856	857	858	859	860	861	862	863	864	865	866	867	868	869	870	871	872	873	874	875	876	877	878	879	880	881	882	883	884	885	886	887	888	889	890	891	892	893	894	895	896	897	898	899	900	901	902	903	904	905	906	907	908	909	910	911	912	913	914	915	916	917	918	919	920	921	922	923	924	925	926	927	928	929	930	931	932	933	934	935	936	937	938	939	940	941	942	943	944	945	946	947	948	949	950	951	952	953	954	955	956	957	958	959	960	961	962	963	964	965	966	967	968	969	970	971	972	973	974	975	976	977	978	979	980	981	982	983	984	985	986	987	988	989	990	991	992	993	994	995	996	997	998	999	1000
---------	---	---	---	---	---	---	---	---	---	----	----	----	----	----	----	----	----	----	----	----	----	----	----	----	----	----	----	----	----	----	----	----	----	----	----	----	----	----	----	----	----	----	----	----	----	----	----	----	----	----	----	----	----	----	----	----	----	----	----	----	----	----	----	----	----	----	----	----	----	----	----	----	----	----	----	----	----	----	----	----	----	----	----	----	----	----	----	----	----	----	----	----	----	----	----	----	----	----	----	-----	-----	-----	-----	-----	-----	-----	-----	-----	-----	-----	-----	-----	-----	-----	-----	-----	-----	-----	-----	-----	-----	-----	-----	-----	-----	-----	-----	-----	-----	-----	-----	-----	-----	-----	-----	-----	-----	-----	-----	-----	-----	-----	-----	-----	-----	-----	-----	-----	-----	-----	-----	-----	-----	-----	-----	-----	-----	-----	-----	-----	-----	-----	-----	-----	-----	-----	-----	-----	-----	-----	-----	-----	-----	-----	-----	-----	-----	-----	-----	-----	-----	-----	-----	-----	-----	-----	-----	-----	-----	-----	-----	-----	-----	-----	-----	-----	-----	-----	-----	-----	-----	-----	-----	-----	-----	-----	-----	-----	-----	-----	-----	-----	-----	-----	-----	-----	-----	-----	-----	-----	-----	-----	-----	-----	-----	-----	-----	-----	-----	-----	-----	-----	-----	-----	-----	-----	-----	-----	-----	-----	-----	-----	-----	-----	-----	-----	-----	-----	-----	-----	-----	-----	-----	-----	-----	-----	-----	-----	-----	-----	-----	-----	-----	-----	-----	-----	-----	-----	-----	-----	-----	-----	-----	-----	-----	-----	-----	-----	-----	-----	-----	-----	-----	-----	-----	-----	-----	-----	-----	-----	-----	-----	-----	-----	-----	-----	-----	-----	-----	-----	-----	-----	-----	-----	-----	-----	-----	-----	-----	-----	-----	-----	-----	-----	-----	-----	-----	-----	-----	-----	-----	-----	-----	-----	-----	-----	-----	-----	-----	-----	-----	-----	-----	-----	-----	-----	-----	-----	-----	-----	-----	-----	-----	-----	-----	-----	-----	-----	-----	-----	-----	-----	-----	-----	-----	-----	-----	-----	-----	-----	-----	-----	-----	-----	-----	-----	-----	-----	-----	-----	-----	-----	-----	-----	-----	-----	-----	-----	-----	-----	-----	-----	-----	-----	-----	-----	-----	-----	-----	-----	-----	-----	-----	-----	-----	-----	-----	-----	-----	-----	-----	-----	-----	-----	-----	-----	-----	-----	-----	-----	-----	-----	-----	-----	-----	-----	-----	-----	-----	-----	-----	-----	-----	-----	-----	-----	-----	-----	-----	-----	-----	-----	-----	-----	-----	-----	-----	-----	-----	-----	-----	-----	-----	-----	-----	-----	-----	-----	-----	-----	-----	-----	-----	-----	-----	-----	-----	-----	-----	-----	-----	-----	-----	-----	-----	-----	-----	-----	-----	-----	-----	-----	-----	-----	-----	-----	-----	-----	-----	-----	-----	-----	-----	-----	-----	-----	-----	-----	-----	-----	-----	-----	-----	-----	-----	-----	-----	-----	-----	-----	-----	-----	-----	-----	-----	-----	-----	-----	-----	-----	-----	-----	-----	-----	-----	-----	-----	-----	-----	-----	-----	-----	-----	-----	-----	-----	-----	-----	-----	-----	-----	-----	-----	-----	-----	-----	-----	-----	-----	-----	-----	-----	-----	-----	-----	-----	-----	-----	-----	-----	-----	-----	-----	-----	-----	-----	-----	-----	-----	-----	-----	-----	-----	-----	-----	-----	-----	-----	-----	-----	-----	-----	-----	-----	-----	-----	-----	-----	-----	-----	-----	-----	-----	-----	-----	-----	-----	-----	-----	-----	-----	-----	-----	-----	-----	-----	-----	-----	-----	-----	-----	-----	-----	-----	-----	-----	-----	-----	-----	-----	-----	-----	-----	-----	-----	-----	-----	-----	-----	-----	-----	-----	-----	-----	-----	-----	-----	-----	-----	-----	-----	-----	-----	-----	-----	-----	-----	-----	-----	-----	-----	-----	-----	-----	-----	-----	-----	-----	-----	-----	-----	-----	-----	-----	-----	-----	-----	-----	-----	-----	-----	-----	-----	-----	-----	-----	-----	-----	-----	-----	-----	-----	-----	-----	-----	-----	-----	-----	-----	-----	-----	-----	-----	-----	-----	-----	-----	-----	-----	-----	-----	-----	-----	-----	-----	-----	-----	-----	-----	-----	-----	-----	-----	-----	-----	-----	-----	-----	-----	-----	-----	-----	-----	-----	-----	-----	-----	-----	-----	-----	-----	-----	-----	-----	-----	-----	-----	-----	-----	-----	-----	-----	-----	-----	-----	-----	-----	-----	-----	-----	-----	-----	-----	-----	-----	-----	-----	-----	-----	-----	-----	-----	-----	-----	-----	-----	-----	-----	-----	-----	-----	-----	-----	-----	-----	-----	-----	-----	-----	-----	-----	-----	-----	-----	-----	-----	-----	-----	-----	-----	-----	-----	-----	-----	-----	-----	-----	-----	-----	-----	-----	-----	-----	-----	-----	-----	-----	-----	-----	-----	-----	-----	-----	-----	-----	-----	-----	-----	-----	-----	-----	-----	-----	-----	-----	-----	-----	-----	-----	-----	-----	-----	-----	-----	-----	-----	-----	-----	-----	-----	-----	-----	-----	-----	-----	-----	-----	-----	-----	-----	-----	-----	-----	-----	-----	-----	-----	-----	-----	-----	-----	-----	-----	-----	-----	-----	-----	-----	-----	-----	-----	-----	-----	-----	-----	-----	-----	-----	-----	-----	-----	-----	-----	-----	-----	-----	-----	-----	-----	-----	-----	-----	-----	-----	-----	-----	-----	-----	-----	-----	-----	-----	-----	-----	-----	-----	-----	-----	-----	-----	-----	-----	-----	-----	-----	-----	-----	-----	-----	-----	-----	-----	-----	-----	-----	-----	-----	-----	-----	-----	-----	-----	-----	-----	-----	-----	-----	-----	-----	-----	-----	-----	-----	-----	-----	-----	-----	-----	-----	-----	-----	-----	-----	-----	-----	-----	-----	-----	-----	-----	-----	-----	-----	-----	-----	-----	-----	-----	-----	-----	-----	-----	-----	-----	-----	-----	-----	-----	-----	-----	-----	-----	-----	-----	-----	-----	-----	-----	-----	-----	-----	-----	-----	-----	-----	-----	-----	-----	-----	-----	-----	-----	-----	-----	-----	-----	-----	-----	-----	------

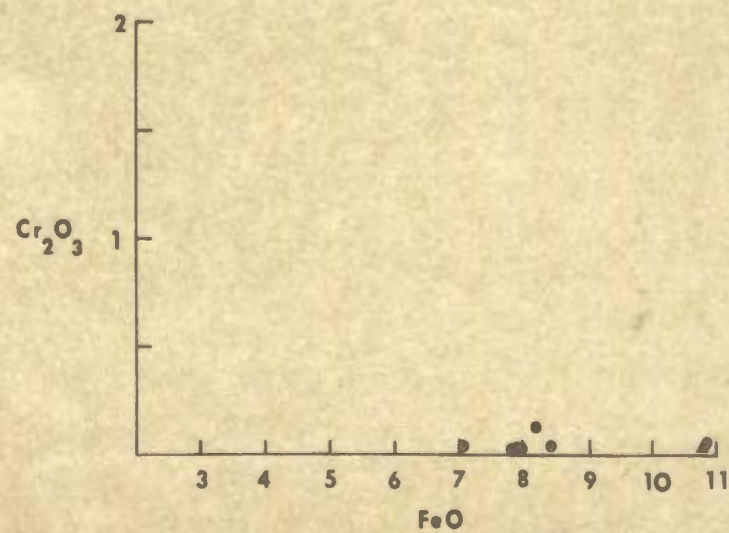
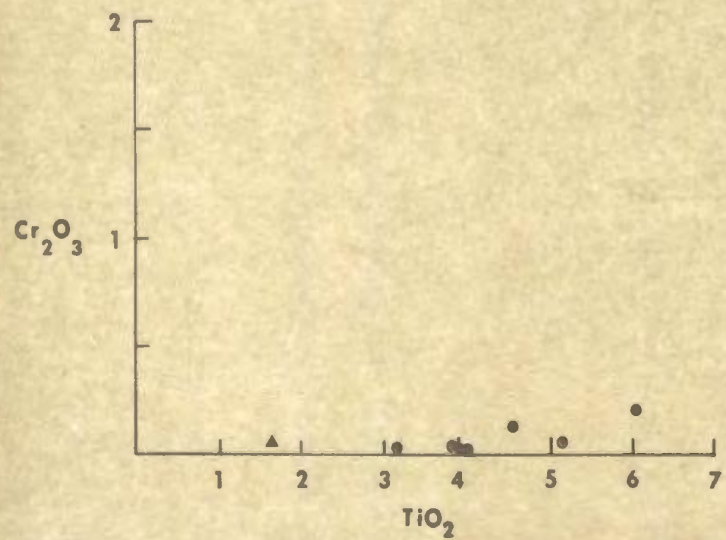
Figure 5.12a Cr_2O_3 vs TiO_2 and FeO diagrams for micas which occur in nodules and megacrysts in kimberlite (after Dawson and Smith, 1975a).

- ◆ Secondary micas in peridotite xenoliths
- Primary micas in peridotite xenoliths
- Mica megacrysts in kimberlite
- ▲ Micas in glimmerite nodules

Figure 5.12b Similar variation diagram to 5.12a however, contains probe analyses for megacrysts in the Aillik kimberlites ● and one glimmerite nodule ▲ from the Aillik association.



A



B

mica analyses from the Aillik kimberlites. The Aillik micas exhibit low Cr_2O_3 contents which are comparable to the African kimberlite megacrysts; however, they contain slightly higher TiO_2 and FeO values. The glimmerite analyses plot within the glimmerite field as outlined by Dawson and Hawthorne (op. cit.) but are not significantly different from megacryst analyses; therefore, implying a genetic relationship between the Aillik megacrystic and glimmeritic micas. This chemical data outlined above supports the earlier observation that the glimmerite nodules are cognate in origin and that the micas are phenocrysts which crystallized from a kimberlitic magma.

5.4.3 Clinopyroxene

Probe data (Collerson, 1973, personal communication) indicate that pyroxenes present in the Aillik kimberlites range in composition from salite to diopside. Salitic pyroxenes within kimberlite have been described elsewhere (Gittins et al., 1975). Pyroxenes are not considered to be an important mineral phase (Mitchell, 1970) although they have been recorded in several kimberlite occurrences (Emeleus and Andrews, 1975; Watson, 1955, 1967a,b).

5.4.4 Opaque Oxides

Probe analyses for several kimberlite opaques in the Aillik dykes (Haggerty et al., 1975) show that the groundmass spinels exhibit a

complex zoning which is similar to that observed in Lesotho kimberlites (Haggerty, 1973, 1975). The earliest formed crystals are Mg and Cr enriched and grade towards Fe^{2+} and Al^{3+} enrichment at their margins. They are then rimmed by Ti^{3+} and Fe^{3+} rich titanomagnetites. Magnesium-rich ilmenites are one of the most characteristic mineral phases present in kimberlite and are usually used as an indicator mineral for rocks of this composition (Dawson, 1971; Mitchell, 1970). The matrix also exhibits a high concentration of magnesium-rich ilmenites which are strongly zoned towards a Mg^{2+} and Fe^{3+} rich margins and rimmed by titanomagnetite and second generation magnesium-poor ilmenite.

Reaction mantles are common on the ilmenite megacrysts (spinel-perovskite) and are similar to those observed in kimberlites from South Africa (Dawson, 1962; Haggerty, 1973, 1975; Mitchell, 1973).

CHAPTER 6

DISCUSSION AND CONCLUSIONS

6.1 Tectonic Setting of Kimberlite Magmatism and Its Relationship to the Aillik Occurrences

Most diamond-bearing kimberlites are confined to the interior of shield areas (Dawson, 1967a, 1970) where they are related to uplift and/or dilation of the earth's continental crust during epirogenic movements. The presence of kimberlites in rift and/or graben structures has been disputed by Mitchell (1970) as most rift zones are characterized by alkaline magmatic activity (Heinrich, 1966; Kumarapeli and Saull, 1966; Doig, 1969; Currie, 1970; Darracott *et al.*, 1973; Bailey, 1974). Recent geological studies indicate that kimberlites occur in both rift systems (Dawson, 1970) and in alkaline provinces (Ferguson, 1973).

Kimberlites have been described from the St. Lawrence rift system (Lee and Lawrence, 1968; Doig, 1969; Currie, 1970) and alnöites, which appear to be genetically related to kimberlites (Allen and Deans, 1965; Nikishov *et al.*, 1972; Dawson, 1967a) are commonly found in association with such structures. For example, a suite of dykes which range in composition from kimberlite to carbonatite have been described by Gittins *et al.* (1975) from the St. Lawrence rift system (Kumarapeli and Saull, 1966; Kumarapeli, 1970).

Kimberlites from the Bushmanland Plateau (Cornelissen and Verwoerd, 1975) are associated with carbonatites, olivine melilitites, phonolites and trachytes on the southwestern margin of the African continent. They consider this extensive group of rocks to have been intruded along a continental warp axis which is parallel to the rift that eventually became the Atlantic Ocean. Janse (1975) considers that kimberlites and related rocks on the Nama Plateau are also related to the same tectonic environment as described by Cornelissen and Verwoerd (1975). He concludes that kimberlites are usually emplaced during the earliest period of epirogenic movements with the distribution of the magmatism around and near the points of warping. The alkaline magmatism is confined to areas where rifting has commenced as many of the channel ways used by the kimberlites are blocked by associated normal faults. This mechanism although simplified may partially account for the kimberlite and associated carbonatite activity in certain rift structures.

Meymechites and picrites with kimberlitic affinities have been described from the Kamchatka Peninsula in the Circum-Pacific mobile belt (Rotman et al., 1972). This occurrence of kimberlite-like rocks within an orogenic zone (some geologists consider meymechnites as an intrusive equivalent of kimberlite; Sheinmann, 1957 quoted by Dawson, 1967; Rotman et al., 1972) implies that kimberlite magmatism may not be confined solely to platformal areas.

The Aillik and Greenland kimberlites are considered to have been emplaced in response to the separation of Greenland from North America (King and McMillan 1975; Andrews and Emeleus, 1971, 1975; Walton, 1966; Walton and Arnold, 1969) as most occurrences lie on a continental margin (Fig. 6.1) and show ages of intrusion similar to that for the breakup of the continent (see below).

The separation of Greenland from North America (Watt, 1969) is believed to have been aided by a mantle plume which is now considered to underlie Iceland (Hyndman, 1973). The initial rupturing of the North American-European continent is regarded as having started in the Jurassic (Burke and Dewey, 1973); however, significant spreading did not occur until the late Cretaceous (Hyndman, 1973; Burke and Dewey, 1973). More recent studies (Van Der Linden, 1975) show that the separation of Greenland from North America may be compared to the evolution of the Red Sea (Fig. 6.2). It was initiated more than 200 m.y. ago by a major updoming presumably related to thermal expansion in the mantle. This doming probably produced a triple point junction (Burke and Dewey, 1973) which is located south of Greenland (Hyndman, 1973) and later became the site for the Mid-Atlantic Sea Ridge.

The Greenland kimberlite dykes were apparently emplaced during the earliest orogenic movements as their age dates (Andrews and Emeleus, 1971, 1975) coincide with such movements (Fig. 6.2). The Aillik dykes however seem to be younger than these movements (cf. King and McMillan,

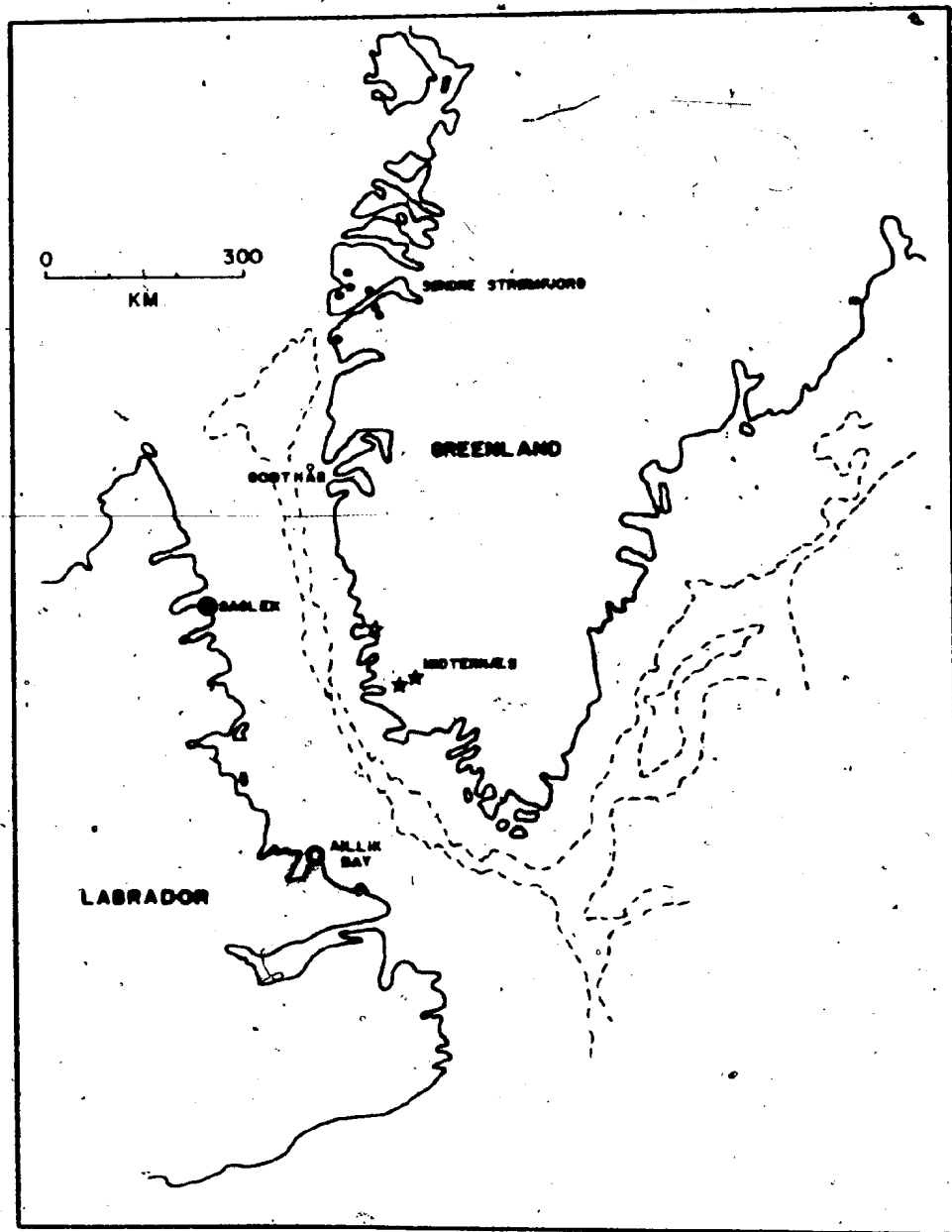


Figure 6.1 Location of Labrador and Greenland kimberlites and lamprophyres on a Bullard *et al.* (1965) fit of the continents, (after Collerson, personal communication).

- ★ ○ ● kimberlites
- ★ lamprophyric carbonatites
- ★ undifferentiated kimberlites & lamprophyres

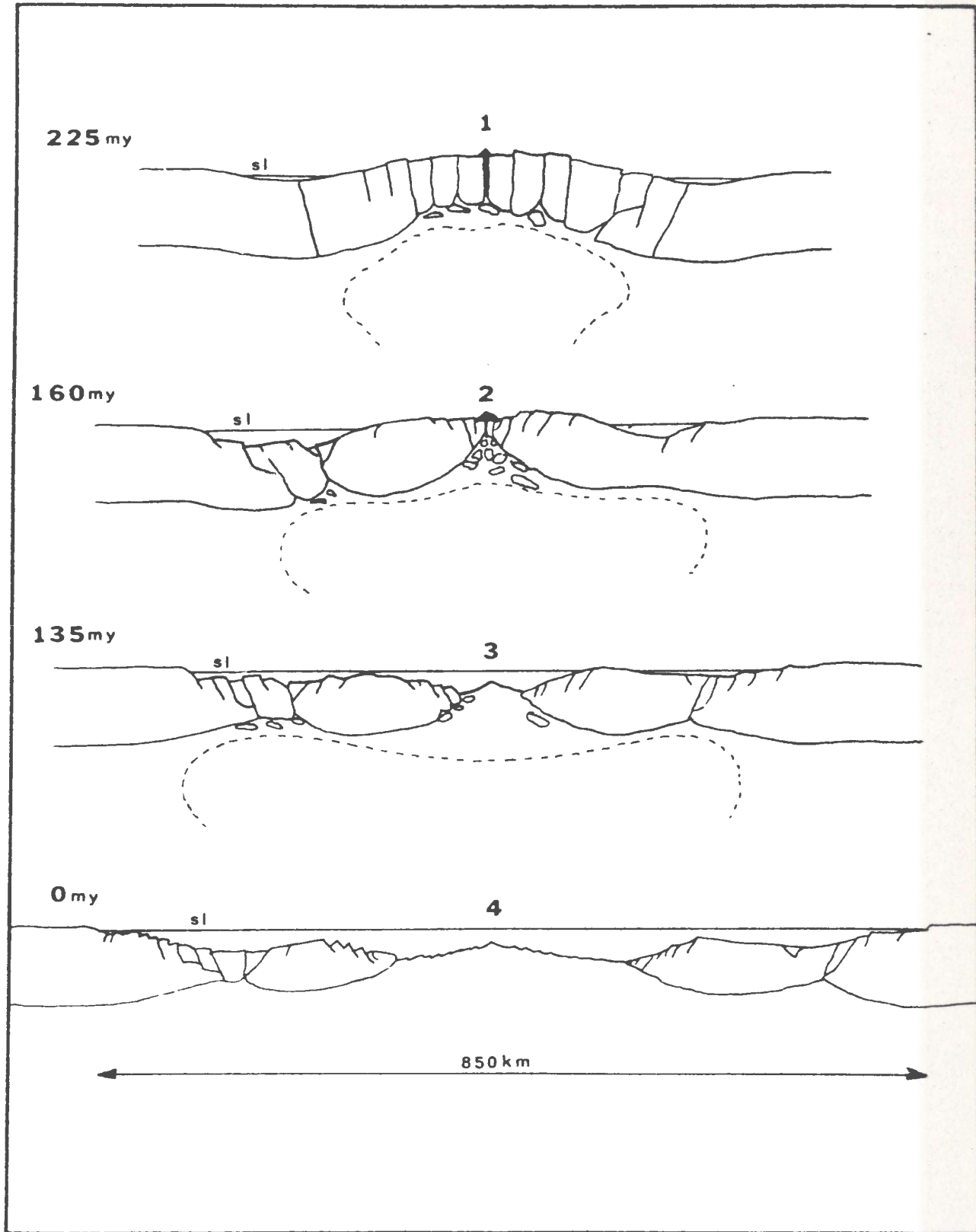


Figure 6.2 Evolution of the Labrador Sea (modified after Van der Linden, 1975).

1975) and coincide with spreading (Fig. 6.2). This discrepancy in age between the Aillik and Greenland dykes may be a result of the limited age dates for the Aillik area and it is probable that both occurrences were intruded at the same time.

6.2 Carbonate: Its Origin in Kimberlites and Carbonatites

Carbonates (calcite, dolomite) are a major constituent of carbonatites and occurs as a major groundmass phase in kimberlites. In kimberlites this carbonate was regarded as of secondary origin (Frant-session, 1970, Smirnov, 1959) possibly after melilite (Lewis, 1887; Wagner, 1914; Williams, 1932; Frankel, 1956; Shand, 1934; Dawson, 1967a; Von Eckermann, 1961, 1967; Stewart, 1970; McCall, 1963). An alternative and more plausible explanation is that the carbonate is a primary phase which crystallized from a magmatic liquid (Watson, 1955, 1967a and 1967b; Mitchell and Fritz, 1973; Dawson and Hawthorne, 1973; Zhabin and Cherepovskaya, 1965; Dawson, 1962; Andrews and Emeleus, 1971, 1975; Johnson, 1961; Walton and Arnold, 1970; Clement, 1975; Robinson, 1975; Clarke and Mitchell, 1975; McCallum and Eggler, 1971).

The petrological evidence for magmatic carbonates is supported by the presence of a number of experimental studies. Wyllie and Tuttle (1960) have shown that calcite can precipitate from melts in the system $\text{CaO-CO}_2\text{-H}_2\text{O}$ through a large pressure range and at temperatures to at least 600°C. Wyllie and Haas (1965, 1966) in an investigation of the

system $\text{CaO-SiO}_2\text{-CO}_2\text{-H}_2\text{O}$ showed that only liquids undersaturated with SiO_2 could lead to the precipitation of either hydrous and/or carbonate phases. Wyllie (1966) and Franz and Wyllie (1967) showed that fractional crystallization of a carbonated ultrabasic magma can produce a residual fraction of carbonatite composition. They also showed that monticellite and forsterite can precipitate with calcite in the system $\text{CaO-MgO-SiO}_2\text{-CO}_2\text{-H}_2\text{O}$, thereby providing an important genetic link between kimberlites and carbonatites as all three phases are found in either rock type.

Wyllie and Boettcher (1969) show that quenched calcite crystals in the system $\text{CaO-CO}_2\text{-H}_2\text{O}$ may be regarded as evidence for the former existence of a liquid phase. They compare their quench textures to those described in carbonatites and kimberlites (Zhabin and Cherepyskaya 1965; Dawson and Hawthorne, 1970, 1973; Johnson, 1961), thereby, supplying further evidence for magmatic carbonates which crystallized from a liquid.

Koster Van Groos and Wyllie (1963, 1966, 1968b) have demonstrated the presence of a wide miscibility gap between silicate liquids and sodium carbonate within the joins $\text{NaAlSi}_3\text{O}_8 - \text{Na}_2\text{CO}_3$; $\text{NaAlSi}_3\text{O}_8 - \text{Na}_2\text{CO}_3 - \text{H}_2\text{O}$ and $\text{NaAlSi}_3\text{O}_8 - \text{CaAlSi}_2\text{O}_8 - \text{Na}_2\text{CO}_3 - \text{H}_2\text{O}$. This miscibility gap is found to decrease with pressure and at 33 bars is nonexistent. They also showed that the crystallization path can lead to the development of immiscible fluid phases of three types; (1) silicate liquid

containing Na_2CO_2 , CO_2 and H_2O , (2) a carbonate liquid containing Na_2CO_3 with dissolved H_2O and a small proportion of silicates, and (3) a vapor phase. These phases under appropriate conditions (determined by P_T , $P_{\text{CO}_2/\text{H}_2\text{O}}$, and bulk composition of the original magma) can be compared to nepheline or ijolite magmas, carbonatite melts and fenitizing solutions, respectively. Their results have important application to central carbonatite complexes where all three of the above liquids are known to coexisted. It also provides a second alternative to carbonatite genesis.

There is now considerable evidence that CO_2 exists in the upper mantle. McGetchin and Besançon (1973) describe carbonate inclusions within mantle-derived pyropes which contain calcite as well as magnesium-iron carbonates. CO_2 has also been found in inclusions from basalts (Lezier, 1966, quoted by Irving and Wyllie, 1975; Rodder, 1965) and in olivine megacrysts from kimberlite and basalt (Green 1972; Green and Radcliffe, 1973). CO_2 has also been recovered during the crushing of natural diamond (Melton et al., 1972) indicating the presence of CO_2 at the time of diamond formation. All of the above data indicate the possibility that carbonates form from primary magmas which are generated within the mantle. Evidence for such a process has received significant support by the presence of ilherzolite-bearing damkjernite in the Fen Carbonatite Complex (Griffin, 1973; Griffin and Taylor, 1975) as well as spinel-ilherzolite xenoliths from the Lashine Volcano, Tanzania (Dawson, et al., 1970).

Experimental work by Irving and Wyllie (1973, 1975) indicates the possibility that carbonatites may exist independantly of silicate melts in the mantle (Boyd and Nixon, 1973). In the system CaCO_3 - MgCO_3 they show that for all mantle pressures there is a range of carbonate solid solutions (calcite-magnesite) for which melting occurs at temperatures lower than the peridotite solidus. Thus, if such minerals do occur in the mantle, they may form a liquid approaching carbonatite in composition. This work also explains the high primary carbonate content of many kimberlites.

Eggler (1973, 1974) during melting experiments with CO_2 show that at mantle depths, basic and ultrabasic magmas contain considerable amounts of CO_2 and rocks of kimberlite composition would have a large CO_2 solubility. The experiments also show that in the presence of CO_2 and $\text{H}_2\text{O}/\text{CO}_2$ mixtures, peridotite melts at higher temperatures than if H_2O was present independently. Eggler (1973) shows that melting of peridotite with a $\text{H}_2\text{O}/\text{CO}_2$ mixture will produce liquids which are less silica saturated than those produced in the presence of H_2O alone. This has important applications for the genesis of kimberlites and carbonatites for by varying the $\text{H}_2\text{O}/\text{CO}_2$ ratio, one can produce liquids of varying silica saturation; a feature noted between kimberlites and carbonatites (Dawson, 1960, 1966, 1967b).

Carbon dioxide is considered by Koster Van Groos (1975) to be an unlikely vapor phase in the mantle (cf. Roedder, 1965) under continental areas but it may occur as such under oceanic plates. He considers

that carbonate under shield areas is in the form of crystalline phases (McGetchin and Besancon, 1973); however at high temperatures they may be partially or completely liquid. These liquids may be present as an interstitial liquid, liquid inclusions or in small pockets and under appropriate conditions crystallize to form carbonatite or carbonate-rich kimberlite.

Wyllie (1975) and Wyllie and Huang (1975) have shown that partial fusion of a CO_2 - bearing mantle can produce liquids of either carbonate or kimberlite composition at depths of between 80 and 100 km. The major factor governing magma composition at this depth is temperature as the first melts produced are carbonatitic and with progressive fusion the melts are converted to kimberlites. According to Wyllie and Huang (op. cit.) fractional crystallization of a kimberlite may produce a carbonatite fraction similar to that observed in the Benfontein Sill (Dawson and Hawthorne, 1973).

Eggler (1976) working in the system $\text{CaO-MgO-SiO}_2\text{-CO}_2$ has shown that liquids formed in the pressure range from 26 to 30 kb are kimberlitic in composition; however, they contain more Ca relative to Mg. He also shows that kimberlitic melts do not form the first melts in this system nor can differentiation of the first melt give rise to carbonatites.

In accordance with the previous discussion, the carbonate present in the minettes, monchiquites, kimberlite, alnöite and carbonatites is regarded to be of magmatic origin. The matrix carbonates in the kimberlites,

alnöite and carbonatite are considered to have crystallized directly from a carbonate-rich fluid phase. In the monchiquites and minettes, carbonate is restricted in its occurrence to the ocelli, which are interpreted to have resulted by processes of liquid immiscibility (cf. Ferguson and Currie, 1971; Philpotts and Hodgson, 1968). Similar carbonate-rich ocelli present in the kimberlites and carbonatites further supports to the role played by liquid immiscibility in the genesis of the suite.

The matrix carbonate in the Aillik kimberlites and carbonatites are therefore considered to have crystallized from a carbonate-rich fluid phase which developed an immiscible fraction at an early stage in the differentiation of the parental magma.

6.3 A Petrogenetic Model for the Aillik Bay Ultrabasic to Basic Dykes

The geographical setting of the Aillik dykes on the west margin of the Labrador Sea implies that the parental magma developed within the mantle in response to epirogenic movements which led to the separation of Greenland from North America. Field data (Chapter 3) and variation diagrams presented in Chapter 6 indicate that the carbonate-rich monchiquites were the first differentiation products of the Aillik parental magma assuming that normal differentiation trends can be applied to rocks of these compositions); however, the lack of nodules or other petrological indicators in the monchiquites precludes the possibility of determining a parental magma composition. A petrological subtraction computer program (Cawthorn and Strong, in press) was applied to the Aillik dykes assuming that a liquid of monchiquitic chemistry

(Table 5.3) approached the primary magma composition. Minerals of the kimberlite suite were subtracted from the monchiquite composition according to their modal percentages, and to the limited probe data from the Aillik dykes as well kimberlites from other areas (Nixon, 1973; Dawson and Smith, 1975a; Frantzsson, 1972; Mitchell, 1973). By subtracting kimberlite mineral phases from a monchiquitic magma, a residual composition approaching carbonatite was attained.

The parental magma of the monchiquites, kimberlites and carbonatites is considered to have been generated within the mantle at depths possibly exceeding 100 km; however, the kimberlites probably evolved at depth < 100 km as they contain nodules of the M.A.R.I.D. suite (Dawson and Smith, 1975b).

It is envisaged that the primary magma began to differentiate at an early stage within or near the generation zone during the initial rifting of the Labrador Sea. Deep fractures tapped this magma source and gave rise to the monchiquite dykes. The remaining magma presumably underwent further differentiation and produced a liquid of kimberlitic composition which was saturated with CO_2 . At this stage, explosive release of volatiles resulted in the emplacement of the kimberlitic magma into the crust and it was subsequently intruded as dykes and sills. Carbonatites formed during the intrusion of the kimberlites principally as a result of liquid immiscibility and flow differentiation.

6.4 Conclusions

The main conclusions which have been deduced from this study are as follows:

1. The Aillik Group in the Aillik Bay area is composed of meta-sediments and metavolcanics. Most units are considered to be equivalent to either the Makkovik or Big Island Formations (as defined by Clark, 1974).
2. The Aillik Group is intruded by a suite of ultrabasic to basic dykes which range in composition from kimberlite, micaceous kimberlite, carbonate-rich kimberlites (micaceous or nonmicaceous), minettes, monchiquites, carbonate-rich monchiquites, alnöites and carbonatites.
3. Emplacement of the ultrabasic to basic dykes was strongly influenced by jointing and hydraulic fracturing in the Aillik Group. The monchiquites are often offset in stepped arrangements and display brittle fracture development indicative of forceful emplacement.
4. Flow differentiation, liquid immiscibility, supercooling and multiple intrusion produced the varied compositional and textural arrangements in the carbonate-rich monchiquites and kimberlites.

5. The kimberlites contain two generations of olivine, opaque oxides, mica and clinopyroxene. The mica commonly exhibits reverse pleochroism and the clinopyroxenes range in composition from diopside to salite. The opaque oxides are magnesium-rich ilmenites; however, perovskite, magnetite and ilmenite also occur. Cognate nodules of the M.A.R.I.D. suite are very common in the Aillik dykes and contain micas which are compositionally equivalent to micas from other glimmerite nodules.
6. The carbonate-rich monchiquites are genetically related to the kimberlites and carbonatites and appear to have been derived from the same parent magma.
7. The minettes are either unrelated to the other dyke suites or their genetic relationship may have been masked by secondary effects.
8. The emplacement of the Aillik dyke swarm and kimberlites in Greenland coincided with the initial rifting phase which preceeded the separation of Greenland from North America. The initial partial melting of the mantle during this stage in the evolution of the Labrador Sea, gave rise to both the Aillik and Greenland dykes.
9. The carbonate present in the Aillik dykes is regarded as being of magmatic origin having solidified late in the crystallization history of the dykes.

BIBLIOGRAPHY

- Abbey, S.T., 1968, Analysis of rocks and minerals by atomic absorption spectroscopy; Part 2; Determination of total iron, magnesium, calcium, sodium and potassium: Geol. Surv. Can. Paper 68-20, 21 pp.
- Allen, J.E. and Balk, R., 1954, Mineral resources of Fort Defiance and Tohatchi Quadrangles, Arizona and New Mexico: New Mex. Bur. Mines Mineral. Resources Bull., 36, 192 pp.
- Allen, J.B. and Deans, T., 1965, Ultrabasic eruptives with alnöitic - kimberlitic affinities from Malaita, Solomon Islands: Mineral. Mag., 34, pp. 16-34.
- Andrews, J.R. and Emeleus, C.H., 1971, Preliminary account of kimberlite intrusions from the Frederikshab district, Southwest Greenland: Gronlands Geol. Unders. Rapn. 31, 26 pp.
- Andrews, J.R. and Emeleus, C.H., 1975, Structural aspects of kimberlite dyke and sheet intrusion in Southwest Greenland: Phys. and Chem. of the Earth, 9, pp. 43-50.
- Aoki, K., 1974, Phlogopites and potassic richterites from mica nodules in South African kimberlites: Contrib. Mineral. Petrol., 48, pp. 1-7.
- Bailey, D.K., 1974, Continental rifting and alkaline magmatism: In: H. Sorensen (ed.), The Alkaline Rocks, John Wiley & Sons, Great Britain, pp. 148-159.
- Beavan, A.P., 1958, The Labrador uranium area: Geol. Assoc. Can. Proc., 10, pp. 137-145.
- Bhattacharji, S., 1967a, Mechanics of flow differentiation in ultramafic and mafic sills: J. Geol., 75, pp. 101-112.

- Bhattacharji, S., 1967b, Scale model experiments on flowage differentiation in sills. In: P.J. Wyllie (ed.), Ultramafic and Related Rocks, John Wiley & Sons, New York, pp. 69-70.
- Bhattacharji, S., and Nehru, C.E., 1972, Igneous differentiation models for the origin of Mount Johnson, a zoned Monteregian intrusion, Quebec, Canada: Int. Geol. Congr., 24th., Montreal, Sect. 14, pp. 3-17.
- Boettcher, A.L., 1967, The Rainy Creek alkaline - ultramafic igneous complex near Libby, Montana: I. Ultramafic rocks and fenite: J. Geol., 75, pp. 526-553.
- Boettcher, A.L. and Wyllie, P.J., 1969, The system $\text{CaO} - \text{SiO}_2 - \text{CO}_2$, III. Second critical end-point on the melting curve: Geochim. Cosmochim. Acta, 33, pp. 611-632.
- Boullier, A.M. and Nicolas, A., 1973, Texture and fabric of peridotite nodules from kimberlite at Mothae, Thaba Putsoa and Kimberley: In: P.H. Nixon (ed.), Lesotho Kimberlites, Lesotho National Development Corporation, Maseru, pp. 57-66.
- Boullier, A.M. and Nicolas, A., 1975, Classification of textures and fabrics of peridotite xenoliths from South African kimberlites: Phys. and Chem. of the Earth, 9, pp. 467-476.
- Bowen, N.L., 1922, Genetic features of alnöitic rocks at Ile Cadieux, Quebec: Amer. J. Sci., 3, pp. 1-35.
- Boyd, F.R. and Nixon, P.H., 1973a, Structure of the upper mantle beneath Lesotho: Carnegie Inst. Wash. Yearbook, 72, pp. 431-445.

Boyd, F.R. and Nixon, P.H., 1973b, Origin of the ilmenite - silicate nodules in kimberlites from Lesotho and South Africa: In: P.H. Nixon (ed.), Lesotho Kimberlites, Lesotho National Development Corporation, Maseru, pp. 254-268.

Brachvogel, F.F. and Kovalsky, V.V., 1970, On the denuded section in the area of the Anabar antecline and nearby structure: In: Geologia i. Polezm. iskop. Yakutii, Yakutsk.

Bridgwater, D., 1970, Observations on the Pre-cambrian rocks of Scandinavia and Labrador and their implications for the interpretation of the Precambrian of Greenland: Grønlands Geol. Unders., Rapp. 28, no. 43-47.

Bridgwater, D., Escher, A., Nash, D.F. and Watterson, J., 1972, Investigations on the Nagssugtoqidian boundary between Holsteinsborg and Kangamiut, Central West Greenland: Grønlands Geol. Unders., Rapp. 55, pp. 22-25.

Bridgwater, D. and Harry, W.T., 1968, Anorthosite xenoliths and plagioclase megacrysts in Pre-cambrian intrusions of South Greenland: Meddr. Grønland, Bd. 185, No. 9, 232 p.

Bullard, E.C., Everett, J.E. and Smith, A.G., 1965, Fit of the continents around Atlantica: In: Blackett, R.M.S., Bullard, E.C. and Runcorn, S.K. (eds.), A. Symposium on Continental Drift, Roy. Soc. London, Phil. Trans., Ser. A, 25B, pp. 41-75.

Burke, K. and Dewey, J.F., 1973, Plume generated triple junctions: Key indicators in applying plate tectonics to old rocks: J. Geol., 81, pp. 406-433.

- Burke, K., Dewey, J.F. and Whiteman, A.J., 1973, Uplift, rifting and the breakup of Africa: In: D.H. Tarling and S.K. Runcorn (eds.), Continental Drift, Sea Floor Spreading and Plate Tectonics, Academic Press, London, pp. 735-755.
- Carswell, D.A., 1975, Primary and secondary phlogopites and clinopyroxenes in garnet lherzolite xenoliths: *Phys. and Chem. of the Earth*, 9, pp. 417-430.
- Carswell, D.A. and Dawson, J.B., 1970, Garnet peridotite xenoliths in South African kimberlite pipes and their petrogenesis: *Contrib. Mineral. Petrol.*, 25, pp. 163-184.
- Cawthorn, R.G. and Strong, D.F., in prep., The presentation of rock analyses in the granite system.
- Christie, A.M., Roscoe, S.M. and Fahrig, W.F., 1953, Preliminary map, Central Labrador coast: *Can. Geol. Surv.*, Paper 53-14.
- Clarke, A.M.S., 1971a, Structure and lithology of part of the Aillik Series, Labrador: *Geol. Assoc. Can. Proc.*, 24, No. 1, pp. 107-117.
- Clarke, A.M.S., 1971b, A structural reinterpretation of the Aillik Series, Labrador: Unpubl. M.Sc. Thesis, Memorial University of Newfoundland, St. John's.
- Clarke, A.M.S., 1974, A reinterpretation of the stratigraphy and deformation of the Aillik Group, Makkovik, Labrador: Unpubl. Ph.D. Thesis, Memorial University of Newfoundland, St. John's.
- Clarke, D.B. and Mitchell, R.H., 1975, Mineralogy and petrology of the kimberlite from Somerset Island, N.W.T., Canada: *Phys. and Chem. of the Earth*, 9, pp. 123-136.

- Clement, C.R., 1975, The emplacement of some diatreme-facies kimberlites: Phys. and Chem of the Earth, 9, pp. 51-60.
- Collerson, K.D., 1973, Unpublished microprobe data on ultrabasic-basic dyke specimens collected by King (1963).
- Copper, A.F., 1971, Carbonatites and fenitization associated with a lamprophyric dyke swarm intrusive into schists of the New Zealand Geosyncline: Geol. Soc. Amer. Bull., 82, pp. 1327-1340.
- Cooper, G.E., 1951, The petrology of some syenites and granites in Labrador: Unpubl. M.Sc. Thesis, McGill University, Montreal.
- Cornelissen, A.K. and Verwoerd, W.J., 1975, The Bushmanland kimberlites and related rocks: Phys. and Chem of the Earth, 9, pp. 71-80.
- Cox, K.G., Gurney, J.H. and Harte, B., 1973, Xenoliths from the Matsoka Pipe: In: P.H. Nixon (ed.), Lesotho Kimberlites: Lesotho National Development Corporation, Maseru, pp. 76-91.
- Currie, K.L., 1970, An hypothesis on the origin of alkaline rocks suggested by the tectonic setting of the Monteregian Hills: Can. Mineral., 10, Pt. 3, pp. 411-420.
- Currie, K.L., 1971a, A study of fenitization around the alkaline carbonatite complex at Callander Bay, Ontario: Discussion: Can. J. Earth Sci., 8, No. 10, pp. 1331-1332.
- Currie, K.L., 1971b, A study of potash fenitization around the Brent Crater, Ontario; a Paleozoic alkaline complex: Can. J. Earth Sci., 8, No. 5, pp. 481-497.

- Currie, K.L. and Ferguson, J., 1970, The mechanism of intrusion of lamprophyre dykes indicated by offsetting of dykes: *Tectonophysics*, 9, pp. 525-535.
- Daly, R.A., 1902, The geology of the northeast coast of Labrador: *Bull. Mus. Comp. Zool. Harvard*, 38, Geol. Ser. 5, No. 5.
- Danchin, R.V., Ferguson, J., Maciver, J.R. and Nixon, P.H., 1975, The composition of late stage kimberlite liquids as revealed by nucleated autholiths: *Phys. and Chem of the Earth*, 9, pp. 235-246.
- Darracott, B.W., Fairhead, J.D., Girdler, R.W. and Hall, S.A., 1973, The East African rift system: In: D.H. Tarling and S.K. Runcord (eds.), *Continental Drift, Sea Floor Spreading and Plate Tectonics*, Academic Press, London, pp. 757-766.
- Davidson, C.F., 1964, On diamantiferous diatremes: *Econ. Geol.*, 59, pp. 1368-1380.
- Dawson, J.B., 1960, A comparative study of the geology and petrology of the kimberlites of the Basutoland province: Unpubl. Ph.D. Thesis, University of Leeds, England.
- Dawson, J.B., 1962, Basutoland kimberlites: *Geol. Soc. Amer. Bull.*, 73, pp. 545-560.
- Dawson, J.B., 1966, The kimberlite-carbonatite relationship: In: Mineral. Soc. India, *Internat. Mineral. Ass. papers*, 4th Gen. Mtg., New Delhi, 1964, pp. 1-4.
- Dawson, J.B., 1967a, A review of the geology of kimberlite: In: P.J. Wyllie (ed.), *Ultramafic and Related Rocks*, John Wiley & Sons, New York, pp. 241-251.

- Dawson, J.B., 1967b, Geochemistry and origin of kimberlite: In: P.J. Wyllie (ed.), Ultramafic and Related Rocks, John Wiley & Sons, New York, pp. 269-278.
- Dawson, J.B., 1970, The tectonic setting of African kimberlite magmatism: In: T.N. Clifford and I.G. Glass (ed.), African Magmatism and Tectonics, Oliver and Boyd, Edinburgh, pp. 321-335.
- Dawson, J.B., 1971, Advances in kimberlite geology: Earth Sci. Rev., 7, pp. 187-214.
- Dawson, J.B., 1972, Kimberlites and their relationship to the mantle: Roy. Soc. London, Phil. Trans., Ser. A, 271, pp. 297-311.
- Dawson, J.B. and Hawthorne, 1970, Intrusion features in some hypabyssal South African kimberlites: Bull. Volcanol., 34, pp. 740-757.
- Dawson, J.B. and Hawthorne, 1973, Magmatic sedimentation and carbonatitic differentiation in kimberlite sills at Benfontein, South Africa: Geol. Soc. London, Quat. J., 129, pp. 61-85.
- Dawson, J.B. and Powell, D.G., 1969, Mica in the upper mantle: Contrib. Mineral. Petrol., 22, pp. 235-237.
- Dawson, J.B. and Reid, A.M., 1969, Ultrabasic xenoliths and lava from the Lashaine Volcano, Northern Tanzania: J. Petrol., v. 11, Pt. 3, pp. 519-548.
- Dawson, J. B. and Smith, J.V., 1975a, Chemistry and origin of phlogopite megacrysts in kimberlite: Nature, 253, pp. 336-338.
- Dawson, J.B., 1975b, Mineral chemistry of amphibole - diopside glimmerite nodules from some South African kimberlites: Unpubl. Abstr., 1975 Kimberlite Conference, Cambridge, England.

- Deans, T., Sukheswala, R.N., Sethna, S.F. and Viladkar, S.G., 1972, Metasomatic feldspar rocks (potash fenites) associated with the fluorite deposits and carbonatites of Amba Dongar, Gujarat, India: Trans, Inst. Mining and Metall., Sect. B, 81, pp. B1-B10.
- Deer, W.A., Howie, R.A. and Zussman, J., 1971, An Introduction to the Rock-forming Minerals: Longman Group Ltd., London, 528 p.
- Doig, R., 1969, An alkaline province linking Europe and North America: Can. J. Earth Sci., 7, pp. 22-28.
- Donaldson, C.H., 1974, Olivine crystal types in harristic rocks of the Rhum Pluton and Archean spinifer rocks: Geol. Soc. Amer. Bull., 85, pp. 1721-1726.
- Douglas, G.V., 1953, Notes on localities visited on the Labrador Coast in 1947 and 1947: Can. Geol. Surv., Paper 53-1.
- Drever, H.I. and Johnston, R., 1957, Crystal growth of forsteritic olivine in magmas and melts: Roy. Soc. Edinburg, Trans., 63, pp. 289-315.
- Eggler, D.H., 1973, Role of CO_2 in melting processes in the mantle: Carnegie Inst. Wash. Yearb., 72, pp. 457-467.
- Eggler, D.H., 1974, Effect of CO_2 on the melting of peridotite: Carnegie Inst. Wash. Yearb., 73, pp. 215-224.
- Eggler, D.H., 1975, CO_2 as a volatile component of the mantle: The system $\text{Mg}_2\text{SiO}_4 - \text{SiO}_2 - \text{H}_2\text{O} - \text{CO}_2$: Phys. and Chem of the Earth, 9, pp. 869-882.
- Egorov, L.S., 1970, Carbonatites and ultrabasic-alkaline rocks of the Maimecha - Kotui region, N. Siberia: Lithos, 3, pp. 341-359.

- Elders, W.A. and Rucklidge, J.C., 1969, Layering and netveining in hornblende lamprophyre intrusions from the coast of Labrador: J. Geol., 77, pp. 721-729.
- Emeleus, C.H. and Andrews, J.R., 1975, Mineralogy and petrology of kimberlite dyke and sheet intrusions and included peridotite xenoliths from Southwest Greenland: Phys. and Chem. of the Earth, 9, pp. 179-198.
- Erlank, A.J., 1973, Kimberlite potassic richterite and the distribution of potassium in the upper mantle: Extended abstracts, International Conference on Kimberlites, Univ. of Cape Town, pp. 103-106.
- Erlank, A.J. and Finger, L.W., 1970, The occurrence of potassic richterite in a mica nodule from the Wesselton kimberlite, South Africa: Carnegie Inst. Wash. Yearb., 69, pp. 320-329.
- Escher, A. and Watterson, J., 1972, Kimberlites and associated rocks in the Holsteinsborg - Søndre Strømfjord region, Central West Greenland: Grønlands Geol. Unders., Rapp. 55, pp. 26-27.
- Faye, C.H., 1968, The optical absorption spectra of iron in six coordinate sites in chlorite, biotite, phlogopite and vivianite. Some aspects of pleochroism in the sheet silicates: Can. Mineral., 9, Pt. 3, pp. 403-425.
- Faye, C.H. and Hogarth, D.D., 1968, On the origin of reverse pleochroism of a phlogopite: Can. Mineral., 10, Pt. 1, pp. 25-34.
- Ferguson, J. and Currie, K.L., 1971, Evidence of liquid immiscibility in the alkaline ultrabasic dykes at Callender Bay, Ontario: J. Petrol., 12, Pt. 3, pp. 561-585.

- Ferguson, J., 1972, The geology and petrology of the alkaline carbonatite complex at Calander Bay, Ontario: Can. Geol. Surv. Bull., 217, 103 pp.
- Ferguson, J., 1973, The Pilanesberg alkaline province, Southern Africa: Geol. Soc. S. Afr., Trans., 76, Pt. 3, pp. 249-270.
- Ferguson, J., Danchin, R.V. and Nixon, P.H., 1973, Fenitization associated with kimberlitic magmas: In: P.H. Nixon (ed.) Lesotho Kimberlites, Lesotho National Development Corporation, Maseru, pp. 207-213.
- Ferguson, J., Danchin, R.V. and Nixon, P.H., 1973, Petrochemistry of kimberlite autoliths: In: P.H. Nixon (ed.), Lesotho Kimberlites, Lesotho National Development Corporation, Maseru, pp. 285-293.
- Ferguson, J., Martin, H., Nicolaysen, L.O. and Danchin, R.V., 1975, Gross Bukkaros: A kimberlite-carbonatite volcano: Phys. and Chem. of the Earth, 9, pp. 219-234
- Fesq, H.W., Kable, E.J.D. and Gurney, J.J., 1975, Aspects of the geochemistry of kimberlites from the Premier mine, and other selected South African occurrences with particular reference to the rare earth elements: Phys. and Chem. of the Earth, 9, pp. 687-708.
- Flanagan, F.J., 1973, 1972 values for international geochemical reference samples: Geochim. Cosmochim. Acta, 32, pp. 1189-1200.
- Fleet, M.E., 1975a, The growth habits of olivine - A structural interpretation: Can. Mineral., 13, Pt. 3, pp. 293-297.
- Fleet, M.E., 1975b, Growth habits of clinopyroxene: Can. Mineral., 13, Pt. 4, pp. 336-241.

- Frankel, J.J., 1956, An inclusion-bearing olivine melilite from Mukorob, Southwest Africa: Geol. Soc. S. Afr., Trans, 35, pp. 115-123.
- Frantsesson, E.V., 1970, The Petrology of the Kimberlites: Trans. from Russian by D.A. Brown, Dept. of Geol., Australian National Univ., Publ. no. 150, 195 pp.
- Franz, G.W. and Wyllie, P.J., 1967, Experimental studies in the system $\text{CaO} - \text{MgO} - \text{SiO}_2 - \text{CO}_2 - \text{H}_2\text{O}$: In: P.J. Wyllie (ed.), Ultramafic and Related Rocks, John Wiley & Sons, New York, pp. 323-326.
- Gandhi, S.S., Grasty, R.L. and Grieve, R.A.F., 1969, The geology and geochronology of the Makkovik Bay area, Labrador: Can. J. Earth Sci., 6, No. 5, pp. 1019-1035.
- Garson, M.S., 1962, The Tundulu carbonatite ring complex in Southern Nyasaland: Nyasaland Geol. Surv., Mem. 2, 248 pp.
- Garson, M.S., 1965, Carbonatites in Southern Malawi: Malawi Geol. Surv. Bull., 15, 128 pp.
- Geijer, P., 1928, Alnoitic dykes from the coast region of Lulea and Kalix in Northern Sweden: Fennia, 50, No. 11.
- Gittins, J., 1963, Further evidence for the existence of carbonatite magmas: Can. Mineral., 7, pp. 817.
- Gittins, J., 1973, The significance of some porphyry textures in carbonatites: Can. Mineral., 12, pp. 226-228.
- Gittins, J., Hewins, R.H. and Laurin, A.I.F., 1975, Kimberlitic-carbonatitic dykes of the Saguenay River Valley, Quebec, Canada: Phys. and Chem. of the Earth, 9, pp. 137-148.

- Gold, D.P., 1963, Average chemical composition of carbonatites: *Econ. Geol.*, 58, pp. 988-996.
- Gold, D.P., 1966, The average and typical chemical composition of carbonatites: In: Mineral. Soc. India, Internat. Mineral. Ass. Papers, 4th Gen. Mtg., New Delhi, 1964, pp. 83-91.
- Green, H.W., II, 1972, A CO₂ charged asthenosphere: *Nature Physical Sci.*, 238, pp. 2-5.
- Green, H.W. and Radcliffe, S.V., 1973, CO₂ exsolution in mantle rocks (abstr.): *Eos. (Amer. Geophys. Union, Trans.)*, 54, pp. 492.
- Griffin, W.L., 1973, Lherzolite nodules from the Fen alkaline complex, Norway: *Contrib. Mineral. Petrol.*, 38, pp. 135-146.
- Griffin, W.L. and Taylor, P.N., 1975, The Fen damkjernite: Petrology of a "Central - Complex Kimberlite": *Phys. and Chem. of the Earth*, 9, pp. 163-178.
- Haggerty, S.E., 1973, Spinel of unique composition associated with ilmenite reactions in the Liqhobong kimberlite pipe, Lesotho: In: P.H. Nixon (ed.), *Lesotho Kimberlites*, Lesotho National Development Corporation, Maseru, pp. 149-158.
- Haggerty, S.E., 1975, The chemistry and genesis of opaque minerals in kimberlite: *Phys. and Chem. of the Earth*, 9, pp. 295-308.
- Haggerty, S.E., Collerson, K.D. and Hawkins, D.W., 1975, Oxide relationships in the Aillik - Makkovik Series of intrusions, coastal Labrador: Unpubl. abstr., 1975 Kimberlite Conference, Cambridge, England.

- Harvie, R., 1909, On the origin and relations of the Palaeozoic breccia of the vicinity of Montreal: Roy. Soc. Can., Trans., 3th. Ser., 3, pp. 249-299.
- Heinrich, E.W., 1966 (ed.), The Geology of Carbonatites: Rand McNally and Co., Chicago, 555 pp.
- Heinrich, E.W. and Moore, D.G., 1970, Metasomatic potash feldspar rocks associated with igneous alkaline complexes: Can. Mineral., 10, pp. 571-584.
- Hogarth, D.D., 1964, Normal and reverse pleochroism in biotite: Can. Mineral., 8, pp. 136.
- Huang, W.L. and Wyllie, P.J., 1974, Eutectic between wollastonite II and calcite contrasted with thermal barrier in $\text{MgO} - \text{SiO}_2 - \text{CO}_2$ at 30 kilobars, with applications to kimberlite - carbonatite petrogenesis: Earth Planet. Sci. Lett., 24, pp. 305-310.
- Huang, W.L. and Wyllie, P.J., 1976, Melting relationships in the system $\text{CaO} - \text{CO}_2$ and $\text{MgO} - \text{CO}_2$ to 33 kilobars: Geochim. Cosmochim. Acta, 40, pp. 129-132.
- Hyndman, R.D., 1973, Evolution of the Labrador Sea: Can. J. Earth Sci., 10, No. 5, pp. 637-644.
- Irving, A.J. and Wyllie, P.J., 1973, Melting relationships in $\text{CaO} - \text{CO}_2$ and $\text{MgO} - \text{CO}_2$ to 36 kilobars with comments on CO_2 in the mantle: Earth Planet. Sci. Lett., 20, pp. 220-225.
- Irving, A.J. and Wyllie, P.J., 1975, Subsolvus and melting relationships for calcite, magnesite and the join $\text{CaCO}_3 - \text{MgCO}_3$ to 36 Kb: Geochim. Cosmochim. Acta, 39, pp. 35-53.

- Janse, A.J.A., 1975, Kimberlite and related rocks from the Nama Plateau of South-west Africa: *Phys. and Chem of the Earth*, 9, pp. 81-94
- Johnson, R.L., 1961, The geology of the Dorowa and Shawa carbonatite complexes, Southern Rhodesia: *Geol. Soc. S. Afr., Trans.*, 64, pp. 101-145.
- Kable, E.J.D., Fesq, H.W. and Gurney, J.J., 1975, The significance of the inter-element relationships of some minor and trace elements in South African kimberlites: *Phys. and Chem of the Earth*, 9, pp. 709-734.
- Kaitaro, S., 1953, Geologic structure of the Late Precambrian intrusives in the Ava Area, Aland Island: *Bull. Comm. Geol. Finlande*, 162, 71 pp.
- King, A.F., 1963, Geology of the Cape Makkovik Peninsula, Aillik, Labrador: Unpubl. M.Sc. thesis, Memorial University of Newfoundland, St. John's.
- King, A.F., and McMillan, N.J., 1975, A mid-Mesozoic breccia from the coast of Labrador: *Can. J. Earth Sci.*, 12, No. 1, pp. 44-51.
- King, B.C. and Sutherland, D.S., 1960a, Alkaline rocks of Eastern and Southern Africa, Part II, Petrology: *Sci. Prog.*, 48, pp. 709-720.
- King, B.C. and Sutherland, D.S., 1960b, Alkaline rocks of Eastern and Southern Africa, Part III, Petrogenesis: *Sci. Prog.*, 48, pp. 709-720.
- Koenig, J.B., 1956, The petrology of certain igneous dykes of Kentucky: *Kentucky Geol. Surv., Bull.*, 21, pp. 1-57.
- Kopécký, L., 1971, Relationship between fenitization, alkaline magmatism, barite - fluorite, mineralization and deep-fault tectonics in the

- Bohemian Massif: Upper Mantle Project, Czechoslovakia (1962-1970), Geology, Final Report, Prague, pp. 73-95.
- Kopécký, L., 1972, Relationship between fenitization, alkaline magmatism, sulphide-barite-fluorite mineralization and deep fault tectonics in the Bohemian Massif and in the Rhinegraben: Int. Geol. Congr., 24th., Montreal, Sect. 14, pp. 3-17.
- Koster, Van Groos, A.F., 1975, The effect of high CO₂ pressure on alkaline rocks and its bearing on the formation of alkalic ultrabasic rocks and the associated carbonatites: Amer. J. Sci., 275, pp. 163-185.
- Koster Van Groos, A.F. and Wyllie, P.J., 1963, Experimental data bearing on the role of liquid immiscibility in the genesis of carbonatites: Nature, 199, pp. 801-802.
- Koster Van Groos, A.F., 1966, Liquid immiscibility in the system Na₂O-Al₂O₃-CO₂ at pressure to 1 kilobar: Amer. J. Sci., 264, pp. 234-255.
- Koster Van Groos, A.F., 1968a, Melting relationships in the system NaAlSi₃O₈-NaF-H₂O to 4 kilobars pressure: J. Geol., 76, pp. 50-70.
- Koster Van Groos, A.F., 1968b, Liquid immiscibility in the join NaAlSi₃O₈-Na₂CO₃-H₂O and its bearing on the genesis of carbonatites: Amer. J. Sci., 266, pp. 932-967.
- Kovalsky, V.V. and Egorov, O.S., 1966, Kimberlite and carbonatite breccias on the eastern side of the Anabar anteklise: In: Soveshchamie po geologiialmaznykh mestorozhdeniy (tezisy dokl.), Perm.
- Kranck, E.H., 1939, Bedrock geology of the seaboard region of Newfoundland, Labrador: Newfoundland Geol. Surv., Bull. 19.

- Kranck, E.H., 1953, Bedrock geology of the seaboard of Labrador between Domino Run and Hopedale: Can. Geol. Surv., Bull. 27, 45 pp.
- Kranck, E.H., 1961, An unusual type of deformation in a basic sill: Bull., Geol. Inst. Univ., Upsaala, 40.
- Kumarapeli, P.S., 1970, Monteregian alkalic magmatism and the St. Lawrence rift system in time and space: Can. Mineral., 10, Pt. 3, pp. 421-431.
- Kumarapeli, P.S. and Saul, V.A., 1966, The St. Lawrence valley system: A North American equivalent of the East African rift valley system: Can. J. Earth Sci., 3, pp. 639-658.
- Kushiro, I., 1970, Stability of amphibole and phlogopite in the upper mantle: Carnegie Inst. Wash. Yearb., 69, pp. 245-257.
- Kushiro, I. and Erlank, A.J., 1970, Stability of potassic richterite: Carnegie Inst. Wash. Yearb., 69, pp. 231-233.
- Kushiro, I., Syono, Y. and Akimoto, S., 1967, Stability of phlogopite at high pressures and possible presence of phlogopite in earth's upper mantle: Earth Planet. Sci. Lett., 3, pp. 197-203.
- Lebedev, A.P., 1964, Kimberlites of Northeastern U.S.S.R. and allied problems: Geol. J., 4, pp. 87-104.
- Lee, H.A. and Lawrence, D.E., 1968, A new occurrence of kimberlite in Gauthier Township, Ontario: Can. Geol. Surv., Paper 68-22, pp. 1-16.
- Leech, G.B., Lowden, J.A., Stockwell, C.H. and Wanless, R.K., 1963, Age determinations and geological studies: Can. Geol. Surv., Paper 63-17, pp. 114-117.

- Lewis, H.C., 1887, On diamantiferous peridotite and the genesis of diamond: *Geol. Mag.*, 4, pp. 22-24.
- Lewis, H.C., 1888, The matrix of diamond: *Geol. Mag.*, 5, pp. 129-131.
- Lézier, J.C., 1966, Inclusions dans quelque nodules de péridotites d'Auvergne: *Compt. Rend.*, 263, pp. 209-211.
- Lieber, O.M., 1860, Notes on the geology of the coast of Labrador: Report of the U.S. Coast Surv.
- Lofgren, G.E. and Donaldson, C.H., 1975, Curved branching crystals and differentiation in comb-layered rocks: *Contrib. Mineral. Petrol.*, 49, pp. 309-319.
- Luth, W.C., 1967, Studies in the system $KAlSiO_4 - Mg_2SiO_4 - SiO_2 - H_2O$.
I - Inferred phase relations and petrological applications: *J. Petrol.*, 8, pp. 372-416.
- Malpas, J., 1976, The petrology and petrogenesis of the Bay of Islands ophiolite suite, Western Newfoundland. Unpubl. Ph.D. thesis, Memorial University of Newfoundland, St. John's.
- Marshintsev, V.K. and Balakshin, G.D., 1969, On the origin of carbonatite formation on the eastern side of the Anabar arched uplift: *Akad. Nauk SSSR, Dokl.*, 188, No. 3.
- Martens, J.H.C., 1924, Igneous rocks of Ithaca, New York and vicinity. *Geol. Soc. Amer., Bull.*, 35, pp. 305-320.
- Maxwell, J.A., 1968, Rock and Mineral Analyses: Interscience Publishers, New York, 584 pp.

- Melton, C.E., Salotti, C.A. and Giardini, A.A., 1972, The observation of nitrogen, water, carbon dioxide, methane and argon as impurities in natural diamond: *Amer. Mineral.*, 57, pp. 1518-1523.
- Métais, D. and Chayes, F., 1963, Varieties of lamprophyre: *Carnegie Inst. Wash. Yearb.*, 62, pp. 156-157.
- Meyer, H.O.A. and Brookins, D.G., 1971, Eclogite xenoliths from Stockdale kimberlite, Kansas: *Contrib. Mineral. Petrol.*, 34, pp. 60-72.
- Mitchell, R.H., 1970, Kimberlites and related rocks - A critical re-appraisal: *J. Geol.*, 78, pp. 686-704.
- Mitchell, R.H. and Fritz, P., 1973, Kimberlite from Somerset Island: *Can. J. Earth Sci.*, 10, No. 3, pp. 384-393.
- Modreski, P.J. and Boettcher, A.L., 1972, The stability of phlogopite and enstatite at high pressures: A model for micas in the interior of the earth: *Amer. J. Sci.*, 272, pp. 852-869.
- Moore, T.H., 1951, Igneous dyke rocks of the Aillik - Makkovik area, Labrador: Unpubl. thesis, McGill University, Montreal.
- Moorhouse, W.W., 1969, The Study of Rocks in Thin Section: Harper and Bros., New York, 514 pp.
- Mukherjee, K.K., 1961, Petrology of lamprophyres of the Bokaro coal field, Bihar: *Mining Metall. Soc. India, Quart. J.*, 33, pp. 69-87.
- McCall, G.J.H., 1963, A reconsideration of certain aspects of the Rongwa and Ruri carbonatite complexes of Western Kenya: *Geol. Mag.*, 100, pp. 181-185.
- McCallum, M.E. and Egger, D.H., 1971, Mineralogy of the Sloan diatreme a kimberlite pipe in Northern Larimer country, Colorado: *Amer.*

- Mineral., 56, No. 9-10, pp. 1735-1749.
- McGetchin, T.R. and Besancon, J.R., 1973, Carbonate inclusions in mantle-derived pyroxenes: Earth Planet. Sci. Lett., 18, pp. 408-410.
- McGetchin, T.R., Nikhanj, Y.S. and Chodos, A.A., 1973, Carbonate-kimberlite relationships in the Cane Valley diatreme, San Juan County, Utah: J. Geophys. Res., 78, No. 11, pp. 1854-1869.
- McGetchin, T.R. and Silver, L.T., 1970, Compositional relationships in minerals from kimberlite and related rocks in the Moses Rock dyke, San Juan County, Utah: Amer. Mineral., 55, pp. 1738-1771.
- Naidu, P.R.J., 1966, Papers and Proceedings, 4th general meeting, International Mineralogical Association, I.M.A. Volume, Mineralogical Association of India, 252 pp.
- Němec, D., 1973, Differentiation series of minettes in the central Bohemian Pluton: J. Geol., 81, pp. 632-642.
- Nikishov, K.N., 1970, Petrology of the kimberlite intrusives: Geologia i uslovia obrazovaniya almaznykh mestorozhdeniy. Permskoe knizhnoye izdatelstvo.
- Nikishov, K.N., Koval'sky, V.V. and Marshintsev, V.K., 1972, Alkaline-ultrabasic rocks (alnöites, kimberlite and carbonatite) of the Northeast Siberian platform: Int. Geol. Congr., 24th, Montreal, Sect. 14, pp. 51-55.
- Nishikawa, M., Kushiro, I. and Uyeda, S., 1971, Stability of a natural hornblende at high water pressures: Preliminary experiments: Jap. J. Geol. Geogr., 41, pp. 41-50.

- Nixon, P.H., 1973, Lesotho Kimberlites: Lesotho National Development Corporation, Maseru, 350 pp.
- Nixon, P.H. and Boyd, F.R., 1973, Petrogenesis of the granular and sheared ultrabasic nodule suite in kimberlite: In: P.H. Nixon, (ed.), Lesotho Kimberlites, Lesotho National Development Corporation, Maseru, pp. 48-56.
- Packard, A.S., 1891, The Labrador Coast: New York.
- Phillips, W.J., 1972, Hydraulic fracturing and mineralization: Geol. Soc. London, Quat. J., 128, pp. 337-359.
- Phillips, W.J., 1973, Interpretation of crystalline spheroidal structures in igneous rocks: Lithos, 6, pp. 235-244.
- Philpotts, A.R., 1972, Density, surface tension and viscosity of the immiscible phase in a basic alkaline magma: Lithos, 5, pp. 1-18.
- Philpotts, A.R. and Hodgson, C.J., 1968, Role of liquid immiscibility in alkaline rock genesis: Int. Geol. Congr., 23th, Prague, 2, pp. 175-188.
- Piloski, M.J., 1955, Geological report on the Aillik - Shoal Lake area: Unpubl. report, British Newfoundland Exploration Company.
- Platten, I.M. and Watterson, J.S., 1969, Oriented crystal growth in some Tertiary dykes: Nature, 223, pp. 286-287.
- Pollard, D.D., 1973, Derivation and evolution of a mechanical model for sheet intrusion: Tectonophysics, 19, pp. 233-269.
- Preston, J., 1963, A columnar crystallization of olivine and plagioclase: Geol. Mag., 100, No. 1, pp. 1-6.

Reid, A.M., Donaldson, C.H., Dawson, J.B., Brown, R.W. and Ridley, W.I., 1975, The Igwishi Hills "Extrusive Kimberlites": Phys. and Chem. of the Earth, 9, pp. 199-218.

Rickwood, P.C., 1969, The nature and occurrence of non-eclogitic ultramafic xenoliths in the kimberlites of Southern Africa: In: Upper Mantle Project, Geol. Soc. S. Afr., Spec. Publ., 2, pp. 395-416.

Rickwood, P.C. and Mathias, M., 1970, Diamantiferous eclogite xenoliths in kimberlite: Lithos, 3, pp. 223-235.

Riley, G.C., 1951, The bedrock geology of the Makkovik and its relation to the Aillik and Kaipokok Series: Unpubl. thesis, McGill University, Montreal.

Rimsaite, J., 1969, Evolution of zoned micas and associated silicates in the Oka Carbonatite: Contrib. Mineral. Petrol., 23, pp. 340-360.

Rimsaite, J., 1971, Distribution of major and minor constituents between mica and host ultrabasic rocks and between zoned mica and zoned spinel: Contrib. Mineral. Petrol., 33, pp. 259-272.

Robinson, D.N., 1975, Magnetite - serpentine - calcite dykes at Premier mine and aspects of their relationship to kimberlite and to carbonatite of alkalic carbonatite complexes: Phys. and Chem. of the Earth, 9, pp. 61-70.

Roedder, E., 1965, Liquid CO₂ inclusions in olivine-bearing nodules and phenocrysts in basalts: Amer. Mineral., 50, pp. 1746-1782.

Rotman, V.K., Markovskiy, B.A. and Khotina, M.I., 1973, The Kamchatka ultrabasic volcanic province: Int. Geol. Rev., 15, No. 9, pp. 1015-1024.

- Saether, E., 1957, The alkaline rock province of the Fen area in Southern Norway: Nor. Vidensk. Selsk., Skr., 1, pp. 1-150.
- Shand, S.J., 1934, The heavy minerals of kimberlite: Geol. Soc. S. Afr., Trans., 7, pp. 57-68.
- Shaw, D.M., 1968, A review of K-Rb fractionation trends by covariance analysis: Geochim. Cosmochim. Acta, 32, pp. 573-603.
- Sheinmann, Y.M., 1957, Location and age of alkalic ultrabasic rocks of the Siberian platform: Razvedka i okrano nedra, 23, pp. 12-16.
- Simkin, T., 1967, Flow differentiation in the picritic sills of North Skye: In: P.J. Wyllie (ed.), Ultramafic and Related Rocks, John Wiley and Sons, New York, pp. 64-69.
- Singewald, J.T. and Milton, C., 1930, An alnöitic pipe, its contact phenomena and ore deposition near Avon, Missouri: J. Geol., 38, pp. 54-66.
- Smirnov, G.I., 1959, Mineralogy of Siberian kimberlites: Int. Geol. Rev., 1, No. 2, pp. 21-39.
- Smith, J.V., Steele, I.M., Hrubec, J. and Dawson, J.B., 1975, Chemistry of mantle minerals: Unpubl. abstr., 1975 Kimberlite Conference, Oxford, England.
- Smyth, W.R., Martin, B.E. and Ryan, A.B., 1975, Geological mapping in the Central Mineral Belt, Labrador: Redefinition of the Croteau Group: Newfoundland Dept. of Mines and Energy, Report of Activities, 1974.

- Sobolev, N.V., 1970, Eclogites and pyrope peridotites from the Kimberlites of Yakutia: *Phys. Earth Planet. Interiors*, 3, pp. 398-404.
- Sobolev, V.S., Dobretsov, N.L. and Sobolev, N.V., 1973, Classification of xenoliths of deep-seated origin and types of the upper mantle: *Int. Geol. Rev.*, 151, Iss. 10, pp. 1197-1202.
- Steele, T.W., 1972, Preliminary report on the analysis of the six Nimroc geochemical standard samples: *Nat. Inst. Metall., Rept. 3151*, Johannesburg, South Africa.
- Steinhauer, H., 1814, Notes on the geology of the Labrador coast: *Trans. Geol. Soc.*, II, pp. 488-491.
- Stevenson, I.M., 1970, Rigolet and Groswater Bay map areas, Newfoundland: *Can., Geol. Surv., Paper 69-48*, 24 pp.
- Stewart, J.W., 1970, Precambrian alkaline - ultramafic/carbonatite volcanism at Qagssiarssuk, South Greenland: *Meddr. Grønland*, Bd. 179, No. 9, 66 pp.
- Strong, D.F. and Harris, A., 1974, The petrology of Mesozoic alkaline intrusives of Central Newfoundland: *Can. J. Earth Sci.*, 11, No. 9, 1208-1219.
- Sutton, J.S., 1972, The Precambrian gneisses and supracrustal rocks of the western shore of Kaipokok Bay, Labrador, Newfoundland: *Can. J. Earth Sci.*, 9, No. 12, pp. 1677-1692.
- Sutton, J.S., Marten, B.E. and Clark, A.M.S., 1971, Structural history of the Kaipokok Bay area, Labrador, Newfoundland: *Geol. Ass. Can., Proc.*, 24, No. 1, pp. 103-106.

- Taylor, F.C., 1971, A revision of Precambrian structural provinces in Northeastern Quebec and Northern Canada: Can. J. Earth Sci., 8, No. 5, pp. 579-584.
- Taylor, F.C., 1972, The Main Province: In: R.A. Price and R.J.W. Douglas (eds.), Variation in Tectonic Styles in Canada: Can., Geol. Surv., Spec. Paper, No. 11, pp. 436-452.
- Taylor, S.R., 1965, The application of trace element data to problems in petrology: Phys. and Chem. of the Earth, 6, pp. 133-213.
- Tuttle, O.F. and Gittins, J., 1966, Carbonatites: Interscience, New York, 591 pp.
- Ukhanov, A.V., 1965, Olivine melilite from the diamond-bearing diatremes on Anabar: Akad. Nauk SSSR, Dokl., 153, pp. 176-178.
- Upton, B.G. and Thomas, J.E., 1973, Precambrian potassic ultramafic rocks: South Greenland: J. Petrology, 14, No. 3, pp. 509-534.
- Vahtra, J., 1975, Unpublished precision and accuracy data for X.R.F. analysis.
- Van Der Linden, W.J.M., 1975, Crustal attenuation and sea-floor spreading in the Labrador Sea: Earth Planet. Sci. Lett., 27, pp. 409-423.
- Von Eckermann, H., 1948, The alkaline district of Alnö Island: Sver. Geol. Under (ARSb.), Ser. Ca. No. 36, 176 pp.
- Von Eckermann, H., 1961, The petrogenesis of the Alnö alkaline rocks: Bull., Geol. Inst. Univ. Upsala, 40, pp. 25-36.
- Von Eckermann, 1966, Progress of research of the Alnö carbonatite: In: O.F. Tuttle and J. Gittins(eds.), Carbonatites: Interscience, New York, pp. 3-32.

- Von Eckermann, H., 1967, A comparison of Swedish, African and Russian kimberlites: In: P.J. Wyllie (ed.), Ultramafic and Related Rocks: John Wiley and Sons, New York, pp. 302-312.
- Wagner, P.A., 1914, The Diamond Fields of Southern Africa: Transvaal Leader, Johannesburg, 347 pp.
- Walker, G.P.L. and Ross, J.V., 1954, A xenolithic monchiquite dyke near Glenfinnan, Inverness - Shire: Geol. Mag., 91, No. 6, pp. 463-472.
- Walton, B.J., 1965, Sinerutian appinitic rocks and Gardar dykes and diatremes, north of Narssarssuaq, South Greenland: Meddr. Grønland, Bd. 179, No. 9, 63 pp.
- Walton, B.J., 1966, Carbonatite - lamprophyre dykes of Mesozoic age: Grønlands Geol. Unders., Rapp. 11, pp. 37-39.
- Walton, B.J., and Arnold, A., 1970, Plutonic nodules in lamprophyric - carbonatite dykes near Frederikshab, Southwest Greenland: Grønlands Geol. Unders., Bull 91, pp. 1-34.
- Watson, K.D., 1955, Kimberlite at Bachelor Lake, Quebec: Amer. Mineral., 40, pp. 565-579.
- Watson, K.D., 1967a, Kimberlite pipes of Northeastern Arizona: In: P.J. Wyllie (ed.), Ultramafic and Related Rocks, John Wiley and Sons, New York, pp. 261-269.
- Watson, K.D., 1967b, Kimberlites of Eastern North America: In: P.J. Wyllie (ed.), Ultramafic and Related Rocks, John Wiley and Sons, New York, pp. 312-323.

Watt, W.S., 1969, The coast - parallel dyke swarm of Southwest Greenland in relation to the opening of the Labrador Sea: Can. J. Earth Sci., 6, pp. 1320-1321.

Watterson, J., 1968, Plutonic development of the Ilordleg Area, South Greenland, 2, Late - Kinematic basic dykes: Grønlands Geol. Unders., Bull., 70, 104 pp.

Wilkinson, J.F.G., 1957, The clinopyroxenes of a differentiated teschenite sill near Gunnedah, New South Wales: Geol. Mag., 94, pp. 123-134

Williams, A.F., 1932, The Genesis of the Diamond: Ernest Benn Limited, London, 636 pp.

Williams, H. Turner, F.J. and Gilbert, C.M., 1955, Petrography: W.H. Freeman and Company, San Francisco, 406 pp.

Williams, J.F., 1891, The igneous rocks of Arkansas: Geol. Surv. Arkansas, Ann. Rep. 2, 457 pp.

Woodland, B.G., 1962, Lamprophyre dykes of the Burke area, Vermont: Amer. Mineral., 47, pp. 1094-1110.

Woolley, A.R., 1969, Some aspects of fenitization with particular reference to Chilwa Island and Kangankunde, Malawi: Brit. Mus. (Natur. Histo.), Bull., Geol., 2, No. 4, pp. 191-219.

Wyllie, P.J., 1966a, Experimental studies of carbonatite problems: The origin and differentiation of carbonatite magmas: In: O.F. Tuttle and J. Gittins (eds.), Carbonatites, Interscience, New York, pp. 311-352.

Wyllie, P.J., 1966b, Experimental data bearing on the petrogenetic links

- between kimberlite and carbonatite: In: Mineral. Soc. India, Internat. Mineral. Ass., Papers 4th. Gen. Mtg., New Delhi, 1964, pp. 67-82.
- Wyllie, P.J., 1975, Liquidus phase relationships involving carbonates and silicates in the system $\text{CaO} - \text{MgO} - \text{Al}_2\text{O}_3 - \text{SiO}_2 - \text{CO}_2$ with applications to kimberlite and carbonatite petrogenesis: Unpubl. abstr., 1975 Kimberlite Conference, Oxford, England.
- Wyllie, P.J. and Boettcher, A.L., 1969, Liquidus phase relationships in the system $\text{CaO} - \text{CO}_2 - \text{H}_2\text{O}$ to 40 kilobars pressure with petrological applications: Amer. J. Sci., Schairer Volume, 267-A, pp. 489-509.
- Wyllie, P.J. and Drever, H.I., 1963, The petrology of picritic rocks in minor intrusions - A picritic sill on the Island of Soay (Hebrides): Roy. Soc. Edinburgh, Trans., 65, pp. 155-177.
- Wyllie, P.J. and Haas, J.L., 1965, The system $\text{CaO} - \text{SiO}_2 - \text{CO}_2 - \text{H}_2\text{O}$; I melting relationships with excess vapor at 1 kilobar pressure: Geochim. Cosmochim. Acta, 29, pp. 871-893.
- Wyllie, P.J. and Haas, J.L., 1966, The system $\text{CaO} - \text{SiO}_2 - \text{CO}_2 - \text{H}_2\text{O}$; II The petrogenetic model: Geochim. Cosmochim. Acta, 30, pp. 525-544.
- Wyllie, P.J. and Huang, W., 1975, Peridotite, kimberlite and carbonatite explained in the system $\text{CaO} - \text{MgO} - \text{SiO}_2 - \text{CO}_2$: Geology, Nov., pp. 621-624.
- Wyllie, P.J. and Tuttle, O.F., 1960, The system $\text{CaO} - \text{CO}_2 - \text{H}_2\text{O}$ and the origin of carbonatites: J. Petrol., 1, pp. 1-46.

Zhabin, A.G. and Cherepyskaya, G.Y., 1975, Carbonatite dykes as related to ultrabasic - alkalic extrusive igneous activity: Acad. Sci. USSR, Dokl., Earth Sci. Sect., 160, pp. 135-138.

APPENDIX I

DETAILED GEOLOGY OF THE AILLIK GROUP AT AILLIK BAY

The following appendix is included to augment the brief description in the text of the thesis (page 14) and contains a more detailed account of the geology of the Early Proterozoic Aillik Group; the country rocks into which many of the basic to ultrabasic dykes were emplaced.

1. Cross-bedded Arkose and Conglomerate

1.1 Distribution and Contact Relationships

This is the oldest unit of the Aillik Group mapped in the Aillik Bay area (Gandhi et al., 1969) and is seen as sporadic exposures from Cape Aillik to an area south of Aillik Village (Fig. 2.1). The arkoses and conglomerate have a total thickness of 396 m in the Makkovik area (Gandhi et al., 1969) but at Cape Aillik the bottom of the succession is not visible.

1.2 Lithology

The arkoses are generally fine grained and have quartzo-feldspathic bands which alternate with more mafic bands on a 2 to 4 cm scale. This variation reflects an original compositional difference between the beds. Sedimentary structures such as cross-bedding and flame structures indicate that the units are upright.

The conglomerate horizon overlies the arkose unit but is known to interfinger with it near the contacts (Clark, 1971). The conglomerate horizon is heterogeneous and contains pebbles and/or cobbles of granitic gneiss, chert and jasper which range from 2 to 10 cm in diameter (Gandhi et al., 1969).

1.3 Correlation with other Horizons in the Aillik Group

The arkoses and conglomerates can be traced southwards to an area southeast of Mark's Bight (Clark, 1971). These sedimentary horizons are tentatively correlated with the cross-bedded arkose and conglomerate members of the Big Island Formation (Clark, 1974).

2. Arkosic Quartzite, Calc-silicate Breccia and Marble

2.1 Distribution and Contact relationships

This unit forms a prominent sedimentary horizon along the eastern shore of Aillik Bay (Fig. 2.1). The arkose may overlie the cross-bedded unit; however, contacts aren't exposed, thus the exact stratigraphic level of this unit isn't known.

2.2 Lithology

The unit is characterized by a well developed banding on a scale of 1 to 3 cm where quartzo-feldspathic bands alternate with more mafic-rich layers. This banding reflects original bedding in the unit; however, it has been folded and contorted during deformation of the Aillik Group.

A zone of calc-silicate breccia within the unit occurs as two isolated exposures southwest of Hawk Pond. The breccia contains abundant subangular arkosic quartzite fragments (60 to 70 percent) in a carbonate matrix. Individual blocks range from 2 to 100 cm in length by 0.5 to 50 cm in width and are flattened into the foliation plane. They are augened by the matrix which contains 70 to 80 percent salmon-red carbonate as well as epidote, diopside, garnet, amphibole and mica (King, 1963). Carbonate pressure fringes are commonly seen at the ends of the flattened blocks indicating migration and recrystallization of the carbonate in areas of low pressure during deformation. The breccias have gradational contacts with the arkose which are characterized by decreasing carbonate content and brecciation. The eastern gradational contacts with the arkose is strongly banded and original bedding is preserved. Cross-bedding in this area indicates that the arkose unit is upright and dips steeply to the east. Northward the breccia is lost under granophyre sheets. Several horizons of a calc-silicate unit are found near the diabase porphyry west of Hawk Pond and are similar in lithology to the matrix of the calc-silicate breccia. The units are 30 cm to 1.5 m thick and probably represent a northern equivalent of the breccia unit.

3. Conglomerate

3.1 Distribution and Contact Relationships

The conglomerate forms a thin sequence approximately 458 m

thick (King, 1963) and crops out from just north of Hawk Pond to an area west of Banana Lake (Fig. 2.1). It conformably overlies the arkosic quartzite unit and has a gradational contact, 46 m wide.

3.2 Lithology

The conglomerate is characterized by a sporadic clast distribution and areas containing 60 percent clasts quickly grade into areas consisting solely of quartzo-feldspathic matrix material. The clasts vary in composition from chloritic quartzite, quartzite to scattered granitoid types (King, 1963) and are contained in a strongly banded matrix consisting of alternating quartz-rich and quartzo-feldspathic layers on a 0.5 to 1.0 cm scale. Most clasts are lenticular in shape and show a marked decrease in abundance both to the north and south. Eastern sections of this unit appear to be lithologically similar to unit 5 (Fig. 2.1).

Marble horizons are not uncommon and occur as salmon red carbonate interbeds which possibly represent limestone horizons.

4. Banded Quartzo-feldspathic Unit

4.1 Distribution and Contact Relationships

This unit forms a northern equivalent of the conglomerate horizon. It has gradational contacts with the former unit near Hawk Pond where a transitional zone 214 m wide exists.

4.2 Lithology

The quartzo-feldspathic unit forms a distinct lithological horizon which is characterized by a well developed banding of quartz and feldspathic layers on a 3 mm to 1 cm scale.

5. Undifferentiated Sediments and Acid Volcanics

5.1 Distribution and Contact Relationships

A unit composed of sediments and acid volcanics forms a wedge shaped outcrop from Buttriss Point to an area southwest of Hawk Pond, (Fig. 2.1). It appears to have a gradational contact with the conglomerate horizon.

5.2 Lithology

This unit is lithologically similar to the clast deficient areas of the conglomerate horizon and exhibits a banding of quartzo-feldspathic and feldspathic layers. It also contains sporadic amphibole-rich pods or veinlets and the latter often transgress the foliation. The unit has a rhyolitic appearance south of Hawk Pond and closely resembles units within the Big Island Formation (Clark, 1974).

6. Sediments (Including Acid Volcanics) Showing Varying Degrees of Secondary Feldspathization

6.1 Distribution and Contact Relationships

Two units of this character were mapped in the Aillik area, but

could be separated by the degree of secondary feldspathization. The smallest exposure (unit 7, Fig. 2.1) crops out from Buttriss Point to northwest of Banana Lake. It has conformable contacts with the Micaceous Unit (King, 1963) while those with the amphibolite are sheared. The more extensive unit crops out from Low Point to immediately west of Banana Lake. This unit usually exhibits sheared contacts.

6.2 Lithology

The smaller unit is similar to the horizon which overlies the conglomerate unit. It is characterized by local concentrations (30 - 60 percent) of alkali feldspar porphyroblasts. The porphyroblasts are regarded to be secondary in origin and have selectively replaced most of the original plagioclase (King, 1963). The secondary feldspathization is most intense in a lenticular zone centered immediately east of Hawk Pond; however, it decreases rapidly both to the north and south.

The larger unit (unit 9, Fig. 2.1) forms a highly feldspathized horizon and in northern sections is characterized by sodic amphibole and pyroxene. Secondary feldspathization decreases to the south but still maintains an appearance similar to the units overlying the conglomerate and micaceous horizons.

Rounded quartz eyes are a characteristic feature of this unit

and modal proportions range from 40 to 65 percent. The sodic ferromagnesian minerals (aegirine, aegirine augite and riebeckite) are of secondary origin and replace mica and/or quartz. They also occur in cross-cutting veinlets, a feature typical of fenitized terrains (Cooper, 1971; Currie, 1971; Deans et al., 1972; Tuttle and Gittins, 1966). At Low Point, this unit can be traced into the cross-bedded arkoses which probably represent the northern equivalent of the feldspathized units.

It is apparent that feldspathization initially occurred by the growth of potash feldspar porphyroblasts along a cleavage or schistosity plane. These horizons show similarities with rocks found in or near Central Carbonatite Complexes (Ferguson and Currie, 1972; Woolley, 1969; Deans et al., 1972; Currie, 1971b; Heinrich and Moore, 1970).

7. Undifferentiated Acid Volcanics and Quartzo-feldspathic Sediments (Possibly Equivalent to the Previous Unit)

7.1 Distribution and Contact Relationships

This unit is the thickest sequence mapped in the Aillik Bay area. It crops out from Cape Makkovik southward to the southern tip of Banana Lake (Fig. 2.2). A smaller exposure is also seen immediately east of Dax Pond where it grades rapidly into the previous unit (unit 9, Fig 2.2). The larger unit has sharp tectonic contacts with the quartzo-feldspathic mylonites.

7.2 Lithology

The unit contains variable amounts of alkali feldspar porphyroblasts (20 to 50 percent) which range in size from 2 to 4 mm and have a hypidiomorphic form. Quartz forms 10 to 30 percent and is accompanied by a medium to fine grained matrix of feldspar, quartz and amphibole. At Cape Makkovik, the unit contains abundant amphibolite pods 1 to 6 cm long and 2 to 5 mm wide which decrease in concentration towards the south. The succession east of the Tidal Flats area has a similar lithological character to the feldspathized parts of unit 9 (Fig. 2.2). The origin of these lenticular pods is unclear. Clark (1971, 1974) has interpreted a similar unit inland from Makkovik (which also contains abundant amphibolite pods) to be an acidic lapilli tuff.

8. Other Units

8.1 Micaceous Unit

8.1.1 Distribution, Contact Relationships and Lithology

The micaceous unit forms a thin band which outcrops from Buttress Point to an area just northwest of Banana Lake. It has a thickness of 14 m and exhibits a gradational contact with the undifferentiated acid volcanic and sediment unit. The unit is fine grained, has a greenish grey color and contains quartz, microcline, chlorite and biotite. Southward the unit becomes a chlorite-biotite schist.

8.2 Amphibolite

8.2.1 Distribution and Contact Relationships

Two horizons of amphibolite occur in the northern part of the map area. The thinnest unit is exposed at Buttress Point while a thicker horizon crops out immediately west of the Tidal Flat area and continues northward to Cape Makkovik (Fig. 2.2). The horizons thicken southward and unit to form one continuous unit.

8.2.2 Lithology

The most conspicuous feature of the amphibolites south of Dax Pond is the abundance of relict pillows which are flattened into the foliation plane. They range in size from 10 to 30 cm long x 10 to 12 cm wide and in some cases, still retain glassy selvages.

9.1 Quartzofeldspathic Mylonite

9.1.1 Distribution and Contact

A unit of mylonite separates the amphibolites from the uppermost horizon mapped in the Aillik Group. It is exposed in a glacially overdeepened valley which extends from Banana Lake to an area east of Low Point.

9.1.2 Lithology

The mylonitic unit occurs in a distinct zone of intense cataclasis in which the original mineralogy is granulated and recrystallized. It consists of alternating quartz-rich (5 to 7 mm wide) and quartzo-feldspathic bands and contains numerous amphibolitic pods which may constitute 30 to 40 percent of the entire outcrop. Quartz porphyroclasts 3 to 8 mm in length commonly occur in local concentrations and are invariably surrounded by fine grained anastomosing layers of quartzo-feldspathic material. Sodic amphiboles and/or pyroxene occur either as small radiating crystals in the matrix or in veinlets which postdate the tectonic foliation.

10. Origin of the Feldspathizing and Fentizing Solutions

The solutions responsible for the secondary alteration in the Aillik Group are considered to have originated from the alkalic ultrabasic magma which gave rise to the Aillik Bay ultrabasic-basic dyke swarm. The localization of the alteration effects to faults and/or areas of microbrecciation implies they were introduced as liquids after the deformation of the Aillik Group and hence may coincide with dyke emplacement. Alteration of this type is not unlike that described near alkaline intrusions in the St. Lawrence Rift System (Currie and Ferguson, 1971) or the Bohemian Massif (Kopecký, 1971, 1972).

APPENDIX II
TERMINOLOGY

The nomenclature of kimberlites, carbonatites and lamprophyres has become extremely complex in recent years, as a result, a discussion of the terminology used by the author in this thesis is included.

The name kimberlite, as first proposed by Henry Carvill Lewis (1887, 1888), was used to describe the porphyritic peridotite that was a host for diamonds in Kimberley, South Africa. By the mid 1900's, a variety of rock types were collectively classified as kimberlites and the original meaning of the word was lost through its varied application. In 1970, Mitchell presented a critical review of kimberlites and related rocks in the light of 70 to 80 years of geological observation since the introduction of the term kimberlite into the geological literature. Mitchell (1970) restricts the term kimberlite to rocks that are "porphyritic, alkalic peridotites containing rounded and corroded phenocrysts of olivine (serpentinized, carbonatized, or fresh), phlogopite (fresh or chloritized), magnesium ilmenite, pyrope and chrome-rich pyrope, set in a fine grained ground-mass composed of second generation olivine and phlogopite with calcite (and/or dolomite), serpentine (and/or chlorite), magnetite, perovskite and apatite. Diamond and garnet peridotite xenoliths may or may not occur."

The presence of pyrope and chrome-rich pyrope is not considered by the author to be an essential mineral in a rock of kimberlite composition as many kimberlite dykes have been recognized which are free of such minerals (Dawson and Hawthorne, 1973). Kimberlites are well known for their dual petrological character in that they exhibit mantle as well as a kimberlite-derived mineralogy (Dawson, 1971, 1972; Mitchell, 1970). It is customary to describe all foreign crystals as xenocrysts (large crystals whose origin cannot be attributed to the crystallization of the kimberlite magma) as they originate by the fragmentation of mantle material. They are similar compositionally to the mineral phases found in mantle-derived nodules, i.e. forsteritic olivine (Fo 90 - 94), enstatite (En 90 - 94), chrome-diopside, pyrope are most common. Crystals which can be shown to be kimberlite-derived are classified as phenocrysts (Mitchell, 1970). These include olivine, phlogopite and magnesium ilmenite (Dawson, 1972; Mitchell, 1970).

Olivine is the most abundant mineral in kimberlites and usually occurs in two generations. Those of the first generation are highly rounded, corroded and may exhibit undulose extinction (Mitchell, 1970). These first generation olivines are often xenocrysts but may also be phenocrysts as Fo contents range from 84 to 93. (Dawson and Hawthorne, 1973) for both types. Second generation olivine is generally euhedral and forsteritic contents from 80 to 84 are common

although second generation crystals are a common matrix phase, they do occur as phenocrysts.

Phlogopite, like olivine, occurs in two generations and contents vary from 1 to 70 percent in extreme types, the latter being referred to as micaceous kimberlites (Dawson, 1971, 1972; Mitchell, 1970). First generation phlogopite is corroded, rounded, kinked and/or folded (Mitchell, 1970). These crystals possibly represent phenocrysts although the presence of phlogopite in the mantle has received significant support from a number of authors (Dawson and Powell, 1969; Dawson, 1964; Dawson et al., 1970; Modreski and Boettcher, 1972; Kushiro, 1970; Kushiro et al., 1967).

The xenocrystal (phenocrystal) micas often exhibit a reverse pleochroism ($\alpha > \beta = \gamma$) and has been found typical of kimberlites (Mitchell, 1970; Watson, 1955); some carbonatites (Singewald and Milton, 1930); alnöites (Von Eckermann, 1948; Hogarth, 1964) and ultramafic rocks (Boettcher, 1967). Second generation phlogopite occurs as small lath to microlithic shaped crystals which lack reaction mantles or deformation effects.

The term megacryst was introduced by Dawson (1971) to describe crystals in kimberlites which are of unknown origin (i.e. xenocrysts or phenocrysts).

Most of the mineral phases in the Aillik kimberlites are believed

to be phenocrysts as dykes lack garnet,¹¹ orthopyroxene and chromium-bearing diopside.

Alnöites (Von Eckermann, 1948; Bowen, 1922) are common intrusive rocks which are sometimes mistaken for kimberlites (Mitchell, 1970). The author considers alnöites as those rocks which contain pyroxene and/or melilite and show considerable petrological (Allen and Deans, 1965) and/or chemical similarities to kimberlites (Dawson, 1966, 1967). Melilite is the major characteristic mineral; however, the genetic association of alnöite with kimberlite cannot be overlooked (Janse, 1975).

The terminology proposed by Von Eckermann (1948) and Heinrich (1966) is followed for carbonatites in the Aillik area.

Members of the lamprophyre clan have been classified according to Williams et al. (1955).

¹¹ Only one garnet-bearing dyke has been discovered in specimens collected by A.M.S. Clark (Collerson, personal communication).

APPENDIX III
LABORATORY METHODS

3.1 Sample Preparation

Representative samples from the dyke suites were initially trimmed to remove as much weathered material as possible and to avoid xenoliths and/or cognate nodules which could cause contamination. All samples were slabbed perpendicular to any apparent banding and the amount crushed depended upon the complexity of banding; hence, more dyke was crushed in strongly banded dykes. The trimmed slabs were then polished to remove saw contamination. The polished slabs were then washed carefully and dried at 100°C. The slabs were then crushed into small chips with a "cutrock" jaw crusher. These chips were ground into a fine powder using a Siebtechnik tungsten-carbide swing mill.

3.2 Analytical Procedure

3.2.1 Major Elements

Forty-nine of the one hundred and one specimens were analyzed by x-ray fluorescence using a Phillips P.W. 1220 C computerized spectrometer. A program allowed determination of eight major elements which were printed out directly on teletype. For X.R.F. analysis, 0.7000 g of the powdered sample was combined with 6.0 g of lithium tetraborate and 0.7500 g of lanthanum oxide. The mixture was fused into a homogeneous glass bead by heating within graphite crucibles at 1050°C in a Thermolyne furnace. The fused bead was then weighed

and sugar was added to make up the original weight for volatiles lost during fusion. The glass bead and sugar was then crushed in a spex ball mill using tungsten carbide vessels for twenty minutes. 1.5 g of the ground powder was pressed at 5 tons for 1 minute into a borax acid disc using a hydraulic compressor. The sample disc was stored in a heated oven until the analysis was carried out. All major elements (SiO_2 , TiO_2 , Al_2O_3 , Total Fe, MgO , CaO , K_2O) were determined using $\text{CrK}\alpha$ radiation and several different analyzer crystals.

Analytical precision and accuracy were determined by using an internal standard NIM-D (National Institute of Metallurgy standard) which was run with every analytical batch. Results of the precision and accuracy are given in Tables (3.1 and 3.2).

MnO and MgO were determined by atomic absorption methods using a Perkin-Elmer 303 Atomic Absorption Spectrometer equipped with a chart recorder read out. Precisely 0.100 g of finely ground rock powder was weighed into a plastic cap and placed in a polycarbonate digestion bottle. Digestion was effected by the addition of 5 ml hydrofluoric acid and heating for 30 minutes. After cooling 50 ml of saturated borac acid was added in order to complex dissolved fluorides. The solution was again heated on a water bath for 20 minutes and upon cooling was made up to 200 ml by the addition of 145 ml de-ionized water. Standard rock solutions were prepared in a similar manner to that described by Abbey, 1968.

TABLE 3.1

Precision of X-Ray Fluorescence Major Element Determinations Based
Upon National Institute for Metallurgy Standard NIM-D (Dunite)

ELEMENT	NUMBER OF DETERMINATIONS	MEAN (Weight %)	STANDARD DEVIATION
SiO ₂	13	38.05	.18
TiO ₂	13	0.06	.02
Al ₂ O ₃	13	0.70	.16
Fe ₂ O ₃	13	17.25	.31
MnO	N.D.	N.D.	N.D.
MgO	13	54.19	4.25
CaO	13	0.18	.01
Na ₂ O	N.D.	N.D.	N.D.
K ₂ O	13	0.05	.006
P ₂ O ₅	13	N.d.	.000
Loss Ign.	N.D.	N.D.	N.D.

N.D. Not Determined

N.d. Not detected

TABLE 3.2

Accuracy of X-Ray Fluorescence Major Element Determinations Based
On National Institute of Metallurgy Standard NIM-D (Dunite)

ELEMENT	S ⁺	MEAN-ANALYSIS
SiO ₂	38.86	38.05
TiO ₂	0.04	0.06
Al ₂ O ₃	0.44	0.70
Fe ₂ O ₃	16.97	17.25
MnO	0.20	N.D.
MgO	43.30	44.19
CaO	0.31	0.18
Na ₂ O	0.10	N.D.
K ₂ O	0.04	0.05
P ₂ O ₅	0.03	N.d.
Loss Ign.	0.18	N.D.

S⁺ Proposed values for NIM-D (Steele, 1972)

N.D. Not determined

N.d. Not detected

The remaining fifty-two samples were analyzed completely by atomic absorption due to technical problems with the X.R.F. and analytical procedure was similar to that described above for MnO and Na₂O. Precision and accuracy for major element analyses are shown in tables 3.3 and 3.4. Accuracy of major element analyses was determined by repeated analysis of U.S.G.S. Standard BCR-1 (Flanagan, 1973).

3.2.2. Trace Elements

All trace elements (Zr, Sr, Rb, Zn, Cu, Ba, Nb, Ni and Cr) were determined by x-ray fluorescence spectrometer. 1.5 g of rock powder was mixed with 3 drops of liquid sugar solution in a mortar and pestle until a uniform color was obtained. This powder was then pressed into a flat disc using a hydraulic compressor.

Precision and accuracy of trace element analysis was determined by repeated analyses of internal control reference rock powders and are shown in tables 3.5 and 3.6.

3.2.3 FeO

FeO concentrations were obtained by a titration method. 0.100 to 0.1500 g of sample powder were treated with ammonium vanadate and 10 ml of hydrofluoric acid and shaken in a wrist action vibrator to ensure complete digestion of the sample. Several blank solutions were also prepared. Each sample was added to a

TABLE 3.3

Precision of Major Element Analyses (After Malpas, 1976)

Element	No. of Determinations	Mean (Wgt. %)		Ci. (Coeff. of vn.)
SiO ₂	10	45.97	0.73	1.59
TiO ₂	10	0.48	0.01	2.08
Al ₂ O ₃	10	22.01	0.18	0.82
Fe ₂ O ₃	10	4.12	0.10	2.43
MnO	10	0.07	0.01	14.29
MgO	10	9.70	0.01	0.10
CaO	10	13.21	0.05	0.38
Na ₂ O	10	1.55	0.02	1.29
K ₂ O	10	0.11	0.04	36.36
P ₂ O ₅	10	0.02	0.01	50.00
L.I.	10	3.48	0.15	4.31

TABLE 3.4

Accuracy of Major Element Analyses (After Malpas, 1976)

Wgt. %	Proposed Value (Abbey, 1968)	Mean Wgt. %		No. of Determinations
SiO ₂	54.36	55.38	0.26	6
TiO ₂	2.24	2.31	0.19	6
Al ₂ O ₃	13.56	13.52	0.25	6
Fe ₂ O ₃	13.40	13.01	0.27	6
CaO	6.94	6.82	0.06	6
MgO	3.46	3.52	0.06	6
Na ₂ O	3.26	3.26	0.04	6
K ₂ O	1.67	1.70	0.04	6
MnO	0.19	0.17	0.01	6

TABLE 3.5

Summary of Precision Data (Vahtra, 1973)

Sample		XC - 1	XC - 2	XC - 3	XC - 4
No. of Pellets		46	18	16	15
Element:					
Zr	Mean (ppm)	129	90	195	109
	ST. Dev.	22	8	23	11
Sr	Mean (ppm)	98	85	51	102
	ST. Dev.	8	5	14	9
Rb	Mean (ppm)	51	123	146	132
	ST. Dev.	7	8	10	12
Zn	Mean (ppm)	27	88	24	29
	ST. Dev.	1	2	1	1
Cu	Mean (ppm)	15	14	14	11
	ST. Dev.	2	3	3	2
Ba	Mean (ppm)	1042	1194	966	973
	ST. Dev.	80	67	57	64
Nb	Mean (ppm)	15	15	19	21
	ST. Dev.	2	4	3	3
Ni	Mean (ppm)	12	69	23	25
	ST. Dev.	3	1	2	2
Cr	Mean (ppm)	12	53	N/A	N/A
	ST. Dev.	4	4		

TABLE 3.6

Summary of Accuracy Data (Vahtra, 1973)

Element	Standard Deviation (s.d.)	Range	Mean	No. of Standards # of Pellets Stds.	
Zr	20	s.d. to 700	200	18	12
Sr	18	s.d. - 1400	250	24	18
Rb	8	s.d. - 400	130	21	15
Zn	10	s.d. - 350	100	24	16
Cu	3	s.d. - 110	35	27	16
Ba	46	s.d. - 1900	700	20	14
Nb	4	s.d. - 300	32	19	13
Ni	21	s.d. - 2400	410	24	16
Cr < 400 ppm	7	s.d. - 400	50	18	12
Cr > 400 ppm	140	400 - 4000	2800	5	4

400 ml beaker containing 100 ml of saturated boric acid and the digestion bottles were then rinsed with an additional 100 ml to ensure that all sample powder and/or ions were removed. 10 ml mixed acid (H_2SO_4 , H_3PO_4), 10 ml of ferrous ammonium sulfate and several drops of barium diphenylamine sulfonate were added to the above solution. It was then titrated with potassium dichromate (K_2CrO_7) and the end point resulted in an aqua blue solution.

The FeO content was determined by the formula:

$$\text{FeO} = \frac{(\text{K}_2\text{CrO}_7 \text{ sample}) - (\text{K}_2\text{CrO}_7 \text{ blank}) \times 0.70353}{\text{sample weight}}$$

where K_2CrO_7 sample = volume of K_2CrO_7 used to reach end point
 K_2CrO_7 blank = volume of K_2CrO_7 used to reach end point in blank
 sample weight = amount (g) of sample digested

The total iron (determined by X.R.F.) was corrected for FeO content and the amount left was regarded as Fe_2O_3 . The loss on ignition was also corrected for oxidation of iron during heating.

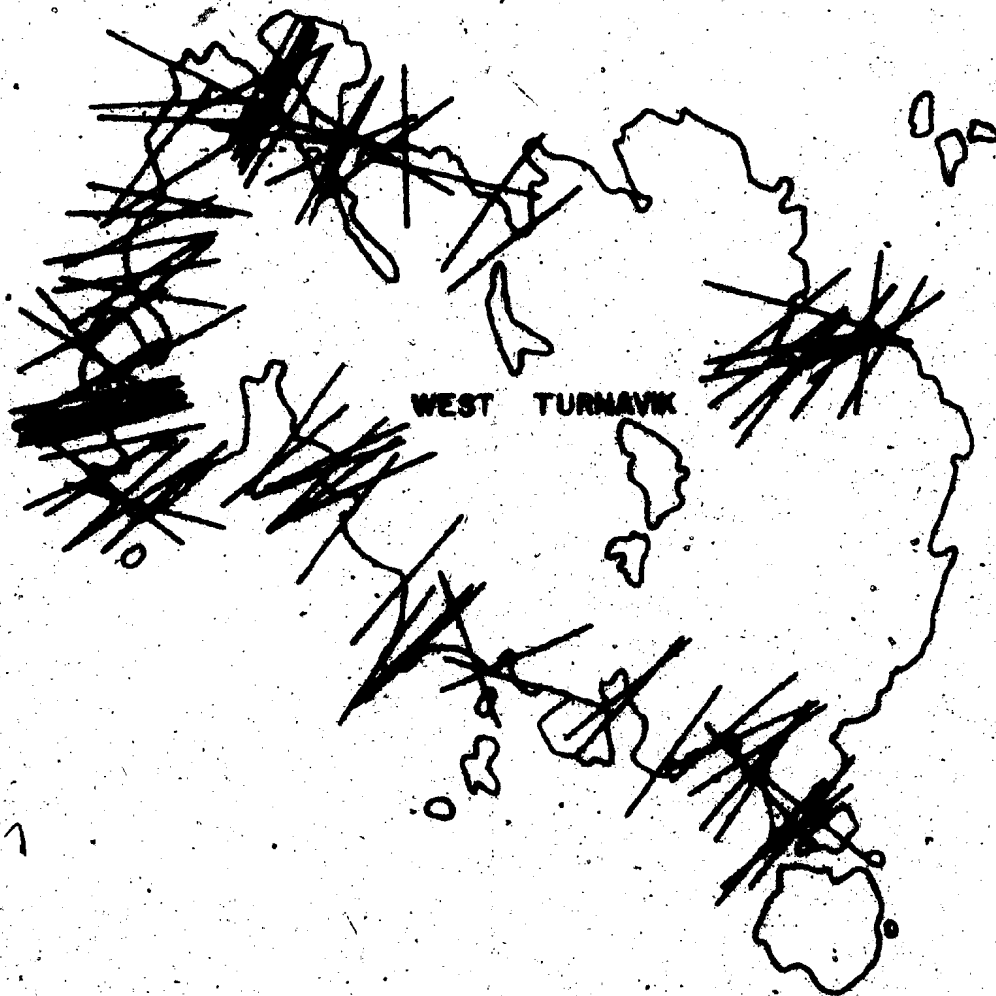
3.2.5 Other Methods

P_2O_5 contents were determined on a Bausch and Lomb Spectronic 20 Colorimeter according to a method modified after Maxwell (1968).

Loss on ignition was determined by weighing approximately 0.5 g of sample into a porcelain crucible, heating to 1050° for two hours, cooling in a dessicator and weighing accurately to determine weight loss of the sample (i.e. volatile content).

CO_2 was measured on a Leco Induction Furnace Analyzer. 0.1000 to 0.5000 g of sample were ignited with iron and tin within porcelain crucibles until the sample was in a molten state. The method and procedure used is that given in the operator manual for the Leco Furnace and results are recorded in percent carbon for each sample analyzed.

59°22'



WEST TURNAVIK

TURNAVIK ISLAND



EAST TURNAVIK

10F

59°15'

59° 15'

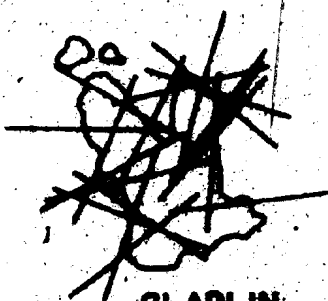
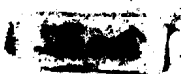
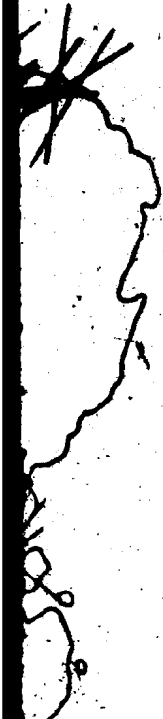
L
A
B
R
A
D
O
R

S
E
A

ISLANDS

EAST TURNAVIK

GLAPLIN
ISLAND



34

ATLANTIC OCEAN

GULL
ROCK

59°08'

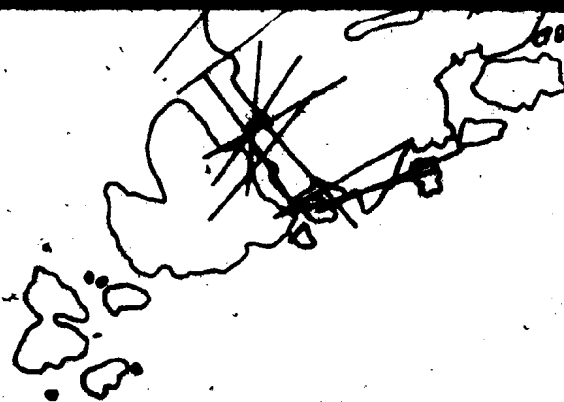
4d

NTIC
OCEAN

55°15'

55°15'

55



EAST TURN

59° 22'

AILLIK AREA, LA SCHEMATIC REPRESENTATION OF DYKE ORIENTATION

SCALE
1:36000

Miles 1



Kilometers 1



EAST TURNVIK

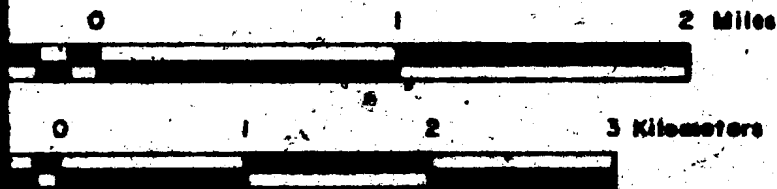
GLAPLIN
ISLAND

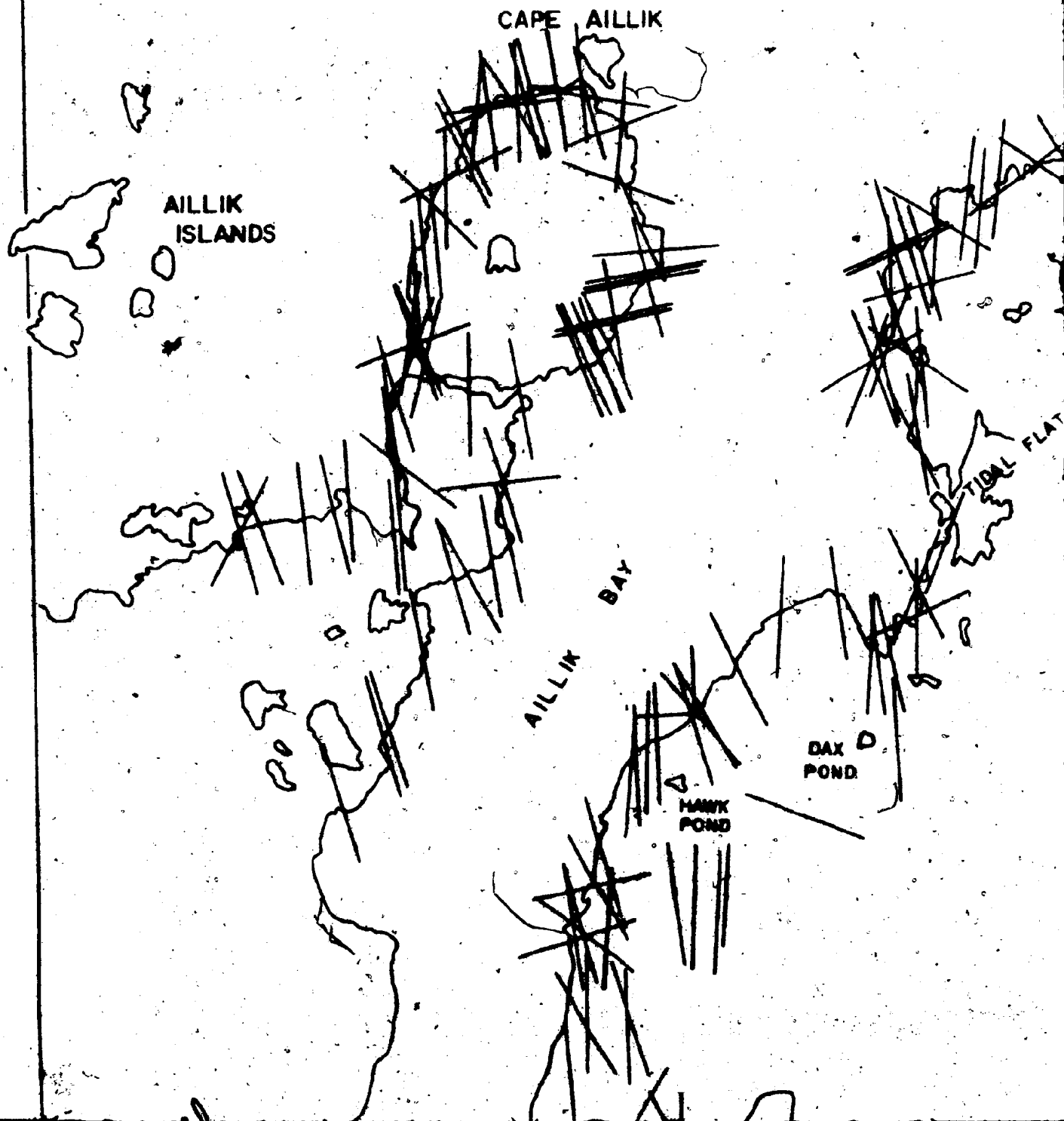
60

X AREA, LABRADOR

**PRESENTATION OF LAMPROPHYRE
KE ORIENTATIONS**

SCALE
1:36000





8 of 1

CAPE AILLIK

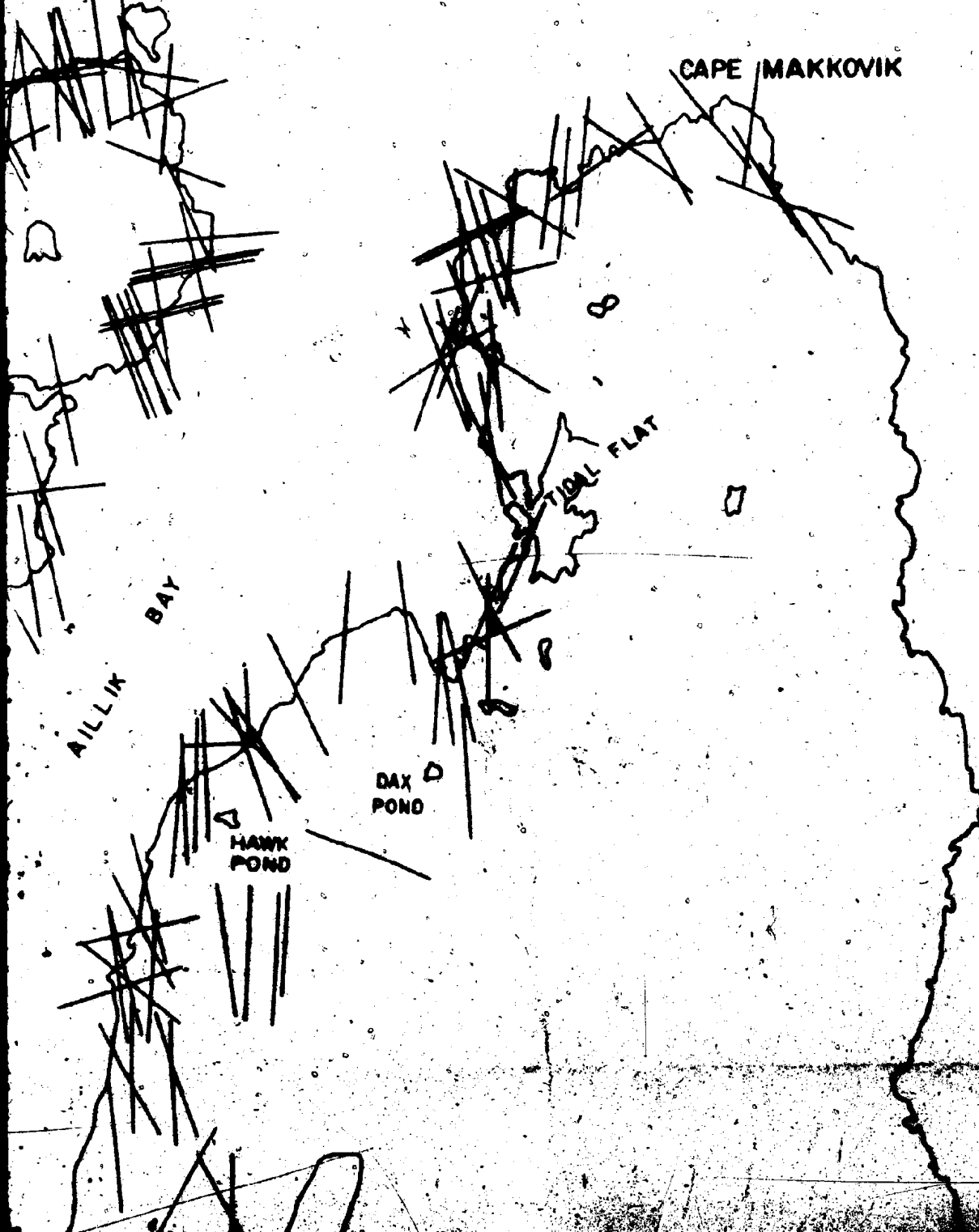
CAPE MAKKOVIK

TIDAL FLAT

AILLIK BAY

DAX POND

HAWK POND



AILLIK AREA, LAB

SCHEMATIC REPRESENTATION OF DYKE ORIENTATION

SCALE
1:36000

Miles |



Kilometers |



9.f

ISLAND

AREA, LABRADOR

DISTRIBUTION OF LAMPROPHYRE
ORIENTATIONS

SCALE
1:36000

2 Miles

3 Kilometers

55°10'

55°10'

10.1

AILLIK
ISLANDS

AILLIK BAY

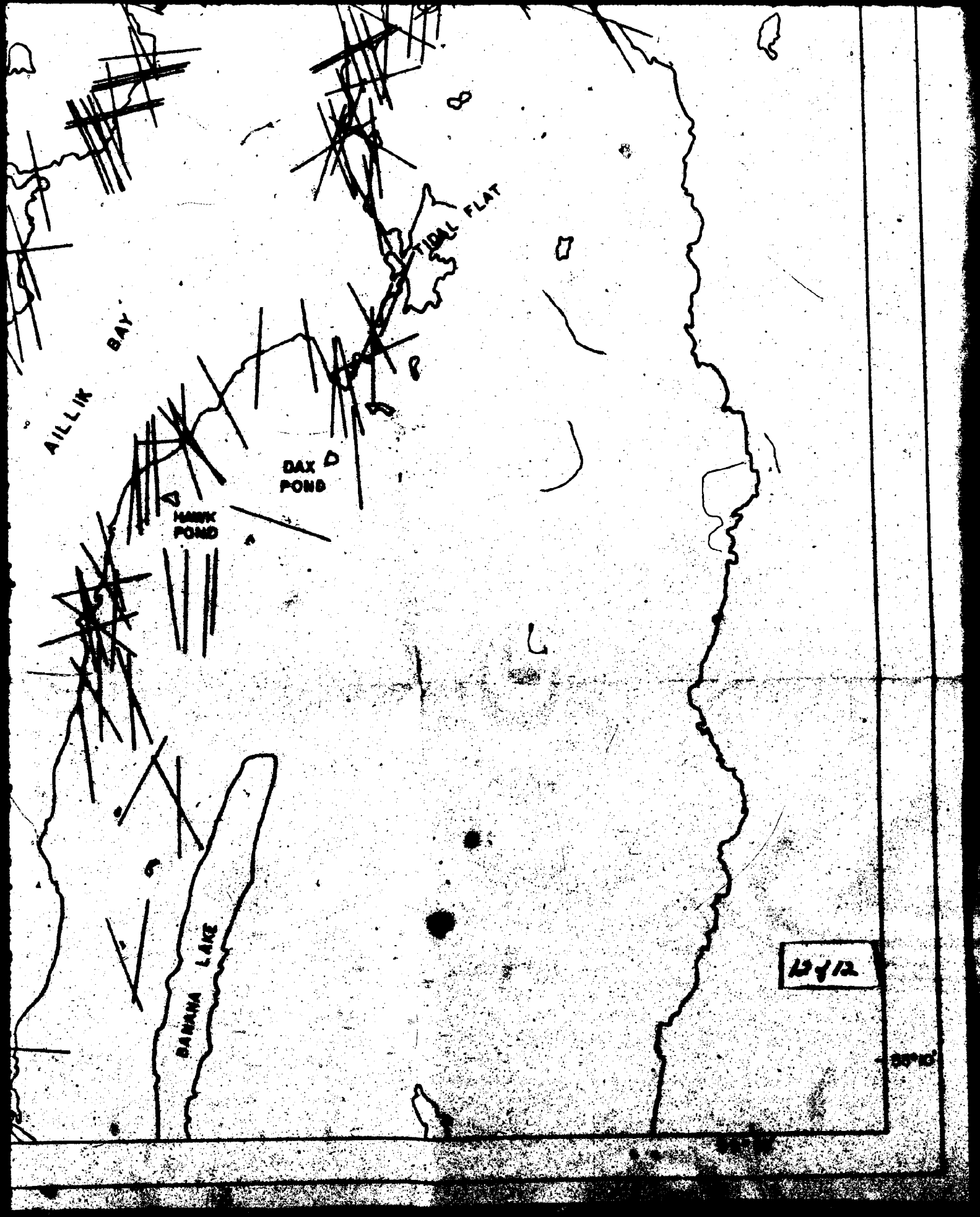
TIDAL FLAT

DAX
POND

HARK
POND

SANAMA LAKE

114



100



WEST THERAPIE

100-100-100

0010

000

000

E
A
B
R
A
D
O
R

A

04-002-003

SLANDS

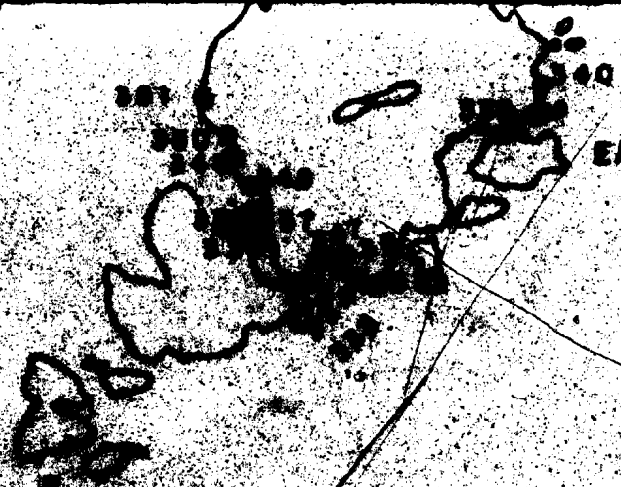
ACT

34

72

5610

56



EAST TURNOUT

SAMPLE LOCATION

OF THE AILLIK B

1000

418 419 424
415 414 425
413 426
409
408

TURNAVIK

GRAPLIN
ISLAND

66

ATION MAP

IK BAY AREA

ADOR

ALLI
ISLAND

7 of

CAPE AILLIK

CAPE MAKKOVIK

AILLIK
ISLANDS



8.0f

CAPE AILLIK

CAPE MAKKOWK

SPR 2487-8



SAMPLE LOCATION

OF THE AILLIK B

LABRADOR

SCALE
1:2500

9.4

CATION MAP

LIK BAY AREA

RADOR

PLE
600

2 Miles

2

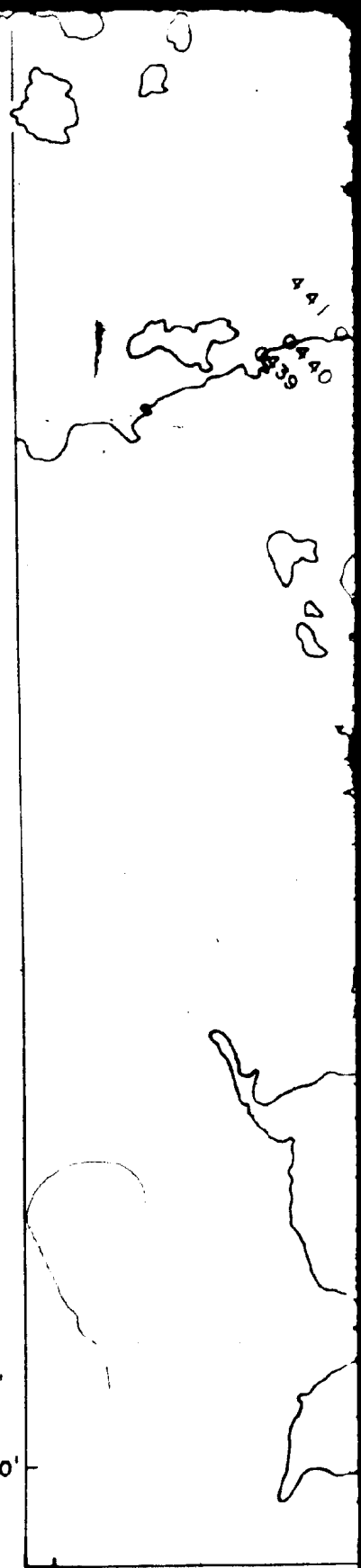
3 Kilometers

55° 10'

10.f

59° 10'

Map 3



59°22'

10F



TURNAVIK ISLAND



EAST TURNAVIK

55°15'

59°15'

120E

L
A
B
R
A
D
O
R

S
E
A

K ISLANDS

AST TURNVIK

GRAPLIN
ISLAND

134

ATLANTIC

OCEAN



GULL
ROCK

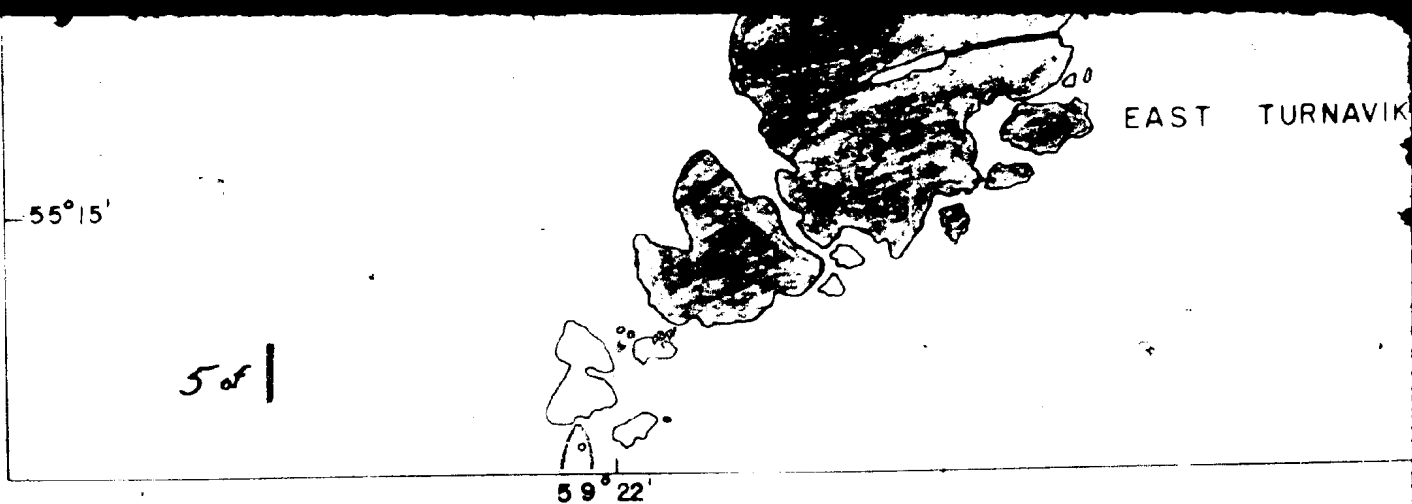
59°08'

4 of

ANTIC

OCEAN

55°15'

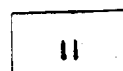


LEGEND

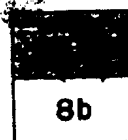
AILLIK GROUP



Sediments, possibly including volcanics,
equivalent to unit 7



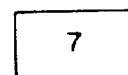
Undifferentiated acid volcanic
and quartzo-feldspathic



Amphibolite, minor quartzite



Quartzo-feldspathic



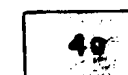
Sediments or acid volcanics showing
secondary feldspathization



Micaceous unit



Undifferentiated sediments
and acid volcanics



Conglomerate, minor marble, in part
equivalent to 5



Banded quartzo-feldspathic unit



Arkose, minor marble and calc-silicate
breccia



Cross-bedded arkose, conglomerate

HOPÉDALE COMPLEX



Undifferentiated quartzo-feldspathic
gneiss, amphibolite, gneissic granite,
omatite

PROTEROZOIC

ARCHEAN

Geological

Fault

Limit of

Pond

Shoal

Anticline

Geological

AST TURNAVIK

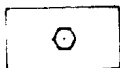
GRAPLIN
ISLAND

6 of 1

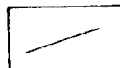
END

ifferentiated acid volcanics
quartzo-feldspathic sediments

quartzo-feldspathic mylonite



Monchiquite diatreme



Diabase



Diabase porphyry



Undifferentiated granitic rocks



Hornblendite to
hornblende diorite

KEY

Geological Contact (approximate, assumed, gradational).....

Fault.....

Limit of geological mapping.....

Pond.....

Shoal.....

Anticline.....

Geology by A F King, 1963 and D W Hawkins, 1973

Compiled by D W Hawkins

AILLIK
ISLANDS

ILLIK-DAV AREA

7 of 1

CAPE AILLIK

CAPE MAKK

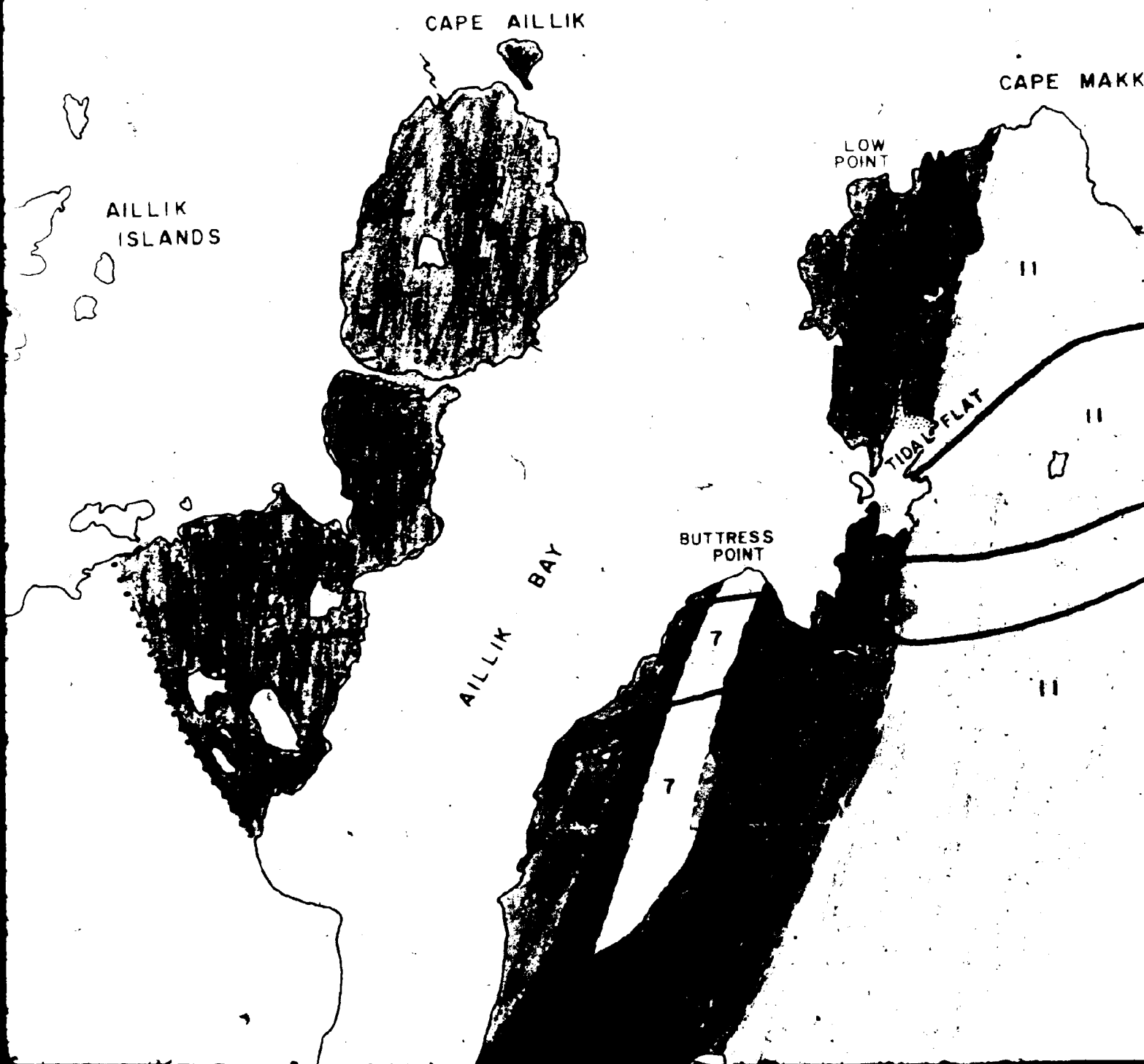
AILLIK
ISLANDS

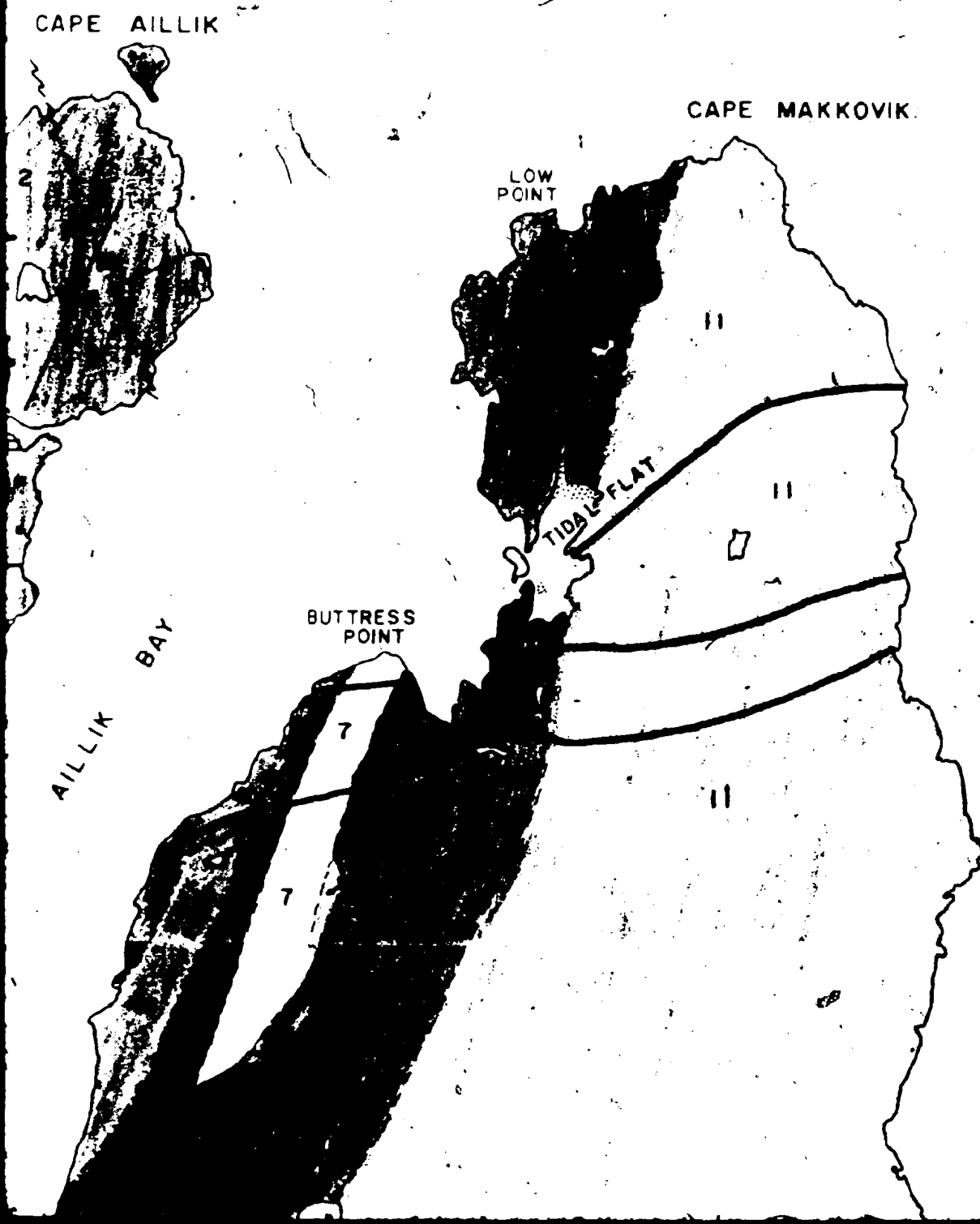
LOW
POINT

TIDAL FLAT

BUTTRESS
POINT

AILLIK BAY





PROTEROZOIC

8b

Quartzite

7

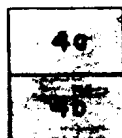
Sediments or acid volcanics showing secondary feldspathization



Micaceous unit



Undifferentiated sediments and acid volcanics



Conglomerate, minor marble, in part equivalent to 5



Banded quartzo-feldspathic unit



Arkose, minor marble and calc-silicate breccia



Cross-bedded arkose, conglomerate

HOPEDALE COMPLEX



Undifferentiated quartzo-feldspathic gneiss, amphibolite, gneissic granite, agmatite

ARCHEAN

GEOLOGY OF THE AILL LABRADO

SCALE
1:36000

Miles



Kilometers

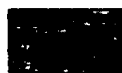


9.8

Map 1



Diabase porphyry



Undifferentiated granitic rocks



Hornblendite to
hornblende diorite

KEY

Geological Contact (approximate, assumed, gradational)

Fault.....

Limit of geological mapping

Pond

Shoal

Anticline

Geology by A F King, 1963 and D W Hawkins, 1973

Compiled by D W Hawkins

AILLIK BAY AREA RADOR

SCALE
1:36000

2 Miles

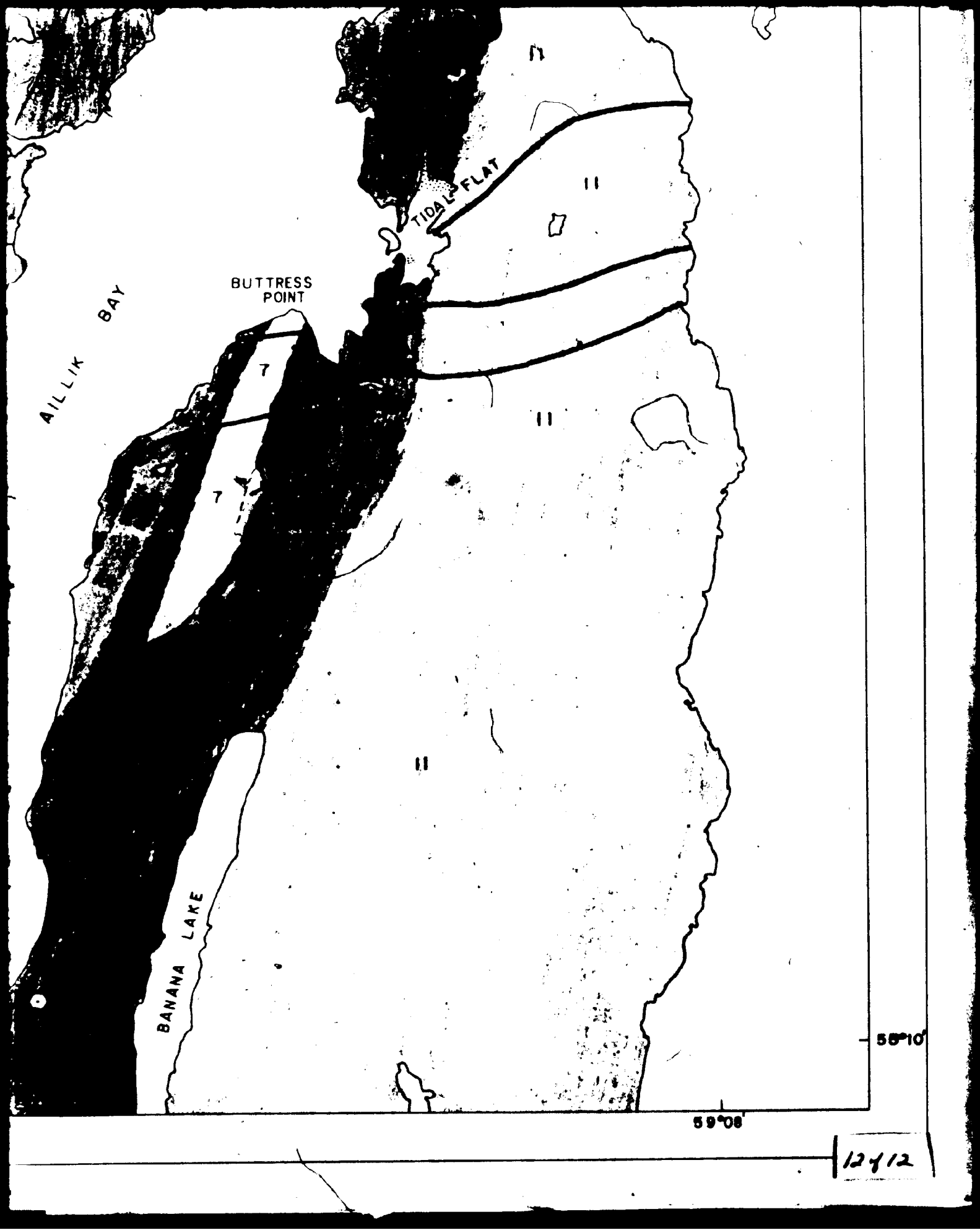
3 Kilometers

55°10'

59°10'

10.f





AILLIK BAY

BUTTRESS
POINT

TIDAL FLAT

BANANA LAKE

55°10'

59°08'

12412

